

The University of Hull

**A Study of Low Force Fabric
Characteristics and Vibrational
Behaviour for Automated Garment
Handling**

being a Thesis submitted for the Degree of

Doctor of Philosophy

in the University of Hull

by

Didier Michel Pollet

B.Sc. Elec. Eng., K.I.H.W.V. Belgium, 1991

M.Sc. Mechatronics, The University of Hull, 1992

November 1998

Abstract

One of the fundamental concepts in automated garment assembly is that the orientation of a fabric panel should never be lost. However, if a panel does become distorted, several techniques, such as vision, air flotation tables, and vibratory conveyors are available to restore the orientation.

This thesis has investigated the behaviour of a fabric panel on a vibratory table. Several table parameters such as amplitude of vibration, frequency and angle of inclination, together with some important fabric properties as friction and compressibility are required to understand the behaviour.

However, most work on friction in textiles considers fibre-fibre or fabric-fabric friction, which is not appropriate to this and so low force frictional properties between unloaded fabric and engineering surfaces (i.e., aluminium, Formica and rubber) have been studied. The influence of several experimental variables on friction is demonstrated, in particular, the effect of humidity and velocity. Further, an in depth study is made on the stick-slip of fabric panels wherein a novel measuring technique is introduced. An estimate of the damping, which is required to model the fabric, has been obtained from an in-plane vibration test.

The second significant fabric property to be studied is the compression both static and impact. Again, only low-force compression tests are carried out since these are the typical forces experienced by fabrics on a vibrating table. The static compressibility of knitted and woven materials is verified with van Wvk's equation. which gives a near indistinguishable fit with the experimental data. The

To my parents

Science is organised knowledge

Herbert Spencer (1820-1903)

Acknowledgements

Six years of work has finally ended and found its way onto paper. There are too many people to thank and I apologise to those I miss out.

I am especially grateful to my supervisor, Paul Taylor, for his encouragement and confidence he has given all this time. His helpful comments and constructive suggestions at each stage of the research have contributed considerably to the improvement of this work.

Thanks also to my fellow colleagues with whom I had the pleasure to work with during this years: Andrew Kaiser, José Mendes, Kevin McKay, Sharon Brady, Sanja Rankov, and special thanks to Paul Abbott for proof-reading the thesis. Thanks to Jo Aspland for cheering me up when 'things' didn't always work, as they should have done.

Furthermore, I gratefully wish to acknowledge the staff and technicians of the Department of Electronic Engineering in particular Dave Joyce and John Hodgson for their mechanical support, Dave Glover, Ernie Thompson, Eric Wright and Sandra Batch for their helpfulness during these years.

I would like to thank the EPSRC for funding the fees and the Department of Electronic Engineering.

I am, of course indebted to all my friends who have made my stay in Hull a pleasurable one, especially Fatima, José and Sam.

And last but not least, my special gratitude goes to my parents for their financial and moral support. Thank you, for everything you have done for me over these years. Without you, none of this would have been possible.

Contents

1	INTRODUCTION	1
1.1	Automation in the Garment Industry: Past Present and Future	1
1.2	Why is Garment Manufacturing Difficult?	4
1.2.1	Fabric Objective Measurement	6
1.2.2	Intelligent Automation	7
1.2.3	Management	7
1.3	Transportation and Orientation Methods for Garment Automation	8
1.3.1	Transportation Mechanisms	9
1.3.2	Orientation and Aligning Mechanisms	10
1.4	Outline and Novelty of the Research	12
2	LITERATURE SURVEY	13
2.1	Friction Properties of Textiles	13
2.1.1	Introduction	13
2.1.2	Classical Friction Models	15
2.1.3	Friction in Textiles	18
2.1.4	Fabric Parameters Affecting Frictional Behaviour	25
2.1.5	Experimental Conditions Affecting Frictional Behaviour	27
2.1.6	Friction Measuring Devices	33
2.2	Compression Properties of Textiles	35
2.2.1	Introduction	35
2.2.2	Van Wyk Model	38
2.2.3	Other Lateral Compression Models	40
2.3	Vibration in Textiles	41
2.3.1	Introduction	41
2.3.2	Longitudinal Vibration	43
2.3.3	Lateral Vibration	46
2.4	Vibratory Feeders	48
2.4.1	Introduction	48
2.4.2	Basic Conveying Theory	49
2.5	Summary	52
3	LOW FORCE FRICTION CHARACTERISTICS OF FABRIC AGAINST ENGINEERING SURFACES	54
3.1	Instrumentation and Method	54
3.1.1	Friction Measuring Table	54
3.1.2	Fabric Details	56
3.1.3	General Test Procedure for Friction Measurements	57
3.1.4	Expression of Results	58
3.2	Surface Roughness	59
3.2.1	Instrumentation and Measuring Method	59
3.2.2	Results	60

3.3	Influence of the Number of Traverses	62
3.4	Influence of the Relative Humidity	66
3.4.1	The Rate of Friction Change from Dry to Standard Conditions	66
3.4.2	The Variation of Friction with Absorption and Desorption of Moisture	70
3.5	The Effect of Static Charge on Friction	77
3.6	Nature of the Sliding Surface	79
3.7	Influence of the Sample Area	81
3.8	Influence of the Normal Pressure	82
3.9	Influence of the Sliding Velocity	86
3.10	Stick-slip Behaviour	88
3.10.1	Instrumentation	88
3.10.2	Results from Diode Bench	91
3.10.3	Stick-Slip Traces	94
3.10.4	Theoretical Stick-Slip Model	100
3.10.5	Defining Parameters for Spring-Damper Model	104
3.10.6	Stick-Slip Simulation	111
3.11	Summary	116
4	LOW FORCE COMPRESSION CHARACTERISTICS	119
4.1	Static Compression	119
4.1.1	Instrumentation and Method	119
4.1.2	Analysis of Loading-Compression Results	121
4.1.3	Some Other Thickness Measurement Techniques	126
4.1.4	Approximation of the Loading-Compression Results	127
4.1.5	Interpretation of the van Wyk Parameters α' and V'	132
4.2	Impact Compression	134
4.2.1	Instrumentation and Method	134
4.2.2	Theoretical Background of the Impact Compression by Pendulum	135
4.2.3	Results	137
4.3	Comparison between Static and Impact Compression	140
4.4	Summary	142
5	VIBRATION CHARACTERISTICS	143
5.1	Instrumentation and Method	143
5.2	Stationary Vibration Tests	145
5.2.1	Non-linear Response	146
5.2.2	Position Dependency of the Vibrating Fabric	147
5.2.3	Amplitude Dependency of the Vibrating Fabric	151
5.2.4	Fabric Vibration Model with Hysteretic Damping	155
5.2.5	Simulation Results	157
5.3	Vibratory Feeding of Fabric	162
5.3.1	Experimental Method	162
5.3.2	Friction Dependency	162

5.3.3	Table Dependency	168
5.4	Some Concepts for the Vibratory Orientation of Fabric	171
5.4.1	Orientation by Fences	172
5.4.2	Orientation by Surface Variations	175
5.5	Summary	177
6	CONCLUSION AND FUTURE WORK	179
6.1	Low Force Friction Characteristics	179
6.2	Low Force Compression Characteristics	181
6.3	Vibration Characteristics	181
	REFERENCES	183
	APPENDIX A FABRIC DETAILS	206
	APPENDIX B TEST EQUIPMENT	214
B.1	Friction Measuring Table	214
B.2	The Ring Dynamometer	216
B.3	Specifications of the Micro-Epsilon® Laser Sensor (LD1605-4)	218
B.4	Diode Bench	219
B.5	Static Compression Tester	221
B.6	Impact Pendulum Tester	224
B.7	Vibrating Table Unit	225
B.8	Gaptek 2004 Non-contact Micro Displacement Transducer	226
B.9	Specifications of the Triaxial Accelerometer (4504)	227
	APPENDIX C SURFACE DETAILS	228
C.1	Instrumentation and Method	228
C.2	Surface Scans	228
	APPENDIX D SOME STATISTICAL ANALYSIS	231
D.1	Kind of Distribution	231
D.2	Number of Samples Required	233
D.3	Precision of KES-FB Tests of Friction and Compression	234

APPENDIX E FRICTION	236
E.1 Detailed Friction Results	236
E.2 Stick-Slip Simulation Parameters and Models	242
APPENDIX F SPRING IMPACT	247
APPENDIX G HYSTERETIC DAMPING	251
APPENDIX H BASIC THEORY OF A SINGLE DEGREE FLIGHT-FREE VIBRATING CONVEYOR	254

List of Illustrations

FIGURE 1.1. PROBLEM-SOLUTION SCHEMA FOR GARMENT AUTOMATION	5
FIGURE 1.2. VIBRATING ALIGNMENT TABLE WITH PINCHING GRIPPER AT THE HULL BRIEF'S ASSEMBLY LINE	11
FIGURE 2.1. SIDE VIEWS OF FABRIC SURFACE FOR FILAMENT YARN FABRIC AND FOR SPUN YARN FABRIC (W1) (MAGNIFICATION X15)	13
FIGURE 2.2. FORCE DIAGRAM OF TWO SOLIDS IN CONTACT	15
FIGURE 2.3. REAL CONTACT BETWEEN TWO SOLIDS	16
FIGURE 2.4. REGULAR STICK-SLIP PLOT	28
FIGURE 2.5. STRIBECK CURVE	29
FIGURE 2.6. REGAIN AS A FUNCTION OF THE RELATIVE HUMIDITY [MORTON 97]	31
FIGURE 2.7. FORCE DIAGRAM OF TWO BODIES ON AN INCLINED PLANE	34
FIGURE 2.8. DREBY'S PRINCIPLE FOR FRICTION MEASUREMENTS	35
FIGURE 2.9. THEORETICAL COMPRESSION-RELEASE CURVE	37
FIGURE 2.10. THREE LAYER MODEL OF WOVEN FABRIC UNDER LATERAL COMPRESSION PROPOSED BY DE JONG ET AL. [DE JONG 86]	38
FIGURE 2.11. CONVENTIONAL VIBRATORY FEEDER	48
FIGURE 2.12. FLOW DIAGRAM OF VARIOUS COMPONENT MOVEMENTS FOR CONTINUOUS CONVEYING [REDFORD 67]	49
FIGURE 2.13. THE CO-ORDINATE SYSTEM AND ANGLES	50
FIGURE 3.1. A SKETCH OF THE FABRIC FRICTION MEASUREMENT	55
FIGURE 3.2. FRICTION TRACE FOR KC11 FABRIC (WALE DIRECTION) AGAINST THE ALUMINIUM SURFACE.	58
FIGURE 3.3. A SKETCH OF THE SURFACE ROUGHNESS TEST	60
FIGURE 3.4. FIRST PROFILE SCAN OF KC11 ALONG THE WALE DIRECTION	61
FIGURE 3.5. SCATTER PLOT OF ROUGHNESS AS A FUNCTION OF DYNAMIC FRICTION FOR SET 1 FABRICS	64
FIGURE 3.6. VARIATION OF THE DYNAMIC FRICTION FOR KC11 CAUSED BY A SUDDEN HUMIDITY CHANGE FROM 0% TO 65% R.H. AS A FUNCTION OF TIME	67
FIGURE 3.7. VARIATION OF THE MASS OF KC11 CAUSED BY A SUDDEN HUMIDITY CHANGE FROM 0% TO 65% R.H. AS A FUNCTION OF TIME	67
FIGURE 3.8. DIAGRAMMATIC REPRESENTATION OF CROSS-SECTIONAL YARN SWELLING WITH INCREASING HUMIDITY	70
FIGURE 3.9. RELATIVE WATER ABSORBENCY FOR SET 2 FABRICS	71
FIGURE 3.10. HYSTERESIS EFFECT OF THE REGAIN FOR KC11	71
FIGURE 3.11. DYNAMIC FRICTION OF C2 AS A FUNCTION OF RELATIVE HUMIDITY	74
FIGURE 3.12. DYNAMIC FRICTION OF KC5 AS A FUNCTION OF RELATIVE HUMIDITY	74
FIGURE 3.13. DYNAMIC FRICTION OF KC11 AS A FUNCTION OF RELATIVE HUMIDITY	74
FIGURE 3.14. DYNAMIC FRICTION OF V1 AS A FUNCTION OF RELATIVE HUMIDITY	75
FIGURE 3.15. DYNAMIC FRICTION OF W2 AS A FUNCTION OF RELATIVE HUMIDITY	75
FIGURE 3.16. DYNAMIC FRICTION OF L1 AS A FUNCTION OF RELATIVE HUMIDITY	75
FIGURE 3.17. DYNAMIC FRICTION OF P2 AS A FUNCTION OF RELATIVE HUMIDITY	76
FIGURE 3.18. DYNAMIC FRICTION OF KN11 AS A FUNCTION OF RELATIVE HUMIDITY	76
FIGURE 3.19. PERCENTAGE CHANGE OF DYNAMIC FRICTION COEFFICIENT WITH RELATIVE HUMIDITY	77
FIGURE 3.20. FRICTION COEFFICIENTS FOR SET 1 FABRICS IN THE WARP (WALE) DIRECTION AGAINST DIFFERENT SURFACES	80
FIGURE 3.21. FRICTION COEFFICIENTS FOR SET 1 FABRICS IN THE WEFT (COURSE) DIRECTION AGAINST DIFFERENT SURFACES	80
FIGURE 3.22. THE EFFECT OF THE SAMPLE AREA ON THE DYNAMIC FRICTION COEFFICIENT FOR SET 1 FABRICS	82
FIGURE 3.23. LOGARITHMIC RELATIONSHIP BETWEEN THE FRICTIONAL FORCE PER AREA (LOG F/A) AND THE NORMAL PRESSURE (LOG N/A) FOR SET 1 FABRICS	83
FIGURE 3.24. RELATIONSHIP BETWEEN WILSON'S MODEL COEFFICIENTS C AND N FOR SET 1 FABRICS AGAINST ALUMINIUM	84
FIGURE 3.25. THE INFLUENCE OF THE SURFACE TYPE ON THE WILSON MODEL COEFFICIENTS N AND C	84

FIGURE 3.26. DYNAMIC COEFFICIENT OF FRICTION FOR FABRIC AGAINST ALUMINIUM AS A FUNCTION OF THE SLIDING VELOCITY	86
FIGURE 3.27. DYNAMIC COEFFICIENT OF FRICTION FOR FABRIC AGAINST RUBBER AS A FUNCTION OF THE SLIDING VELOCITY	86
FIGURE 3.28. THEORETICAL SENSOR OUTPUT FOR A 'RIGID' BODY UNDER STICK-SLIP MOVEMENT	89
FIGURE 3.29. THEORETICAL SENSOR OUTPUT FOR A 'STRETCHABLE' BODY UNDER STICK-SLIP MOVEMENT	89
FIGURE 3.30. SKETCH OF THE DIODE BENCH FOR MEASURING LOCAL FABRIC STICK-SLIP	90
FIGURE 3.31. BASIC OPTICAL ARRANGEMENT	90
FIGURE 3.32. TYPICAL UNPROCESSED SENSOR OUTPUT FROM PHOTODIODES FOR PERSPEX SLED MOVEMENT	92
FIGURE 3.33. MAGNIFIED AND FILTERED SECTION FROM FIGURE 3.32 ABOVE	92
FIGURE 3.34. PHOTO-DIODE OUTPUTS FOR A REPRESENTATIVE KNITTED MATERIAL (KA1)	93
FIGURE 3.35. PHOTO-DIODE OUTPUTS FOR A REPRESENTATIVE WOVEN MATERIAL (C3)	93
FIGURE 3.36. IRREGULAR STICK-SLIP TRACE OF KA3 ON ACETATE	96
FIGURE 3.37. REGULAR STICK-SLIP TRACE OF C3 ON ACETATE	96
FIGURE 3.38. AUTOSPECTRAL DENSITY OF STICK-SLIP TRACE OF KA3	98
FIGURE 3.39. AUTOSPECTRAL DENSITY OF STICK-SLIP TRACE OF C3	98
FIGURE 3.40. VARIATION OF THE WAVELENGTH PEAKS FOR DIFFERENT YARN SPACING (0.12 MM/S)	100
FIGURE 3.41. CLASSICAL AND APPROXIMATED FRICTION MODEL	101
FIGURE 3.42. THEORETICAL SPRING DAMPER MODEL	102
FIGURE 3.43. A SKETCH OF THE LONGITUDINAL VIBRATION MEASUREMENT OF FABRIC	104
FIGURE 3.44. SDOF SPRING-DAMPER MODEL FORCE-VIBRATED AT THE BASE	105
FIGURE 3.45. FREQUENCY RESPONSE FOR DIFFERENT DAMPING RATIOS OF A BASE EXCITED VISCOUS-DAMPED SYSTEM	106
FIGURE 3.46. TRANSMISSIBILITY OF C3 AT 50 μ M EXCITATION	107
FIGURE 3.47. TRANSMISSIBILITY OF KC3 AT 50 μ M EXCITATION	107
FIGURE 3.48. TRANSMISSIBILITY OF KA1 AT 50 μ M EXCITATION	107
FIGURE 3.49. TRANSMISSIBILITY OF KA3 AT 50 μ M EXCITATION	108
FIGURE 3.50. TRANSMISSIBILITY OF AC1 AT 50 μ M EXCITATION	108
FIGURE 3.51. TRANSMISSIBILITY OF L2 AT 50 μ M EXCITATION	108
FIGURE 3.52. TRANSMISSIBILITY OF PA1 AT 50 μ M EXCITATION	109
FIGURE 3.53. STATIC EXTENSION MEASUREMENTS FOR SOME SET 3 FABRICS	110
FIGURE 3.54. COMPARISON BETWEEN THE SIMULATED AND EXPERIMENTAL STICK-SLIP FOR KC3	113
FIGURE 3.55. DISPLACEMENT OF SPRING AND MASS IN A SINGLE-MASS MODEL (KC3)	113
FIGURE 3.56. SPRING VELOCITY IN A SINGLE-MASS MODEL (KC3)	114
FIGURE 3.57. SIMULATED STICK-SLIP FOR A TWO-MASS MODEL (KC3)	114
FIGURE 3.58. SIMULATED MASS DISPLACEMENT (ENLARGEMENT) OF KC3 WITH A TWO-MASS MODEL	115
FIGURE 3.59. SIMULATED MASS DISPLACEMENT (ENLARGEMENT) OF C3 WITH A TWO-MASS MODEL	115
FIGURE 4.1. A SKETCH OF THE EXPERIMENTAL COMPRESSION RIG	120
FIGURE 4.2. COMPRESSION HYSTERESIS FOR C1	122
FIGURE 4.3. COMPRESSION HYSTERESIS FOR P1	122
FIGURE 4.4. COMPRESSION HYSTERESIS FOR W1	122
FIGURE 4.5. COMPRESSION HYSTERESIS OF W1B (SHAVEN W1)	123
FIGURE 4.6. COMPRESSION HYSTERESIS FOR KC1	123
FIGURE 4.7. COMPRESSION HYSTERESIS FOR KC11	123
FIGURE 4.8. COMPRESSION HYSTERESIS FOR KA11	124
FIGURE 4.9. SURFACE ROUGHNESS OF THE SET 1 FABRICS AS A FUNCTION OF THEIR 'SPRINGINESS' (WC)	125
FIGURE 4.10. VAN WYK APPROXIMATIONS TO THE COMPRESSION OF C1	129

FIGURE 4.11. VAN WYK APPROXIMATIONS TO THE COMPRESSION OF P1	129
FIGURE 4.12. VAN WYK APPROXIMATIONS TO THE COMPRESSION OF W1	129
FIGURE 4.13. VAN WYK APPROXIMATIONS TO THE COMPRESSION OF W1B	130
FIGURE 4.14. VAN WYK APPROXIMATIONS TO THE COMPRESSION OF KC1	130
FIGURE 4.15. VAN WYK APPROXIMATIONS TO THE COMPRESSION OF KC11	130
FIGURE 4.16. VAN WYK APPROXIMATIONS TO THE COMPRESSION OF KA11	131
FIGURE 4.17. SKETCH OF THE IMPACT COMPRESSION MEASURING DEVICE	134
FIGURE 4.18. THEORETICAL DYNAMIC PENDULUM COMPRESSION OF FABRIC	136
FIGURE 4.19. FORCE DIAGRAM OF A SIMPLE PENDULUM	136
FIGURE 4.20. FREE OSCILLATION OF THE IMPACT PENDULUM	138
FIGURE 4.21. ENERGY LOSS OF THE PENDULUM IN FREE OSCILLATION	138
FIGURE 4.22. IMPACT RESPONSE OF KC11	139
FIGURE 4.23. IMPACT RESPONSE OF C1	139
FIGURE 4.24. IMPACT RESPONSE OF W1	140
FIGURE 4.25. COMPARISON BETWEEN THE STATIC AND DYNAMIC ENERGY FOR SIMILAR COMPRESSION THICKNESSES	141
FIGURE 5.1. SKETCH OF THE OUT OF PLANE VIBRATION MEASUREMENTS	144
FIGURE 5.2. SCHEMATIC DIAGRAM OF THE EQUIPMENT SET-UP	145
FIGURE 5.3. RAW DATA FOR OUT OF PLANE VIBRATION OF W1	146
FIGURE 5.4. RAW DATA FOR OUT OF PLANE VIBRATION OF C1	146
FIGURE 5.5. LOCATION OF THE MEASURING SPOTS ON A FABRIC SAMPLE	147
FIGURE 5.6. FREQUENCY RESPONSE OF C1 MEASURED AT THREE DIFFERENT POINTS	148
FIGURE 5.7. FREQUENCY RESPONSE OF P1 MEASURED AT THREE DIFFERENT POINTS	149
FIGURE 5.8. FREQUENCY RESPONSE OF W1 MEASURED AT THREE DIFFERENT POINTS	149
FIGURE 5.9. FREQUENCY RESPONSE OF W1B MEASURED AT THREE DIFFERENT POINTS	149
FIGURE 5.10. FREQUENCY RESPONSE OF KC1 MEASURED AT THREE DIFFERENT POINTS	150
FIGURE 5.11. FREQUENCY RESPONSE OF KC11 MEASURED AT THREE DIFFERENT POINTS	150
FIGURE 5.12. FREQUENCY RESPONSE OF KA11 MEASURED AT THREE DIFFERENT POINTS	150
FIGURE 5.13. AMPLITUDE DEPENDENCY OF C1	151
FIGURE 5.14. AMPLITUDE DEPENDENCY OF P1	152
FIGURE 5.15. AMPLITUDE DEPENDENCY OF W1	152
FIGURE 5.16. AMPLITUDE DEPENDENCY OF W1B	152
FIGURE 5.17. AMPLITUDE DEPENDENCY OF KC1	153
FIGURE 5.18. AMPLITUDE DEPENDENCY OF KC11	153
FIGURE 5.19. AMPLITUDE DEPENDENCY OF KA11	153
FIGURE 5.20. EXPERIMENTAL HYSTERESIS FOR KC11 AND W1	154
FIGURE 5.21. BASE EXCITED MODEL WITH HYSTERETIC DAMPING SIMULATING FABRIC VIBRATION	155
FIGURE 5.22. THEORETICAL FREQUENCY RESPONSE OF A BASE EXCITED SPRING-DAMPER MODEL WITH HYSTERETIC DAMPING	157
FIGURE 5.23. COMPARISON OF THEORETICAL AND MEASURED FREQUENCY RESPONSE FOR W1 AT 75 μ M EXCITATION	158
FIGURE 5.24. COMPARISON OF THEORETICAL AND MEASURED FREQUENCY RESPONSE FOR W1B AT 75 μ M EXCITATION	158
FIGURE 5.25. COMPARISON OF THEORETICAL AND MEASURED FREQUENCY RESPONSE FOR KC1 AT 75 μ M EXCITATION	158
FIGURE 5.26. COMPARISON OF THEORETICAL AND MEASURED FREQUENCY RESPONSE FOR KC11 AT 75 μ M EXCITATION	159
FIGURE 5.27. COMPARISON OF THEORETICAL AND MEASURED FREQUENCY RESPONSE FOR KA11 AT 75 μ M EXCITATION	159
FIGURE 5.28. RELATIONSHIP BETWEEN THE BENDING STIFFNESS AND THE RESONANCE FREQUENCY	160
FIGURE 5.29. OUT OF PHASE MOTION WHEN INCLINING THE TABLE	163
FIGURE 5.30. VIBRATORY FEEDING OF FABRIC SAMPLES ON AN ALUMINIUM SURFACE IN BOTH PRINCIPAL DIRECTIONS	163

FIGURE 5.31. FRICTION DEPENDENCY FOR VIBRATORY FEEDING OF C1	164
FIGURE 5.32. FRICTION DEPENDENCY FOR VIBRATORY FEEDING OF P1	164
FIGURE 5.33. FRICTION DEPENDENCY FOR VIBRATORY FEEDING OF W1	165
FIGURE 5.34. FRICTION DEPENDENCY FOR VIBRATORY FEEDING OF W1B	165
FIGURE 5.35. FRICTION DEPENDENCY FOR VIBRATORY FEEDING OF KC1	165
FIGURE 5.36. FRICTION DEPENDENCY FOR VIBRATORY FEEDING OF KC11	166
FIGURE 5.37. FRICTION DEPENDENCY FOR VIBRATORY FEEDING OF KA11	166
FIGURE 5.38. CONVEYING VELOCITY OF FABRICS ON DIFFERENT SURFACES	167
FIGURE 5.39. RELATIONSHIP BETWEEN THE FABRIC DAMPING AND THE SLIDING VELOCITY	167
FIGURE 5.40. CONVEYING VELOCITY OF C1 FOR AN INCREASING TABLE INCLINATION	168
FIGURE 5.41. CONVEYING VELOCITY OF P1 FOR AN INCREASING TABLE INCLINATION	169
FIGURE 5.42. CONVEYING VELOCITY OF W1 FOR AN INCREASING TABLE INCLINATION	169
FIGURE 5.43. CONVEYING VELOCITY OF W1B FOR AN INCREASING TABLE INCLINATION	169
FIGURE 5.44. CONVEYING VELOCITY OF KC1 FOR AN INCREASING TABLE INCLINATION	170
FIGURE 5.45. CONVEYING VELOCITY OF KC11 FOR AN INCREASING TABLE INCLINATION	170
FIGURE 5.46. CONVEYING VELOCITY OF KA11 FOR AN INCREASING TABLE INCLINATION	170
FIGURE 5.47. THEORETICAL AND EXPERIMENTAL SLIDING VELOCITY OF SOME FABRICS FOR AN INCREASED TABLE EXCITATION OF 150 μ M	171
FIGURE 5.48. STABLE AND UNSTABLE EDGE ALIGNMENTS OF AN ARM SHAPED FABRIC PANEL	172
FIGURE 5.49. PREDICTING THE ROTATION OF A RECTANGULAR PANEL HITTING A FENCE (AFTER [MASON 84])	173
FIGURE 5.50. SOME CONCEPTUAL IDEAS OF ORIENTATING FABRIC PANELS ON A LINEAR VIBRATORY FEEDER	174
FIGURE 5.51. CROSS SECTIONAL VIEW OF AN ELECTORRHEOLOGICAL ORIENTING TABLE	176
FIGURE B.1. PICTURE OF THE FRICTION TABLE	214
FIGURE B.2. DISPLACEMENT OF THE FRICTION TABLE AT VARIOUS VELOCITIES	215
FIGURE B.3. CLOSE-UP OF THE RING DYNAMOMETER AND AMPLIFIER	216
FIGURE B.4. RING CONFIGURATION BASED ON THE CLASSICAL MOREHOUSE PROVING RING	217
FIGURE B.5. CALIBRATION GRAPH OF THE RING DYNAMOMETER	217
FIGURE B.6. TRIANGULATION MEASURING PRINCIPLE [MICRO-EPSILON 94]	218
FIGURE B.7. DIODE BENCH	219
FIGURE B.8. STATIC COMPRESSION TESTER	221
FIGURE B.9. INHERENT HYSTERESIS OF THE STATIC COMPRESSION TESTER	222
FIGURE B.10. CLOSE UP OF THE STATIC COMPRESSION TESTER	222
FIGURE B.11. TOTAL VIEW OF THE IMPACT TESTER	224
FIGURE B.12. EXPERIMENTAL SET-UP OF THE VIBRATION UNIT	225
FIGURE C.1. ROUGHNESS PROFILE OUTPUT OF THE ALUMINIUM SURFACE	229
FIGURE C.2. ROUGHNESS PROFILE OUTPUT OF THE FORMICA SURFACE	230
FIGURE C.3. ROUGHNESS PROFILE OUTPUT OF THE RUBBER SURFACE	230
FIGURE D.1. GRAPHICAL REPRESENTATION OF THE NORMALITY TEST FOR KC11	232
FIGURE D.2. NORMALITY TESTS FOR OTHER SET 1 FABRICS	233
FIGURE E.1. SINGLE-MASS MODEL FOR SIMULATING STICK-SLIP BEHAVIOUR IN FABRIC	240
FIGURE E.2. TWO-MASS MODEL FOR SIMULATING STICK-SLIP IN FABRIC	241
FIGURE E.3. REPRESENTATION OF A ONE MASS ELEMENT AS A SUBSYSTEM (FRICTION1 M1) IN FIGURE E.2	241
FIGURE E.4. FOUR-MASS MODEL FOR SIMULATING STICK-SLIP BEHAVIOUR IN FABRICS	242
FIGURE E.5. SIMULATED FRICTION FOR KC3 WITH A FOUR-MASS MODEL	243

FIGURE E.6. SIMULATED MASS MOVEMENT FOR KC3 WITH A FOUR-MASS MODEL	243
FIGURE E.7. EXPERIMENTAL MOVEMENT OF FABRIC PARTS IN KC3 DETECTED ON THE DIODE BENCH	243
FIGURE E.8. COMPARISON BETWEEN THE EXPERIMENTAL STICK-SLIP TRACE FROM KC3 AND THE SIMULATED TRACE WITH A FOUR-MASS MODEL (0.12 MM/S)	244
FIGURE F.1. LOAD DEFLECTION CHARACTERISTIC OF TEST SPRING	245
FIGURE F.2. PENDULUM OSCILLATION FOR TEST SPRING	245
FIGURE F.3. COMPARISON BETWEEN THE STATIC AND DYNAMIC WORK FOR SIMILAR COMPRESSION OF THE TEST SPRING	246
FIGURE F.4. IMPACT LOAD ON A HELICAL SPRING	247
FIGURE F.5. THEORETICAL COMPARISON BETWEEN THE STATIC AND DYNAMIC COMPRESSION ENERGY	248
FIGURE G.1. BASE EXCITED SPRING-DAMPER MODEL	249
FIGURE H.1. THE CO-ORDINATE SYSTEM AND ANGLES	252
FIGURE H.2. 'SLIP STICK' CYCLE OF A VIBRATING FABRIC PANEL	254
FIGURE H.3. THEORETICAL SLIDING VELOCITY OF A SOLID OBJECT IN FLIGHT-FREE MOTION FOR A TABLE EXCITATION OF 100 μM	255
FIGURE H.4. THEORETICAL SLIDING VELOCITY OF A SOLID OBJECT IN FLIGHT-FREE MOTION FOR A TABLE EXCITATION OF 150 μM	256
FIGURE H.5. THEORETICAL SLIDING VELOCITY OF A SOLID OBJECT IN FLIGHT-FREE MOTION FOR A VARIABLE TABLE INCLINATION	256

List of Tables

TABLE 1-1. COST FROM RAW FIBRE TO MADE-UP SHIRT [VERRET 91]	3
TABLE 1-2. COST PER PROCESS FROM RAW FIBRE TO MADE-UP SHIRT [VERRET 91]	3
TABLE 1-3. LABOUR COST PER PROCESS FROM RAW FIBRE TO MADE-UP SHIRT [VERRET 91]	3
TABLE 2-1. FOUR CASES FOR THE MATERIAL CONSTANT (N) [WILSON 63]	20
TABLE 2-2. AVAILABLE FABRIC FRICTION MODELS	25
TABLE 2-3. SOME TYPICAL FRICTION COEFFICIENTS FOR FIBRES [MORTON 97]	26
TABLE 3-1. MEAN ROUGHNESS VALUES OF THE SIX STANDARD SAMPLES (MM)	61
TABLE 3-2. DYNAMIC FRICTION COEFFICIENT OF KC11 MEASURED OVER A 5 DAYS PERIOD	63
TABLE 3-3. THE EFFECT OF THE NUMBER OF TRAVERSES ON FABRIC FRICTION	65
TABLE 3-4. TIME CONSTANTS OF FRICTION AND MASS FOR A SUDDEN HUMIDITY CHANGE	68
TABLE 3-5. MOISTURE ABSORPTION AND HYSTERESIS FOR SET 2 FABRICS	72
TABLE 3-6. INFLUENCE OF STATIC CHARGE ON FRICTION	78
TABLE 3-7. THE EFFECT OF THE NORMAL PRESSURE ON THE DYNAMIC FABRIC FRICTION	85
TABLE 3-8. FRICTION COEFFICIENTS FOR SET 3 FABRICS AT STICK-SLIP CONDITIONS	97
TABLE 3-9. RESULTS FROM AUTOSPECTRAL DENSITY ANALYSIS FOR REGULAR STICK-SLIP TRACES	99
TABLE 3-10. ESTIMATED SPRING-DAMPER COEFFICIENTS FROM LONGITUDINAL VIBRATION MEASUREMENTS FOR SET 3 FABRICS	109
TABLE 3-11. SIMULATED STICK-SLIP TIMES FOR A SINGLE-MASS MODEL	112
TABLE 4-1. KES-FB3 COMPRESSION PARAMETERS (SEE 2.2.1) FOR SET 1 FABRICS (+ W1B)	125
TABLE 4-2. AVERAGE MIN-MAX THICKNESSES OF SET 1 FABRICS MEASURED WITH DIFFERENT SYSTEMS	126
TABLE 4-3. VAN WYK PARAMETERS A' AND V' FOR THE TWO AND THREE PARAMETER MODEL	131
TABLE 4-4. PACKING FRACTION OF THE 'INCOMPRESSIBLE' VOLUME, V', FOR SET 1 FABRICS (+ W1B)	132
TABLE 4-5. ESTIMATED COMPRESSED FIBRE MASS IN THE SURFACE LAYER OF SOME SET 1 FABRICS	133
TABLE 4-6. RATIO OF THE DYNAMIC COMPRESSION ENERGY TO THE STATIC COMPRESSION ENERGY FOR SUCCESSIVE IMPACTS	141
TABLE 5-1. ESTIMATED SPRING-DAMPER COEFFICIENTS FROM VIBRATION MEASUREMENTS OF SET 1 FABRICS	160
TABLE 5-2. COMPARISON BETWEEN STATIC AND DYNAMIC STIFFNESS	161
TABLE B-1. SPECIFICATIONS OF THE STEPPER MOTOR (20-3437D200-F075) [SIGMA 90]	214
TABLE B-2. SPECIFICATIONS OF THE PDX15-D SERIES MINI-STEPPING DRIVES [PARKER 96]	215
TABLE B-3. TECHNICAL SUMMARY OF THE LD1605-4 [MICRO-EPSILON 94]	218
TABLE B-4. ELECTRO-OPTICAL CHARACTERISTICS OF OD-880F AT 25°C [OPTO DIODE CORP. 92]	220
TABLE B-5. ABSOLUTE MAXIMUM RATINGS OF OD-880F AT 25°C CASE [OPTO DIODE CORP. 92]	220
TABLE B-6. ELECTRO-OPTICAL CHARACTERISTICS OF AEPX65 AT 22°C AND 5V REVERSE [CENTRONIC 95]	220
TABLE B-7. ABSOLUTE MAXIMUM RATINGS OF AEPX65 AT 22°C [CENTRONIC 95]	220
TABLE B-8. SPECIFICATIONS OF THE TQ-401/5M [VIBRO-METER 95]	223
TABLE B-9. SPECIFICATIONS OF THE LCF-50G [OMEGA 95]	223
TABLE B-10. ELECTRO-MECHANICAL SPECIFICATIONS OF THE COLOSSUS 15 X B [WHARFEDALE 93]	226
TABLE B-11. SPECIFICATIONS OF THE OMP/MF1000 [B.K. ELECTRONICS 93]	226
TABLE B-12. SPECIFICATIONS OF THE GAPTEK 2004 WITH PROBE CG8PO1 [GWI 85]	227
TABLE B-13. SPECIFICATIONS OF THE TRIAXIAL DELTATRON® ACCELEROMETER TYPE 4504 [B & K 96]	227

TABLE C-1. SPECIFICATIONS OF THE ENGINEERING SURFACES	229
TABLE C-2. AVERAGE SURFACE ROUGHNESS OF ENGINEERING MATERIALS	229
TABLE D-1. TEST FOR NORMALITY ON KC11	232
TABLE D-2. VALUES FOR THE STUDENT T-DISTRIBUTION [CHATFIELD 70]	234
TABLE D-3. COEFFICIENT OF VARIANCE FOR KES-F FRICTION AND COMPRESSION TESTS [MAHAR 87]	235
TABLE E-1. FRICTION COEFFICIENTS FOR SET 1 FABRICS AGAINST DIFFERENT SLIDING SURFACES	236
TABLE E-2. THE EFFECT OF THE SAMPLE AREA ON FABRIC FRICTION FOR SET 1 SAMPLES	237
TABLE E-3. EXPERIMENTAL VALUES OF C AND N FOR SET 1 FABRICS	238
TABLE E-4. COEFFICIENTS A_3 AND B FOR DYNAMIC FRICTION COEFFICIENT WITH VARIABLE SPEED AGAINST ALUMINIUM AND RUBBER	239
TABLE E-5. FRICTION MODEL PARAMETERS FOR SINGLE-MASS MODEL	240
TABLE F-1. STATIC AND DYNAMIC COMPRESSIONAL WORK FOR IDENTICAL COMPRESSIONS	246

List of Symbols

Symbol	Meaning	Units
<i>A</i>	area	m ²
<i>a, a₁</i>	friction constant	
<i>a₂</i>	material parameter (area)	
<i>a₃</i>	material parameter (sliding)	
<i>b</i>	velocity coefficient	
<i>C</i>	Wilson constant	N/m ²
<i>c</i>	damping coefficient (viscous)	N s/m
<i>c_{eq}</i>	equivalent viscous damping coefficient	N s/m
<i>D</i>	deformation force	N
<i>E</i>	modulus of elasticity (Young's modulus)	N/m ²
<i>F</i>	force	N
<i>f</i>	frequency	Hz
<i>G</i>	flexural rigidity	Nm ²
<i>g</i>	acceleration of gravity	m/s ²
<i>Hz</i>	Hertz	
<i>h</i>	height	m
<i>I</i>	moment of inertia of the cross section	m ²
<i>Int.</i>	integral expression on the dimension	
<i>i</i>	index	
<i>j</i>	√-1	
<i>K</i>	Van Wyk constant (0.01)	
<i>k</i>	spring constant, stiffness, stiffness constant	N/m
<i>l</i>	length	m
<i>m</i>	mass	kg
<i>m_a</i>	mass per area (area density)	kg/m ²
<i>N</i>	normal force	N
<i>n</i>	frictional index	
<i>n_a</i>	frictional index of the asperity	
<i>P</i>	pressure	N/m ²
<i>p</i>	yield-pressure	N/m ²
<i>Q</i>	number of asperities	
<i>r</i>	radius	m
<i>r²</i>	correlation coefficient	
<i>r.h.</i>	relative humidity	%
<i>S</i>	shear force	N
<i>SMD</i>	mean deviation of surface roughness	m
<i>s</i>	number of samples	
<i>T</i>	thickness	m
<i>T_r</i>	transmissibility	

t	time	s
t_c	Student t distribution	
u_0	amplitude of the displacement	m
V	volume	m^3
v	velocity	m/s
W	work (energy)	Nm
W_p	potential energy	Nm
w	width	m
X	linear displacement of table in direction of X axis	m
x	linear displacement of object in direction of X axis	m
Y	linear displacement of table in direction of Y axis	m
y	linear displacement of object in direction of Y axis	m
Z	natural damping loss of the pendulum	Nm
α_1, α_2	curve parameters	
ε	strain	
ϕ	inclination angle	rad
γ	hysteretic (structural) damping constant	
η	dynamic viscosity	Pa s
λ	wavelength	m
μ	friction coefficient	
θ	pendulum inclination angle	rad
ρ	mass density	kg/m^3
σ	stress	N/m^2
σ	standard deviation	
σ_{rip}	dynamic ripple (standard deviation)	
τ	shear strength	N/m^2
ω	angular velocity	rad/s
ω_n	undamped natural frequency	rad/s
ξ	time constant for humidity change	s
ψ	phase angle	rad
ζ	fraction of critical damping	

Other symbols of special or limited application are defined in the respective chapters as they are used.

1 Introduction

1.1 Automation in the Garment Industry: Past Present and Future

Textiles are some of the oldest products known to mankind and yet have changed so little. The exact origin of textile production is lost in prehistory and no one knows precisely when spinning and weaving began, but archaeologists have found evidence of these processes dating back to between 7000 and 5000 BC [Tortora 87]. Originally, textiles were either worn for reasons of protection and modesty or used for utilitarian purposes. As the complex social and political organisations of people evolved, textile technology changed rapidly and fabrics became world trade products; silk, cotton and dyes were highly valued next to spices and gold. At the same time, textiles developed into fashion items, involving social factors and status. Now a huge industry has emerged, employing in the USA alone twice as many workers as in the car industry and three times as many as in the steel sector [Redman 94]. Outside apparel, a whole new side industry is appearing where speciality fabrics are woven or knitted for composites. For example, 3D knitting made it possible to knit a static engine part in 100% silicon carbide [Ashton 94].

Yet, the textile and fashion industry is a complex network of interrelated industries ranging from the relatively well developed and automated yarn spinning and weaving sector to the more labour intensive garment making. Although computers and robotics have made a large impact on the industry since the first Industrial Revolution, garment manufacturing is still based on the use of needles and thread. Today, the fabric design, apparel design, pattern making, spreading and cutting processes can be totally integrated into a series of linked processes forming a compact CAD-CAM system. As the designer specifies the fabric patterns and the shapes to make up the garment, this information is used during the laying up process of the cloth and eventually directed to a robotic cutter to physically cut the plies. Unfortunately, it is from this point onwards that difficulties arise. The manipulation and handling of fabric parts is far less advanced than the computer technology used to prepare them. Bundles of partly constructed garments are usually passed from operator to operator, each individually performing a specific task in an assembly-line fashion until the garment is completed. Sewing is still the basic joining technique in the garment industry, some apparel companies claim that it forms as much as 80% of the labour cost though closer inspection brings it back to a maximum of 20% [Berkstresser III 86]. The remaining part is consumed by material handling and although a number of devices are already available to bring the material in an orderly fashion to the sewing operators, material flow remains one of the main handicaps in garment manufacturing. This obviously makes the garment industry more labour intensive than many other manufacturing industries if the necessary flexibility, in terms of products and manufacturing time, is required.

Therefore, since the 1980s, considerable funds in the USA, Japan and Europe have been directed to research and development to automate the garment industry. In the USA, there was the

(TC)² project that integrated a robot with an articulated pinch gripper, an overhead vision system, and an X-Y sewing station [Abernathy 86], [Bray 86] and [Tyler 89]. The system was able, for example, to complete a sleeve for men's tailored suits by guiding it through a series of sewing and folding operations [Bernardon 85]. Japan invested around £8000 million in the nine year TRAASS project, which aimed to reduce production times to less than 50% of those achieved currently [Taylor 90]. Extensive use of high performance robots and sophisticated vision systems resulted in the design of a total test plant to manufacture ladies' blazers. The layout comprised four clusters: an intelligent cloth inspection system, a high-speed laser-cutting module, a flexible sewing and assembly unit, and a 3D flexible pressing device [Off 91]. Initiatives in Europe took place under the BRITE-EURAM [BRITE-EURAM 91] scheme. One of the projects, for example, involved the development of a prototype 2D-assembly system for cost-effectively manufacturing garments in different sizes and styles.

The Robotics Research Unit at The University of Hull has also played an active role in a range of UK funded projects. A research project, carried out under the aegis of the ACME Directorate of the Science and Engineering Research Council, produced a laboratory prototype capable of automatically assembling briefs [Gibson 90], [Taylor 91]. The system comprised pallets restraining the various plies during sewing and low cost UMI-RTX robots with appropriate grippers for transfer and manipulation of the parts between the individual sewing cells. The majority of the stitching was performed in 2D and constrained to straight lines apart from some contour stitching for the 'top taping' of the men's briefs. Eventually, a complex folding gripper held the brief while a sequence of sewing operations closed the garment into a 3D structure [Taylor 92a]. Again in 1990, Hull joined the £7 million CIMTEX project (Computer Integrated Manufacturing of Textiles) together with 4 other British universities and 42 industrial collaborators. The target of the project was to showcase a state-of-the-art garment manufacturing system focusing the UK industry on the latest high-tech and ultimately making the industry again competitive on a worldwide scale. Hull's role was to research and produce an automated assembly line for sweatshirts made from medium weight fleecy knitted material [Taylor 94b]. The line had to sew the side seams from the cuff up to the sleeve, to the arm pit and then down the side of the sweatshirt to the waist. Normally, such a sewing operation would require curved sewing, which is exceedingly difficult to automate effectively. However, the complexity of the process was significantly reduced by a straightening mechanism consisting of a vertically rotating overhead conveyor, which steered the fabric in a straight line through the sewing machine. A stationary cuff and waistband attaching-machine using 3D sewing techniques finished the garment.

Unfortunately, most of these ambitious projects have only shown a glimpse of the future and highlighted some major problems but have not had the anticipated impact on industry. Governments failed to prevent part of the garment industry moving towards the lower-wage countries. A comparison in manufacturing costs of a cotton/polyester dress shirt between the USA and Southeast Asia shows clearly why [Verret 91]. Even with the best technology available today, the cost of the shirt in Southeast Asia (SEA) is only 67% of the USA cost. As can be seen in Table 1-1, the difference in labour cost of \$1.34 makes up 83% of the total difference. However, Table 1-2 shows the

manufacturing costs broken down by process then there is no question that shirting fabric made in the USA is competitive with SEA. The cost difference in making up the shirt is \$1.32 compared with a difference of \$0.31 for the fabric manufacturing cost. Unfortunately, shirts made in SEA will also use fabrics from SEA. Comparing, however, the labour cost in Table 1-3 then of the total labour cost difference of \$1.34, \$1.15 or 85% is needed for the making-up process. Thus, if a cost difference of 85% between the USA and SEA is assumed competitive then the making-up technology in the USA (and Europe) will have to increase its labour productivity by 130%. Material handling is an obvious target for automation though it is not sufficient to reduce labour costs.

Table 1-1. Cost from raw fibre to made-up shirt [Verret 91]

	Cost per Dress shirt (\$U.S.)		
	USA	SEA	Ratio
Raw material	0.90	0.78	87
Labour	2.44	1.10	45
Energy	0.27	0.46	170
Manufacturing expenses	0.79	0.63	80
Depreciation	0.48	0.29	60
Total manufacturing cost	4.88	3.26	67

Table 1-2. Cost per process from raw fibre to made-up shirt [Verret 91]

	Cost per Dress shirt (\$U.S.)		
	USA	SEA	Ratio
Spinning (a) including fibre	0.84	0.71	85
Weaving (b) added value	0.76	0.65	86
Dyeing (c) added value	0.46	0.39	85
(a) + (b) + (c)	2.06	1.75	85
Making up (d) added value	2.82	1.50	53
Total manufacturing cost	4.88	3.25	67

Table 1-3. Labour cost per process from raw fibre to made-up shirt [Verret 91]

	Cost per Dress shirt (\$U.S.)		
	USA	SEA	Ratio
Spinning (a)	0.119	0.068	57
Weaving (b)	0.240	0.190	79
Dyeing (c)	0.201	0.104	52
(a) + (b) + (c)	0.560	0.362	65
Making up (d)	1.884	0.733	39
Total labour cost	2.444	1.095	45

1.2 Why is Garment Manufacturing Difficult?

The problem of garment automation may be split into two as schematically presented in Figure 1.1. Fabrics are categorised as solids but, at the same time, they are very limp. This limpness makes fabrics on the one hand unique in that they cover a 3D body without disturbing its movement but, on the other hand, this brings serious difficulties for automation. As exemplified by Aisaka [Aisaka 87], “the shape of a handkerchief is different according to the holding method – holding it by one hand at one corner or at the centre, or by two hands at two corners”. Fabrics are further distinguished from most other ‘solids’ in being viscoelastic and anisotropic and, in addition, all fabric properties are time and environment dependent. Thus, different climatic conditions will change the behaviour of the fabric and therefore an automated process, which works perfectly in Europe, might fail in Southeast Asia where the humidity levels are most of the time much higher. The second important factor in garment automation is the required production flexibility and turnarounds. Considering that textiles are fashion items, small volumes with high diversity are needed, preferably with a short delivery time. Retailers are becoming increasingly more reluctant to stock huge numbers of garments but if one item sells well, it is impossible to place an extra order when production lead times are 60 weeks [Kurt Salmon 88]. It is just this flexibility of fast delivering small extra quantities of garments, which can offset the cost advantage of the lower-wage countries (see 1.1 above). Referring again to Figure 1.1, the solutions for automating the garment industry can be split into three main components though automation will only be successful if each is interrelated with each other.

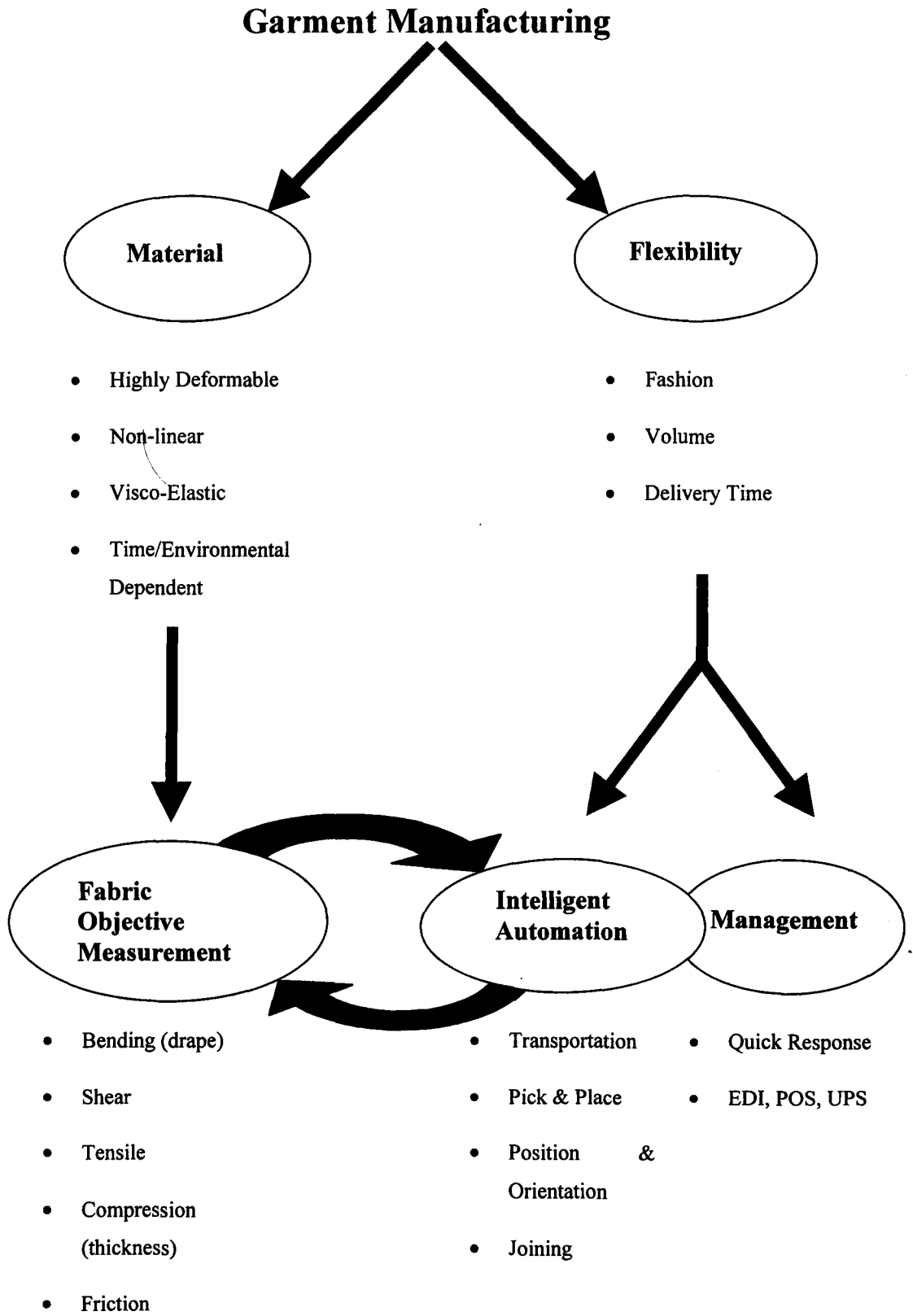


Figure 1.1. Problem-solution schema for garment automation

1.2.1 Fabric Objective Measurement

Fabric is still mainly evaluated subjectively on its quality and performance by a panel of textile experts [Kawabata 91], [Bishop 96]. For example, they decide by touching or rubbing the fabric whether it is suitable for a specific design (tailorability) or give advice on how to assemble the garment. However, a subjective evaluation requires a set of criteria against which judgements can be made though it is obvious that these are based on individuals' likings or preferences. Hence, decisions vary from person to person and are often described in a confusing vocabulary using descriptions such as fullness, softness and crispness. Yet, objective measurement of fabric has been the subject of research since the pioneering work by Peirce [Peirce 30, 37] in the 1930s where he wisely states in his introduction that: 'The evidence of the sense, . . . , depends on the physical properties of the material, so that physical measurements can be of great value in providing data upon which to exercise judgement'. Subsequently, Lindberg [Lindberg 60] and his co-workers Waesterberg and Svenson at TEFO in Sweden further introduced standards and instruments to quantify fabric handle which might today perhaps be seen as the most important work on objective measurement. Since then, various groups at the University of Leeds and Manchester have made many theoretical and experimental contributions though despite the efforts to promote the philosophy (e.g., EC-funded SPRINT project [SPRINT 83]), objective measurement remained largely in the research domain. Under the incentive of Kawabata and his co-workers Niwa in Japan and Postle in Australia, a set of physical parameters for instance friction, bending and shearing has been identified to describe the fabric handle and quality. Subsequently, Kawabata designed the KES-F system (*Kawabata Evaluation System for Fabrics*) [Kawabata 80] comprising four instruments to measure those mechanical parameters. However, the astronomic cost price (i.e., £100,000) and the tedious measuring procedures, which have been proven very much operator dependent, are partly responsible for the slow take-up by the textile industry [Bishop 96]. An alternative to KES-F is the FAST system (*Fabric Assurance by Simple Testing*) [De Boos 90], which involves three instruments and a test method (i.e., friction not included) originally developed by CSIRO (Australia) to measure the properties of wool. The system is simpler and quicker to use than the KES-F system though at still one-fifth of the cost of the KES-F system, it is relatively expensive for many textile companies, which are on the whole small to medium sized.

However, objective measurements are vital to evaluate reliably the mechanical properties of fabrics and to allow a basis for quality assurance and process control throughout the whole textile industry ranging from fibre to garment. Previous automation projects often only worked satisfactorily for a limited range of different fabrics, which were relatively easy to handle, because a good understanding of the relation between basic mechanical handling parameters and the dynamic behaviour of fabric was lacking. An understanding of the interaction between automation and material properties is fundamental for garment automation and up to now this has only been partly established for sewing [Clapp 92], [Amirbayat 92, 95] and [Zeto 96]. For instance, seam puckering is thoroughly evaluated objectively [Kawabata 90], [Barndt 90], [Park 97] in order to optimise the sewing processes. This leads us towards the second important factor for competitive garment automation: intelligent automation.

1.2.2 Intelligent Automation

Humans have the natural ability through their hand, eye, and hearing co-ordination to manipulate materials even in very complex situations where conditions are continuously changing. As an increasing flexibility demands smaller lots with greater product variability, the automated processes become inefficient due to the frequent trial and error alterations of parameters to match changes in the fabrics; hence, the need for self-adapting processes. However, intelligent automation should not result in operations, which emulate human handling as earlier projects have failed in doing, but in systems where a complex interaction between fabric and machine (and man) compensates for changes in the process [Stylios 96a]. Research is currently concentrating on implementing this strategy in sewing machines because the optimisation of sewing machine settings is one of the most important requirements in the industry. An on-line system measures the necessary fabric properties, passes them on to the sewing machine, which optimises its setting and eventually monitors the quality of the seam. The data from the monitoring system is then fed back into a self-learning model, which trains itself for future problems [Barrett 96a], [Stylios 96b].

Intelligence is also indispensable for the handling of fabrics if garment automation is to be effective [Govindaraj 92]. Although the fabric/gripper (feeder) interaction is less complex than for sewing machines, many of the handling operations still fail because of variations in the fabric properties. So far, both of the above improvements in garment automation have dealt with technological aspects only, a third and last key factor examines some approaches from a managerial and organisational viewpoint.

1.2.3 Management

Although one might have automated one level of the garment industry very successfully, competitiveness is very much dependent on maximum efficiency of the whole chain right from the producers of yarn up to the sales outlets. The reduction of response times between the various manufacturers is one of the main goals in the textile chain. Now, distributors have to place orders six to eight months in advance, which are a forecast in terms of volume, product and time-spans involved. This, no matter how refined the predictions are, results in high stocks and garments eventually sold as sale goods at the end of the fashion season. Further, if garment manufacturers can reduce the time between orders and delivery to a minimum than this gives a major advantage over the lower-wage countries, which must contend with a two to three month transit time for the goods. In order to achieve this, a new philosophy has emerged, called *Quick Response*, which is in fact an extension of the well-known Just-in-Time philosophy in that it is applied over the whole manufacturing chain [Berkstresser III 86, 95] [Forza 97]. Quick Response (QR) concerns the realisation of an information pipeline, which guarantees a precise and accurate flow of information to and from all the sectors in the textile industry. Manufacturers obtain accurate up-to-date sales information about which items sell and which do not through point-of-sale (POS) tracking so that forecasts can be made more easily. Product orders, commercial information and administrative documents are sent to all the various links in the chain through the adoption of electronic data interchange (EDI). Yet, information technologies and telecommunications constitute not the only means, which can be exploited by the textile-apparel

industry to improve time performance. Flexible production systems such as modular production cells where a group of multifunctional operators is responsible for the assembly of one garment could replace the typical long assembly lines [Chuter 88], [Lowder 91]. Furthermore, the introduction of a unit-production system (UPS) [Colgate 89] in which partly constructed garments are open to inspection by the next operator in the line can improve quality standards and reduce the work in progress.

However, modernisation and adaptation to a Quick Response will not be easy for the garment industry because the vast majority of it comprises small or medium sized enterprises that employ fewer than 500 people [Redman 94]. These companies will find it difficult to invest in high-technology production processes let alone in research and development. A strategy for combating competition will have to merge companies into a network with other public or private organisations (i.e., universities and research centres) so that problems can be solved collectively. One of the technological problems in garment automation discussed earlier involves the movement and orientation of fabrics, which will now be looked at in some more detail.

1.3 Transportation and Orientation Methods for Garment Automation

Transportation of fabric panels and partially made-up garments from one automation cell to another is a frequent operation in garment manufacture, yet an irrational approach leads many times to unnecessary handling, reorientation and lost manufacturing time. Traditionally, the garment industry relies on the bundling system otherwise known as the progressive bundle system (PBS) where large 'ordered' stacks (e.g., 50 units) are passed down the production system. Neatly piled fabric stacks coming from the cutter have a positional variation between the top and bottom layer of maximum a few millimetres, though when passed down in the system, the stack becomes more irregular and distorted. Separating the plies from the stack does not cause any problems for human operators but for an automated process, this becomes a difficult control and sensing task. Hence, fully automated systems had to convert to the unit-production system (UPS) where only one ply (or garment) at a time is routed through the production system. Obviously, this will put greater demands on the transport system in terms of speed, accuracy, orientation and the ways of presenting the panel to the station.

A selection of various techniques, which can be divided into two main classes, is currently available, each with its advantages and drawbacks. The first group comprises the pure transporting mechanisms, which cannot alter the orientation of the fabric during transport, whereas the second group consists of mechanisms, which can position and orientate the material during its movement. Grippers combined with a 'robotic' system can also be used to move fabric panels or garments although, generally, they are considered more as manipulation tools and will therefore not be considered here. The reader is referred to [Hall 87], [Karakerezis 94] and [Taylor 94a, b], for further reading on gripping technology in textiles. Pure movement of fabric panels or garments, which is regarded here as the first group, can be obtained by four commonly used transport devices in textile automation: jigs, conveyors, sliding surfaces and, for completeness, monorails.

1.3.1 Transportation Mechanisms

Most monorail systems (i.e., the Eaton system and the Gerber Mover system) are made of a chain of hangers with each hanger holding the various garment piece parts in a passive clamp system. Depending on the level of sophistication the system is either powered by a motorised chain or simply pulled by the operators on the factory floor. Strictly speaking, a monorail system is more suited for assembly line manufacturing than for automation since the fabric panels totally lose their orientation from the moment that they are removed from the cutting table. Recently, De Montfort University designed a robotic system for stripping the panels and loading them automatically onto hangers [Czarnecki 95]. The CIMTEX project at Hull used a similar hanger system (i.e., the Gerber Mover) to introduce the body of the sweatshirt to the first cell in the automation line. However, the hangers were adapted to hold the sweatshirt at the four corners of the waistband so that the orientation of the garment was not totally random.

Total orientation of the fabric is kept when using jigs, where the material (i.e., one or several panels) is clamped during transportation. This technique is ideal for sewing along one edge where panels are restrained on a pallet while the pallet is co-ordinated with the speed of the sewing head [Taylor 94a]. However, fabric panels come in many different sizes and shapes, which will require some flexibility of the system.

Conveyors are by far the most frequently used transportation mechanisms in manufacturing. However, dependent on whether the conveyor can be stopped or not, their simplicity might be slightly misleading when it comes to placing or removing the material. Obviously, the simplest case occurs when the conveyor can be stopped during the operation since the fabric can then be placed or removed as from a stationary flat surface. If, however, the conveyor is continuously moving then tracking of the belt needs to take place before the fabric can be laid down. A more simple method of placing a panel on a moving conveyor consists of holding the fabric stationary along one edge and allowing the opposite free trailing edge to be pulled onto the conveyor. Removing the fabric from a rolling conveyor is an even more complex task because the gripper mechanism needs to synchronise exactly with the conveyor. In addition, conveyor belts are rarely flat across their width, which not only increases the difficulty in gripping the material but also due to inherent vibrations in the conveyor causes the material to move slightly during transport. A 'scoop' method, originally designed at The University of Hull to remove shirt collars from a conveyor [Taylor 92a], seems to be a very simple alternative. The idea consists of a low friction plate onto which the fabric panel is dropped or pushed dependent on whether the scoop is positioned at the edge of the conveyor or on the top surface of the conveyor. Furthermore, conveyors cannot only be used for transporting fabric panels but also for performing simple 2D manipulation such as sewing along a straight edge [Abernathy 86], [Tyler 89] or even for folding garments [Taylor 92b], [Taylor 94b].

Finally, the last and simplest device of all, which purely moves fabric panels, is an inclined low friction surface where the panels are allowed to slide under gravity [King 95]. The guide must be inclined properly to ensure that the panel slides completely down but, at the same time, one has to be careful that the leading edge does not crumple when hitting a possible alignment edge at the end. In

order to secure the alignment or to increase the conveying speed some small vibrations or air jets can assist the movement.

1.3.2 Orientation and Aligning Mechanisms

From the above mentioned examples it is clear that fabrics can easily be out of place for the next process. Furthermore, uncertainties in the pick and place operations along the automation line often result in buckled panels or furled edges. If subsequent tasks cannot cope with these errors then an orientation process needs to be implemented to correct the position and orientation of the fabric. Two fundamental techniques are available. A passive location method observes the area in which the panel is located and calculates its position relative to an origin, an active method, on the other hand, directs the fabric immediately to a preordained place. Both methods can be used either to orientate a full sized panel or to align only one edge of the fabric. However, edge alignment, which is often required prior to sewing, will not be considered here.

Passive orientation methods generally require some form of vision module whether it is a full area scan camera or a more simple line scan camera. Yet, if a high accuracy is required, overhead area cameras either do not have the resolution needed to scan large fabric panels or are not cost effective. However, since a number of salient features of the fabric such as edges or corners are sufficient to align the panel, several small cameras, selectively positioned, form an effective and cheaper alternative [Taylor 86], [Iype 89]. Furthermore, the lighting in fabric sensing particularly the positioning of the light source(s) is crucial. A good contrast between the fabric and the background can reduce the image processing time severely. Top lighting is generally easy to achieve but requires a contrasting background to operate reliably and is therefore less suitable when a wide range of coloured or patterned fabrics is used. Back-lighting on the other hand, can give a better contrast especially if only the perimeter of the shape is needed but becomes less viable for pale dyed fabrics or fabrics with a very open structure. Finally, the actual manipulation of the fabric can be performed either with a gripper as the end-effector of a robot [Iype 89], [Paraschidis 95] or with a more dedicated device such as an XY-theta table [Taylor 82] and [Barrett 96b]. An XY-theta table, which is capable of moving in two linear directions and providing an angular rotation, is for a similar accuracy level less expensive than a robotic system, which might require a complex multi-degree of freedom gripper.

The same conclusion can be made for an active orientation system. Since they have a minimum number of sensors and an absence of camera systems, active orientation systems are far less expensive in computing power and financial terms than a passive system. However, active systems might not be able to orientate all kinds of shapes, for example, I-shapes or L-shapes will easily deform when slid over a surface. Air flotation and vibration, which are established techniques in moving and orientating solid materials (e.g., vibratory bowl feeders), have been applied also in active orientation of textiles. Yet, both approaches, originally reviewed in a study on limp material handling by Arthur D. Little Inc. [Little 65] [Saibel 68] and recently investigated at The University of Hull [Gunner 92], showed a mixed outcome. Air flotation, in particular, encountered problems in controlling the direction of the fabric and, in addition, large pieces of fabric tended to parachute. On the other hand, controlled vibrations proved to be a more effective way. Arthur D. Little Inc.

[Little 65] showed in an experimental set up that a 60 Hz vibration was adequate and obtained linear feeding rates of 12 to 15 cm/s, which could be further improved by tilting the table. This has been used to good effect in orientating knitted cotton panels as part of the garment assembly line at Hull [Gunner 92], [Taylor 94a]. As depicted in Figure 1.2, a fabric piece is aligned on a tilted linear feeder before being assembled together with other pieces on a jig ready for sewing (jig is not visible in picture). By tilting the table perpendicularly to the direction of vibration, the fabric moves down the slope until it hits the constraining bar (left in the vibratory table). A simple reflective sensor, imbedded in the table surface, stops the vibrations at the moment that the panel is orientated and one of the corners of the panel blocks the sensor.



Figure 1.2. Vibrating alignment table with pinching gripper at the Hull brief's assembly line

The table was capable of successfully orientating all the double knit fabric panels (i.e., KC11) used in the assembly line though failed to do so for some lightweight woven or polyester fabrics. As with many handling and manipulation tasks in garment automation, the relation between the mechanical parameters and the fabric behaviour is not always understood.

The initial aim of the research was to gain a scientific understanding of the vibratory feeding of fabrics. However, it soon became apparent that much of the crucial information about fabric properties under zero or very low normal loads was unavailable. Consequently, the bulk of this thesis is concerned with research in this area and culminates in a study of the vibrating problem.

1.4 Outline and Novelty of the Research

The thesis is divided into three main chapters (literature review not included), each investigating one particular fabric property: starting with friction, followed by compression and ending with vibration, which in fact can be seen as a special form of compression. However, the present state of the work on these three fabric properties is first given in the literature review in chapter 2.

The chapter reviews extensively friction, compression and vibration in fabrics. However, literature on friction between fabric and non-fibrous materials is scarce since textile research has mainly been concentrated on friction between fabric and fabric under medium to high normal forces. Static compression, which is the second parameter to be reviewed, is still largely dominated by the van Wyk equation, which up to now has almost not been challenged by others. The third and last property in the review considers vibration of fabrics. Again, practically no work has been published on this subject apart from some dynamic compression in carpet and felt by Dunlop, which thereby forms a good starting point for this research. Finally, the chapter concludes with a brief explanation of how solids are conveyed on a vibratory feeder and which mechanical parameters are involved.

Chapter 3 investigates the frictional properties between six different fabrics and three different engineering surfaces under zero or extremely low external normal forces. Various parameters such as velocity, pressure and humidity are varied to measure their influence on friction and Wilson's pressure model, which originally describes fabric-fabric friction, is verified for non-fibrous friction. Special attention is given to stick-slip where a new measuring technique reveals the actual fabric movement at extremely low speeds. Further, a classical friction model is used to model and simulate this low velocity behaviour and crucial model parameters such as the damping are measured directly on the fabric through a longitudinal vibration test.

Chapter 4 studies the static compression of woven as well as of knitted materials. The various KES-F parameters, which characterise compression, are calculated and compared. Further, the van Wyk equation is used to model the compression and the various simplifications of the model are correlated with each other. Finally, a novel impact test is introduced in the second half of the chapter and compared with the static tests. The compressional energy lost during each impact is related to the stiffness of the material.

Chapter 5 extends the dynamic compression properties of fabric and looks at the out of plane vibration of fabric. Fabrics vibrating in a 'stationary mode' reveal an amplitude dependent behaviour, which is represented in a Kelvin-Voigt model. Furthermore, the conditions for optimal conveying are investigated and several novel ideas are proposed for fabric alignment using vibrational force.

Chapter 6 summarises the thesis and indicates some gaps in the knowledge, which need further research in the future.

2 Literature Survey

As highlighted in the introduction of this thesis, objective assessment of fabrics comprises five modes of fabric deformation: bending, shearing, tensile, compression and surface or friction tests. The last two of these properties, namely, compression and friction, will be discussed here in more detail, though from a different point of view to the literature. Friction is mostly measured between fabrics (fabric-fabric) either with an identical or with a different type, and under an external normal force higher than the fabric weight. In this thesis, however, friction will be studied between fabrics and engineering materials (fabric-non-fabric) under zero or slightly loaded conditions. Consequently, the fabrics will behave differently. For example, the surface fibres in spun woven fabrics cannot entangle with each other, as it is the case in fabric to fabric friction. Only the surface fibres and crowns of the yarn will be important during the sliding since the fabric samples rest under their own weight. In the same way with compression tests at very low pressures, the surface fibres in spun woven fabrics will bend first, and only larger pressures will eventually deform the yarns. Figure 2.1 shows the obvious difference in surface between a filament woven fabric and a spun woven fabric.

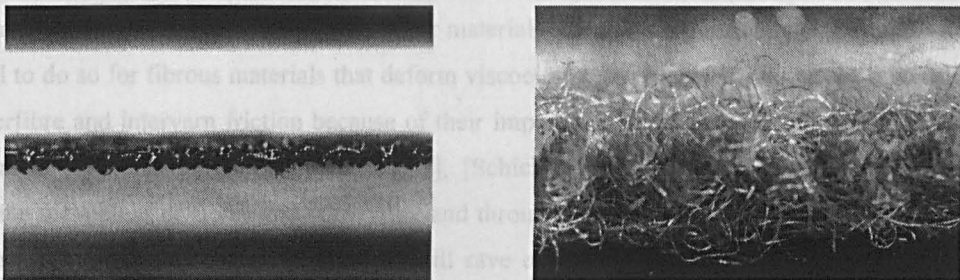


Figure 2.1. Side views of fabric surface for filament yarn fabric and for spun yarn fabric (W1) (magnification X15)

Compression tests are normally static tests where the pressure increases or decreases relatively slowly with time. This thesis, however, will also investigate the dynamic compression by vibrating the fabric samples but again under no extra normal forces. It will be seen that only a small number of studies have been conducted on dynamic compression of carpet and felt pads subjected to large normal forces. The vibration characteristics of fabrics are studied here as a preliminary investigation into the possibility of orientating fabrics with vibration. Therefore, a brief theoretical explanation on vibratory conveyors with solid objects is included in a final section of this chapter but first the friction properties of textiles will be discussed.

2.1 Friction Properties of Textiles

2.1.1 Introduction

The presence or lack of frictional forces is essential for successful handling and joining operations in garment automation. During sewing of multiple plies, for example, the fabric-fabric surface forces must be adequate to prevent slippage between the individual plies but the fabric-sewing

table friction should be low to facilitate sliding. This dualistic nature of friction is important in garment design as well. For instance, between shirts and the inside surface of trousers, high friction is preferred but lining materials should have a low friction when in contact with the fabrics worn next to them. This tactile comfort is often subjectively assessed by rubbing the cloth between fingers and thumb [Bishop 96].

However, the subjective evaluation of friction is a quite complex problem where both physical fabric parameters and psychological factors are involved. Peirce [Peirce 30] was the first in his famous analysis on cloth handling to mention that the smoothness of a cloth could be quantified by its friction coefficient. This single correlation has now been questioned by several authors [Dreby 43], [Hoffman 51] and [Viallier 92]. They had some doubts whether or not the coefficient of friction alone adequately represented the tactile sensation of smoothness, or if the compressibility also was to be included. Many studies have been carried out to relate the sensory and physical values of friction [Röder 53], [Ajayi 88].

Friction has been defined simply as the force resisting relative motion between two bodies in contact, i.e., sliding, rolling or flowing. The classical friction models based on Amontons' Laws adequately describe the frictional behaviour for materials that deform plastically (e.g., metals and ice) but fail to do so for fibrous materials that deform viscoelastically. Many studies have been carried out on interfibre and interyarn friction because of their importance in yarn production and the effects on mechanical properties of fabrics [Morrow 31], [Schick 75]. The process of textile manufacturing needs the movement of fibres and yarns over and through a number of guiding surfaces in spinning, weaving and stitching. Lower fibre friction will save energy and leads towards a faster production, while a consistent friction guarantees uniform product quality. Interfibre and interyarn friction will not be reviewed in detail in this thesis though many friction effects in fibrous materials were first described in fibre friction. In contrast to the vast amount of literature on fibre and yarn friction, very little attention has been given to the frictional behaviour of fabrics. In addition, most of these studies on fabric friction have been concentrated on the importance of friction with regard to fabric handle [Dreby 43], [Hoffman 51]. As an illustration of this, Howell *et al.* [Howell 59] devoted only eight pages out of 250 on fabric friction in their book "Friction in Textiles". Hardly any studies [Yoon 84], [Nishimatsu 84a, b], [Ajayi 92], [Hosseini Ravandi 94] and [Virto 97] have investigated the friction between fabric and engineering surfaces (fabric-non-fabric) and all measure friction under normal force conditions. Up to now, also no standard friction test has been available, which makes hard any comparison between results from various sources.

2.1.2 Classical Friction Models

Historically, tribology is based on the classical laws enunciated for the first time by Leonardo da Vinci in 1519 [da Vinci 1519] and later rediscovered by Amontons in 1699 [Amontons 1699]. Both laws may be summarised as follows:

1. The frictional force, F , is directly proportional to the normal force, N , (e.g., mass of the material) see Figure 2.2, that is:

$$F = \mu N \quad (2.1)$$

2. The coefficient of friction, μ , is independent of the geometric area of contact between the two surfaces providing that the mass and frictional force remain in proportion.

These two laws were further verified by Coulomb in 1785 [Coulomb 1785] who introduced the concepts of static and dynamic (or kinetic) friction. The static friction is the force necessary to initiate motion and is usually higher than the kinetic friction or the force that is necessary to sustain the motion. Coulomb found what is often regarded as the third friction law, that the dynamic friction was independent of the velocity.

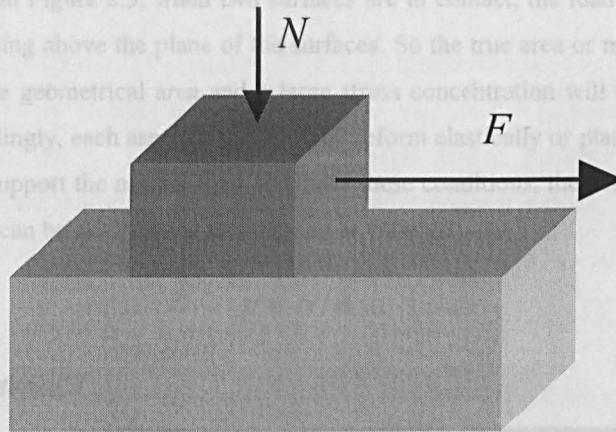


Figure 2.2. Force diagram of two solids in contact

In the past, two hypotheses were used to explain the friction phenomenon. Amontons propounded that friction was the force necessary to overcome the irregularities or roughness between the two surface areas. Other workers [Chapman 55] believed that friction was due to some attractive forces between the atoms of the two surfaces or to some electrostatic forces. While some of these explanations are still valid up to now, the universally accepted theory of friction between solids is based on the adhesion-shearing theory originally proposed by Ernst and Merchant [Ernst 40]. This theory has then later been improved in the fifties by Bowden and Tabor [Bowden 50].

The adhesion-shearing theory is founded on two basically different processes. First, there is the macro process of mechanical interference between the surfaces when asperities engage upon sliding. Secondly, there is the tendency for adhesion or cold welding at the interfacial regions of the real

contact caused by the high pressure on these asperities. Consequently, the deformation between the two surfaces will be dependent on the shear strength and the compressibility of the asperities. In other words, the deformation mechanism deals with large volume deformations and small strains while the shearing mechanism involves only thin interfacial regions and large strains. The total observed friction, F , is then the sum of both the deformation or ploughing force, D , and the shearing force, S , so that:

$$F = D + S \quad (2.2)$$

Both mechanisms are not necessarily equally significant. In certain arrangements for example, where a hard material slides over a softer surface, the deformation term may be more important than the shearing and the hard material may act as an abrasive. On the other hand, for polymers (e.g., fibrous materials) and rubbers sliding over a relatively smooth hard surface, the ploughing term may be almost non-existent. For most situations with metal surfaces, the shearing term is greater than the deformation term. The deformation part of the friction force is expressed in terms of the geometry of the moving surfaces, and a factor that is of the same order of magnitude as the yield-pressure of the softer material. In the following pages, we will only consider the shearing factor.

As illustrated in Figure 2.3, when two surfaces are in contact, the load is only supported by a few asperities projecting above the plane of the surfaces. So the true area or microscopic contact will be much less than the geometrical area and a large stress concentration will take place at the tip of each asperity. Accordingly, each asperity surface will deform elastically or plastically until the area of true contact, A , can support the normal load N . Under these conditions, the average yield-pressure, p , of the softer material can be described at equilibrium as follows:

$$p = N/A \quad (2.3)$$

Material A



Material B

Figure 2.3. Real contact between two solids

On average, the yield-pressure, p , at the asperities for metals is three times the yield-strength of the bulk material [Bowden 50]. For relative motion to take place between both surfaces, the force to shear the adhered asperities, which is essentially the frictional force ($F=S$), is given by:

$$F = A\tau = N\tau/p, \quad (2.4)$$

with, τ , the shear strength of the weaker material per unit area. From the above expression, it is clear that the frictional force is directly proportional to the normal load and independent of the area of the surfaces providing that the yield-pressure and the shear strength remain constant. In accordance with Amontons' Laws, Equation (2.1), the coefficient of friction, μ , is then given by:

$$\mu = \tau / p \quad (2.5)$$

As shearing mainly occurs at the softer material during sliding, it is shown from the above Equation (2.5) that the friction coefficient, μ , is purely a material property of the softer material. Considering that this ratio (shear strength to yield-pressure) is roughly the same for the most diverse materials, it becomes clear that the coefficient of friction does not vary by a very large factor (i.e., generally $\mu = 0.6-1.2$). However, this simple friction model has a serious theoretical deficiency because the normal yield-pressure and the tangential stress are both considered here as independent properties. Plasticity theory shows that a combination of normal and tangential stresses is required for plastic yielding to take place [Bowden 64] though this is beyond the scope of this thesis. With regard to friction of polymers and elastomers, the above mentioned shearing-deformation mechanism is still valid but some modifications need to be taken into account considering their viscoelastic nature.

For the friction properties of polymers, three main differences need to be considered. First, the contact area does not only depend on the pressure but also on the geometry of the surfaces, for example, the curvature of the indenting surface. Several studies [Lincoln 52], [Howell 53], and [Bowden 64] have shown that the area of contact, A , varies proportionally to a power of the normal force, N , as given below:

$$A = a_2 N^n \quad n \in (\frac{2}{3}, 1) \quad (2.6)$$

The lower value of the frictional index, n , corresponds to a purely elastic deformation of the asperities whereas the higher value corresponds to a perfectly plastic deformation (e.g., metals). If the shear strength is considered constant and the frictional force varies in the same way with the area as the area varies with the normal force then the friction can simply be written as [Lodge 54]:

$$F = a_1 N^n \quad (2.7)$$

Secondly, in relation to metals, polymers have a low elasticity modulus that is very sensitive to temperature variations. Therefore, frictional heating in polymeric surfaces can no longer be neglected at velocities for instance, higher than 10 mms^{-1} [Briscoe 79], which consequentially makes friction in polymers velocity dependent. Thirdly, the ploughing term of friction, if present, does not take the form of a plastic deformation but of an elastic hysteresis.

Elastomers such as rubber have the same exemptions as polymers concerning the general shearing-deformation theory. However, elastomers differentiate from polymers in that both their

deformation and shearing force can be expressed in terms of the loss angle ($\tan \delta$) [Moore 72]. In 1952, Schallamach [Schallamach 52] concluded that rubber on a glass surface formed spherical asperities that only changed their contact area according to the Equation (2.7) above but remained equal in number. This agrees well with the elastic contact theory of Hertz [Hertz 1881]. During further research in 1971, Schallamach observed that when sliding a rubber hemisphere over a smooth glass surface, the rubber surface buckled and generated ‘waves of detachment’ resembling the movement of a caterpillar. This theory, generally referred to as the rate theory, assumes that bonds between the elastomer and the sliding surface are continuously formed and broken.

2.1.3 Friction in Textiles

Over the past decades, friction in fibrous materials (viz., fibres, yarns and fabrics) has been the subject of many investigations, of which the majority were conducted to find out the divergence from the classical Amontons’ Laws. It is now well established that textile materials do not completely conform to Amontons’ simple linear relationship (2.1) between the frictional force and the applied normal force [Howell 53]. Fibrous materials do not deform purely plastically and therefore the friction coefficient may increase or decrease to a constant value with a diminishing pressure. Consequently, the frictional force is non-linear with the normal force.

Although this thesis will not discuss any modelling of fibre or yarn friction in detail, it is necessary to state that many effects in fibre and yarn friction will also appear in fabric friction. However, when comparing friction coefficients between fabrics and their component yarns, it was found that the coefficient of friction for fabric-fabric was significantly higher than for the yarns [Zurek 85], [Ajayi 94].

Compared to the vast number of publications on fibre and yarn friction, limited information on friction modelling for fabric is available in the literature, [Miura 54], [Wilson 63], [Ohsawa 66], [Kawabata 79], [Nishimatsu 84b], and recently [Virto 97]. One of the first attempts to model the influence of pressure on the friction in between fabric surfaces (fabric-fabric) has been undertaken by Wilson [Wilson 63]. In this empirical study, which has now become a classical reference for fabric friction, Wilson based his model on a powered relationship between the pressure and the frictional force (Equation (2.7)). This relationship has been applied first on fibres and yarns by Huffington and Stout [Huffington 60], and is consistent with the adhesion theory of Bowden and Tabor. Both his theoretical analysis and experimental results indicated clearly the importance of the apparent area in frictional characterisation of fabric and thereby rejected Amontons’ second law.

Wilson’s friction model is based on two basic hypotheses generally used in friction in textiles:

adhesion takes place at the real contact points (asperities),

the junctions at the interface have a constant shear strength, τ , per unit area.

Assuming that α_i is the real area of contact for any asperity, i , the frictional force, F_i , necessary for shearing to take place can be written as follows:

$$F_i = \tau \alpha_i \quad (2.8)$$

The variation of the real area of contact, α_i , with the normal force, N_i , at asperity i is analogue to Equation (2.6) and given as:

$$\alpha_i = a_2 N_i^{n_a} \quad (2.9)$$

The constants a_2 and n_a are material constants with n_a being the *frictional index of the asperity* varying between 0.5 and 1.0 respectively for pure elastic or pure plastic deformation of a cylinder against a plane. Substituting Equation (2.9) in Equation (2.8), one obtains a relationship between the frictional force, F_i , and the normal force, N_i , as follows:

$$F_i = \tau a_2 N_i^{n_a} = a N_i^{n_a} \quad (2.10)$$

where $a = \tau a_2$

Let Q_p indicate the total number of real contacts per unit apparent area at pressure P then the total frictional force, F_p , per unit area at pressure P becomes:

$$\begin{aligned} F_p &= \sum_{i=1}^{Q_p} F_i = \sum_{i=1}^{Q_p} a N_i^{n_a} \\ &= a Q_p \overline{N^{n_a}} \\ &= a Q_p \left[\frac{\overline{N^{n_a}}}{(\overline{N})^{n_a}} \right] (\overline{N})^{n_a} \\ &= a Q_p^{1-n_a} (Q_p \overline{N})^{n_a} \\ &= a Q_p^{1-n_a} P^{n_a} \end{aligned} \quad (2.11)$$

For any reasonable distribution of the normal force over the asperities, $\left[\frac{\overline{N^{n_a}}}{(\overline{N})^{n_a}} \right] \approx 1$, taking the

logarithmic of the frictional force per unit area gives:

$$\log \left(\frac{F_p}{A} \right) = \log(a) + (1 - n_a) \log(Q_p) + n_a \log(P) \quad (2.12)$$

The factors a and n_a are material parameters and are assumed constant irrespective of the fibre morphology (staple or continuous filament) and independent of the geometric structure of the fabric.

Dependency of a and n_a on the fibre diameter was ignored by Wilson considering the limited variation of fibre diameter in his investigation. Wilson assumed further that the number of contacts varies with pressure according to the following relationship:

$$Q_p = \iota P^\beta$$

$$\text{where } \beta = \left(\frac{n - n_a}{1 - n_a} \right) \quad (2.13)$$

$$\text{and } \log(\iota) = \frac{C - \log(a)}{1 - n_a}$$

Furthermore, at unity pressure the number of contacts will be mathematically equal to ι or:

$$\log(\iota) = \log Q_{p=1} = \frac{C_{p=1} - \log(a)}{1 - n_a} \quad (2.14)$$

Under these conditions the theoretical equation correlates with the following experimental log-log relationship given by:

$$\log\left(\frac{F_p}{A}\right) = C + n \log(P) \quad (2.15)$$

Thus, from the above definition of β in (2.13), it can be seen that for a given fibre material, n will be exclusively controlled by β . In other words, the slope of the linear log-log curve depends upon the way the number of asperities, Q_p , varies with the pressure P . In fact, n can be regarded as the overall frictional index of the fabric whereas n_a is the frictional index for the contacts. Four special cases given in Table 2-1 evolve directly from Equation (2.13). Case 1 agrees with Hertz elasticity theory whereas case three conforms to Amontons' Law. Case 2 will appear mostly for fibrous materials. Case 4 is an exceptional case where the coefficient of friction will increase with an increasing load until most likely a constant value is reached. Such an example has been reported for the friction between cotton fibres [Schick 75].

Table 2-1. Four cases for the material constant (n) [Wilson 63]

Case	β	Q_p in relation to pressure	Relation between n and n_a
1	0	Independent	$n = n_a$ (minimum value of n)
2	$0 < \beta < 1$	Increase but less rapidly	$n_a < n < 1$
3	$\beta = 1$	Directly proportional	$n_a = n = 1$
4	$\beta > 1$	Increase more rapidly	$n > 1$

Wilson's experimental dynamic friction results revealed a distinct grouping of the tested fabrics regarding the yarn being either of the spun type or the filament type. From Equation (2.14), it can be seen that the value of C is directly associated for a certain fabric, given values a and n_a , with the number of asperity contacts at unity pressure. This was experimentally verified [Wilson 63]. Fabrics made out of spun yarns tend to give larger numbers of contact points at low pressure which did give a large value for C and vice-versa for continuous filament fabrics. Furthermore, when increasing the pressure, the number of contacting points between spun fabrics increased less rapidly than between filament fabrics. This resulted in low values of n and β for the spun type fabrics and high values of n and β for the filament types (see Table 2-1). In some cases at high pressures, the number of asperities between two continuous filament fabrics can even exceed that of the spun fabrics. Thus, a negative correlation between n and C splitting the test samples into two groups can be observed. High values of n and low values of C are associated with spun fabrics while low values of n and high values of C are related to filament fabrics.

Wilson [Wilson 63] also carried out some dynamic friction tests between fabric (spun and filament type) and a viscose sheet under varying normal load. His conclusions are very useful with reference to friction of fabrics on solid surfaces (fabric-non-fabric). The results obtained showed that the number of contacts per unit area at unit pressure was smaller between a spun fabric and the viscose sheet than it was between two spun fabric surfaces. An opposite effect was found in the case of the filament fabrics but the number was, however, still smaller than that between the spun fabric and the viscose sheet. Wilson explained this again in terms of variations of asperities. In a filament fabric most of the raised points can make contact with the viscose sheet. However, when two filament fabrics slide across each other, the tips of one surface can be juxtaposed to troughs of the other surface and thus reduce the number of real contacts. On the other hand, a spun fabric will not be able to penetrate or entangle with the viscose surface and therefore will be unable to increase its number of asperities. In addition, the variation of the number of contacts with pressure is now similar for both spun fabrics and filament fabrics. This explains why fabric-fabric friction gives a better discrimination in the friction coefficient. Similar conclusions were made by Morrow [Morrow 31] and Ajayi [Ajayi 92a]. Morrow found that all his tested fabrics showed very much the same coefficient of dynamic friction (≈ 0.22) under a 'small' unknown normal load against a polished steel surface.

It is now well reported that the friction coefficient of both fabric-fabric and fabric-non-fabric [Virto 97] friction diminishes with an increasing pressure. Yet, the pressure sensitivity in friction is more pronounced at lower pressures than it is at higher pressures. At higher pressures (i.e., $P > 10 \text{ kN/m}^2$), the friction coefficient approaches a constant value. Several studies have now correlated ($r^2 > 0.9$) their experimental static and dynamic frictional data by using Wilson's model. Generally, the results of these studies (all fabric-fabric friction) are expressed in the form of a power equation similar to Equation (2.7), with a_1 replaced by C . Various ranges for the frictional index n have been reported. Wilson originally found a value for n between (0.57-1.06), while Ohsawa and Namiki [Ohsawa 66] recorded a slightly higher minimum value (0.85-1.07), considering that their samples only comprised filament fabrics. More recently, Carr *et al.* [Carr 88] confirmed Wilson's

model and found n varying between (0.67-0.94). In a summarised study on the frictional behaviour of textile fabrics, Clapp *et al.* [Clapp 91] observed the same clear grouping in spun type and filament type among their samples and found a value for n between (0.54-0.92). Ajayi [Ajayi 92a] reported the lowest values of frictional index (0.5-0.87) and describes it due to the relatively lower pressure used in his experiments. No unanimous explanation has been given for the inverse relationship between n and C , Ohsawa and Namiki [Ohsawa 66] attributed it to structural interlocking whereas Viswanathan [Viswanathan 66] ascribed it in a study on cotton fibre friction as fibre cohesion.

In a recent study on friction between fibrous materials (*viz.*, interfibre and interyarn), Gupta and El Mogahzy [Gupta 91] proposed a structural model to give some theoretical significance to the friction parameters n and C from Wilson's model (2.15). After all, Wilson's equation is also valid for interfibre and interyarn friction. Only a summary of Gupta and El Mogahzy's improved theory will be given here. A general pressure-area relationship applying to a wide range of fibrous materials is postulated as follows:

$$P = JA^\kappa \quad (2.16)$$

The pressure and true area are respectively symbolised by P and A , the constant J might be considered as a hardness or stiffness factor and κ as a kind of shape factor. The underlying mechanism for their derivations is still assumed the adhesion theory of Bowden and Tabor though it is understood that one stress distribution cannot be applicable to all cases. The stress distribution at the contact regions is expected to vary broadly with the fibre structure and the testing conditions, including the magnitude of the applied normal force. Therefore, Gupta and El Mogahzy assumed three different stress distributions namely a uniform distribution, a spherical and a conical distribution. Eventually, the contact area for all three stress distributions lead to a general expression of the form:

$$A = D_i J^{-\varphi} Q^{1-\varphi} N^\varphi \quad (2.17)$$

where $\varphi = (\kappa + 1)^{-1}$

In the above Equation (2.17), Q is again the number of asperities between the two contacting bodies, N is the total normal force, and D_i is a constant dependent on φ and the nature of the stress distribution ($D_i = [0.924-1]$). Substituting the area from Equation (2.17) in the friction-shear Equation (2.4) yields:

$$\begin{aligned} F &= \tau A \\ &= \tau D_i J^{-\varphi} Q^{1-\varphi} N^\varphi \end{aligned} \quad (2.18)$$

If now Equation (2.18) is compared with Wilson's Equation (2.15), the following relations can be immediately obtained:

$$\begin{aligned} n &= \varphi \\ C &= \tau D_i J^{-n} Q^{1-n} \end{aligned} \quad (2.19)$$

Again, the above derivations show that the normal force has a direct influence on the true contact area and the frictional force. The nature of the influence, however, is controlled by the frictional index n . For a plastic deformation, n and D_i become unity ($\kappa = 0$), the friction force and area increase in direct proportion to the normal force and Amontons' Law is again confirmed. The 'stiffness factor', J , equals the yield-pressure and C becomes the coefficient of friction μ . If n is less than unity, the frictional force and the area increase with the normal force, but at a decreasing rate. Thus, also the friction coefficient μ between fibres and yarns will decrease with an increase in normal force. Although Wilson's model is most widely accepted, it is originally intended to model fabric-fabric friction. The following three models, however, will look at fabric-non-fabric friction.

Yoon *et al.* [Yoon 84] believed that the friction coefficient, μ , (fabric-fabric and fabric-non-fabric) consists of two contributions in compliance with the shearing-deformation theory of Bowden and Tabor [Bowden 50]. One part of the friction, μ_D , is due to the deformation of the material around the contact points (i.e., ploughing term) while the other part is due to molecular interaction at the contact (i.e., the adhesion term, μ_s). The relative importance of these two terms was thought to vary according to the type of surfaces in contact and the applied normal force though no actual comparison was made between theory and experiments. Experimental results between knitted polyester and two non-fibrous surfaces showed a reasonably sharp increase in friction coefficient at a specific load with a decreasing surface hardness. A knitted polyester (100% T310 PET) was tested against a hard plastic surface (Celcon[®]), against itself and against a rubber surface. The friction coefficient for the rubber surface test was approximately 3.0 ($\mu = 3$), which was about 6 times higher compared to the plastic surface and 1.5 times compared to the fabric itself. In all three tests the friction coefficient decreased with an increase in pressure, sharply at first to 241 N/m² then moderately towards higher pressures (483 N/m²). This changeover in friction coefficient could mark a load level where apart from fibre bending also yarn deformation starts to count. The decrease in friction is further believed to be the result of a more homogenous load distribution on the contact surface, though no further theoretical explanation or modelling has been reported. Similar findings with regard to classification of the surface hardness have been published for a normal pressure of 470 N/m² by Ajayi [Ajayi 92a] but he gave much smaller coefficients of friction (i.e., $\mu_s < 0.9$). Yoon *et al.* [Yoon 84] presumed that the high friction coefficient for the rubber tests was caused by a lateral ploughing of the rubber and the fabric.

Another two-component model for fabric-non-fabric friction has been proposed by Kawabata and Morooka [Kawabata 79]. The first component, μ_a , is due to the friction between a fibrous surface and a rigid surface. The second component, μ_b , is supposed to relate to the energy loss, W , caused by the interfibre friction during the compressive deformation in the rubbing process and is expressed as follows:

$$F_b = Ww = \frac{F_w - F_l}{l - w} w \quad (l > w) \quad (2.20)$$

where F_w and F_l are respectively the friction force in the width, w , and length, l , of the sample. The authors found a high correlation between the calculated energy losses derived from lateral compression tests and the experimentally measured values from friction tests. Nevertheless, the experimentally measured values were two to five times larger than the derived ones. It is further understood that this fibre deformation will be more evident at the moving edge of the fabric. Kawabata's hypothetical model has further been used by Nishimatsu and Sawaki [Nishimatsu 84a] to study the frictional properties between a pile fabric and a slider (unknown material) under various pressures discovering a good agreement between measured and calculated values.

A more recent attempt at modelling fabric-non-fabric friction comes from Virto and Naik [Virto 97]. They have developed a model, based again on Bowden and Tabor's deformation-shearing theory, to explain the sliding friction behaviour of fabrics on solid surfaces. This theoretical model is distinctive from all previous models in two ways. At first, Virto and Naik view the adhesion force, F_{ad} , as a van der Waals electrostatic interaction resulting from electric dipole fluctuations between the fabric and the solid surface. Secondly, the deformation force not only consists of a shearing force, F_s , on the asperities but also of an impact force, F_i , between the moving sled and the asperities. The latter considers the relative velocity between the two surfaces. Thus, the total force required to slide a fabric over a surface at a certain speed under a normal force is given as follows:

$$F = F_{ad} + (-F_s) + F_i \quad (2.21)$$

The forces in the theoretical model of Virto and Naik [Virto 97] contain several unknown constants (i.e., the Hamaker constant for the adhesion, the curvature of the asperities, etc.), which make a numerical assessment of the model impossible. Experimentally, seven fabrics very different in fibre nature and construction (wool, cotton, flax, and polyester) are tested against a stainless steel surface, a nylon surface and a synthetic rubber surface. They found a similar classification as Yoon *et al.* [Yoon 84] and Ajayi [Ajayi 92a] with regard to surface hardness but the measured friction coefficients are even lower due to the extremely high normal pressures used (1736-14580 N/m²). A summary of the available models and the minimum and maximum normal pressure used during the experiments is given in Table 2-2. Generally, it appears that irrespective of the friction model, the main difficulty lies in accurately determining the true area of contact.

Table 2-2. Available fabric friction models

Authors	Law	Friction Type	Verification	Normal Pressure (N/m ²)
Wilson [Wilson 63]	(2.15)	Fabric-fabric	[Wilson 63]	20-30000
		Fabric-fabric	[Carr 88]	345-34500
		Fabric-fabric	[Clapp 91]	460-15860
		Fabric-fabric	[Ajayi 88, 92a]	63-630
		Fabric-non-fabric	[Ajayi 88, 92a]	470
Yoon <i>et al.</i> [Yoon 84]	$\mu_D + \mu_S$	Fabric-fabric	[Yoon 84]	103-483
		Fabric-non-fabric	[Yoon 84]	103-483
Kawabata and Morooka [Kawabata 79]	$\mu_a + \mu_b$ (2.20)	Fabric-non-fabric	[Kawabata 79]	Unknown
		Fabric-non-fabric (pile fabric)	[Nishimatsu 84a, b]	48-462
Virto and Naik [Virto 97]	(2.21)	Fabric-non-fabric	[Virto 97]	1736-14580

2.1.4 Fabric Parameters Affecting Frictional Behaviour

From the above analyses of Wilson [Wilson 63], [Carr 88] it has been highlighted that friction between fabrics (fabric-fabric) is clearly dependent on the contact pressure and the yarn type. However, also processing parameters such as fibre composition, yarn construction, fabric structure and finishing treatments [Ajayi 95a, 95b] may have an importance in the frictional behaviour between fabrics. On the other hand, according to Virto and Naik [Virto 97] these morphological factors of the fabric have been found to have an insignificant influence when sliding fabrics over a solid surface (fabric-non-fabric). Yet, in order to study the effect of the different construction parameters on fabric friction only the parameter under study should vary. Therefore, special precautions such as identical weaves and similar yarn diameter need to be considered before testing. Furthermore, when comparing various publications obviously the fabrics are different from each other but also the test method can be influential.

Although, a constant true coefficient of friction does not exist either for fibres nor for fabrics (i.e., always pressure dependent), it might be useful for comparison to quote some typical values for fibres and yarns first (see Table 2-3). Note that wool fibre has a directional friction effect. So, when pulling two wool fibres against their scales, entangling will take place and a higher friction will be measured.



Table 2-3. Some typical friction coefficients for fibres [Morton 97]

	Crossed Fibres [Mercer 47]	Yarn passing over hard steel [Buckle 48]
Nylon	0.14-0.6	0.32
Viscose Rayon	0.19	0.39
Silk	0.26	
Acetate (dull)*	0.29	0.30*
Cotton (grey)*	0.29,0.57	0.29*
Wool, with scales	0.20-0.25	
Wool, against scales	0.38-0.49	

* Friction for dull acetate or cotton grey yarn passing over hard steel

A limited number of studies have tried to investigate the importance of the fibre type in friction. Wilson [Wilson 63] made four series of fabrics from blended yarns and notified a predictable change in the frictional characteristics when altering the blends. Shuck and Loeb [Shuck 70] reported a lower coefficient of friction for wet fabrics with decreasing cotton content. More recently, Yoon *et al.* [Yoon 84] and Carr *et al.* [Carr 88] conducted some frictional tests for knitted and woven material with various blending ratios. However, both studies are contradictory to each other. Carr *et al.* could not discern the effect of fibre type on fabric friction while Yoon *et al.* reported an increase in both static and dynamic friction between fabrics with increasing cotton content. On the other hand, when testing the polyester-cotton samples against a rubber surface, Yoon *et al.* observed a decrease in friction with an increase in cotton percentage. Still, there is no conclusive study about the fibre's effect on fabric friction and further research is definitely needed.

Other yarn parameters that might affect the fabric friction are the yarn twist and the spinning method. Again, little is known about their influence. Only one study reported the influence of the spinning mechanism on fabric-fabric friction [Thorndike 61] where worsted Panama fabrics made from high draft yarns displayed a lower coefficient of friction than the samples obtained from normal yarns (Bradford system). With regard to yarn twist, Nishimatsu and Sawaki [Nishimatsu 84b], noticed a fall in friction force (fabric-non-fabric) in both warp and weft direction when the twist number of the pile warp yarns increased. They attributed this reduction in friction to the fact that with an increased twist number the yarn diameter reduced, which in turn decreased the real area of contact between the pile fabric and the slider.

Another very important fabric parameter to influence fabric friction is the configurational shape taken up by the yarns in the weave, normally referred to as the fabric geometry. Two geometrical factors are pertinent to fabric friction, namely the yarn crown height and the fabric balance. The yarn crown height describes the relative protrusion of the yarn tips from the plane of the fabric surface (i.e., surface roughness) and can be calculated using Peirce geometrical models [Peirce 37] for woven fabrics from the yarn profiles. The crown height of the yarn is shown to have a remarkable effect on the anisotropic behaviour of friction for a given fabric [Ohsawa 66]. Protruding yarns will create a 'ribbed' effect on the fabric surface and hence restrain the motion by mechanical

interlocking when sliding across another fabric surface. The second geometric parameter important in friction is the fabric balance [Ajayi 97a] or the total true area of fabric-to-fabric contact. From the above analysis, this is seen as being of major importance in the fabric friction modelling. An increase in the number of threads per centimetre increases the area and by this, results in a higher frictional resistance and a smoother fabric surface. Studies by [Żurek 85], [Ajayi 92b, 97a] confirmed a positive relation between an increasing fabric balance and the frictional force.

2.1.5 Experimental Conditions Affecting Frictional Behaviour

In addition to the influence of fibre content, yarn and fabric structure discussed in the previous section (2.1.3), fabric friction is also affected by several experimental conditions. In a review on friction, Rubenstein [Rubenstein 58] points out several factors such as the sliding velocity, the number of traverses and environmental factors affecting the friction measurements. A recent more detailed survey by Clapp *et al.* [Clapp 89] identifies several areas of further research on these affecting factors. Five influencing factors will be discussed below starting with the stick-slip effect (1) resulting from a very low velocity of sliding, followed by the overall velocity effect (2) on friction and the influence of the number of traverses (3) on the same sample. To conclude, the effect of the humidity (4) on friction will be reviewed in addition to static charging (5) as a result of low humidity.

(1) From the shearing theory of Bowden and Tabor, it is clear that when two bodies are sliding against each other, contacts are continuously formed and broken. The frictional force necessary to break this cold adhesion has been successfully modelled for non-fibrous materials by using the intimate contact area, the yield-pressure and the shear strength of the junctions, which were assumed constant. However, the latter is not true. At extremely low speeds of sliding, the resultant strength of the junction proved to be greater than at higher speeds. This means, as often has been experimented even in fabric-fabric friction, that the static friction is higher than the dynamic friction. If therefore one of the sliding bodies has a certain degree of elasticity, the motion will be intermittent at low speeds. This phenomenon is called 'stick-slip' and has been illustrated for various surfaces including metals [Bowden 39], [Rabinowicz 58], fibres [Hearle 71] and fabrics. Particularly in control, stick-slip friction can be responsible for many problems, which in some cases can have severe indirect effects. For example in textile automation, oscillations caused by stick-slip in machinery can lead to objectionable patterning in the cloth [Catling 60]. Theoretical analysis by Bowden and Leben [Bowden 39] showed that the difference between the static and dynamic friction caused stick-slip in non-lubricated metallic surfaces to occur. The stick-phase is due to the higher static friction, F_s , whereas the slip-phase to the lower kinetic friction, F_d . The larger the difference between the static and dynamic friction the more regular the stick-slip will be (see Figure 2.4). This relative difference in static and dynamic friction has been encountered as a good indicator for subjectively ranking the tactile sensation of fibres [Röder 53] and fabrics [Ajayi 92a, 92b, 95a]. Hearle and Husain [Hearle 71] characterised the stick-slip topographically during their friction tests on rayon fibres (fibre-fibre) giving six features, namely:

1. frictional force corresponding to the first peak (F_s , static friction);
2. frictional force at beginning of a peak line;
3. frictional force at the end of a peak line (i.e., peaks might not be constant);
4. frictional force at the beginning of a trough line;
5. frictional force at the end of a trough line (i.e., troughs might not be constant to); and
6. number of peaks/cm moving (peak frequency).

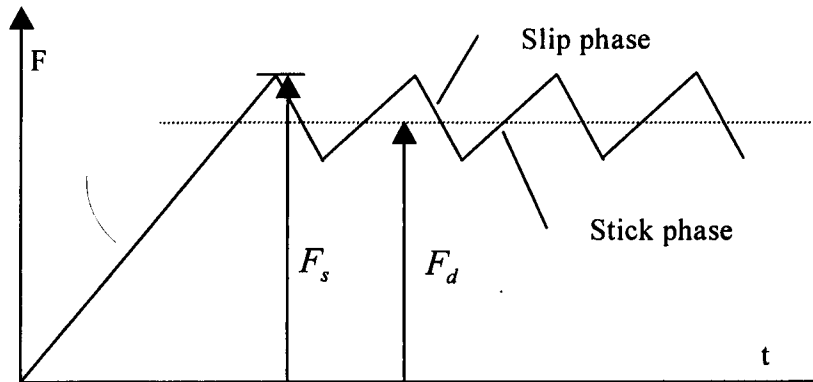


Figure 2.4. Regular stick-slip plot

Note that the definition of beginnings and ends of peak and trough lines is rather ambiguous in that it assumes that the peaks and trough of the stick slip trace are not constant. Rabinowicz [Rabinowicz 58] further included for non-fibrous materials two temporal phenomena necessary to predict correctly the range of speeds and structural conditions over which stick-slip will occur. First, an increase in dwell time or the time a junction is stuck together will increase the static friction [Pascoe 56]. Secondly, Rabinowicz noticed a delay between the change in velocity and the corresponding change in friction and referred to this as frictional lag. Hence, increasing the speed of sliding will reduce this dwell time, which will lower the static friction at breakaway and will abruptly terminate the stick-slip at a certain characteristic velocity.

Stick-slip motion has now been successfully used by several researchers [Ajayi 92b, 95], [Hosseini Ravandi 94] in relating the frictional characteristics of fabric with the topographic structure of its surface. Ajayi showed that there was a positive relationship between the yarn crown height and the peak to peak values of the slip traces, and that the number of peaks correlated well with the yarn density or number of cords. Hosseini Ravandi *et al.* [Hosseini Ravandi 94] explored the periodicity of stick-slip patterns of fabric against a Perspex sled by using an autospectral density function. Out of the frequency information, they could easily calculate the fabric density in a particular direction (warp or weft) knowing the velocity of sliding. Furthermore, they noticed that where yarns protrude from the surface of the fabric a repeated stretching and releasing occurred when a sled under normal load was sliding over the fabric which produced extra broad peaks in the autospectral density plot. When

increasing the normal load on the fabric, the stick-slip amplitude increases (not the friction coefficient) and the broader peaks in the density plot move up in frequency. Hosseini Ravandi and Toriumi [Hosseini Ravandi 96] have also applied this technique during yarn pullout tests with great success to measure the thread interaction at the crossing points in fabrics.

(2) A further increase in velocity implies a decrease in the time of contact between the two bodies and thus a change in friction. The velocity dependence in fibres and yarns has been extensively reported by several studies, [Röder 53], [Howell 59], [Wilson 66] and [Kalyanaraman 88a, b] but also fabric studies mention the velocity dependency [Nishimatsu 84b], [Ajayi 92a] and [Virto 97]. In a study of frictional properties of pile fabrics against a slider (fabric-non-fabric), Nishimatsu and Sawaki [Nishimatsu 84b] noticed a considerable drop in frictional force between 0.5-5 mm/s that gradually increased again at higher sliding speeds. Ajayi [Ajayi 92a] discovered that the velocity of sliding (fabric-fabric) was connected also with the geometry of the fabrics with friction between knitted fabrics with large ribs less susceptible to velocity. However, Virto and Naik [Virto 97] found that in their study on sliding fabrics over solid surfaces, the velocity had no significance at all. This is most likely because of the high normal forces used in the tests.

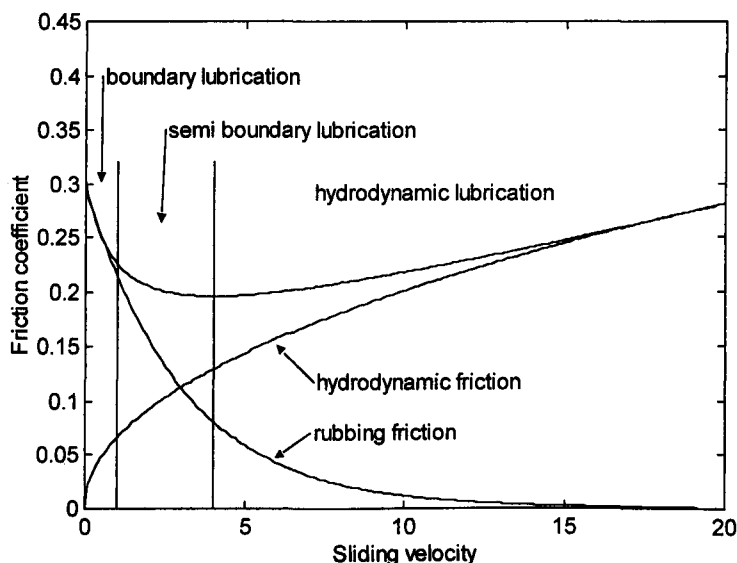


Figure 2.5. Stribeck curve

Originally, it was thought that the increase in friction at high speeds was due to frictional heating, affecting the yield-pressure and shear strength of the fibres [Howell 59]. This heating will have some effect on the friction in fibres and fabrics and will be more pronounced in synthetic fibres, though the main mechanism is now explained by lubrication [Kalyanaraman 88a]. The resemblance between the velocity curves for fibrous materials (lubricated or clean yarn) and those for journal bearings was striking [Hansen 57], [Kalyanaraman 88a]. Friction initially decreases with increasing speed, reaches a minimum, and eventually increases again with increasing speed towards a constant

value (see Figure 2.5). This type of curve has been referred to in tribology as the Stribeck curve. Four regimes of lubrication can be distinguished: static friction (velocity independent), boundary lubrication, partial or semi boundary lubrication and hydrodynamic lubrication. With reference to the velocity effect in yarn-metal friction, the following hypothesis can be given [Kalyanaraman 88b]. At low speed (boundary lubrication), the fibrous materials are supported on their hairs which gradually rise when the velocity is increased. This 'bristle effect' lifts the fibrous material up and reduces the contact area that in turn decreases the friction. With the speed increasing further, the projecting surface hairs will bend down and the contacting surface area will increase again, contributing to a rise in friction. In the case of man-made fibres, the explanation has to be more directed towards various lubricating effects.

(3) A direct result of this hairiness in natural fabrics is that the friction becomes dependent on the number of traverses. Successive traverses of fabric over fabric will align and flatten the surface hairs in the direction of motion and hence reduce the frictional force. Dreby [Dreby 43] found a 50% and 20% reduction in static and dynamic friction forces respectively after five traverses, similar findings were reported by [Mercier 30], [Morrow 31], [Thorndike 61], [Wilson 63], [Carr 88] and [Ajayi 92a]. Furthermore, the direction of testing is important. Due to the anisotropy in fabric geometry, friction in the warp direction will be different to that in the weft direction. Ohsawa and Namiki [Ohsawa 66] therefore introduced a coefficient to express this directionality (i.e., coefficient of the *Directional Frictional Effect*).

(4) Changes in ambient temperature and humidity cause fibres to adjust their moisture content and their own temperature to be in equilibrium with the surrounding atmosphere. The absorption of water, whether liquid water or water vapour, is an exothermic reaction evolving heat (i.e., heat of absorption) in the fibres. This property, known as hygroscopicity, changes the fibre properties, dimensionally as well as mechanically [Clayton 29], [DeLuca 92], and [Inoue 97]. It causes the fibres to swell, which alters their dimensions, and this in turn will change the size, shape, stiffness, and permeability of the yarns and fabrics. Wehner *et al.* [Wehner 87] modelled successfully the variation in air permeability in fabrics (woven and non-woven) for changing humidity. They noticed a type of sigma shaped curve for most natural fibre types with a rapid increase of resistance to air from 0-40% r.h., a plateau region between 40-70% r.h. and again an increase above 70% r.h. The mechanical and frictional properties will be changed affecting also the fabric's processing and end use. The amount of water in a specimen can be expressed in terms of either the regain (mostly used) or the moisture content [Morton 97]:

$$\text{regain} = \frac{\text{mass of absorbed water in specimen}}{\text{mass of dry specimen}} * 100\%;$$

$$\text{moisture content} = \frac{\text{mass of the absorbed water in specimen}}{\text{mass of undried specimen}} * 100\%.$$

The regain for different materials can vary considerably as seen from Figure 2.6; some synthetic and mineral fibres absorb very much less than 1% water at saturation, while the corresponding uptake by natural protein and cellulosic fibres can exceed 30%.

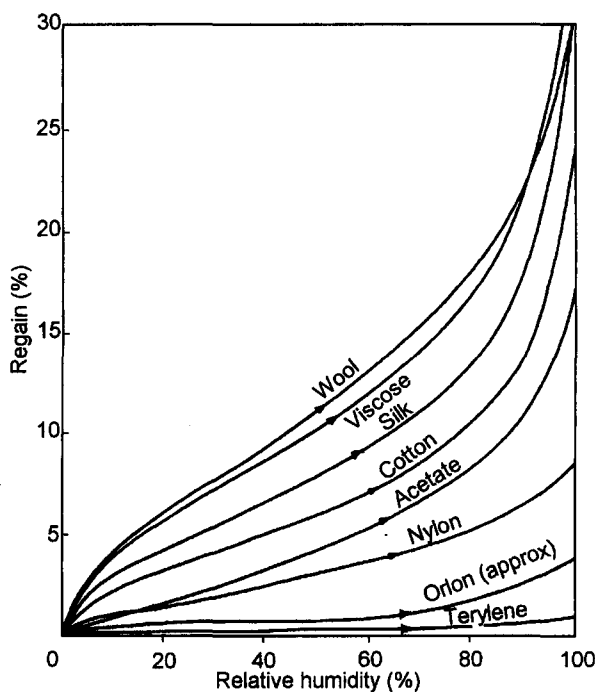


Figure 2.6. Regain as a function of the relative humidity [Morton 97]

Furthermore, a hysteresis effect exists between the regain of the textile material and the relative humidity of the atmosphere. If the relative humidity of the environment is reduced, the fibres desorb water but the regain will be higher than if the same condition had been achieved through absorption. This hysteresis effect will obviously have implications on the dimensional and mechanical parameters of the fabrics. For instance Cookson and Slota [Cookson 93] noted that the hygral expansions (change in length) were greater on desorption than on absorption. Regarding the atmospheric influence on friction in textile materials, little information is available. Clearly, the effect of the humidity on friction will depend considerably on the hygroscopicity of the fibre and in the case of fabrics on their construction too. For instance, for viscose staple fibres, Röder [Röder 53] found only a small increase (12%) in the interfibre friction above 70% r.h. On the other hand, Morrow [Morrow 31] measured a friction coefficient for cotton fibre against steel varying from 0.27-0.44 for a relative humidity from 0% to 100% r.h. respectively. Similar increases in interfibre friction (0.34-0.72) were found in jute and some other long vegetable fibres [Bandyopadhyay 51]. More recently, El Mogahzy and Gupta [El Mogahzy 93a] conducted a detailed study of friction in yarns in which they tested the effect of wet conditions. Although synthetic yarns were used for the tests, polypropylene and acrylic are considered hydrophobic, surprisingly an increase in friction was found for the wet states. Referring to the constants in the Equation (2.19) for friction, results indicated that the frictional index n was not affected by changes in the environment whereas C increased significantly (22%). They ascribed this

increase to be either due to a growth of the total contact area caused by captured water in between the fibre spaces or to the shear of the water film around the yarns. In a further study on friction between pile fabric and a slider (fabric-non-fabric), Nishimatsu and Sawaki [Nishimatsu 84b] incorporated a humidity factor in an experimental equation similar to the Kawabata equation for friction [Kawabata 79]. The frictional force, F , increased with humidity and was related to the contact area, A , and the loss energy, W , both being dependent on humidity, as follows:

$$F(r.h.) = f_{AY} A(r.h.) + wW(r.h.)$$

$$\text{with } f_{AY} = \frac{F_{AY}}{A_Y} \quad (2.22)$$

with (F_{AY}) the frictional force between the yarn bundle and the true contact area, A_Y , and w the width of the sample. Some other recent studies also reported an increase in friction for a higher water content when investigating the influence of humidity on fabric-to-skin friction [Kenins 94], [Sukigara 97].

(5) Finally, there is the effect of static charging on the frictional behaviour of fabrics. However, this influence is mostly neglected in fabric friction because the majority of frictional processes are performed under normal forces that are sometimes very high. Hence, limited quantitative information is available on the effect in fibrous friction [Gonsalves 53], [Hersh 55], [Ramer 68], and [Onogi 96] even though rubbing (e.g., friction) is one of the main ways of generating static charges. Electrostatic forces are well known in textiles, not so much as a useful force but rather as a nuisance. Similarly charged fabrics repel each other and will cause difficulties in handling, for example when fabric comes off a finishing machine the cloth may not fold down neatly. On the other hand, unlike charges will attract causing fabric panels to stick to earthed machine parts and to each other. In addition, the earthing of machinery usually increases the charge on the textile even further. Another consequence is the attraction of oppositely charged particles of dust and dirt from the atmosphere. Few practical applications use static charges; one of them is the versatile electrostatic gripper [Monkman 89]. Despite the considerable effort that has been expended over the past in eliminating the disadvantageous effects [Henry 53c], the mechanism for generating triboelectric charges in polymers still remains to be clarified. One of the surprising features for instance, is the capacity of nominally identical materials to charge each other when they are rubbed together. It is still unclear whether the electric charge carrier is electrons [Montgomery 59] [Lowell 86b], ions or both. Similar properties and experimental parameters influencing the friction in textiles such as material type, normal pressure, surface conditions, sliding velocity and environmental conditions will play a role in triboelectrification, though little is known about their exact contribution to the process. In addition to these factors, there is also the importance of the rubbing process. Henry [Henry 53a, b] showed that the direction of charging is dependent on whether the materials are rubbed symmetrically or asymmetrically. For example, a wool fibre pulled at the tip from an aligned bundle of fibres will have an opposite charge than when it is pulled from its root [Martin 41].

The two parameters characterising static charging are the rate of generated charge and the rate of charge dissipation. The amount of static-charge varies from one material to another and is affected by geometrical fabric constructions (e.g., the yarn crimp). In practice, it is found that cellulosic fibres are least troubled by static charges; wool and silk intermediate; and acetate, nylon and other synthetic fibres are mostly affected [Morton 97]. However, Ramer and Richards [Ramer 68] found that the initial charge generation for a wide range of fabrics was approximately of the same order of magnitude for one rubbing surface and independent of the humidity (25%, 38% and 65% r.h.). The initial static charges varied with different rubbing surfaces (i.e., PTFE > polyethylene > nylon), but unrelated to their respective coefficient of friction (i.e., $\mu_{\text{polyethylene}} > \mu_{\text{nylon}} > \mu_{\text{PTFE}}$).

The effect of sliding speed on static charge is more complicated and very much dependent on the rubbed materials. Hersh and Montgomery [Hersh 55] found that the static charging was independent of the rubbing speed in case of two insulators but linearly increased in case of metals on insulators. Except, in cases where PTFE (Teflon®) was rubbed against an insulator, the charge sometimes increased linearly or remained constant. Further, Hersh and Montgomery [Hersh 55] found also a linear relationship between the generated static charge and the normal force.

Finally, the moisture content of both the air and the sample will be perhaps the most crucial parameter determining the static electrification because fabric regain severely affects the electrical properties. Onogi *et al.* [Onogi 96] concluded that static charges dissipate mainly exponentially with time by electric conduction into the earth. However, atmospheric dissipation by evaporating water molecules is also possible. They noticed that the rate of charge dissipation suddenly increased at a water content critical for each textile material and smaller than the water content at standard conditions. This explains why the usual standard textile testing atmosphere of 65% r.h. and 20°C is too moist for static charging to occur. Hence raising the humidity of the air is generally a sufficient, but not always practical way to reduce static charges. A more successful approach is to ionize the air. Onogi *et al.* [Onogi 97] also found in a later study that this critical water content is dependent on the absolute humidity of the environment. Further research is conducted in minimising the accumulation of electrostatic charge including the addition of surfactants [Jeffries 89], blending of hydrophilic polymers, blending of electrically conductive fibres (ECF) [Tabata 88], copolymerization of hydrophilic monomers [Uchida 91] etc.

2.1.6 Friction Measuring Devices

Considering the fact that the friction coefficient of a fabric cannot be extrapolated from its fibre or yarn friction, measuring-devices for fabric friction are indispensable. The majority of instruments have been designed to measure fabric to fabric friction but all can be converted to measure fabric to non-fibrous materials. However, some of the testing rigs are limited in altering the influencing factors in fabric friction (i.e., sliding speed, pressure, etc.). Two main categories of devices can be distinguished; the inclined plate method and the linear motion types either in a unidirectional or reciprocating motion. Only two methods used in this study will be discussed in more detail, the others will be mentioned briefly.

Mercier [Mercier 30] was one of the first to describe the inclined plate method as a simple and quick way to measure static friction. A sample of cloth is attached to a horizontal plate with on top a sled covered with either an identical or a different type of fabric. Next, the angle of the plate to the horizontal is increased until the fabric-covered sled starts moving (see Figure 2.7). The tangent of this angle is the friction coefficient between the two tests fabrics. Morrow [Morrow 31] found very erratic readings when using this testing method especially when using identical fabric samples and therefore suggested it was better to measure the slope at which the motion ceased when the inclination was gradually decreased. Some other disadvantages of this method are the impossibility to measure dynamic friction or vary the sliding speed. Furthermore, large coefficients of friction (large ϕ) will be erratic because the forces do not act purely normal to the surfaces. From the above description, it can easily be seen that the fabric-covered sled can be substituted by any other engineering material. The inclined plate method has now become an ASTM-standard (D3334.15 derived from TAPPI T503) to measure the coefficient of static friction of fabrics woven from polyolefin monofilaments.

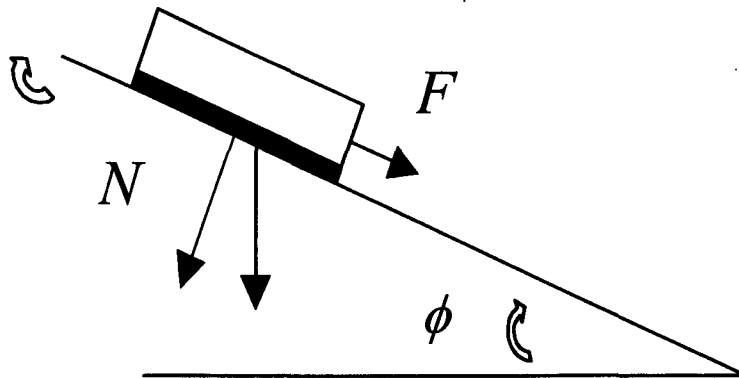


Figure 2.7. Force diagram of two bodies on an inclined plane

$$\mu = \frac{F}{N} = \frac{mg \sin \phi}{mg \cos \phi} = \tan \phi \quad (2.23)$$

The most widely used method of measuring friction nowadays is based on the friction device developed by Dreby [Dreby 43]. The principle of measurement simply consisted of the shearing of two pieces of fabric; one sample was connected to a rotary drum supplying the movement, the other sample to a registration device, a torque sensor in the case of Dreby. This method has now been modified to a system where either a fabric-covered sled is pulled over a stationary table [Ajayi 88] or where a linear motion table is slid underneath a fabric-covered sled as in this research (see 3.1.1). The tested fabrics can be identical or different in type and the table or sled can be left uncovered and be substituted with any engineering material. The sled is connected to a force sensor or dynamometer directly registering the frictional force (see Figure 2.8). This method allows measurement of both the static and dynamic friction under variable conditions of distance, speed, acceleration and normal loads. Many research laboratories are now equipped with a versatile tensiometer (e.g., Instron®) which can easily be adapted to measure friction. Considering that the cross-head of a tensiometer

moves in a vertical plane, the sled or fabric sample will have to be connected with a towing yarn passing over a 'frictionless' pulley.



Figure 2.8. Dreby's principle for friction measurements

Other methods include the chainomatic balance technique by Morrow [Morrow 31], and several abrasive friction devices. A more recent friction tester measuring fabric to metal was introduced by Kawabata [Kawabata 80] as part of the KES-F. The friction tester (KES-FB4) comprises two testers, a surface friction tester and a geometrical roughness tester. The surface friction tester uses a stationary steel finger consisting of 10 piano wires each 0.5-mm in diameter and 5 mm long. The probe, 5 mm² in total, is pressed with a 50-g normal force onto the moving fabric sample. The fabric specimen is rolled on two drums and can be moved forward or backwards at different speeds. Great care must be taken to decontaminate the steel finger from any softeners or other textile lubricants picked up from previous tests as this can increase the friction coefficient by a factor of two to three. The roughness tester contains only one piano wire (0.5 x 5 mm) and uses a 10-g contact force while the fabric sample is moved underneath. The probe measures displacement and is sufficiently sensitive to distinguish differences in yarn and fabric structure. However, all contact methods apply a minimum pressure on the stylus that to a certain degree can disturb the fabric surface and, depending on the type and size of the contactor might oversee some irregularities. Nevertheless, contact methods will be very useful in tactile roughness measurements for the estimation of fabric handle and comfort where the minimum pressure will better imitate the striking of the fabric with ones fingertips.

Non-contacting methods on the other hand are using laser sensors so that the fabric is not disturbed. In a study by Ramgulam *et al.*, [Ramgulam 93] large discrepancies were found between roughness tests performed on the KES-F tester and tests with a laser sensor (spot diameter 25-microns). In all cases, and especially for knitted material (e.g., mean roughness KES-F 6.4 μm , laser 183.04 μm), the surface estimations on the KES-F tests were significantly lower than with the laser method.

2.2 Compression Properties of Textiles

2.2.1 Introduction

The compressibility of fabrics (i.e., lateral compression) is again considered a basic mechanical property closely related to fabric handle. That means that, the compressibility is concerned with the softness and fullness of the fabric [Elder 84], and likewise with the surface smoothness

[Ajayi 88, 97b], [Viallier 92]. A fabric that compresses easily is likely to be deemed soft, and to be found to possess a low compression modulus or high compression. Elder *et al.* [Elder 84] successfully correlated results of subjective finger pressures (20 g/cm^2) with fabric softness. Hence, any surface finishing of the fabric such as singeing (or gassing), milling and pressing, generally applied to improve the hand will have an essential impact on the compressibility of the fabric. Furthermore, the compressibility is related to the fabric geometrical structure, the surface properties of the yarns and/or fibres and their lateral compressibility.

The fabric compressibility test quantifies the thickness (ASTM D1777) and compressional stiffness of fabrics. As an indirect measurement, compressibility has successfully been used to assess dry abrasion of fabrics [Ukponmwan 94] and the wear of carpets referred to as the carpet resilience. However, compression can be distinguished either statically when the pressure varies slowly in time or dynamically when the sample is repeatedly loaded and unloaded. The dynamic compression will be discussed in the next section (2.3.3).

Compression is defined as the decrease in intrinsic thickness with an appropriate increase in lateral pressure. The intrinsic thickness of a fabric is in fact the maximum fabric thickness and is determined as the thickness of the space occupied by the fabric subjected to a barely perceptible pressure (1% of the maximum pressure). Two effects are noteworthy in compression. At first there is the irrecoverable strain during the initial compression cycle, and secondly, there is a mechanical hysteresis observed during a compression-release cycle (see Figure 2.9) resulting in a lower volume (stress) during the release cycle. Successive compression cycles (20 or more) will continually reduce the hysteresis. In order to compare different compression curves Kawabata [Kawabata 80] introduced four parameters as part of the compression test in his KES-F system. The KES-FB3 compression test takes several thickness measurements between T_0 and T_m at a 0.5 gf/cm^2 and 50.0 gf/cm^2 (P_m) pressure interval respectively. The four parameters express the work of compression, WC , as the area under the pressure-thickness curve; (WC' area release curve), the linearity, LC , as the deviation from a straight line between the thickness limits; the resilience or hysteresis of the fabric compression, RC and the relative compressibility, EMC .

$$\begin{aligned}
 WC &= \int_{T_0}^{T_m} PdT \\
 LC &= WC / (0.5P_m(T_0 - T_m)) \\
 RC &= WC' / WC \\
 EMC &= 1 - (T_m / T_0)
 \end{aligned}
 \tag{2.24}$$

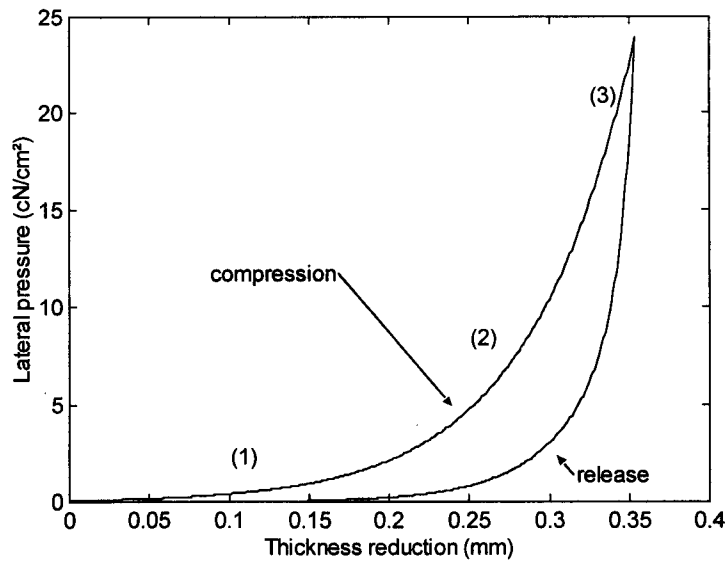


Figure 2.9. Theoretical compression-release curve

In general, any woven fabric structure can be approximated by a three-layer structure consisting of the inner core and two outer layers at each face as seen in Figure 2.10 [de Jong 86]. The core is a dense assembly of fibres/yarns with air spaces in between, whereas the outer layers consist mainly of air with some projecting fibres (2% of total fabric mass per unit area for wool [de Jong 86]). In the process of fabric compression (woven and knitted), three stages can now be distinguished depending on the pressure (see Figure 2.9) [Postle 71], [de Jong 86] and [Matsudaira 95]. First at low pressure, the compression plate comes into contact with the hairs and/or protruding fibres from the outer face of the fabric and the compression force varies linearly with the thickness. This first region (1) of the compression characteristic is presumed to be elastic. Increasing the pressure overcomes the interyarn and interfibre friction, any buckles are flattened and fibre slippage takes place reducing the air spaces between the fibres. The fabric thickness decreases non-linearly with increasing pressure in this second region (2). Increasing the pressure even further compresses the fibres laterally hence the pressure rises greatly for a small reduction in thickness. This third region (3) can be considered as the initial elastic region of the fibres. For filament spun fabrics only two stages can be considered because of the absence of any protruding surface fibres. More recently, Hu and Newton [Hu 97] proposed a five-layer structure by subdividing the outer layers of de Jong's model into two separate layers. The introduction of the model was revealed by an unexpected discrepancy that was found between the smaller geometrical thickness, which was calculated and measured principally under zero pressure, and T_0 which was measured at 0.5 gf/cm^2 . The first layer in their model still containing hairy fibres now also includes crowns above the average geometrical thickness (i.e., calculated from the crimp height and the thread diameter). The second layer is 'another' compressible layer forming the firm structure of the fabric whereas the third layer is the incompressible layer as in de Jong's model.

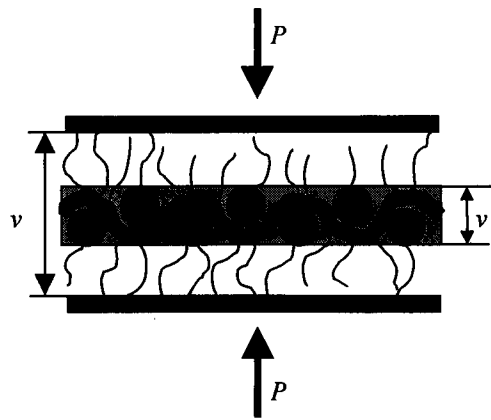


Figure 2.10. Three layer model of woven fabric under lateral compression proposed by de Jong et al. [de Jong 86]

Again, as with all fabric parameters, fabric compressibility is susceptible to humidity changes. Sukigara and Niwa [Sukigara 96] investigated the effect of moisture transfer on the properties of wool futon padding and found that samples with a higher water content were more easily compressed. They also observed an increase in volume for the wool padding during desorption of moisture. Similar results have been reported by Tester [Tester 90] and Shishoo [Shishoo 90]. Both studies found an increase in fabric thickness at lower regain mainly due to rising of the surface hairs.

The compression properties of fibrous materials have been the subject of many studies and investigations [Peirce 30], [van Wyk 46a, b], [Bogaty 53], [Komori 77], [Dunlop 83] and [Lee 85]. However, the majority has been of an empirical nature in that the fibre compression and decompression curves have been fitted to various equations. First, the pressure-volume model of van Wyk [van Wyk 46a, b] that has been dominating the field for many years will be discussed, followed by some other approaches by Bogaty, Matsudaira, Dunlop and Schneider in 2.2.3.

2.2.2 Van Wyk Model

Van Wyk presented an elegant proof of a relationship previously found by Schofield [Schofield 38], stating that the exerted pressure (on wool) was inversely proportional to the cube of the sample's volume. The proof starts from several hypotheses as follows:

possible twisting, extension and slippage of the fibres is ignored,

the fibre mass is regarded as a system of bending units, and

the fibre elements are randomly orientated and uniformly packed.

Based on a simple model where fibres are supposedly cylindrical rods subjected to simple bending when applying compression stress, van Wyk extrapolated the following equation:

$$P = KE \frac{m^3}{\rho^3} \left(\frac{1}{V^3} - \frac{1}{V_0^3} \right) \quad (2.25)$$

Equation (2.25) is independent of the fibre diameter and the elasticity, but is dependent on the Young's modulus, E , the mass of the fibres, m , and the bulk density, ρ , at a relatively low pressure (300 N/m^2). The volume V and V_0 are respectively under pressure P and zero pressure. The dimensionless constant K includes the fibre characteristics and will vary with fibre orientation and crimp [van Wyk 46b]. Although it is probably impossible to derive the K -constant theoretically, it may be found experimentally if one can determine the Young's modulus independently. Van Wyk first assumed unity for the constant but found later a typical value of 0.01 for K . Furthermore, Dunlop [Dunlop 74] reported a close correlation ($r^2 = 0.95$) between (KE) and ρ but found that the K -constant and the Young's modulus were the dominant parameters in distinguishing the compression of different types of fibre (e.g., different types of wool).

Van Wyk suggested further corrections to the equation because the relationship was only found to hold well for moderate compression rates. At very low compression rates, the disparity was due to the lack of uniformity in the packing density of the fibres whereas at high pressures, the incompressible volume, V' , could still be significant. Attempts by Larose [Larose 53] to apply the more simple Equation (2.25) to fabrics failed because of neglecting the limiting fibre volume, V' , at large pressure. In order to fit van Wyk's equation to the compression of pile fabrics, Larose had to reduce the order of the volume to 2.5 instead of three. De Jong *et al.* [de Jong 86] found that V' was still between 0.5 to 0.9 of the fabric's original thickness at a pressure of 50.0 gf/cm^2 . Thus a more elaborate equation must be used, such as:

$$P = KE \frac{m^3}{\rho^3} \left[\frac{1}{(V - V')^3} - \frac{1}{(V_0 - V')^3} \right] \quad (2.26)$$

In spite of the usefulness, van Wyk's model has some limitations. Namely, the real physical meaning of the K -constant is undetermined, and the model does not take account of hysteresis, which is probably caused by fibre slippage and fibre friction during compression and decompression. Dunlop investigated both deficiencies and came to some astonishing conclusions. Fibre slippage and friction was clearly detectable by means of acoustic emission [Dunlop 79] during compression and decompression of fibre wads. Further evidence of fibre slippage was found during measurements of the dynamic bulk modulus (elastic modulus of the fibre mass) [Dunlop 81]. This modulus was determined from an acoustic impedance measurement, which minutely deflects the fibres so that fibre slippage hardly can occur. Hence, Dunlop found estimates of (KE) much higher than van Wyk, which could only be attributed to fibre slippage and frictional effects occurring during slow compression in van Wyk's experiments. Overall, Dunlop [Dunlop 81] concluded that van Wyk's basic concept of fibre bending during compression was correct though still inadequately described the distribution of fibre element length and the regularity of fibre loading points.

Recently, Dupuis *et al.* [Dupuis 95], [Viallier 92] showed that in fabric compression the interlacing of the yarns in the fabric is more essential than the yarns from which the fabric was made. All specimens could be classified according to their limit of compression in three groups; non-woven and knitted, woven fabrics and finally film structures. They found a good agreement between the

compression results and the calculated results for pressures even less than 0.1 kPa using van Wyk's equation. De Jong *et al.* [de Jong 86] fitted van Wyk's equation to their experimental data by varying the three unknown parameters (V' , V_0 , and KEm^3/ρ^3), the fitted curves were in many cases indistinguishable from the measured compression curves.

Furthermore, several theoretical studies [Komori 77], [Lee 85], [Carnaby 89] and [Komori 91] have been conducted to improve van Wyk's theory, specifically in replacing the random fibre abstraction. After all, yarns and fibres are organised according to a specific pattern (weave or knit) in a fabric structure and will therefore have a preferential orientation during compression (K -constant alters during compression). Stearn [Stearn 71] originally showed that even a random mass of fibres had a preference to bend perpendicularly to the direction of compression. This result has been confirmed by Komori and Makishima [Komori 77] who introduced an orientation density distribution in order to calculate the number of fibre contact points better. Lee and Lee [Lee 85] have extended this density distribution theory in relating the tangential elastic modulus and Poisson's ratio of an isotropic mass to the orientation density and properties of fibres. A further addition was made by Carnaby and Pan [Carnaby 89] who succeeded for the first time in theoretically predicting the compression hysteresis in fibrous masses. The essential principle is based on classifying the fibre contact point as either slipping or non-slipping so that the deformations then can be calculated by using a non-linear iteration technique. Although a rather high Poisson's ratio (> 0.5) was obtained during Carnaby and Pan's analysis, reasonable agreement was found with the experimental results. More recently, Lee and Carnaby [Lee 92] have introduced a new approach to the compressional mechanism by using an energy method based on continuum mechanics. The bending energy of each fibre under compression, derived in terms of the strain and the Poisson's ratio, is summed using a density function combining length and orientation of each fibre. A further theoretical explanation of the density models would lead us too far-afield.

2.2.3 Other Lateral Compression Models

In addition to van Wyk's equation there are numerous empirical equations [Peirce 30], [Hoffman 51], [Bogaty 53], [Matsudaira 95] and some mechanical models [Dunlop 83], [Schneider 91] relating thickness of a fabric to the applied pressure. Only the most relevant will be mentioned, starting with a hyperbolic approach from Bogaty [Bogaty 53].

Bogaty *et al.* [Bogaty 53] suggested an equation, similar to the van der Waals' gas equation, relating pressure, P , to fabric thickness, T , of the following format:

$$T = e_1 + \frac{e_2}{P + e_3} \quad (2.27)$$

The lack of any physical significance of the constants (e_1 , e_2 , e_3) of this equation in particular and others is the main disadvantage of empirical equations. Originally, Bogaty *et al.* considered the constant e_1 as a thickness correction factor, which was defined as the fabric thickness at maximum

pressure (1.38 N/cm^2). The e_3 -constant was also a correction factor, but for pressure. The value of e_3 was assumed constant for all fabrics (0.034 N/cm^2) and accounted for the fact that the fabric's thickness is limited at zero pressure. Only the e_2 -constant was found more fabric characteristic and related directly to the height and density of the surface fibres.

However, Larose [Larose 53] applied this equation to fit the compression of pile fabric but with little success. The results showed that Bogaty's equation did not represent compressibility over a wide range of pressures unless the values of e_1 and e_3 are changed for each fabric.

Considering that the compression mechanism can be split in three stages (see 2.2.1), Matsudaira and Qin [Matsudaira 95] proposed a regression curve for each individual stage. The initial and last part of the compression curve together with the first part of the recovering curve is approximated by a linear equation. The middle part of the compression and recovering curve are both regressed by an exponential curve. Hence, in total five equations and several constants are necessary to describe the full compression/recovery graph. An attempt is made at relating the constants used in the regression analysis with some mechanical parameters (e.g., fibre bending on the surface and compressional modulus of the fibres) though the model is still empirical. The following two models approach compression from a phenomenological point of view.

Dunlop [Dunlop 83] combines van Wyk's fibre bending theory, simulated as non-linear springs, with Coulomb friction blocks accounting for the fibre slippage effect. The non-linear springs obey an inverse cube force-extension relation while the friction elements simulate the stiffness in the model and indirectly account also for the point to point contact in between the fibres. Three different models are suggested: two series Coulomb-spring friction models and a parallel model.

Finally, in a study on the sensation of warmth or coolness of fabrics, Schneider and Holcombe [Schneider 91] needed an estimate of the outer surface thickness of a fabric. The outer surface of fabrics is found to be closely related to the thermal resistance and needed measurements under pressures of the order of the fabric's weight. They therefore proposed a fibre-bending model based on the point deflection of a clamped cantilever. However, again the model needs several parameters such as the fibre diameter and the number of protruding fibres per unit area that are difficult to establish. Consequently, they assumed that these fibre constants would not change much in their experiment and only measured relative thickness at two different pressures.

2.3 Vibration in Textiles

2.3.1 Introduction

Although fabrics are continuously subjected to dynamic loading during the manufacturing process as well as during the wearing of garments, the overall majority of studies on their mechanical properties are concentrated on static or quasi static loading. This can at least partly be explained by the

lack of suitable measuring equipment. The earliest techniques were only based on modified static measurement devices or employed impact loading conditions. From the moment that techniques such as acoustic pulse propagation became available, dynamic measurements were given more attention particularly in the case of fibres [Ballou 49], [Dunell 51], [Meredith 56], [King 70], [Zorowski 70] and [Morton 97]. Mostly a rheological model is used in which springs and dashpots (viscous or Coulomb) approximate the dynamic properties. For yarns and especially fabrics, however, the field of dynamic modelling has received less attention because usually cross-sectional properties of the specimen are required. Only recently, thanks to the computer graphics industry, dynamic modelling has been given another boost [Weil 86], [Terzopoulos 87], [Aono 90] and [Carignan 92]. However, the purpose of these studies is not so much as to predict an accurate deformation but rather to simulate a cloth-like behaviour for computer animation.

A fibrous body whether it is a fibre, a yarn or a fabric panel can be dynamically excited in two ways either in plane or out of plane. Longitudinal excitation in plane which is discussed first in 2.3.2 will measure the dynamic elastic modulus (i.e., dynamic Young's modulus) while lateral excitation out of plane, discussed in 2.3.3, will give the dynamic compression. One exception can be mentioned with regard to the Vibroscope method of Gonsalves [Gonsalves 47]. This method uses lateral vibration on a single fibre under tension to determine its linear density (ASTM D1577-66). But, also other parameters such as the dynamic shear modulus or the Poisson's ratios that are very difficult to measure by conventional methods, and are becoming more and more in demand in complex modelling, can be studied.

A variety of techniques has been employed for the measurement of the dynamical properties of fibres [Morton 97], less for yarns and fabrics but basically three classes can be identified; free vibration (1), resonance methods (2) and wave propagation (3).

1. In a free vibration method, the continuing result of an initial disturbance is monitored in the form of a logarithmic decrement. One has to be cautious when the system is non-linear or when the period of oscillation is dependent on the amplitude (e.g., fibrous systems). The logarithmic decrement is extremely useful in identifying the type and degree of damping of a system. Although the damping will likely be a combination of dry friction, viscous or hysteresis damping, the dominant mechanism can be estimated from a semi-logarithmic plot of the maximum amplitude versus the number of cycles [Steidel 89]. The next two methods both use continuous forces.
2. The resonant method finds the maximum system response when the body is vibrated with constant amplitude and varying frequency. The resonance frequency at which the maximum response occurs, will give some information on the elastic properties while the sharpness or width of the response curve will give a measure of the dissipative forces present in the system.
3. The last technique is based on wave propagation through the material. Three types of elastic waves can appear in solid rods (e.g., fibres and yarns) namely torsional, extensional or flexural. Only the last two types can propagate through plates (e.g., fabrics). The velocity of propagation of

all types of waves will depend on the elastic properties and density of the material. Hence, the dynamic elastic modulus can easily be calculated from the velocity. When the material includes a viscous behaviour, in addition to the elastic, then the parameters describing the dissipative forces can be measured at any two points along the specimen as follows:

- from the amount of dissipated energy,
- from the phase relation between stress and strain, or
- from the amplitude ratio of the measured stresses (or strains).

2.3.2 Longitudinal Vibration

One of the first reported works on dynamic mechanical measurements in textiles was made by Ballou and Silverman [Ballou 44] in 1944. Their work on the propagation of low frequency longitudinal waves in filaments has been the start of very few other studies mainly on fibre dynamics [Hillier 49], [Chaikin 55] and [Alptekin 68]. Apart from a dynamical fibre/yarn model and some quasi-static fabric models, no true modelling of in plane dynamics of fabric has been found in the literature. A linear viscoelastic yarn model based on work by Zorowski and Murayama [Zorowski 67] and further expanded for low frequencies by Alptekin [Alptekin 68], [Zorowski 70] will first be discussed in more detail. This section further includes some stress relaxation models (quasi-static) by Johnson [Johnson 85] and Vangheluwe [Vangheluwe 96], and finally discusses some helpful techniques used in a study on the dynamic characterisation of TABI (Tailorable Advanced Blanket Insulation).

Alptekin [Alptekin 68] proposed a simple linear Voigt element consisting of a spring in parallel with a dashpot to model the steady state dynamic properties of yarn. The spring represents the steady state elasticity, E , whereas the dashpot the steady state viscosity, η . Any significant inertial effects can eventually be included by an extra mass element. Considering now a periodically varying strain of the form, $\varepsilon = \varepsilon_0 e^{i\omega t}$ with angular velocity ω , the constants specifying the spring and dashpot can be defined as follows:

$$E = E' = \int_0^{\infty} \frac{\omega^2 t^2}{1 + \omega^2 t^2} E(t) dt$$

$$\eta = E'' = \int_0^{\infty} \frac{t^2}{1 + \omega^2 t^2} E(t) dt$$
(2.28)

The function $E(t)$ specifies the contribution of a constituent element with relaxation time t (no viscous flow possible) and differs from the static modulus, which is measured by holding the specimen a number of seconds under strain. From Equation (2.28), it can be seen that at high frequencies the viscosity becomes negligible whereas at extremely low frequencies ($\omega \ll 1$) the viscosity becomes dominant and makes the steady state elasticity virtually negligible.

Alptekin measured the dynamical parameters for three different continuous filament yarns (i.e., nylon 66, acetate and polyester) with various twist levels (10° to 45°). The measurements are performed on what is called a 'Vibron Viscoelastometer' [Takayanagi 63]. The instrument imposes a sinusoidal tensile strain between 10-110 Hz on one end of a yarn sample and registers the resulting sinusoidal tensile stress at the other end of the yarn that is held fixed. The output stress amplitude, σ , to the input strain amplitude, ε , and the phase angle, δ , between these two quantities are measured to calculate the two elements in the Voigt model as follows:

$$|E| = \frac{|\sigma|}{|\varepsilon|} = \sqrt{(E')^2 + (E'')^2} \quad (2.29)$$

$$\delta = \tan^{-1} \frac{E''}{E'}$$

Both measured quantities are found to be influenced by inertial effects (i.e., density of the material), the sample size and the structural geometry (e.g., twist level and internal pressure between fibres). In describing now the dynamics of a one-dimensional longitudinal vibration of a fixed yarn with length, l , and density, ρ , the displacement u of an infinitesimal free viscoelastic body at location x can be written as:

$$E_y \frac{\partial^2 u}{\partial x^2} + \eta_y \frac{\partial^3 u}{\partial x^2 \partial t} = \rho \frac{\partial^2 u}{\partial t^2}$$

with boundary conditions :

$$u(0, t) = u_0 \sin \omega t \quad u(l, t) = 0 \quad (2.30)$$

The elasticity and viscosity of the yarn both include an integral expression, $Int.$, for the yarn geometry, which can be determined either analytically or experimentally from the sonic velocity, v_s , as follows:

$$v_s = \sqrt{\frac{E'Int.}{\rho}} \quad \text{with} \quad E_y = E'Int. \quad (2.31)$$

Ryan and Postle [Ryan 81] applied the sonic wave technique to fabrics and found that only flexural waves were propagating through the fabric panels. The orthotropic character of fabric was clearly visible in their results when comparing measurements in both warp and weft direction.

Furthermore, Alptekin [Alptekin 68] showed that the damping mechanism is not purely viscous but that Coulomb friction due to filament rubbing must be assumed as a secondary dissipation mechanism. In addition, an analysis, similar to Equation (2.30), was given for the dynamic response of simple fibre networks based on a distribution function specifying the number of filaments on each node. Generally, these node techniques generate huge amounts of dependent variables [Leech 77], [Mansell 78]. Therefore, other approaches studying wave propagation in fabrics are based on assuming the fabric panel to be an orthotropic continuum medium having only stiffness in the

principal directions (i.e., warp and weft) [Sun 73], [Leech 79]. However, further explanation of these theories is beyond the scope of this review.

Some more complex rheological models compared to the simple Voigt element of Alptekin were proposed in two studies on (quasi-static) relaxation behaviour in fabric. Johnson [Johnson 85] proposed two viscoelastic models to predict fabric stress-strain and recovery from stress behaviour. One model combines two parallel Maxwell elements (spring and damper in series) in series with another Maxwell element; a second model consists of a spring in series with a Voigt element. However, a poor fit was found between the theoretical and experimental results. A more recent non-linear extended Maxwell model taking into account the loading history has been proposed by Vangheluwe *et al.* [Vangheluwe 96]. The model consists of a non-linear spring with a quadratic characteristic in parallel with several Maxwell elements.

Another study on the dynamical characterisation of thermal protection material for space investigates various helpful techniques to measure the necessary in-plane dynamic parameters [Clayton 92]. The material known as TABI (Tailorable Advanced Blanket Insulation) is built from a three-dimensional rectangular or triangular ceramic fabric (silicon carbide) core structure filled with fibrous ceramic insulation and can be used for deployable space vehicles. The measurements are twofold, estimating the elastic stiffness and the damping characteristics. The elastic modulus was simply derived from a stress-strain test and found non-linear in both warp and fill directions. For the damping properties two tests were performed, one free vibration test using the logarithmic decrement and another forced vibration test revealing the hysteresis of the material. The logarithmic decrement was rather inconclusive and identified the presence of all three damping mechanisms with an overall dominant viscous damping. In addition, the material behaved in a non-linear way because viscous damping was only visible at low amplitudes whereas a different test at higher amplitude indicated dry friction. For a further identification of the damping mechanism and the degree of damping, some forced damping tests between 20-50 Hz were performed. Elliptical hysteresis curves proved again that the main damping mechanism was viscous. Several other interesting observations were made. First, the damping energy was found to increase consistently with increasing excitation amplitude and varied with frequency in a complicated manner. Secondly, for each frequency, the stiffness diminished as the amplitude increased which is a similar phenomenon as in rubber isolators containing carbon [Harris 96].

Furthermore, two models were proposed, one model represented the logarithmic decrement, the other model the hysteresis tests. Numerical solutions of the first model showed initially poor agreement with the experiments mainly because the static stiffness was used and found to deviate significantly from the dynamic stiffness. A dynamic magnification factor was therefore calculated from the resonance frequency and multiplied by the static stiffness to estimate the dynamic stiffness. The second model included a damping coefficient dependent on the frequency and excitation

amplitude as the hysteresis tests indicated. It was further found that dynamic stiffness obtained from several experimental hysteresis curves gave better simulation results than the modified static stiffness.

2.3.3 Lateral Vibration

Work on lateral vibration in fibrous materials has primarily been concentrated in felt pads [Tyzzer 47], [Dunlop 90, 92] investigating their dynamic properties as vibration isolation mountings and in carpet resilience [Dunlop 89, 91]. These studies are considered a good starting point for this thesis and will be discussed in this section. More recently, a growing number of analyses on lateral dynamics in polymer matrices are reported mainly because of their applications as body armour and their superior lightweight and strength in mechanical applications in aerospace and the automotive industry [Jeng 96]. However, all of these studies are (high velocity) impact load tests and therefore not applicable to this work. Only one article by Hearle and Turner [Hearle 61] dealing directly with lateral vibrations (i.e., flexural) in fabrics could be traced.

Hearle and Turner [Hearle 61] reported in 1961 a preliminary study on the flexural vibrations in fabrics in which a formula for the resonance frequency, f_{res} , has been derived as follows:

$$f_{res} = \frac{1}{2\pi} 3.52 \sqrt{\left(\frac{Gg}{m_a l^4}\right)} \quad (2.32)$$

with $G = \frac{EI}{g}$

The resonance frequency of a fabric panel with length, l , unit width, and mass per unit area, m_a , is dependent on the flexural rigidity, G . The flexural rigidity, G , of a fabric is calculable as the bending length of a fabric (i.e., overhanging length in a stiffness test (ASTM D1388-75) divide by two) to the power of three multiplied by its weight per area, m_a , [Peirce 30]. Vibrations, other than the fundamental will require a different numerical constant. The analysis assumes only these forces involved in flexing the fabric, in reality also gravitational forces need to be taken into account. Nevertheless, as long as the ratio of these two forces (flexural and gravitation) $(m_a l^3 / 3G)$ is far less than unity, the mass of the fabric can be neglected. The above ratio suggested that only fabric samples of 1 cm could be used in order to avoid the effect of the fabric mass. Experiments were performed in which hanging fabric samples with a small piece of iron fixed at their base were brought into an alternating electromagnetic field. The specimen partially obscured a beam of parallel light that fell on a photodiode thereby generating an alternating signal and measuring the flexural amplitude of the fabric. However, the results were distorted by torsional vibration and some harmonics induced in the electromagnet and thereby initially deviated severely from the calculated results. A better estimate of the sample length (yarns have a different length as to the fabric because of the crimping) gave straight lines according to Equation (2.32). Again, little correlation was found between the static and the dynamic elasticity. Further, amplitude dependency has not been investigated.

The compression properties of carpets, particularly the dynamic response, are especially relevant to their mechanical performance. As floor coverings, carpets are constantly subjected to compressive forces developed during standing and walking, and more recently to extreme reactions in sporting activities. A lot of the work on the dynamic compression of carpets has been conducted far from realistic situations either at too low frequencies (quasi-static) or at too high pressures [Horino 71]. Dunlop and Sun have rectified both inadequacies. In a first paper, Dunlop and Sun [Dunlop 89] have studied carpet compressions at frequencies in the range 20-100 Hz and pressures between 4.9-7.0 kPa. In a second paper, the pressure was further increased to 22 kPa [Dunlop 91]. A similar approach was conducted on felt pads [Dunlop 90, 92].

During compression normal to the pile, the carpet is assumed to behave as a compression spring with an energy dissipating mechanism. The characteristics can therefore be approached as a spring-damper model. An extra weight is put on top of the carpet to produce the initial compression [Dunlop 89]. In total, a double-mass damped harmonic oscillator is obtained with one reaction mass as weight and a smaller carpet mass at the bottom directly connected to the driving system. Hence, the system is second order with the usual amplitude curve sweeping up at resonance frequency and the phase lagging 90° to 110° depending on the system's damping.

As expected the results indicated a resonance frequency that is dependent on amplitude. Further, the resonance frequency and phase lag shifted to lower frequencies when increasing the driving amplitude. This clearly pointed out that the spring in the model is non-linear, giving a smaller dynamic modulus at higher amplitudes. Comparing again the dynamic and static compression moduli at equal compression loads revealed that the smallest dynamic moduli (i.e., at highest excitation amplitudes) were generally greater than those derived from the slope of the static compression tests. This can be accounted for in terms of friction controlled slippage of the piles in the carpet. It is thought that the static compression induces larger displacements that consequently result in much greater slippage. On the other hand, the damping was found independent of the frequency though slightly increased at higher amplitudes, which would indicate that the damping mechanism is friction controlled rather than viscoelastic. Similar conclusions are made in the case of the vibration of felt pads [Dunlop 90].

In a second set of papers [Dunlop 91, 92], the initial pressure is further increased by allowing the vibrator to activate a pressure plate resting on the sample (e.g., carpet or felt pad). In effect, the sample is sandwiched between the vibrator and a rigid support. Similar results were observed with regard to the amplitude dependence of the resonance frequency, however, the shifts were smaller, due to the larger pressures. Overall, higher compression moduli were observed with higher pressures supporting again the theory of fibre slippage. For carpets the damping was independent of the amplitude but increased with an increase in amplitude in the case of felt pads. For both carpets and felt pads, lower damping was observed for increased pressures.

2.4 Vibratory Feeders

2.4.1 Introduction

Vibratory conveying of solid materials has been in use for a long time, some studies [Guthrie 65] even quote that, old civilisations such as the Greeks and Romans made use of these techniques. The principle is very simple in that a trough vibrating backwards and forwards causes objects on it, such as granular materials or solids, to slide and/or hop along it. Nowadays, the increasing use of automation in industry widely use vibratory conveying whenever an orienting, feeding or conveying system is needed. The various types of vibratory feeders can be classified according to a combination of these functions, but the vibratory bowl feeders in particular are by far the most versatile and used types of feeders. These devices are custom-designed for the orientation of single or small numbers of parts and rely on mechanical filters to reject parts in unwanted orientations. Despite their widespread use, vibratory feeders have several disadvantages; they have to be redesigned when the geometry of the part changes and they are quite noisy or may even damage fragile parts. The vibratory manipulator used for this thesis is of the 'in line'-type, which is mainly used for feeding.

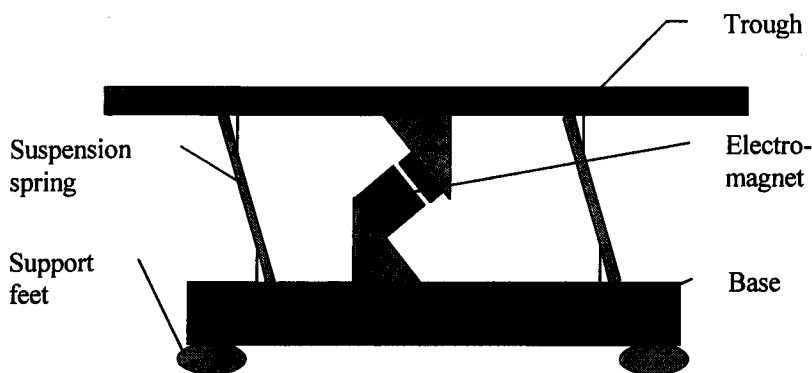


Figure 2.11. Conventional vibratory feeder

The basic configuration of a conventional vibratory feeder illustrated in Figure 2.11 consists of a trough or pan that is attached to a heavy base via a set of springs constraining the trough to move relative to the base. Various types of feeders can be distinguished according to the type of suspension (e.g., rubber, pneumatic or spring steel) or the kind of driving mechanism. For the majority of small mass units, the power is applied to the system by an alternating electromagnet but other various mechanical crank systems and rotating unbalancing systems have been used successfully [Parameswaran 79]. Generally, a single periodic sine wave is used though also non-sinusoidal excitations, proved to give considerably larger conveying velocities, can be applied [Okabe 85], [Srinath 88]. Five main factors affecting the performance of a vibratory conveyor are listed below:

- the frequency of vibration,
- the amplitude of vibration,
- the angle between the plane of the trough and the plane of vibration,

- the inclination of the trough to the horizontal, and
- the dynamic coefficient of friction between the parts and the trough.

At first, it is useful, before looking into the mechanical analysis, to visualise the behaviour of an object that is placed on a vibratory table. Assuming the forcing agency provides a very low amplitude force to the table, the frictional force is likely to keep the object in the same relative position. So, there will be no net movement and the object is riding (*Ride*) on the table. However, increasing the driving force with a normal acceleration lower than the gravity of the components may initiate forward sliding (*Upwards*) along the plate. Further increasing the force amplitude, greater than the gravitational force of the objects, will cause the objects to lose contact with the table surface and travel in free flight for some part of the cycle. After landing the objects will either stay stationary or slide forward but also sliding backwards (*Backwards*), is possible. A combination of these four modes can designate a particular motion of the objects dependent on the driving conditions of the table. Gaberson [Gaberson 67] anticipated as many as 21 theoretically different solution forms. Although non-contact conveying is considered the most efficient operating condition, it is thought that in the case of vibrating textiles, this mode of vibrating is virtually excluded due to the low transverse stiffness of the fabric. Therefore, only the three possible modes of component motion during one cycle in continuous contact with the table (no free flight) are shown in a flow diagram in Figure 2.12.

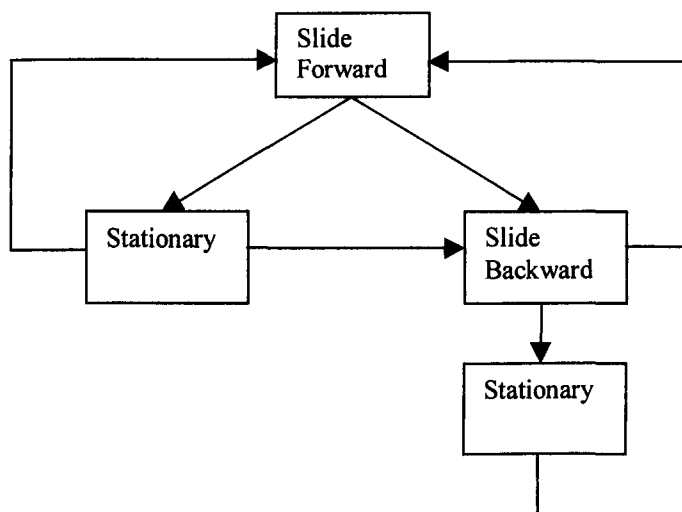


Figure 2.12. Flow diagram of various component movements for continuous conveying [Redford 67]

2.4.2 Basic Conveying Theory

In the above section (2.4.1), it has been shown that a vibratory feeder can work in two main modes, namely the contact mode or the flight mode. The theoretical analysis for both operating modes differs slightly. The flight mode analysis has to account for the impact at the end of the flight cycle, which might change the coefficient of friction due to the high pressures at impact [Gaberson 72]. However, consideration will be given only to the motion of a non-rolling particle in flight free mode [Böttcher 58], [Booth 63] and [Nedderman 90].

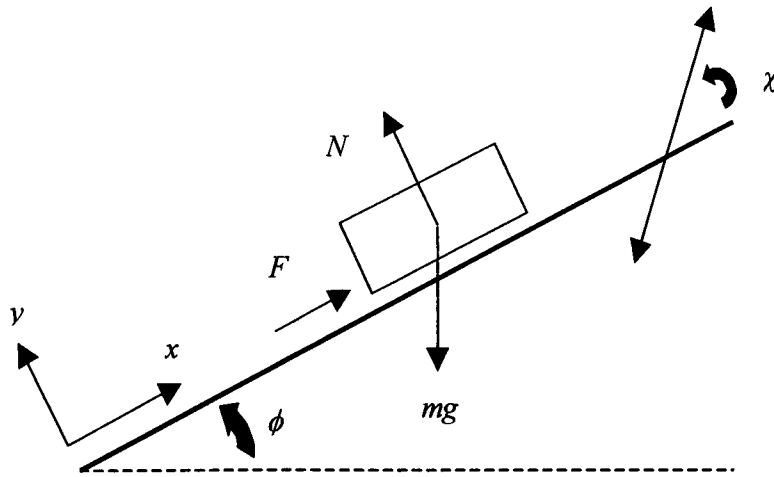


Figure 2.13. The Co-ordinate system and angles

Figure 2.13 shows the co-ordinate system used to describe the motion of the conveying surface and the particle, the x-axis is directed along the surface and the y-axis is perpendicular to it. The plane track of the conveyor is inclined at an angle, ϕ , to the horizontal and vibrates sinusoidally with an amplitude, u_0 , and angular velocity, ω , in a direction inclined at χ to the normal of the track. Thus any point on the conveyor surface moves in a plane inclined at an angle $(\phi + \chi)$ to the horizontal. It is, however, necessary to prevent the object from just sliding down, for that reason the angle of the table inclination, ϕ , must be less than the angle of repose ($\tan^{-1} \mu_s$, see 2.1.6). For the analysis, it is presumed that the coefficient of friction remains constant. Further, it is assumed that the motion of the track is unaffected by the presence of the component, that the motion of the component is independent of its shape, and that any air resistance to the component motion is negligible. Denoting by X and Y the co-ordinates of any particular point on the table surface, the displacement of the table may be written as:

$$X = u_0 \sin(\omega t) \cos \chi \quad Y = u_0 \sin(\omega t) \sin \chi \quad (2.33)$$

If the particle maintains contact with the table then the particle's y-velocity, \dot{y} , and acceleration, \ddot{y} , will be equal to the y-velocity and y-acceleration of the table, respectively. Hence, the dynamic force equilibrium of the particle (with co-ordinates x, y) in the y-direction yields:

$$m\ddot{y} = N - mg \cos \phi \quad (2.34)$$

Contact between the particle and the track will be lost if the normal force, N , becomes zero and hence for a flight free conveying:

$$g \cos \phi > u_0 \omega^2 \sin \chi \quad (2.35)$$

Note that the normal force can not be negative. The ratio of the two components of Equation (2.35) is called the 'throw-number' [Böttcher 58] and is an important factor in the non-contact analysis to

determine the number of flights per cycle [Ahrens 83]. As mentioned previously in 2.4.1, three modes can be distinguished for the horizontal motion of the particle, specifically the forward slide (*Upwards*), the backward slide (*Backwards*) and the stationary mode (*Ride*). The direction of the tangential force, F , due to friction will decide the mode of operation as follows:

$$\begin{aligned} F &= \mu N && \text{when } x < X \text{ for slide (B)ackwards} \\ F &= -\mu N && \text{when } x > X \text{ for slide (U)pwards} \\ -\mu N &\leq F \leq \mu N && \text{when } x = X \text{ for ride (R)} \end{aligned} \quad (2.36)$$

Further, resolving the particle motion along the conveyor surface gives:

$$m\ddot{x} = F - mg \sin \phi \quad (2.37)$$

Thus, a given set of operating conditions (u_0 , ω , ϕ , and χ) will determine the complete motion and transition times of a mass with parameters m and μ throughout one cycle.

The above analysis assumed that the air resistance of the particle was negligible during the conveying though this is only true in the case of materials with a high permeability, K_p . Brickman [Brickman 63] assessed the air effect on bulk material in a standard atmosphere (ρ_0 air density at *S.T.P.*) and defined a factor, c_a , expressing the air damping during conveying as follows:

$$c_a = \frac{\rho_0 / \rho}{K_p \omega} \quad (2.38)$$

As can be seen from the above Equation (2.38), the material density, ρ , and the angular velocity, ω , of the conveyor have the same influence on the air damping. Consequently, a conveyed material with a large permeability (large K_p) will give a small damping which will hardly influence the objects' motions whereas an impermeable material causes large attenuation.

Finally, because of the importance of feeders in automated assembly several studies [Redford 66], [Okabe 85] and [Srinath 88] have searched for ways to increase the conveying speed of the material. Obviously, increasing the frequency and amplitude of the table will increase the conveying speed but the noise level will also increase. Some more specific adaptations have been made in the driving mechanism by introducing a phase shift between the normal and parallel component of the excitation force [Redford 66, 67], [Myagkov 67]. The experimental results indicated that by introducing an appropriate phase shift, high conveying velocities could be achieved which were virtually independent of the friction between the component and the track. Furthermore, Redford [Redford 66] found that the travel rate was inversely proportional to the vibration frequency. However, one disadvantage of an out-of-phase conveyor is the mechanical construction, which demands an individual motion of the track in both normal and parallel direction. Some other attempts

at improving the conveying rate are reducing the 'friction coefficient' by using bristled tracks for instance, which act as cantilever springs tossing the transported component in the proper direction [Mansour 75] [Okabe 80]. Both studies found an appreciable gain in velocity.

2.5 Summary

This chapter reviewed at first the present and past research on two crucial fabric parameters namely friction and lateral compression, followed next with the present status on vibration in textiles and finally concluded with a brief explanation on vibratory feeders. The first section on fabric friction showed that mainly friction has been investigated between individual fabric samples (fabric-fabric). Only five studies could be traced considering friction of fabric against non-fibrous materials. Unfortunately, all of these studies were using moderate to high normal force where this thesis will investigate friction under zero added normal force. Until now, also no numerically solvable model has been produced for fabric-non-fabric friction. On the other hand fabric-fabric friction has been successfully modelled as a function of the normal force by Wilson and is now generally accepted and verified. Furthermore, it has been shown that fabric friction is susceptible to many experimental parameters that will demand great care during tests.

Literature on compression in fabrics has revealed that a woven fabric structure can be abstracted in a three-layer model consisting of an inner core and two outer layers at each face containing the protruding surface fibres. With regard to physically modelling lateral compression of fabric, van Wyk's pressure-volume model is still largely dominating the field. However, several studies have since been performed to improve this theory, specifically in replacing the random fibre abstraction in van Wyk's original theory. In addition to van Wyk's theory, some other empirical and phenomenological models relating fabric thickness to pressure have been addressed. Compression tests are usually performed statically but dynamic investigations have shown large discrepancies between dynamic and static parameters.

However, research on dynamic fabric parameters is scarce mainly because of the difficulties in measuring and the complexity of the problem. Two different ways of excitation namely in plane and out of plane of the fabric have been discussed with the latter being most relevant for this thesis. The few studies on lateral excitation by Dunlop were performed again under normal force investigating carpets or felt pads. In spite of the enormous structural difference between carpets, felt pads and fabric the study points out an interesting fact that might also occur in fabric vibration. Dunlop found that the dynamic elasticity decreased with an increase in excitation amplitude and modelled this as a non-linear spring in a spring-damper mechanism. The damping in carpets, however, was found independent of the amplitude.

Finally considering that the dynamic tests in this thesis will be performed on a vibratory feeder, the last section of this chapter reports briefly their operation. Vibratory conveying of solids has already been used for a long time in automation and is therefore theoretically well established. The theoretical analysis showed that the objects could either stay in contact with the vibrating surface or

fly during some part of the cycle. However, it is speculated that the latter mechanism of free flight will not appear in fabric vibration due to the low transverse stiffness of fabric.

The review on fabric friction in 2.1.5 pointed out several influencing experimental factors, such as sliding speed and the number of traverses, which may affect the frictional behaviour. Many of these influencing factors need further research and verification against non-fibrous materials and are the subject of the following chapter.

3 Low Force Friction Characteristics of Fabric against Engineering Surfaces

When a fabric is sliding either over another fabric or over a solid surface, various parameters are influencing the frictional force as has been documented in the literature (section 2.1). These effects can be divided in two categories. On one hand, we have what could be called ‘invisible’ effects such as the number of traverses or history of the fabric and the environmental conditions where humidity plays an important role in the frictional process. Sometimes as a direct consequence of low humidities, static charges are developed which will increase the friction dramatically. On the other hand, there are the directly ‘visible’ influences such as the decrease of friction with an increasing normal pressure, the nature of the surface, which the fabric is sliding against, and the velocity of sliding. The last section of this chapter is dedicated to the stick-slip phenomenon, which can be regarded as a special type of friction only occurring at very low sliding speeds. All the above mentioned influential parameters will be discussed in a similar order in this chapter but first some details will be given about the instrumentation and experimental method used to measure the friction.

3.1 Instrumentation and Method

3.1.1 Friction Measuring Table

Any contacting method for measuring the friction as for example the KES-F tester [Kawabata 80] will influence the measurement however small the contacting pressure. In addition, all directly contacting methods only measure the friction locally where the stylus rubs over the surface hence a full picture of the friction can never be obtained. On the other hand, pilot measurements with the inclined plate method were found too erratic for unloaded samples. Besides, the method only reveals the static friction and does not allow velocity tests. Hence, the friction instrumentation used here, is based on Dreby’s principle [Dreby 43] (see 2.1.6) and does not experience any of the above mentioned disadvantages. The method tests friction without any normal force and under variable sliding speeds. A static (viz., non-moving) measuring device was preferred to a moving sensor, commonly used in Instron® testers, because of the very small forces that will be involved in the measurement. Any movement of the sensing device can cause unnecessary vibrations giving rise to erratic signals. In addition, the method does not need any pulleys or guides because the fabric sample is directly connected to the measuring device. Figure 3.1 pictures the main set-up, which comprises an X-Y table providing the shearing movement between the engineering surface and the fabric, and a ring dynamometer. A computer controls the table and logs the data.

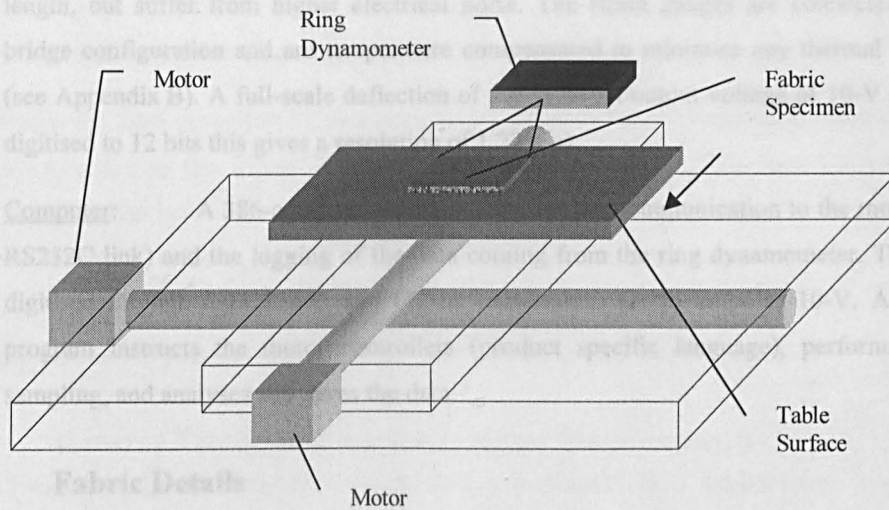


Figure 3.1. A sketch of the fabric friction measurement

1. **X-Y table:** The X-Y table consists of a movable rectangular surface (250 x 350 mm) to which different test surfaces can be attached easily. Three different test surfaces were chosen representing some commonly used materials in the garment automation industry. A pure aluminium surface was selected as a lightweight construction metal, a rubber surface, which is often used for conveyor belts, and a Formica surface that is covering many tabletops on sewing machines. Further details regarding the roughness of the three test surfaces can be found in Appendix C. Only one driving axis of the X-Y table is used for the tests. The table slides on camroller guides and is directly connected to a permanent magnet stepper motor via a 4-mm pitch leadscrew. Special precautions, both mechanical and control-wise, are needed to minimise vibrations caused by the stepper and the mechanical movements. On the mechanical side, vibrations are reduced by introducing a flexible shaft coupling connecting the stepper to the leadscrew. Furthermore, a rubber pad physically decouples the motor from the X-Y table, and the mass of the table is increased significantly by a 12.6-kg brass plate. For the control of the steppers, a MOSFET chopper regulated drive (DIGIPLAN PDX15-D) with micro stepping options is used. The micro stepping increases the motor resolution up to 4000 steps/rev and therefore a smoother rotation is obtained even at very low velocities (< 0.2 mm/s). The control is performed in open loop considering that there is no need for extreme accurate positioning (accuracy < 1mm). The reader is referred to Appendix B for further details on the X-Y table and the motor controllers.
2. **Ring dynamometer:** The ring dynamometer is constructed in-house from a spring steel ring (\varnothing 150 mm) with four single-axis strain gauges bonded at the mid length of the ring. This particular configuration of force sensor was chosen because of its high mechanical amplification. Further increase of the sensitivity was obtained by using semiconductor strain gauges instead of the more common resistive strain gauges. Semiconductor gauges have the largest gauge factor, defined as the relative change of resistivity with relative variation of

length, but suffer from higher electrical noise. The strain gauges are connected in a full bridge configuration and are temperature compensated to minimise any thermal elongation (see Appendix B). A full-scale deflection of 5-g gives an output voltage of 10-V (i.e., when digitised to 12 bits this gives a resolution of 1.22 mg).

3. **Computer:** A 386-computer is responsible for the communication to the motor (via an RS232C link) and the logging of the data coming from the ring dynamometer. The latter is digitised through a PC30AT card (12-bit conversion) set to unipolar 10-V. A PASCAL program instructs the motor controllers (product specific language), performs interrupt sampling, and analyses and saves the data.

3.1.2 Fabric Details

Three groups of fabrics are used in this investigation. The fabrics are grouped together according to the case study in subsequent sections of this chapter and successive chapters, and are coded to facilitate the comparison of results. A single capital letter with a number stands for a woven (or non-woven) sample pointing to the material, for example W for wool and P for polyester; the number is just a classification number. A double capital letter coding represents a knitted structure and always starts with the letter K first, followed by a letter and a number, again abbreviating the material of the sample and ranking the fabric respectively. The ranking, however, is slightly different than for woven materials, a single digit stands for a single knit stitch, for example KC1 which is a single cotton knit, a double digit stands for a rib stitch such as double-knits. A brief summary of the three fabric groups is given below but the reader is referred to Appendix A for more detail on the fabric properties.

The first group of fabrics (set 1) is a collection of six standard fabrics and is used throughout the full investigation of the thesis. The fabric samples encompass three woven and three knitted structures with a wide diversity of physical properties regarding their mass, thickness, and compressibility. The area density (at standard conditions, $20^{\circ}\pm 1^{\circ}\text{C}$, $65\pm 4\%$ r.h.) varies from 105 g/m^2 for a lightweight plain weave polyester (P1) to 517 g/m^2 for the heavyweight twill cotton (C1 denim). The group of fabrics also reflects a wide difference in surface properties such as smoothness, i.e., plain weave (P1), roughness due to the ribs in the twill of C1 and hairiness on a fleece knit (KC1). Regarding the material content, both natural (cotton, wool) and synthetic (polyester, acrylic) fibres are represented.

The second group of fabrics (set 2) is chosen deliberately to study the effect of humidity on friction (see 3.4) and therefore includes a wider variety of materials compared to set 1. This group now also includes a regenerated material (viscose rayon V1), which is chemically processed from cotton fibres, a knitted nylon sample, KN11, as synthetic material and a linen sample, L1, as extra natural fibres. The group further consists of a polyester plain weave, P2, a woollen even twill, W2, and three cotton samples, a single knit, KC5, a double knit, KC11, and a plain weave C2. Note that only one sample of the set 1 fabrics is included in this group, namely KC11. The area density (at 21°C

and 60% r.h.) of the set 2 fabrics varies from 118 g/m² for a single knit cotton (KC5) to 226 g/m² for the medium weight even weave linen (L1).

Finally, the third group (set 3) comprises seven specially selected fabrics samples each with a rather open structure so that a light beam can easily shine through it. This feature is necessary to measure the stick-slip behaviour in 3.10, which uses a totally new approach. The fabrics include a single-knit, two open rib knits, a gauze weave, two plain weaves and a non-woven sample. The area density (at standard conditions, 20±1°C, 65±4% r.h.) varies from 48.3 g/m² for the extreme lightweight non-woven polyamide (Pa1) to 197 g/m² for the knitted acrylic (KA3).

3.1.3 General Test Procedure for Friction Measurements

All tests on the friction-measuring table are performed in a similar way, except where otherwise stated. The fabrics are conditioned at standard testing atmosphere (20±1°C, 65±4% r.h.) for at least one day with the face resting upwards (fabrics are stored in wooden shelves). Note that the temperature and the relative humidity are out of bounds from the prescribed ASTM standard of 20±2°C and 65±2% r.h. (ASTM D1776-85). Most of the time a maximum variation of 2% on the relative humidity was not feasible because of the limitations of the air conditioning system at The University of Hull. All tests were performed in the same room where the fabrics were conditioned. During the full length of the friction tests, the air is ionised with a portable ionizer close to the table to prevent the fabric samples from becoming electrically charged (see 3.5).

Before the start of each friction test, the mass of the sample is accurately measured with an electronic balance (METTLER Toledo PB302, resolution ±0.01-g) and entered in the computer together with the fabric code. Next, the table velocity, acceleration and travelling distance together with the sampling rate are added into the program. The total number of samples necessary for the test is calculated from the sampling rate and the total run time. In case the maximum allowed number of samples (max. 7600) is exceeded, the user is asked to reduce either the total sampling time of the test or the sampling rate. The fabric specimen is then carefully connected to the ring dynamometer with a fine polyester thread and rested with the measuring face up on the cover plate of the force sensor. A keystroke starts the actual program and returns the X-Y table to its home position. When the table has come to a standstill, the fabric specimen is neatly placed on the table with the measuring face down as depicted in Figure 3.1. No stress is put on the connecting thread between the sample and the force sensor. A short measurement is taken to calibrate the zero level and offset the weight of the fibre attachment, followed by a dwell time of 30 s in accordance with ASTM D3334-80. After the dwell time has passed, the table (only one axis of the X-Y table) starts to move away from the sensor and the frictional force is logged by the computer. At the end of the sampling time, the frictional force trace is normalised to the dimensionless 'coefficient of friction', μ , based on the simple linear relationship, $F = \mu N$, between the frictional force and the normal force. In most cases, the normal force to consider is only the fabric's own weight. The program first searches for the highest peaks at the start of the friction trace and allocates this as the static friction. Next, the dynamic friction and ripple is calculated by averaging the friction trace starting from the static friction position up to the end of the

trace (see 3.1.4). Before terminating the test, the user can ask for a display on the screen and has the opportunity to save the data in either ASCII or MATLAB™ format.

Six tests in total are averaged to determine the friction coefficient ($\bar{\mu}$) for each fabric type against an engineering surface at specific conditions of velocity and humidity. The standard error of the measurements of six tests (i.e., $\sigma_{\bar{\mu}}$, error on the error) is then within 11% of the accurate 68% confidence limit. A more detailed explanation for this particularly selected sample size can be found in Appendix D together with some statistical calculations and formulas. For set 1 fabrics both the warp (wale) and the weft (course) direction are tested. Hence, in order to speed up the measurements two sets of six fabric specimens, one for warp and one for weft testing, are available. The fabric specimens are thus re-used in different tests because the low force tests are non-destructive (e.g., no attrition). A relaxation period of one full day is used between each test so that any possible surface alignment can recover. However, a fresh sample of set 1 fabrics was used in the repetitive transverse tests (see 3.3). For set 2 fabrics, tested under various humidity conditions (3.4), only one group of six fabric specimens is examined in one principal direction. Tests on set 3 fabrics contain three specimen of each fabric type. Both set 1 and set 2 fabric specimens have a dimension of 100-mm square, set 3 specimens are oblong (305 x 60 mm) in order to make the stick-slip behaviour more prominent.

3.1.4 Expression of Results

The frictional parameters enumerated in this section are determined in accordance with the procedures of several other investigators, namely: Hearle and Husain [Hearle 71], Carr *et al.* [Carr 88], and Ajayi [Ajayi 92a]. Figure 3.2 illustrates a typical friction trace of KC11 against the aluminium surface indicating the various defined parameters below. Note that the rising of the curve in Figure 3.2 and subsequent figures does not represent the friction coefficient since the fabric only starts to move from the static friction onwards. Further, due to the low fabric forces involved any forces required for the acceleration of the fabric are insignificantly small and therefore not visible in the traces.

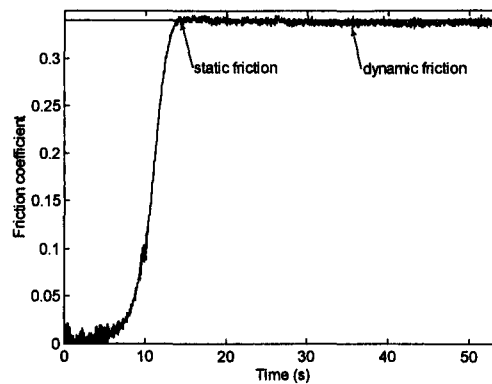


Figure 3.2. Friction trace for KC11 fabric (wale direction) against the aluminium surface.

Standard conditions, velocity: 0.5 mm/s, mass sample: 1.78 g, area of the sample: 1 dm², static friction coefficient, μ_s : 0.341, dynamic friction coefficient, μ_d : 0.339, dynamic ripple, σ_{rip} : 0.004

1. **Frictional coefficients:** Both static and dynamic frictions were determined directly from the friction trace. The static friction coefficient, μ_s , is taken as the highest peak at the beginning of the motion whereas the mean of the peaks and troughs is regarded as an estimation of the dynamic (kinetic) friction coefficient μ_d . The discrimination, however, between the static and dynamic friction for low-pressure tests is not always very clear, especially at higher velocities. The dynamic friction coefficient is indicated in Figure 3.2 by the straight line through the pulses of the friction trace and calculated as follows:

$$\mu_d = \frac{\sum_1^s \mu_i}{s} \quad (3.1)$$

The number of samples μ_i , starting from the static friction reading, is denoted by s .

2. **Dynamic ripple (σ_{rip}):** This is a measure of the oscillations (i.e., standard deviation) of the kinetic value, μ_i , above and below the mean value, μ_d (dynamic friction coefficient). The dynamic ripple is calculated as follows:

$$\sigma_{rip} = \sqrt{\frac{\sum_1^s (\mu_i - \mu_d)^2}{s}} \quad (3.2)$$

3.2 Surface Roughness

3.2.1 Instrumentation and Measuring Method

As seen in section (2.1.6), surface roughness of a fabric can be measured in two ways, either using a contacting method such as in the KES-F test (KES-FB4) or a non-contacting method. The non-contact laser method has here been chosen to profile the surface because of the much higher accuracy of the method and the fact that no pressure is applied on the sample. After all, the friction tests will be performed mainly in unloaded conditions.

The test arrangement seen in Figure 3.3 consists of a laser sensor that is firmly mounted on a stand pointing downwards onto the slowly moving surface of a piece of fabric which is placed on the X-Y table. The laser (further used for vibration tests in chapter 5) is using the triangulation technique (see Appendix B) to measure the distance between itself and the fabric surface. Triangulation has the advantage of not being susceptible to colour changes or patterns providing that sufficient light is reflected back from the surface and is therefore well suited for fabric testing. A beam of red light (675-nm) with a 300- μ m diameter spot is projected from a laser diode onto the surface of the fabric. Part of the emitted light is scattered back onto a photosensitive detector, which then signals the position of the image from it. As the reflected light strikes the detector at different locations depending on its distance from the fabric surface, the signal strength indicating the location of the reflected light is converted to distance. The sensor used for the present work (LD1605-4 by $\mu\epsilon\text{®}$) is capable of measuring a distance range of 4 mm with a resolution of 1- μ m. Further technical

specification of the laser sensor can be found in Appendix B. Bearing in mind that the total measuring range corresponds to a linear voltage output of ± 10 V, a 12 bit A/D conversion (i.e., PC30AT-card) as used in these measurements will have a 5 mV resolution. Hence, the minimum detectable analog voltage is identical to the resolution of the laser sensor (i.e., 5-mV represents 1 μm).

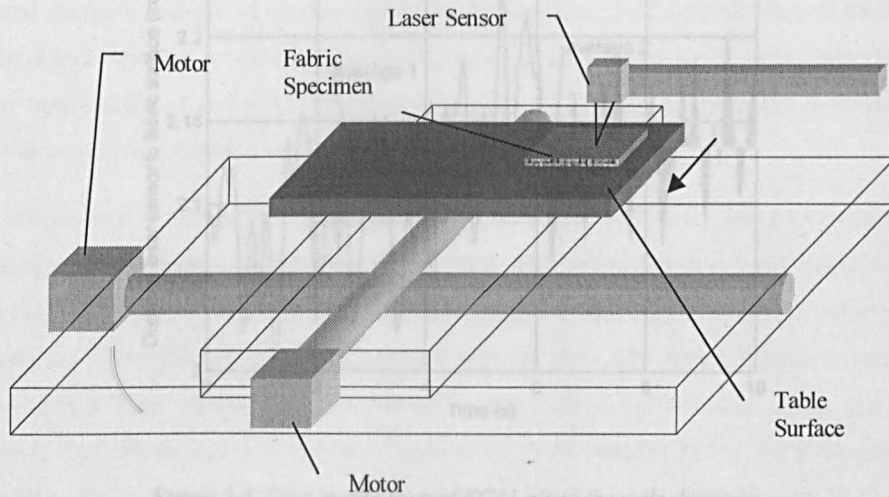


Figure 3.3. A sketch of the surface roughness test

Fabric heights of the six standard (set 1) samples are measured six times in the forward X-direction by the laser sensor over a 1-cm length, at Y-step size of 0.1 mm. The fabrics are placed stress free on the rubber surface of the X-Y table with the face or right side of the fabric upwards. The table is moved then at a velocity of 1 mm/s while the voltage signal from the laser sensor is sampled at a rate of 500 Hz, giving 5000 samples in total for each pass in the X-direction. Next, whilst keeping the fabric untouched, the table moves back to its home position (in the X-direction) and shifts 100-microns in the Y-position ready for the next line scan. After a full test of six scans in one fabric direction, the fabric is turned 90° to face along the other principal direction. Thus, all fabric samples are tested six times in the warp (wale) direction and six times in the weft (course).

3.2.2 Results

The surface roughness (*SMD*) of a fabric is in accordance with the KES-FB4 test [Kawabata 80], calculated from its height profile, h_i , obtained by the laser sensor at s different points and is defined as the mean deviation, which is given as follows:

$$SMD = \frac{1}{s} \sum_{i=1}^s |h_i - \bar{h}| \quad (3.3)$$

with \bar{h} representing the mean value of the heights. In order to compensate for any undulations of the fabric, two mean heights and the local roughness based on them are calculated for 4-mm subdivisions;

(SMD_1) was calculated between 2-6 mm and (SMD_2) between 6-10 mm as used by Ramgulam *et al.* [Ramgulam 93] (see Figure 3.4). The filled area in Figure 3.4 between the mean value and the actual surface height of the second subdivision represents graphically the numerator of Equation (3.3).

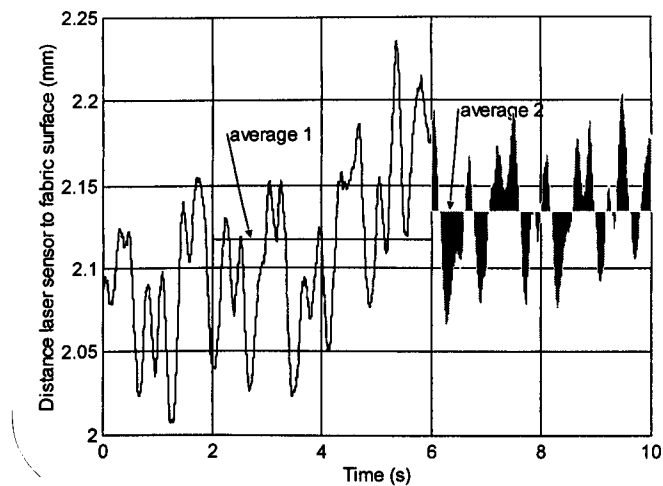


Figure 3.4. First profile scan of KC11 along the wale direction

Scanning the table in an identical way as the fabrics produced an average surface roughness of 7-microns indicating a smooth table surface. Hence, the table will not superimpose any profile on the fabric. As a comparison, the rubber surface has also been measured with a stylus, giving however, a ten times lower surface roughness ($PRa = 0.7 \mu m$). This shows, as has been detected for fabrics [Ramgulam 93], that a contact method gives a smaller roughness figure than a non-contacting method. More details on the method and results of scanning the rubber surface (and the other engineering surfaces) can be found in Appendix C.

Twelve roughness values thus obtained from Equation (3.3) are averaged to give the mean roughness of the fabric along each principal direction (see Table 3-1).

Table 3-1. Mean roughness values of the six standard samples (mm)

Fabric code	Warp (Wale)	Weft (Course)
C1	0.086	0.105
P1	0.016	0.026
W1	0.077	0.048
KC1	0.071	0.064
KC11	0.027	0.034
KA11	0.079	0.073

A first glimpse at Table 3-1 shows that all roughness figures are of the same order of magnitude, with the lowest values for P1 and the highest for C1. This result is expected because the polyester fabric P1 has a high sett (i.e., large number of threads/cm in both warp and weft, see Appendix A), which gives a smooth surface. The denim cotton C1, on the other hand, has a distinct diagonal ribbed pattern on the face surface, characteristic for a twill weave, which gives a rougher surface. KC1 and W1 have both fuzzed surfaces and give a similar roughness although the fabrics differ in structure; KC1 is a fleece single knit whereas W1 is a woollen twill. A rather unexpected result is the large difference in roughness between KC11 and KA11 for both directions. KC11 and KA11 differ in material but are very similar in structure only the course count is smaller for KA11.

A closer look at the results for the woven materials reveals that C1 and P1 have a remarkably rougher surface in the weft direction than in the warp. This effect has also been objectively verified when rubbing a finger over the surface in the respective directions. Similar observations were made by Ramgulam *et al.* [Ramgulam 93] who found that 90% of their 650 tested fabrics showed a higher roughness with a laser sensor along the warp (in the weft direction) than along the weft. This anisotropy is most likely due to the greater number of yarns running in the warp direction of most fabrics, which would explain why the surface roughness for W1 is reversed. Sample W1 has a higher roughness in the warp direction because of a higher weft sett. With regard to the knitted samples, no clear distinction is visible between the roughness values in the principal directions.

In general, one can conclude that the surface test gives a reasonable discrimination between a rough and a smooth sample (factor five between P1-C1). It remains now to be seen whether the roughness of the surface will have a notable effect on the friction between a fabric and a non-fabric surface. The surface roughness test, however, did not separate a fuzzed surface from an ordinary surface; both roughness values of KC1 and KA11 were found identical. This shortcoming is likely caused by the averaging of the laser spot (300 μm). Nevertheless, these protruding hairs might have an influence on the friction as will be investigated in the next section.

3.3 Influence of the Number of Traverses

As shown in Table 3-3 successive traverses of the fabrics over the aluminium table (ionised) with no relaxation time between the individual tests caused a 3 to 15% increase in the dynamic friction for all fabrics but one. Fabric C1, which has a ribbed non-hairy surface, shows a decrease in friction in the warp direction while remaining constant in the weft. For all other fabrics, it is postulated that an alignment effect gradually increases the contact area, which as a result increases the frictional force. This finding is however opposite to what happens in fabric-fabric friction. Several investigators [Dreby 43], [Wilson 63], [Carr 88] and [Ajayi 92a] have reported a decrease in friction with an increase in traverses. It was proposed by Ajayi [Ajayi 92a] that the higher friction measured initially between fresh samples was caused by intermeshing of the surface fibres which, after repeated sliding, then gradually aligned in the sliding direction consequently reducing the friction. However, an intermeshing of fibres is in our case impossible regarding that the fabric is slid over a non-fibrous material. Rather the increase in friction must be caused by an aligning which is proven when the

samples are reversed through 180° as in test 11 in Table 3-3. A sudden dip in friction between test 10 and 11 is found for all 'hairy' fabrics (not C1 and P1). Furthermore, KC1, KC11 and KA11 display a large dynamic ripple, σ_{rip} , for the first test, which indicates a more fluctuating irregular movement. Increasing the number of consecutive slides gradually polishes the fabric surface resulting in a more smooth motion and a smaller ripple value. The polyester sample P1 is rather an exception, in that both the coefficient of friction and the dynamic ripple keep increasing in spite the fact that this fabric has the lowest surface roughness (Table 3-1) of all samples.

Hence, from the above results, it is further clear that one has to take care when testing the friction successively on the same specimens. Nearly all samples have shown a serious increase in friction after ten tests therefore, all specimens will have to relax (i.e., not be used for any test) for at least one day before being used in another test. To prove this, three samples of KC11 have been tested over a period. One specimen has been tested every day, a second specimen every odd day and a third and last specimen, at the beginning and end of the test. The results tabulated in Table 3-2 evidence that a one-day relaxation period is sufficient for the test fabrics.

Table 3-2. Dynamic friction coefficient of KC11 measured over a 5 days period

	Specimen 1		Specimen 2		Specimen 3	
	μ_d	σ_{rip}	μ_d	σ_{rip}	μ_d	σ_{rip}
Day 1	0.384	0.003	0.385	0.002	0.392	0.003
Day 2	0.384	0.003				
Day 3	0.380	0.003	0.384	0.003		
Day 4	0.397	0.005				
Day 5	0.390	0.004	0.384	0.004	0.396	0.007

Velocity: 1-mm/s, aluminium surface, tested in the wale direction

Furthermore, some remarkable conclusions can now be drawn from Figure 3.5 if we compare the results from the surface roughness tests in the previous section (3.2.2) with the friction results from this section. A first examination of Figure 3.5 shows that all knitted samples have a higher dynamic friction against aluminium than the woven samples. In addition, an inverse proportional relation is visible between the surface roughness of the fabric and its dynamic friction. For example, fabric C1 has been measured as the roughest surface from all specimens and consequently resulted in the lowest coefficient of friction. On the other hand, fabric P1 was found to have the smoothest surface but this fabric did not give the highest frictional resistance; the highest friction coefficient is found for fabric KC11, which had the second smallest surface roughness. Furthermore, the difference in friction in the principal directions is here not as clear as for the surface roughness tests, only the friction for all the knitted fabrics is significantly higher in the wale direction than in the course.

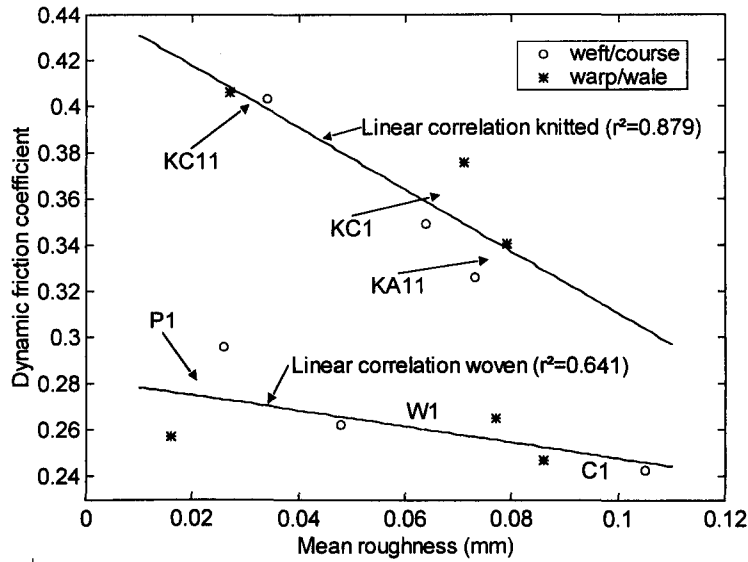


Figure 3.5. Scatter plot of roughness as a function of dynamic friction for set 1 fabrics

A linear regression (least squares) of the form $\mu_d = \alpha_1 \overline{SMD} + \alpha_2$ indicates the trend between the friction coefficient and the roughness with $\alpha_1 = -0.34$, $\alpha_2 = 0.28$ for woven structures and $\alpha_1 = -1.34$, $\alpha_2 = 0.44$ for knitted structures

Thus, in general, the smoother the fabric's surface the higher the friction will be. Yet, the fabric roughness is not the only determining factor. However, ranking the friction coefficient according to the content material is unfortunately not possible in our case considering that the structure of the samples in the test is not identical. For example, both cotton samples C1 and KC11 have a very different friction coefficient (C1 $\mu_d = 0.247$, KC11 $\mu_d = 0.406$).

Until now, all samples were tested under standard conditions of temperature and humidity but as will be seen in the next section, changing these environmental conditions has a serious influence on the frictional behaviour of fabrics.

Table 3-3. The effect of the number of traverses on fabric friction

Fabric code		Warp/Wale						Weft/Course					
		1	5	10	11*	% ₁₋₁₀	Trend	1	5	10	11*	% ₁₋₁₀	Trend
C1	μ_d	0.247	0.246	0.243	0.240	-2	↓	0.243	0.247	0.246	0.251	1	~
	σ_{rip}	0.006	0.008	0.008	0.008			0.007	0.008	0.007	0.009		
P1	μ_d	0.257	0.277	0.283	0.287	10	↑	0.296	0.318	0.319	0.322	8	↑
	σ_{rip}	0.006	0.007	0.008	0.011			0.005	0.006	0.007	0.009		
W1	μ_d	0.265	0.277	0.291	0.283	10	↑	0.262	0.279	0.289	0.284	10	↑
	σ_{rip}	0.002	0.002	0.008	0.004			0.003	0.004	0.003	0.005		
KC1	μ_d	0.376	0.407	0.412	0.392	9	↑	0.349	0.373	0.361	0.346	3	↑
	σ_{rip}	0.008	0.005	0.006	0.005			0.005	0.003	0.005	0.005		
KC11	μ_d	0.406	0.434	0.439	0.410	8	↑	0.403	0.424	0.425	0.410	6	~
	σ_{rip}	0.012	0.008	0.005	0.007			0.010	0.005	0.005	0.005		
KA11	μ_d	0.341	0.386	0.393	0.373	15	↑	0.326	0.354	0.366	0.357	12	↑
	σ_{rip}	0.009	0.003	0.005	0.003			0.009	0.005	0.003	0.004		

Trend: upwards ↑, downwards ↓, fluctuating ~, * test 11 is turned 180° end-to-end

Standard conditions, velocity: 1 mm/s, aluminium surface, sampling frequency: 75 Hz, sample area: 1 dm²

3.4 Influence of the Relative Humidity

The study on the influence of humidity on friction in fabrics is approached in two ways. First, one almost dry specimen of each fabric is placed in a standard environment and friction testing is carried out in time to find the rate of fabric conditioning. Secondly, the friction coefficient of six specimens is measured and averaged at various humidities. The friction measurements start with dry fabrics, which are then stepwise increased in humidity by 10% r.h. up to a maximum humidity of 87% r.h. followed by a decrease again to 0% r.h. Any hysteresis effect present will be revealed in this test. The experiments were limited to a maximum humidity of 87% r.h., not only because of the restrictions of the air conditioning but also because of the increasing experimental difficulty near saturation. All tests have been completed in an infinite atmosphere of the required conditions, no forced conditioning or ventilation has been used and the temperature remained $20^{\circ}\pm 1^{\circ}\text{C}$ for all humidities.

All humidity tests are performed on set 2 fabrics (Appendix A) against the aluminium surface. The specimens are tested only in the warp (wale) direction, and are all subjected to the same sliding velocity of 1-mm/s, and sampled at 75 Hz.

For the environmental experiments, dried specimens were required to start with. However, reducing the humidity in the laboratory to an absolute minimum is not sufficient. Dry fabric samples can be obtained in two ways either by exposing the fabric to a chemical drying agent such as phosphorus pentoxide or simply by drying the fabric in an oven [Morton 97]. Enclosing the fabric specimen with a drying agent in a container is the most accurate technique because the temperature of the specimen is kept constant and therefore other changes, apart from the moisture, are not likely to occur. This method, however, has the disadvantage of being extremely slow. Therefore, all samples for this test have been oven dried at about 110°C for one hour [Cookson 91]. The raising of the air temperature lowers the relative humidity since the saturation humidity increases enormously, though the absolute humidity of the air in the oven changes very little. Hence, the relative humidity in the oven can never be zero. For example, if the air outside the oven has a humidity of 50% r.h. at 20°C , heating the oven to 110°C will create a humidity of 0.8% r.h. in the oven. The moisture that is left in the fabric is known as the residual regain and is regarded as an inherent source of error. Furthermore, heating the fabric specimens may also remove substances other than water such as oils or wax and could even cause some geometrical changes in the specimen (e.g., shrinkage) [Cookson 91].

3.4.1 The Rate of Friction Change from Dry to Standard Conditions

The specific test procedure is as follows; an oven-dried specimen at near zero humidity is taken out the oven and brought into the standard conditioned laboratory ($20^{\circ}\pm 1^{\circ}\text{C}$, $65\pm 4\%$ r.h.), weighed and friction tested as the time starts counting. Next, the weighing and testing are repeated six times while the elapsed time between each friction measurement is registered (total experimental time is 90 min.).

In essence, when a mass of fibrous material is exposed to a new environmental condition the changes are passed in two waves of diffusion, one for the heat conduction and one for the moisture change [Morton 97]. Both diffusions, however, are strongly coupled for hydrophilic textile materials. Therefore, in fact, two combinations of both waves will travel through the material but each wave at a different speed with the slowest wave almost entirely determining the transmission of moisture (at constant ambient temperature). A detailed mathematical calculation of the conditioning rates of the fabrics, however, is beyond the scope of this thesis [Crank 49] but the change of regain for the fabrics will roughly follow an exponential pattern [Morton 97]. Hence, a similar exponential increase in the dynamic friction coefficient with time is observed as shown for example in Figure 3.6 for KC11. A similar picture is found for all other fabric samples except for P2. The polyester sample, P2, is more or less a hydrophobic material, and therefore neither the regain nor the friction changed in between the 0% to 65% r.h. humidity range.

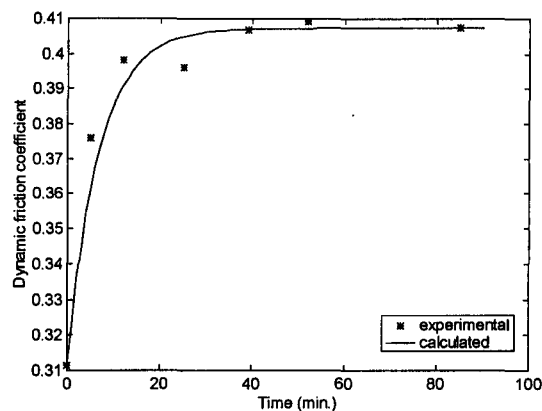


Figure 3.6. Variation of the dynamic friction for KC11 caused by a sudden humidity change from 0% to 65% r.h. as a function of time

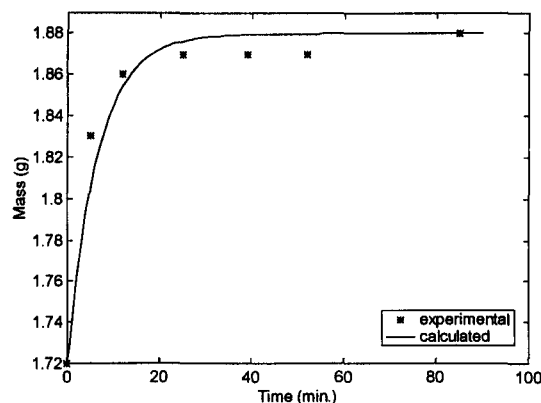


Figure 3.7. Variation of the mass of KC11 caused by a sudden humidity change from 0% to 65% r.h. as a function of time

Laboratory at standard conditions, velocity: 1 mm/s, aluminium surface, weight (0% r.h.): 1.72 g, weight (65% r.h.): 1.88 g, tested in the wale direction

Thus, theoretically a given proportion of the total change in friction between 0% and 65% r.h. will always take the same time irrespective of the magnitude of the total change. Under this condition we can write:

$$\frac{d\mu}{dt} \propto \mu_{65\%} - \mu$$

$$\frac{d\mu}{\mu_{65\%} - \mu} = \frac{dt}{\xi} \quad (3.4)$$

On integrating, and assuming as initial condition the friction at $t=0$ to be the friction for a dry fabric ($\mu_{0\%}$), this gives:

$$\ln(\mu_{65\%} - \mu) = \frac{-t}{\xi} + \ln(\mu_{65\%} - \mu_{0\%}) \quad (3.5)$$

Equation (3.5) leads eventually to:

$$\mu = \mu_{65\%} \left(1 - e^{-t/\xi}\right) + \mu_{0\%} \left(e^{-t/\xi}\right) \quad (3.6)$$

Using now a least squares procedure on Equation (3.6) gives the time constant ξ which best fits the experimental points for every fabric type. At $t = \xi$, 63% of the total change will be completed. A similar procedure can also be followed for the change in mass with time as seen in Figure 3.7. Both time constants are listed in Table 3-4 below.

Table 3-4. Time constants of friction and mass for a sudden humidity change

Fabric code	ξ for friction (min.)	ξ for mass (min.)	Increase (%) in μ_d between 0% to 65% r.h.	Increase (%) in mass between 0% to 65% r.h.
C2	5.2	6.3	17.6	4.8
KC5	3.2	9.3	21.7	4.4
KC11	6.8	6.6	30.8	9.3
V1	6.0	9.0	22.4	10.2
W2	10.3	10.0	9.5	10.6
L1	9.0	9.0	26.1	7.4
P2	-	-	-	-
KN11	6.4	7.3	22.1	10.2

From Table 3-4, it can be seen that all time constants are in the order of several minutes. This is reasonably fast compared to the one-hour conditioning for pile fabrics found by Nishimatsu and Sawaki [Nishimatsu 84b]. However, they conditioned the fabrics up to 90% r.h., which might explain this large conditioning time. Furthermore, there is also not a great difference between the time for the mass of the samples to increase and the rate of friction change. However, it is hard to make any conclusions based on the comparison of individual specimens regarding the differences in structure and geometry, but one can see that the woollen and linen sample W2 and L1 have the slowest increase in friction. The most striking result in Table 3-4 is the enormous difference in percentage increase between the mass of a specimen and its rise in friction. In nearly all fabrics, except W2, the friction increased far more compared to the mass, up to even 300% for KC11 (30.8% increase in friction for a 9.3% increase in mass). This table also indicates that the increase of mass with humidity is non-linear to the increase of frictional force with humidity. In other words, the change in mass is not the only varying parameter when the humidity changes. The water absorption (or desorption) from the air will have a direct implication on the geometry of the specimens.

When fibres absorb water, their dimensions are changed, axial and transversal swelling occur. As would be expected this hygral expansion will, in spite of the fabric structure, vary between the materials in much the same way as the regain (Figure 2.6): the fibres that absorb most water swell to the greatest extent. One exception is that cotton and viscose rayon have a larger transverse swelling than wool whereas wool normally has the highest regain of all fibre materials. However, the extension of fibres is not isotropic, most textile materials apart from nylon have a predominant transverse swelling which will cause the fibres and yarns to straighten [Morton 97]. This diametrical growth will have severe consequences in the dimensional stability of woven and knitted structures. The extension of the yarn will only continue until the interyarn forces (i.e., stress) at the crossing point become too high to allow any further straightening. A further swelling of the yarns can then only be accommodated if the yarn crimp decreases, which results in an overall extension in both warp and weft of the fabric and a minimisation of the strain energy in the fabric. A reduction in the yarn crimp will also induce a reduction in the fabric thickness. Furthermore, the porosity of the fabric decreases significantly [Wehner 87] and the surface area will become more smooth (see Figure 3.8). Consequently, an increase in surface contact between the fabric and the sliding surface should result in an increase in friction. The above explanation, however, remains hypothetical considering that no measurements were taken with regard to dimensional changes. In addition, also the shear strength (see Equation (2.8)) between the fabric and the sliding surface might be affected by the humidity change, but the author could not trace any information regarding this. In the case of hydrophobic materials, a water film most likely adheres to the fibres at higher moisture levels to act as a kind of 'lubricant' which consequently changes the shear strength between the fabric and the sliding surface.

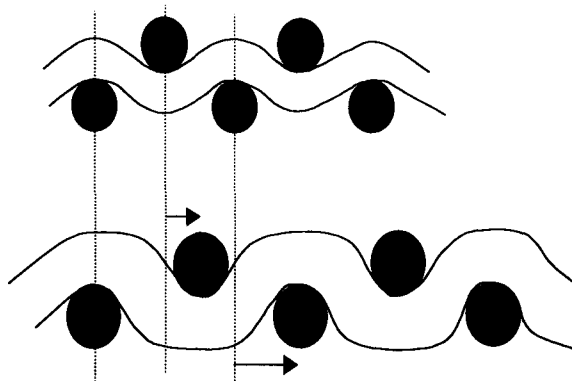


Figure 3.8. Diagrammatic representation of cross-sectional yarn swelling with increasing humidity

The above tests only showed the rate of friction change from dry conditions to a 65% relative humidity though the friction for a specific humidity level cannot be extracted from these experiments. Further, in the literature review it was shown that the regain has a hysteresis, which most likely will affect the friction. Both questions are the subject of the next section where the fabric samples will be tested at various humidities.

3.4.2 The Variation of Friction with Absorption and Desorption of Moisture

The friction and mass of the samples are measured at seven humidity levels over a period of 21 days. All specimens are conditioned for at least 24 hours in order to relax (directionality effect see 3.3) and to allow the lab to attain and operate at the new conditions. The test cycle is started again with oven-dried specimens (3.4.1 above) which are tested at a minimum lab humidity of 40% r.h. and further stepwise increased by 10% r.h. for each measurement until a maximum humidity of 87% r.h. A similar procedure is followed for a decrease in humidity (desorption). Finally, the tests finish with drying the samples in the oven and measuring their corresponding friction. First, we will discuss the regain or variation in mass with humidity and secondly, the influence this has on the friction together with other factors, caused by the humidity variation.

The amount of water absorbed or desorbed in a fabric sample can be expressed as a percentage increase in the fabric mass already known as the regain:

$$\text{regain} = \frac{\text{mass of absorbed water in specimen}}{\text{mass of dry specimen}} * 100\%$$

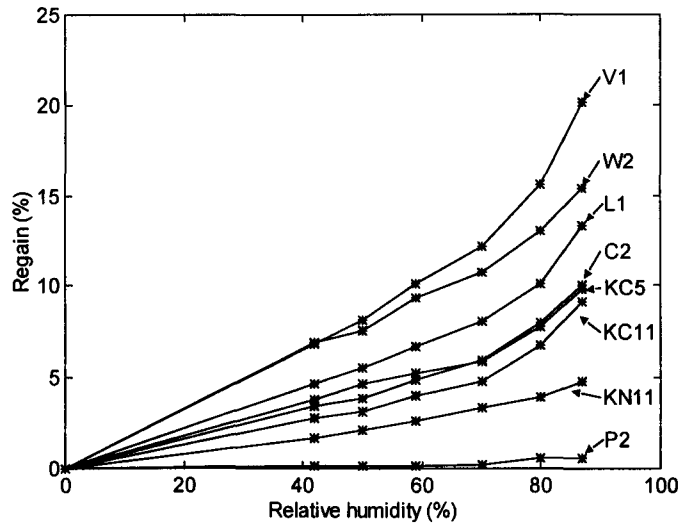


Figure 3.9. Relative water absorbency for set 2 fabrics

Figure 3.9 shows that all natural fibre samples in the tests experience the largest regain as expected whereas the man-made materials as for example P2 and KN11 have the lowest regain. The three cotton samples, C2, KC5 and KC11 have a very similar absorbency, the small differences between the samples are possibly due to the variations in structure or the type of cotton (origin or process, e.g., mercerization). One disagreement compared with Figure 2.6 is that the viscose sample, V1, has the largest regain, and not the woollen specimen W2, though this could again be due to some structural difference in the samples. Generally, viscose is very absorbent and although it is mainly processed from cotton, its regain is always higher than for cotton.

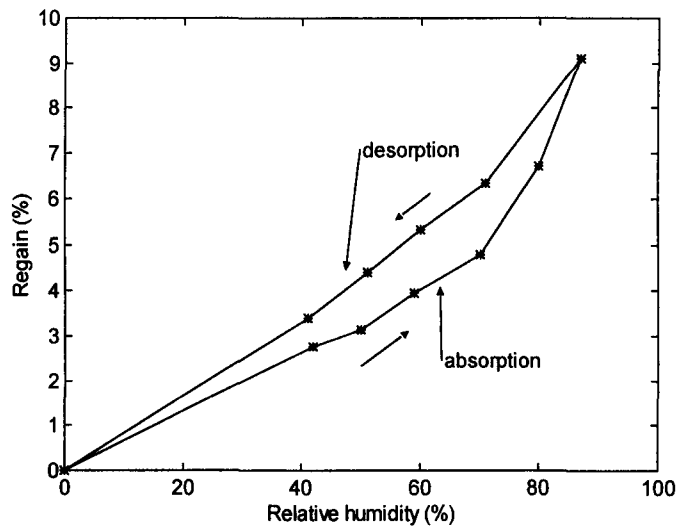


Figure 3.10. Hysteresis effect of the regain for KC11

Furthermore, as mentioned in the literature review (section 2.1.5), a hysteresis is observed in the relationship between the regain of textile materials and the relative humidity of the atmosphere.

The curves usually have a sigmoidal shape with a rapid increase in regain at low humidities, followed by a 'linear' portion, and then again towards higher humidities a steeper increase. However, the theoretical steep increase of regain for lower humidities is not so clear in Figure 3.10 for KC11 because of the lack of data between 0% and 40% r.h. Thus, two specimens of an identical fabric can have a different regain dependent on their history. The bottom curve of Figure 3.10, commonly called the absorption isotherm, plots the regain for successively higher humidities of a specimen initially bone dry. The upmost curve or desorption isotherm, plots the regain for specimens initially humid at successively lower humidities.

The absorption regains at 65% r.h. and the width and area of the hysteresis loops for all samples are given in Table 3-5. The table shows that the magnitude of the hysteresis is ordered in much the same way as the order of the regain (Figure 3.9). Wool and viscose have the highest regain of all samples and hold the largest hysteresis. The linen sample, L1, has a hysteresis area that is similar in size to the cotton samples though its regain is about 50% higher. The smallest hysteresis is as usual found for the synthetic materials; in fact, hysteresis in P1 is nearly absent. Nevertheless, note that nylon, though a man-made material has still about half the regain of cotton.

Table 3-5. Moisture absorption and hysteresis for set 2 fabrics

Fabric code	Total area of the hysteresis	Absorption regains (%) ⁺	Difference in desorption and absorption regains (%) ⁺	Difference in desorption and absorption regains of fibres (%) (20°C, 65% r.h.) after [Morton 97]
C2	6.26	5.43	1.17	0.9-1.5*
KC5	6.52	5.53	1.32	0.9-1.5*
KC11	6.65	4.41	1.38	0.9-1.5*
V1	13.18	11.24	2.16	1.8
W2	13.40	10.10	2.26	2.0
L1	6.80	7.38	1.08	-
P2	0.54	0.18	0.27	-
KN11	1.12	2.97	0.07	0.25

* Mercerised cotton, + (20°±1°C, 65±4% r.h.)

Further, a good agreement is found when comparing the results with some values for fibre absorbency [Morton 97] despite the structural complexity of fabrics. Absorption of water in fibres is a complicated phenomenon in which several factors, arising from the moisture change and the mechanical swelling, are interacting. In addition, when studying absorbency in fabrics, an extra difficulty is introduced due to structure of the fabric itself. A general view of the subject shows the

action of various mechanisms of absorption (i.e., from molecular or thermodynamic viewpoint), which is beyond the scope of this thesis. In the following paragraphs of this section, we will now investigate whether the hysteresis of the regain is also noticeable in the friction measurements.

Figure 3.11 to Figure 3.18 display the full variation of dynamic friction in a relative humidity interval from dry (0% r.h.) to 87% r.h. for all set 2 fabrics respectively. The raw data has been fitted with a double exponential of the form $\mu_d = cte_1e^{-\alpha_1(r.h.)} + cte_2e^{-\alpha_2(r.h.)}$, which is optimised with a least squares method (i.e., Levenberg-Marquardt algorithm). Apart from the cotton samples, a small but distinct hysteresis is visible in the friction of all other fabrics. The hysteresis loop follows a similar path as for the regain: the lower curve is representing the absorption cycle while the upper curve is giving desorption. However, the friction curves show no steep rise in friction at low humidities (cf., Figure 3.10). Further, notice on closer inspection at the 0% r.h. point that the friction after oven drying is smaller for desorption than for absorption. This is, however, not an experimental error but more probably a fabric characteristic. Cookson and Slota [Cookson 93] reported that in spite of well-considered precautions the final length of a fabric, subjected to a 0→90→0% r.h. conditioning cycle, was significantly less at 0% r.h. than the initial length started with. Only after a second cycle, were the final and initial lengths identical. This relaxation shrinkage is due to the fast rate of drying introduced during oven drying of wet fabric samples [Cookson 91]. Baird [Baird 63] suggested that cycling a fabric between 0% and 15% of its regain was an effective way of reducing the shrinkage. Thus, if the length is different for both drying points (0% r.h.) so will be the surface geometry of the fabric and the contacting area with a surface. Therefore, one can deduce that also the friction will be less for the desorption dry point (0% r.h.) than for the absorption dry point.

For all fabric samples the friction increases significantly above 70% r.h., a similar conclusion was made for fibres (fibre-fibre) by Röder [Röder 53]. Most of the friction curves change the gradient around 60% to 70% r.h. and one could therefore dispute whether the standard testing conditions of 65% r.h. for fabrics is the most appropriate to test friction. A lower humidity would cause less fluctuation in the results but might then introduce other problems such as static charges (see 3.5). Further note that the ripple on the dynamic friction, σ_{rip} , pictured in the figures as vertical lines through the sampling points, also increases for higher humidities indicating a more irregular movement.

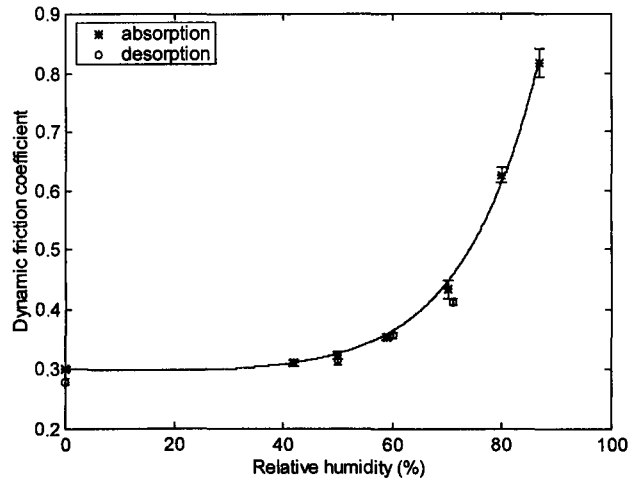


Figure 3.11. Dynamic friction of C2 as a function of relative humidity

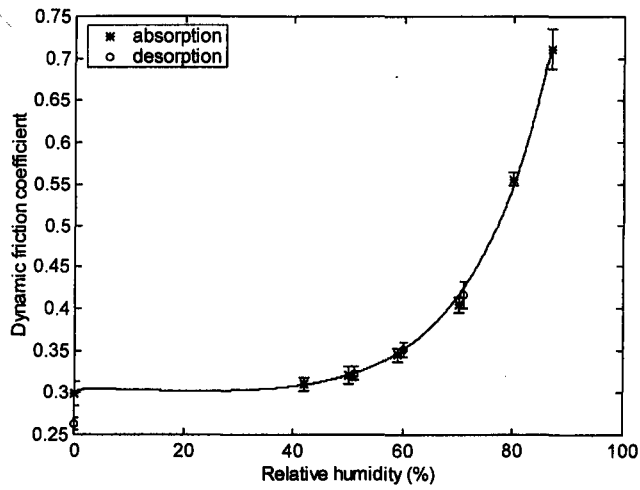


Figure 3.12. Dynamic friction of KC5 as a function of relative humidity

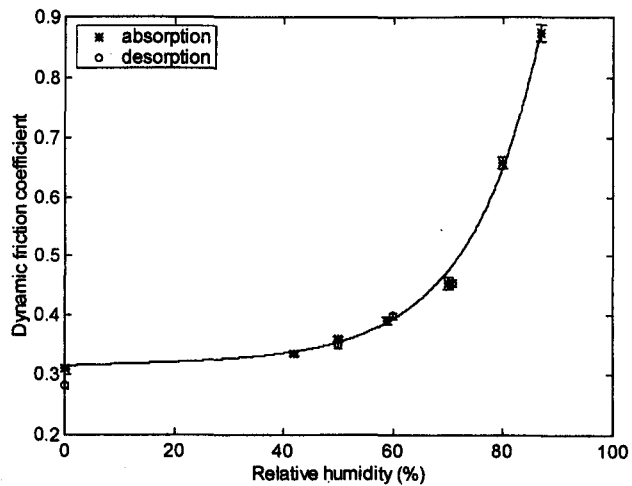


Figure 3.13. Dynamic friction of KC11 as a function of relative humidity

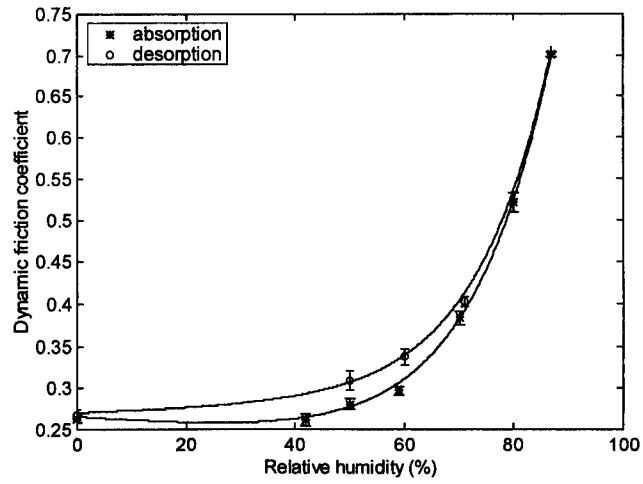


Figure 3.14. Dynamic friction of V1 as a function of relative humidity

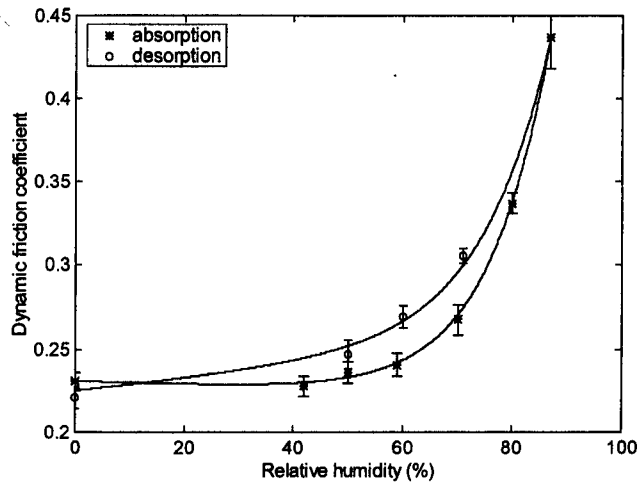


Figure 3.15. Dynamic friction of W2 as a function of relative humidity

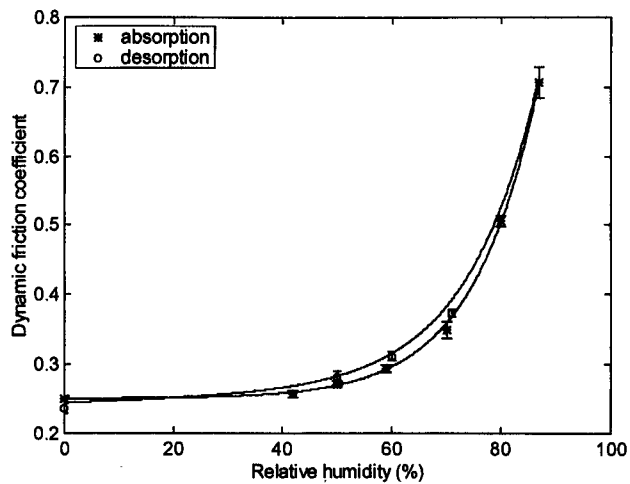


Figure 3.16. Dynamic friction of L1 as a function of relative humidity

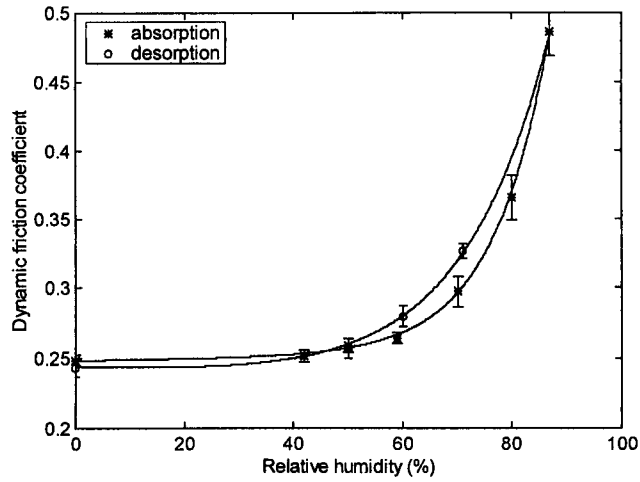


Figure 3.17. Dynamic friction of P2 as a function of relative humidity

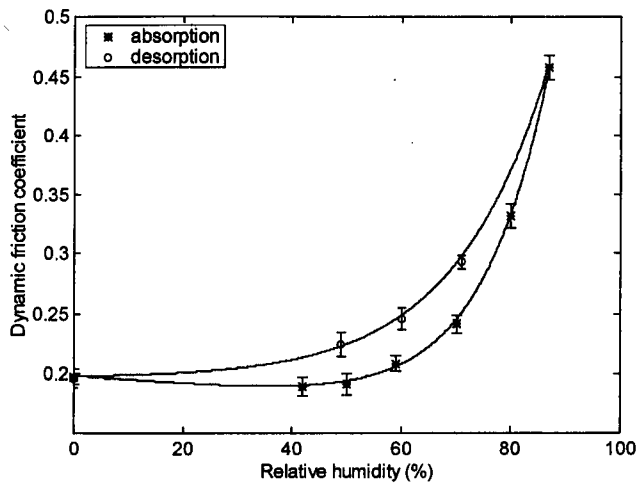


Figure 3.18. Dynamic friction of KN11 as a function of relative humidity

To end this section on friction and humidity some interesting conclusions can be drawn from Figure 3.19 showing the percentage increase in dynamic friction with the increase in relative humidity (percentage increase is calculated in the same way as regain). All tested fabric samples have a 2 to 3 fold increase in friction between 0% to 87% r.h., with the natural materials representing the highest increase. The ranking, however, does not match the regain ranking. The viscose sample, V1, does not have the highest increase in friction and most remarkably, the wool sample, W2, which is a very hygroscopic material, gives the lowest percentage increase in friction. Unfortunately, there is not another wool sample included in the study so it is impossible to deduce whether this is a typical wool characteristic. Another unexpected result is the significant increase in friction for the nylon sample, KN11. Nylon is exceptional in that its axial swelling is larger than the transverse swelling. Thus, the discrepancies between the regain and the friction of a particular fabric can be explained as a difference between the absorption of moisture and the resulting swelling of the fibres. Some fibres can absorb a certain quantity of water but will have a limited swelling.

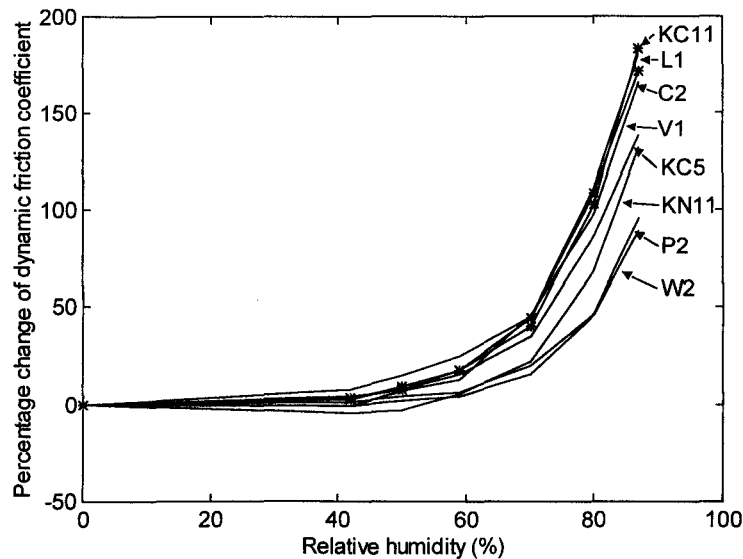


Figure 3.19. Percentage change of dynamic friction coefficient with relative humidity

It has earlier been suggested in this section that reducing the relative humidity to below 60% r.h. during friction tests would give more repeatable results favourable to inter-laboratory experiments for example. However, in the next section, it will be seen that the chances of statically charging the samples will rise which can severely increase the friction again.

3.5 The Effect of Static Charge on Friction

The static charge test is mainly performed to show the influence electrostatics can have on the friction between a fabric sample and a non-fibrous material when no extra normal force is applied on the specimen. Unfortunately, the charge generated initially on the fabric samples could not be quantified but the same procedure has been applied to all set 2 samples, except KC5 (the edges of the specimen curl and therefore give unreliable results). After all, Ramer and Richards [Ramer 68] found in their experiments that charges produced on a large range of fabrics were approximately all of the same order of magnitude, only the charge-decay varied from fabric to fabric. For this test, the fabrics have been charged by placing one specimen per fabric, for one day on a Perspex surface. The Perspex has previously been charged by rubbing the surface several times (≈ 10 times) with a woollen cloth. The environment of the lab is set at a dry condition ($20^{\circ}\pm 1^{\circ}\text{C}$, $40\pm 4\%$ r.h.) especially to augment the effect. In addition, at this condition, atmospheric discharging of the specimens will be slowly exponential (e.g., discharging wool to 0.5 of its initial charge takes 15 min. [Onogi 96]) and will therefore give sufficient time to perform the tests. To have a realistic situation the specimens have been tested on the aluminium surface which considering the electrical conductivity of the material would more easily discharge the samples than an insulating material such as Perspex. The aluminium surface has been earthed although according to Ramer and Richard [Ramer 68] this has little effect on the rate of charge-decay. The test is divided in two stages, first the charged fabric specimens are tested, and one hour later, in the second stage, the air surrounding the samples is intensively ionised

for 15 minutes and the sample is tested again. All fabric specimens were carefully transferred from the Perspex surface onto the aluminium surface with the charged (or discharged) side down.

Table 3-6. Influence of static charge on friction

Fabric code	Static charged			Static discharged			Percentage Difference μ_d charged/discharged (%)
	Static friction	Dynamic friction	Dynamic ripple	Static friction	Dynamic friction	Dynamic ripple	
	μ_s	μ_d	σ_{rip}	μ_s	μ_d	σ_{rip}	
C2	0.348	0.327	0.008	0.330	0.308	0.007	6.3
KC5	-	-	-	-	-	-	-
KC11	0.373	0.347	0.009	0.343	0.323	0.007	7.3
V1	0.362	0.327	0.011	0.339	0.303	0.012	7.7
W2	1.183	0.901	0.111	0.241	0.220	0.007	309.3
L1	0.301	0.277	0.006	0.285	0.266	0.007	4.2
P2	0.899	0.763	0.050	0.274	0.241	0.007	216.8
KN11	2.316	1.742	0.187	0.235	0.204	0.011	752.0

Laboratory at ($20^{\circ}\pm 1^{\circ}\text{C}$, $40\pm 4\%$ r.h.), velocity: 1 mm/s, sample rate: 75 Hz, aluminium surface, tested in the wale direction, only one test per fabric

The friction coefficients in Table 3-6 indicate a slight increase in friction due to electrostatic charge for the cellulosic materials such as cotton and linen (4 to 8%). On the other hand a huge increase (200 to 700%) can be seen in the friction for wool and the man-made materials, polyester and nylon. The latter samples (i.e., W2, P2 and KN11), which are less susceptible to humidity (see Figure 3.19), indicate well the relationship between regain and static-charge because fibre regain greatly affects the electrical properties. Further, note the large variation between the static friction coefficient and the dynamic coefficient. All fabrics registered a clear peak force at the beginning of the friction trace and especially the very sensitive materials, which were visibly attracted to the aluminium surface. The sliding of statically charged fabrics is also more irregular, resulting in a higher dynamic ripple value, σ_{rip} , (see Table 3-6).

Static charging of a fabric material is closely linked with its resistivity; low resistance materials such as cotton and viscose will rarely get charged but high resistance materials such as wool and polyester will often cause trouble. Therefore, lowering the resistance of either the material or the air is an effective method of getting rid of static charges as seen from Table 3-6. Ionising the air around the fabrics removes the static charge and consequently brings the friction back to normality. Using additional normal forces during friction tests might make the effect of the static charge unnoticeable,

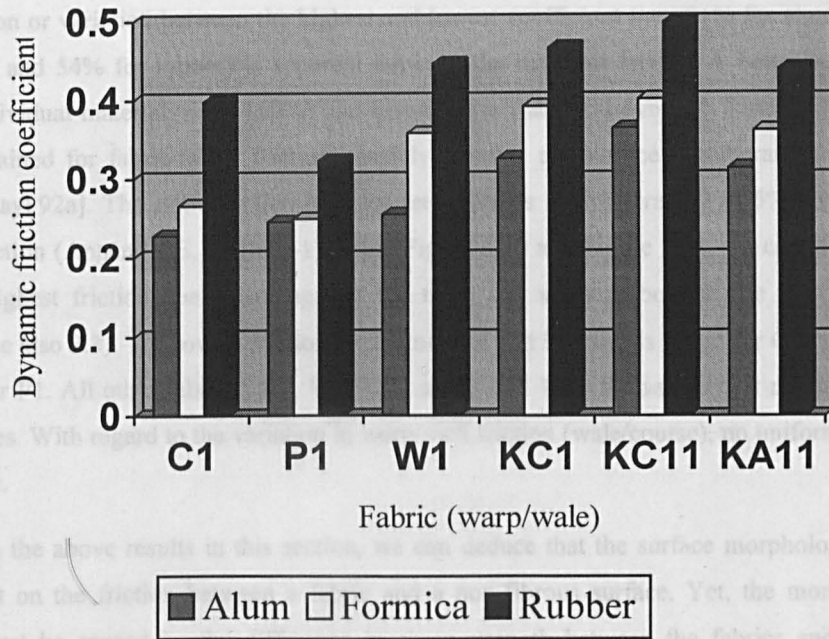
although the static generation for fibres on itself increases with normal force [Hersh 55] the friction decreases and may balance the effect. However, no experiments were made to prove this hypothesis and definitely more research on this is necessary.

3.6 Nature of the Sliding Surface

As can be seen from Figure 3.20 and Figure 3.21 for the warp and weft direction respectively, the influence of the sliding surface on the friction is quite evident (detailed numerical results can be found in Appendix E, table E-1). For the same test conditions (standard humidity and 1 mm/s), the maximum values of friction are found against the rubber surface and the minimum values against the aluminium surface. This finding is identical to what Yoon *et al.* [Yoon 84], Ajayi [Ajayi 92a], and Virto and Naik [Virto 97] reported. However, all friction coefficients for set 1 fabrics are more in the order of magnitude similar to the results of Virto and Naik [Virto 97] despite the very large forces, they used (see Table 2.2). For example Yoon *et al.*, who used the lowest forces of all reference studies (103-483 N/m², other tests conditions unknown), published a friction coefficient of three for a knit polyester fabric against rubber. This result is 6 times higher than the highest value measured in this study and far too high if also compared with some values reported by Ajayi (fabric-rubber, $\mu = 0.8 - 0.9$). The above comparison, demonstrates that it is very difficult to relate results with each other in particular when tested against rubber because the compressibility of the sliding surface can have a pronounced effect on friction under normal forces (see 3.7). Furthermore, great care needs to be taken that the tests surface is free of any contamination (e.g., grease or powders). For instance, preliminary results on a slightly greased aluminium surface displayed a 30% to 50% higher friction.

Thus, the friction coefficient depends strongly on the nature of the sliding surface but from Appendix C, it can be seen that the surface roughness, PR_a , is very similar for the three surfaces (i.e., aluminium, Formica and rubber). Hence, we must draw the conclusion that here the shear strength (see Equation (2.8)) between the fabrics and the sliding surface changes (not to be confused with the shear modulus in a fabric sample).

When comparing the individual friction coefficients for one sliding surface with a moderate discrimination of 14% for Formica, 14% for Alum and 14% for Rubber. The variation between individual fabrics will only be observed when they are put together [Alum (24) and Rubber (24)] will give the highest friction coefficient in the case of rubber for the three surfaces. With the above results, no conclusion can be made.



From the above results in this section, we can assume that the surface morphology has not a great impact on the friction coefficient. Yet, the more significant variation must be caused by the difference in the fabrics and the sliding surface. Until now, some other variables in friction (i.e., number of transverses and humidity) were investigated. In the next section of this chapter, we will investigate what happens to the friction if physically larger samples are tested.

Figure 3.20. Friction coefficients for set 1 fabrics in the warp (wale) direction against different surfaces

Standard conditions, velocity: 1 mm/s, sample area: 1 dm²

3.7 Influence of fabric structure on friction

In order to investigate the influence of fabric structure on friction, the friction coefficient was measured in the weft (course) direction for the same fabrics and surfaces. The results are shown in Figure 3.21. The friction coefficient is limited to a small reduction in friction coefficient compared to the warp direction. Only P1 against Alum shows a 27% rise in friction coefficient when the fabric is tested in the weft direction.

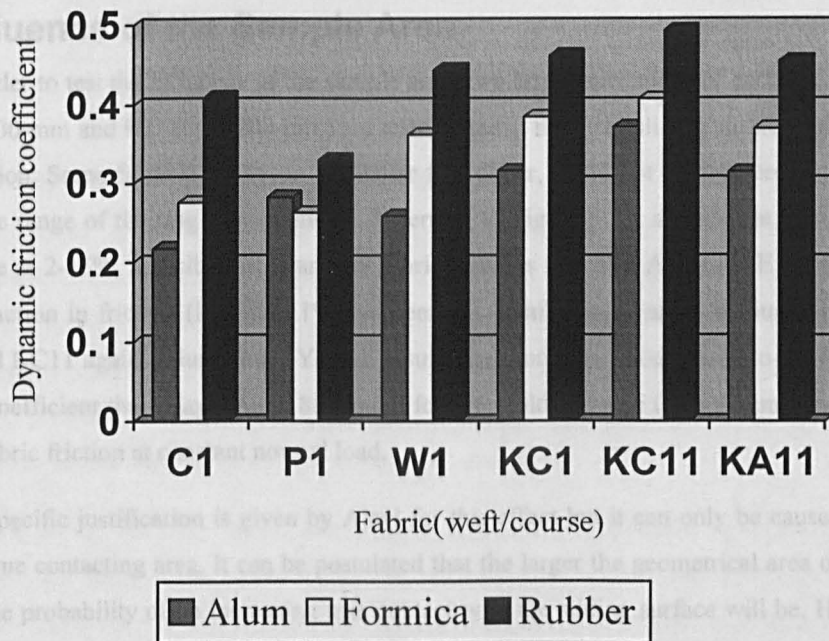


Figure 3.21. Friction coefficients for set 1 fabrics in the weft (course) direction against different surfaces

Standard conditions, velocity: 1 mm/s, sample area: 1 dm²

When comparing the individual friction coefficients for one sliding surface, only a moderate discrimination or variation between the highest and lowest coefficient (i.e., 71% for aluminium, 64% for Formica and 54% for rubber) is apparent between the different fabrics. A better differentiation between individual materials (i.e., 160%) and between the static and dynamic friction (20-40%) will only be obtained for fabric-fabric friction possibly because the surface protuberances can fit well together [Ajayi 92a]. The static friction here for set 1 fabrics is on average 3 to 5% higher than the dynamic friction (Appendix E, Table E-1). From Figure 3.20 and Figure 3.21, we can see that KC11 gives the highest friction coefficient against the three test surfaces both in the wale and course direction (see also 3.3). The lowest friction for aluminium and Formica is found for C1 but in the case of rubber for P1. All other fabric types, W1, KC1 and KA11 keep the same order magnitude for the three surfaces. With regard to the variation in warp/weft friction (wale/course), no uniform conclusion can be made.

From the above results in this section, we can deduce that the surface morphology has not a great impact on the friction between a fabric and a non-fibrous surface. Yet, the more significant variation must be caused by the difference in shear strength between the fabrics and the sliding surface. Until now, some other variations in friction (i.e., number of transverses and humidity) were induced by differences in the real contacting area between the fabrics and the sliding surface, however, the geometrical area of the test specimens remained constant. In the next section of this chapter, we will investigate what happens to the friction if physically larger samples are tested.

3.7 Influence of the Sample Area

In order to test the influence of the sample area, two larger specimens of each set 1 fabric (i.e., R1: 100 x 200-mm and R2: 200 x 200-mm) are tested against the three sliding surfaces in the weft (or wale) direction. Some friction values, in particular for rubber, could not be measured because of the limited force range of the ring dynamometer. Referring to Figure 3.22, a moderate increase, ranging from as little as 2-15%, is visible for nearly all fabric samples (see also Appendix E Table E-2). Only a small reduction in friction (less than 1%) between the small sample areas is found for P1 against Formica and KC11 against aluminium. Yet, all results are much lower compared to the 66-207% rise in friction coefficient that Ajayi [Ajayi 88] found for a tenfold increase (4 to 40 cm²) in sample area for fabric-fabric friction at constant normal load.

No specific justification is given by Ajayi for this effect but it can only be caused again by a rise in the true contacting area. It can be postulated that the larger the geometrical area of the sample the larger the probability of an increasing true contact with the sliding surface will be. However, this influence will fade away, for some fabrics after doubling the area for others after a fourfold increase of the area. Anyway, this test proves once more that the classical friction laws do not pertain to fabrics. In the following two sections, more evidence will be given that proves this divergence.

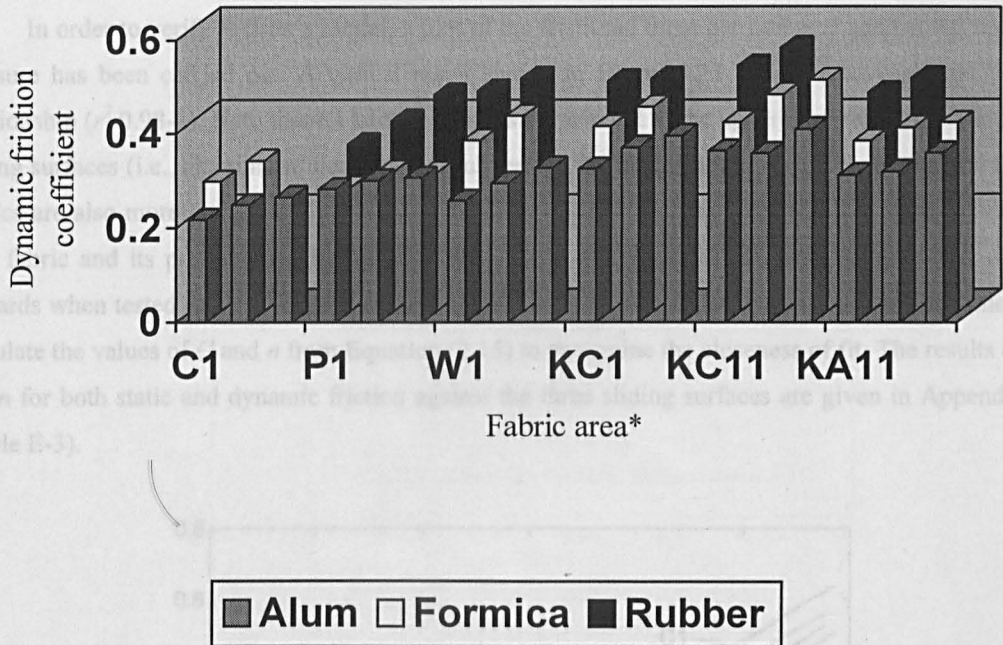


Figure 3.22. The effect of the sample area on the dynamic friction coefficient for set 1 fabrics

Standard conditions, velocity: 1 mm/s, * first row of each fabric category sample area: 1 dm², second row sample area (R1): 100 x 200 mm, third row sample area (R2): 200 x 200 mm (except for C1 area is 165 x 173 mm). Some values are missing due to the limited force range of the sensor

3.8 Influence of the Normal Pressure

The effect of the normal pressure on the frictional properties of fabrics has been extensively reported in the literature and is here investigated to find if any similar or other relationship exists for the case of slightly loaded fabrics. The normal pressure has been increased at random (one test per fabric per day) by placing similar fabric specimens on top of the sample under test. By doing so, small evenly spread pressure increases can be realised. The friction for all set 1 fabrics has been measured against the three engineering surfaces in both principal directions.

The results of the experiment, summarised in Table 3-7, all show a decrease in dynamic friction coefficient for a rising pressure. This is in accordance with results found for fabric-fabric friction by several other workers [Wilson 63], [Carr 88], [Ajayi 92a] and for fabric-non-fabric friction by [Yoon 84] and [Virto 97]. The non-linearity between the frictional force and the normal pressure indicates once more that the classical friction laws are not applicable to fabrics. According to Wilson [Wilson 63] this is because of the viscoelastic nature of the fabric whereby the apparent area of contact increases less rapidly than the load. Hence, this implies that the value of the friction index, n ,

in the relation $F = a_1 N^n$ (Equation (2.7)) lies between 0-1 (viz., $n = 1$: apparent area is directly proportional to pressure).

In order to verify Wilson's model, a plot of the frictional force per unit area against the normal pressure has been carried out. A typical result shown in Figure 3.23 indicates an excellent linear relationship (r^2 0.98-1). Note that all knitted samples correspond to the uppermost curves for the three sliding surfaces (i.e., aluminium, Formica and rubber). In the next chapter, it will be shown that these fabrics are also more compressible which might point out a dependency between the compressibility of a fabric and its pressure sensitivity in friction. Only the curve for the wool sample, W1, shifts upwards when tested against Formica and rubber. A linear regression analysis is further performed to calculate the values of C and n from Equation (2.15) to determine the closeness of fit. The results of C and n for both static and dynamic friction against the three sliding surfaces are given in Appendix E (Table E-3).

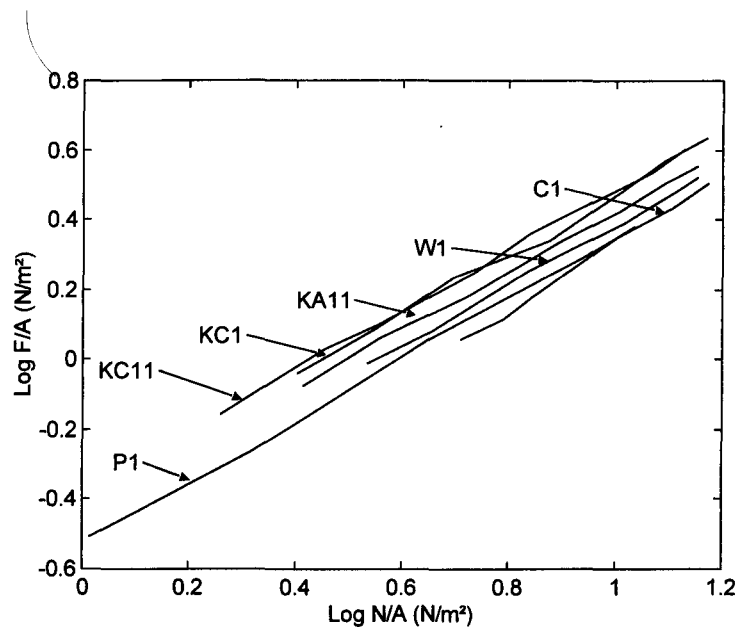


Figure 3.23. Logarithmic relationship between the frictional force per area ($\log F/A$) and the normal pressure ($\log N/A$) for set 1 fabrics

Standard conditions, velocity: 1 mm/s, aluminium surface, weft or wale direction, sample area: 1 dm²

The values of C and n range from -0.26 to -0.64 and 0.83 to 1.09 respectively. However, the values of n higher than one are likely to be erratic due to fitting errors and need to be interpreted as equal to one. In other words, the friction for those fabrics is directly proportional to the pressure. Note also that the C -value has the unit of pressure (N/m²). In Figure 3.24, n is plotted against C and likewise Wilson's results, an inverse 'linear' relationship is found. Yet, the relationship is weak (r^2 0.6) and no distinct grouping dependent on the yarn type (filament or spun) is visible (P1 is a 'spun filament' type fabric but should be regarded as spun type). All fabrics seem to have high values of n (highest in the direction of the lowest yarn sett) and low values of C , which corresponded in Wilson's experiments to the filament group. On the other hand, when displaying all the C and n values for

friction against the three surfaces (aluminium, Formica and rubber), a clustering of the values according to the rubbing surface is visible as shown in Figure 3.25.

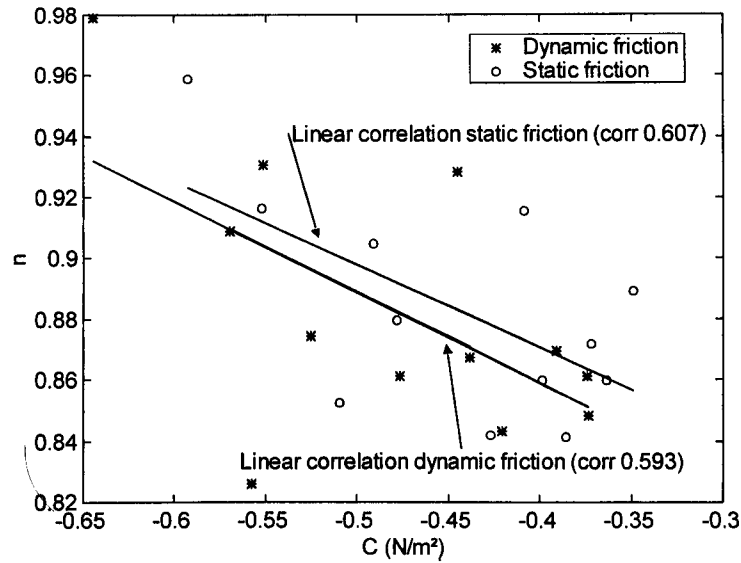


Figure 3.24. Relationship between Wilson's model coefficients C and n for set 1 fabrics against aluminium

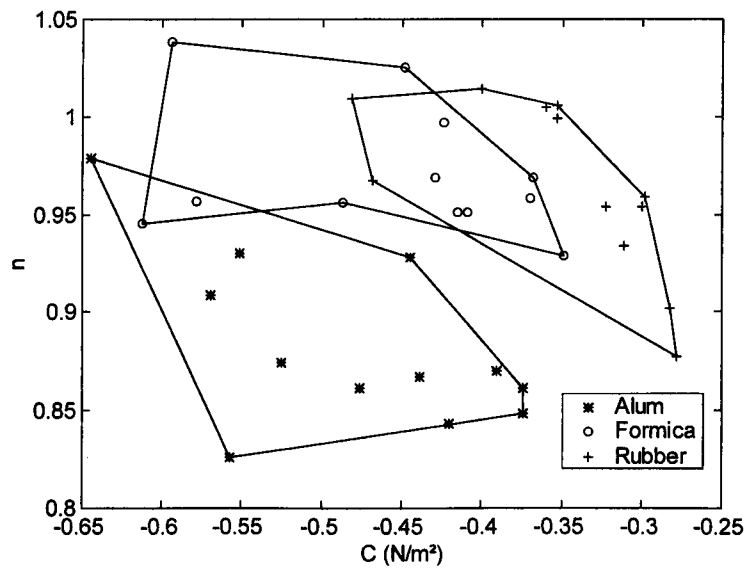


Figure 3.25. The influence of the surface type on the Wilson model coefficients n and C

Thus, Wilson's model works well for correlating both static and dynamic frictional data with varying normal force but values of C and n are more dependent on the sliding surface than on the type of yarn used in the fabric. In the next section, the influence of the sliding velocity on the friction will be studied.

Table 3-7. The effect of the normal pressure on the dynamic fabric friction

Fabric code		μ_d Aluminium			μ_d Formica			μ_d Rubber		
		0*	8 (g/dm ²)	12 (g/dm ²)	0*	5 (g/dm ²)	10 (g/dm ²)	0*	4 (g/dm ²)	7 (g/dm ²)
C1	Warp	0.226	0.220	0.215	0.270	-	0.270	0.410	-	0.410
	Weft	0.218	0.217	0.215	0.280	-	0.264	0.409	-	0.406
P1	Warp	0.248	0.193	0.182	0.240	0.231	0.212	0.329	0.323	0.320
	Weft	0.290	0.231	0.220	0.263	0.253	0.240	0.332	0.332	0.331
W1	Warp	0.255	0.245	0.236	0.359	0.356	0.348	0.443	0.442	0.440
	Weft	0.264	0.253	0.235	0.364	0.364	0.363	0.444	0.443	0.443
KC1	Wale	0.331	0.306	0.296	0.400	0.393	0.385	0.467	0.449	0.412
	Course	0.321	0.306	0.299	0.385	0.381	0.379	0.469	0.454	0.441
KC11	Wale	0.364	0.324	0.296	0.410	0.400	0.396	0.496	0.475	0.465
	Course	0.373	0.314	0.287	0.411	0.402	0.391	0.485	0.476	0.456
KA11	Wale	0.324	0.276	0.258	0.362	0.355	0.343	0.440	0.435	0.420
	Course	0.316	0.282	0.262	0.371	0.365	0.349	0.454	0.448	0.437

Standard conditions, velocity: 1 mm/s, sampling frequency: 75 Hz, sample area: 1 dm²

0* original fabric sample without extra load, for all other pressures fabric weight is included, values of one test only

3.9 Influence of the Sliding Velocity

There is still some controversy on the influence of the sliding velocity on fabric friction but this is likely caused by the difference in experimental conditions, in particular the normal pressure. The friction-velocity tests here are performed on the set 1 fabrics against aluminium and rubber surfaces without applying normal pressure on the fabric. Again, to prevent any aligning effect or other unknown influences, the experiments are conducted at random speeds, one test a day with a relaxation period of 24 hours. The results in Figure 3.26 and Figure 3.27 (single values) for the aluminium and rubber surface respectively, show a small to moderate increase of friction with an increasing velocity.

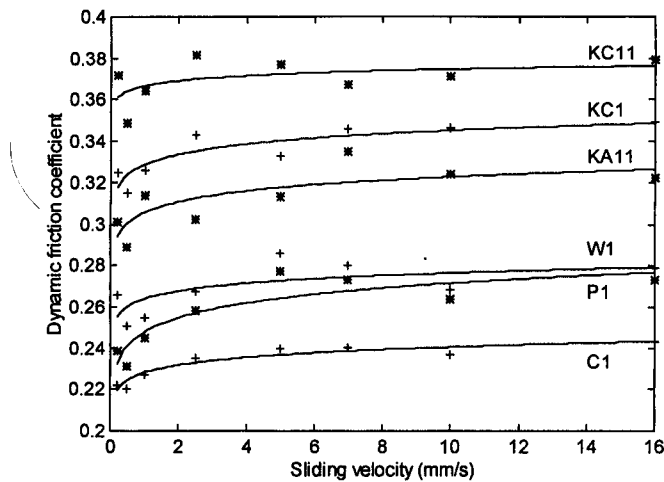


Figure 3.26. Dynamic coefficient of friction for fabric against aluminium as a function of the sliding velocity

Standard condition, warp or wale direction, and sample area: 1 dm^2

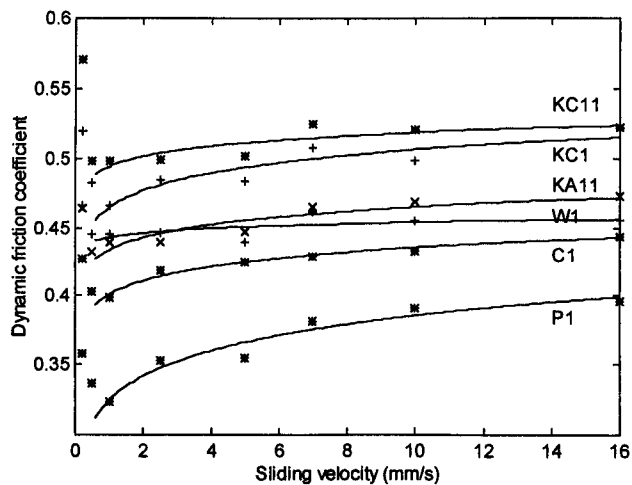


Figure 3.27. Dynamic coefficient of friction for fabric against rubber as a function of the sliding velocity

Standard condition, warp or wale direction, sample area: 1 dm^2 , note that the first and second measurements are excluded from the curve fitting (see below)

From the literature review in chapter 2, we have seen that the velocity effect of friction between fibres (or yarns) and rollers can be explained by a lubrication mechanism. It is well known in tribology that in hydrodynamic lubrication the velocity, v , has exactly the same effect as the viscosity, η , of a lubricant. In other words, if the velocity rises by a factor of two, the frictional behaviour will be the same as if the velocity had been kept constant and the viscosity had been increased twice. However, the friction will not only depend on the product of v and η but, as seen from the previous section, also on the normal load. Lyne [Lyne 55] reported a decrease in friction for acetate yarn over a chromium pin for higher loads at varying velocities. In conventional journal bearing lubrication under hydrodynamic conditions, the coefficient of friction is found as a dimensionless single-valued function of $\eta\omega/P$, where ω is the angular velocity and P the nominal pressure (i.e., normal load divided by the area) on the bearing. Because of the analogy with the hydrodynamic effect in bearings, Hansen and Tabor [Hansen 57] have adopted the following empirical equation for describing the velocity in yarns with a constant width:

$$\mu_d = cte_1 \left(\frac{\eta v}{P_{1,2}} r \right)^{cte_2} \quad (3.7)$$

with r the radius of the pulley, v the velocity of the yarn, $P_{1,2}$ the resultant load with which the yarn presses against the cylinder (i.e., nearly equal to the sum of the tension on both sides of the yarn), and cte_1 and cte_2 two experimental constants. This equation will now be adapted for linear sliding of fabric.

The fabric samples in the tests here do not have any lubrication and hence a dry friction has to be assumed in which air (η 18 Pa s at 20°C) is the lubricant. Furthermore, if v is the velocity of sliding, the angular velocity, ω , in the formula for bearing lubrication is proportional to v/l , with l the length of the sample (in the sliding direction). Hence, the coefficient of dynamic friction can be related empirically to the velocity of sliding as follows:

$$\mu_d = a_3 \left(\frac{\eta v/l}{P} \right)^b \quad (3.8)$$

From the above Equation (3.8), it is clear that at higher pressures the friction coefficient will decrease, which could explain why Ajayi [Ajayi 92a] and Virto and Naik [Virto 97] noticed a continuous declining friction for an increase in velocity. The coefficient a_3 is a material parameter while b is expressing the nature of sliding or with regard to bearings, the type of bearing (e.g., 1 for conventional bearing, 0.5 for tilted pad and 0.3 for foil bearings). Applying now a linear regression on the data calculates the coefficients a_3 and b , which are tabulated in Table E-4 (Appendix E) for the set 1 fabrics against aluminium and rubber. Next, the coefficients are fitted back into Equation (3.8) and used in curve fitting the data (see Figure 3.26 and Figure 3.27). Overall, a better correlation (see Appendix E, Table E-4) is found for the friction against rubber (r^2 0.85) than against aluminium

(r^2 0.75). Note also that the hydrodynamic lubrication for friction on the rubber surface cannot exist at very low speeds (< 0.5 mm/s) but is determined by ordinary rubbing friction and therefore excluded from the calculations (first two measurements). No rubbing friction is visible for fabric against the aluminium surface.

The values of a_3 (see Appendix E, Table E-4) are fabric specific and converge to the dynamic friction coefficient for high speed. The values of b differ from fabric to fabric and are greater for the rubber surface than for the aluminium surface. However, the values for b are ten times smaller, compared to the value of 0.38 that Hansen and Tabor [Hansen 57] found in their experiments for nylon over a steel cylinder. This large contrast could be due to the fact that fabrics are geometrically more complex than fibres. In essence, the parameter b expresses the sensitivity of friction to velocity (viz., the higher the value of b the more sensitive friction is to velocity). Further, b is closely related to the fabric geometry because the largest values appear in the sliding direction with the highest yarn sett (except for KC1 and W1 against aluminium).

Thus, a hydrodynamic lubrication effect is slowly increasing the frictional force for fabrics at higher speeds. As could be seen from Figure 3.27, the frictional force of fabric against rubber at very low speed (0.2-0.5 mm/s) will increase again and another phenomenon called 'stick-slip' will occur. This will be the topic of the next and last section in this chapter together with the question on how a fabric exactly slides over a surface.

3.10 Stick-slip Behaviour

Stick-slip has fascinated many researchers in the past, in particular, for control purposes though the precise mechanism is still not well understood. The aim of the study here is to examine stick-slip for fabrics sliding over a non-fibrous material and eventually to build a model that simulates this behaviour. The few stick-slip studies in textiles [Hearle 71], [Ajayi 92b, 95], [Hosseini Ravandi 94] have always been conducted on a tensile tester where either a sled is moved over the fabric or the front edge of the sample is moved. However, these methods do not reveal the exact fabric movement and considering the limpness of fabrics it can be questioned whether a fabric moves simultaneously as one piece or whether the fabric moves in a kind of 'caterpillar' manner. Therefore, we will enquire into the fabric deformation mechanism when sliding over a surface at very low speeds and in order to perform the test a special device needed to be built which will be discussed first.

3.10.1 Instrumentation

The testing device is required to measure the local movement simultaneously at different places of a fabric sample when sliding at very low speed over a surface. In essence, there are two non-contacting approaches to this problem either by using a reflective method (e.g., triangulation laser sensor (see 3.2.1) or cameras) or a transmissive method. However, cameras are more costly and would require large magnification whereas most of the reflective sensors suffer from a low power reflection due to the diffuse optical properties of fabric. On the other hand, acoustical methods (reflective or transmissive) would not give the required accuracy due to the large beam angles of the currently

available sensors thus an optical transmission method seems the best option. Furthermore, the data can be collected either in the frequency domain or in the time domain. Though due to their mesh structure, textiles tend to create second order components in the FFT, which make the image in the Fourier plane more confused [Lipson 72]. Besides, the FFT-image of a consistent moving web structure will be more or less 'stationary' so it would be impossible to measure any delays due to the fabric movement. Hence, a transmissive IR time domain method was opted for. A similar approach, though with laser light, has been proposed by Monkman [Monkman 96] as a thread counting device.

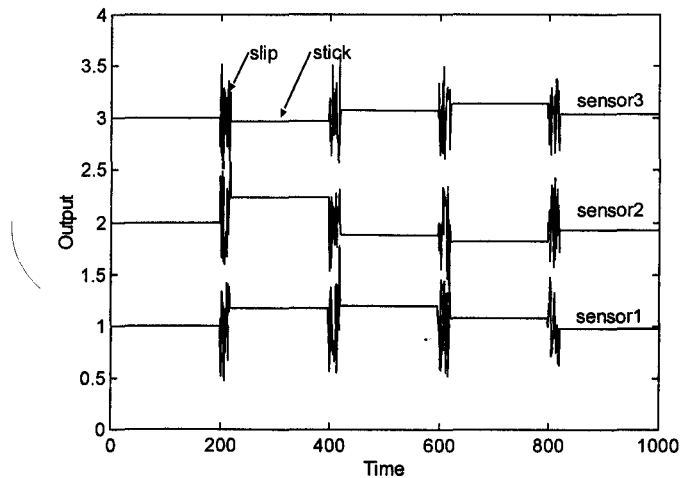


Figure 3.28. Theoretical sensor output for a 'rigid' body under stick-slip movement

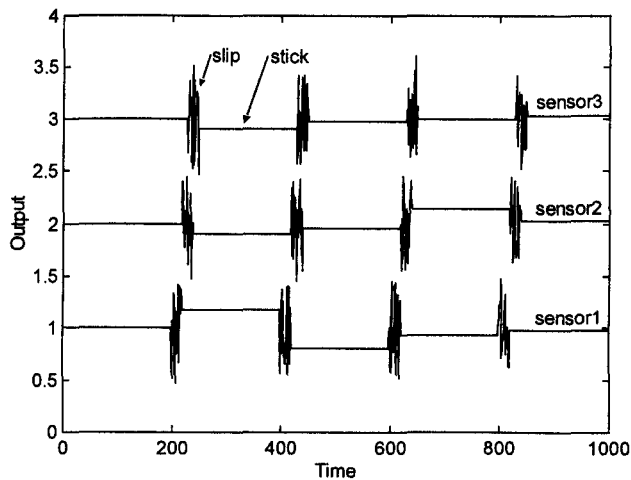


Figure 3.29. Theoretical sensor output for a 'stretchable' body under stick-slip movement

An offset on the sensor signals (1, 2 and 3) is here just introduced to distinguish better the level though in reality the three sensor levels will be almost identical. Further, the stick 'levels' are dependent on the light intensity and are therefore varying between the different sensors

The concept of testing is simple in that the light transmission either will fluctuate whenever the underlying fabric moves in between the sensor or will remain constant when the fabric is still. Thus, the transitions from constant to fluctuating signal indicate the transition between the stick to slip phase

in between the particular sensor. Note however that the constant light level is likely to change between each stick phase because of the fabric not being a flat continuum (i.e., fabric sett also varies). If now several sensors are aligned across the fabric then one can easily detect whether the fabric moves as one body or as a kind of ‘caterpillar’. For example, when the fabric moves as one body, all sensors, three in this case here, should register the same transitions at the same time as illustrated in Figure 3.28. Otherwise, if for instance the pulling side of the fabric moves first then a time delay should be visible between the individual sensors as in Figure 3.29. Sensor 1, which is closest to the pulling side of the fabric, changes first, followed by sensor 2 and sensor 3 respectively. The implementation of the concept is depicted in Figure 3.30.

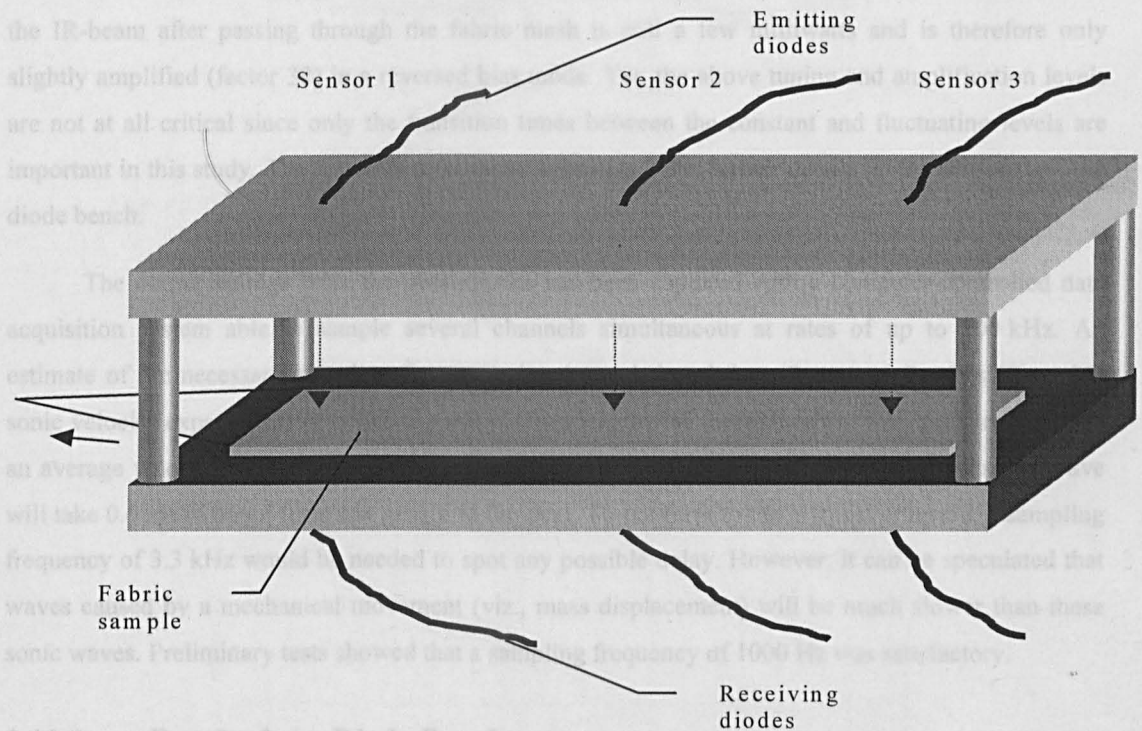


Figure 3.30. Sketch of the diode bench for measuring local fabric stick-slip

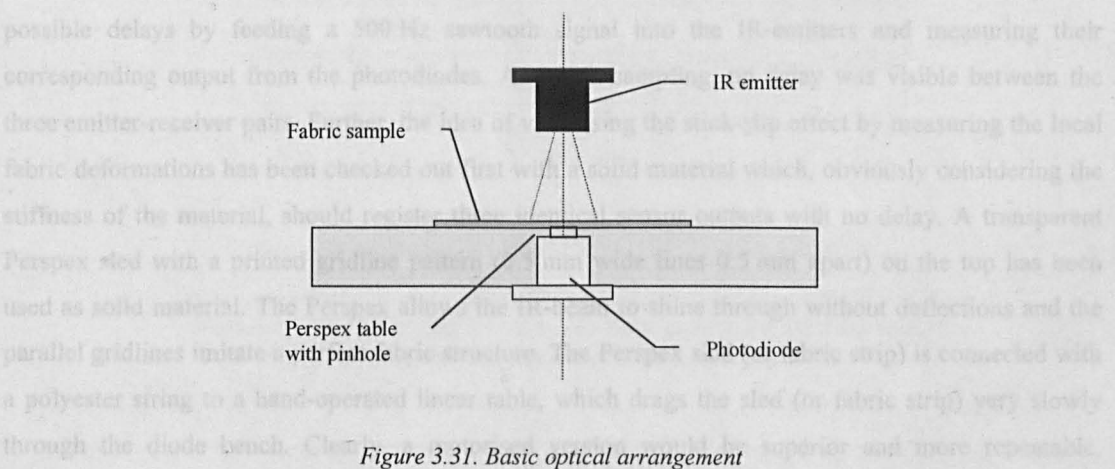


Figure 3.31. Basic optical arrangement

The test rig (Figure 3.30) consists of three emitter-receiver units, 150-mm apart from each other, embedded in a black Perspex ‘gantry’ structure through which the fabric sample can be passed. A

black structure has been chosen to stop any influences from direct light to affecting the measurements. Each unit comprises a small angle gallium-aluminium-arsenide (GaAlAs OD-880F) emitter in the top plate and a high-speed silicon photodiode in the bottom plate (AEPX65) as seen schematically in Figure 3.31. A 0.8-mm diameter pinhole between the fabric sample and the photo-sensor (\varnothing 0.84-mm) reduces the beam. Further, a thin sheet of acetate covers the top of the table acting as the sliding surface and avoiding any possible obstructions during sliding due to burrs on the pinholes yet allowing light transmission. The diameter of the receiver and the pinhole is selected in a way not to measure in between the individual gauges of the fabric but to average over a small area. Hence, a change of brightness is measured when the fabric mesh is sliding over the pinholes. The IR-emitters (880 nm) are supplied from a single DC-voltage and tuned to give the same light output. The power of the IR-beam after passing through the fabric mesh is still a few milliwatts and is therefore only slightly amplified (factor 30) in a reversed bias mode. Yet, the above tuning and amplification levels are not at all critical since only the transition times between the constant and fluctuating levels are important in this study. The reader is referred to Appendix B for further details on the sensors and the diode bench.

The output voltage from the photodiodes has been captured with a computer-controlled data acquisition system able to sample several channels simultaneous at rates of up to 200 kHz. An estimate of the necessary sampling frequency has been deduced from Ryan and Postle's [Ryan 81] sonic velocity experiments in which a pulse passing lengthwise through fabric was measured to have an average velocity of 250-m/s. Thus, for an interval of 150-mm between each diode, a sonic wave will take 0.6 ms to travel from one sensor to the next. To conform to the Nyquist criterion, a sampling frequency of 3.3 kHz would be needed to spot any possible delay. However, it can be speculated that waves caused by a mechanical movement (*viz.*, mass displacement) will be much slower than these sonic waves. Preliminary tests showed that a sampling frequency of 1000 Hz was satisfactory.

3.10.2 Results from Diode Bench

Before starting the actual stick-slip tests, the diode bench has been verified electrically for any possible delays by feeding a 500 Hz sawtooth signal into the IR-emitters and measuring their corresponding output from the photodiodes. At 5-kHz sampling, no delay was visible between the three emitter-receiver pairs. Further, the idea of visualising the stick-slip effect by measuring the local fabric deformations has been checked out first with a solid material which, obviously considering the stiffness of the material, should register three identical sensor outputs with no delay. A transparent Perspex sled with a printed gridline pattern (0.5 mm wide lines 0.5 mm apart) on the top has been used as solid material. The Perspex allows the IR-beam to shine through without deflections and the parallel gridlines imitate a perfect fabric structure. The Perspex sled (or fabric strip) is connected with a polyester string to a hand-operated linear table, which drags the sled (or fabric strip) very slowly through the diode bench. Clearly, a motorised version would be superior and more repeatable. However, a consistent manual speed of approximately 0.18 mm/s has been attempted in all tests. A typical output from the three photodiodes when sliding the Perspex sled over the diode table is given in Figure 3.32 together with a magnification of a specific section in Figure 3.33.

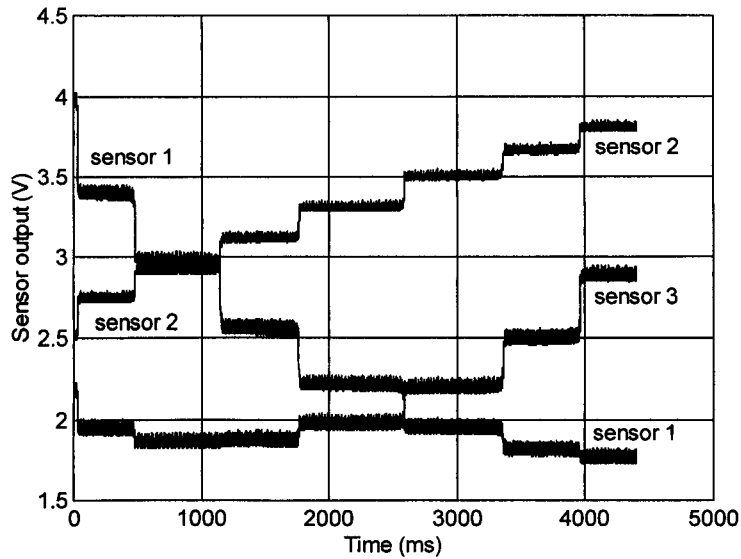


Figure 3.32. Typical unprocessed sensor output from photodiodes for Perspex sled movement

Perspex sled with gridline pattern (0.5 mm wide-0.5 mm apart) on top, sensor 1 is closest to the pulling side, sampling frequency: 1000 Hz, sliding speed: ≈ 0.18 mm/s

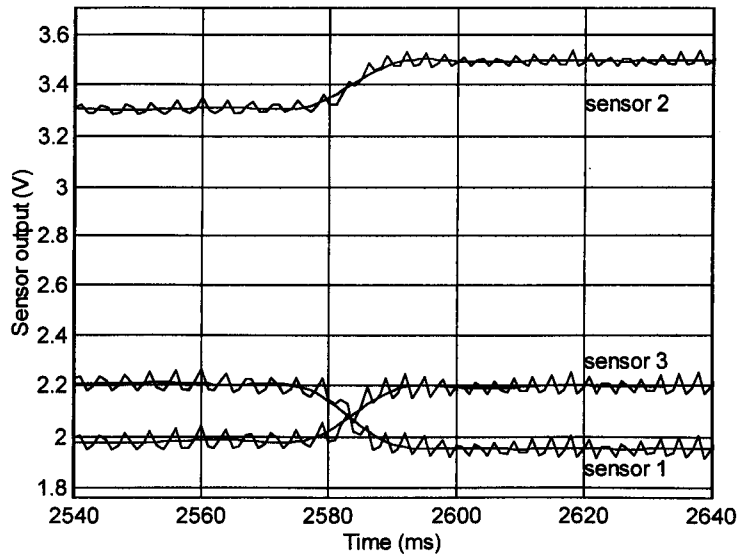


Figure 3.33. Magnified and filtered section from Figure 3.32 above

Perspex sled with gridline pattern (0.5 mm wide-0.5 mm apart) on top, sampling frequency: 1000 Hz, sliding speed: ≈ 0.18 mm/s, solid line is the result of a 5th order lowpass Butterworth filtering with cut-off frequency at 70 Hz

In Figure 3.32 a rectangular ‘histogram like’ signal is obtained for all three sensors changing voltage level whenever the Perspex sled makes an abrupt forward movement. Note that the voltage levels do not change identically for all three sensors but that this is dependent on the light intensity received by the photodiodes. Hence, some signals go up in voltage (max. 10 V) when less area of the

pinhole is covered (viz., more light is transmitted) while others decrease when a gridline darkens the photodiodes. Unfortunately, the signals are polluted with electrical noise partly due to inherent noise in the photodiodes and noise generated in the amplifier. Therefore, a 5th order lowpass Butterworth filtering has been applied to the signals (and to the signals for the fabric stick-slip) [MATLAB 88]. A cut-off frequency of 70 Hz is found adequate to remove the noise while keeping the signal data intact because a voltage transition or 'slip' takes about 18 ms (55 Hz) to change (see Figure 3.33).

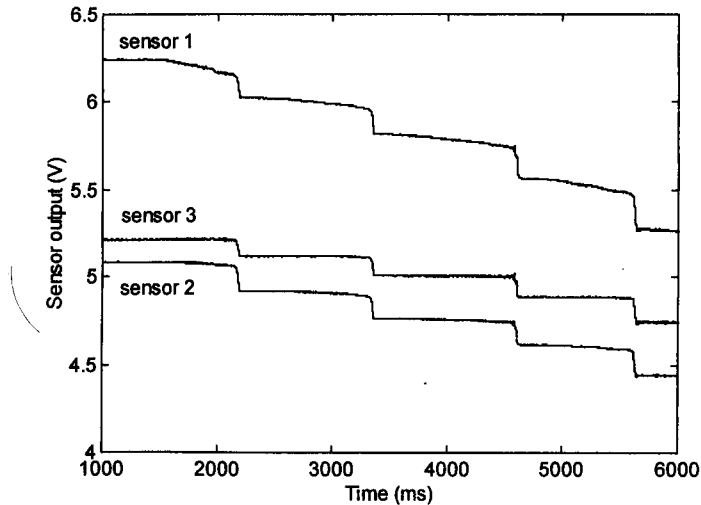


Figure 3.34. Photo-diode outputs for a representative knitted material (KA1)

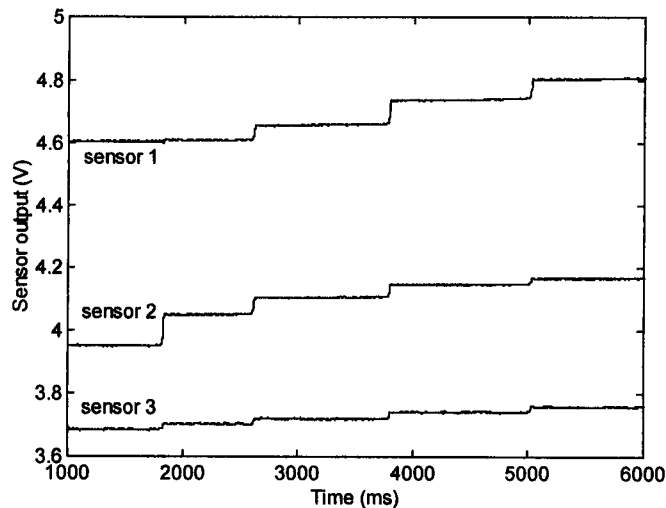


Figure 3.35. Photo-diode outputs for a representative woven material (C3)

Sensor 1 is closest to the pulling side, sampling frequency: 1000 Hz, sliding speed: ≈ 0.18 mm/s, 5th order lowpass Butterworth filtering applied with cut-off frequency at 70 Hz

Obviously, the slip time or transition time will also be dependent on the sliding speed. As expected when sliding a solid surface sample (Figure 3.33), no time delay is visible between the individual sensor signals, which indicates that the material is sliding as one body. Yet, when sliding fabrics

across the diode table totally different outputs are obtained from the sensors as seen in Figure 3.34 and Figure 3.35 for a knitted and woven material respectively.

All seven fabrics (set 3) have been subjected to the stick-slip test on the diode table though not all samples produced a good analysable signal. Very dense weaves as for example the linen fabric, L2, did not give large voltage transitions whereas, the non-woven material, Pa1, produced a continuous signal showing no signs of stick-slip movement at all. When analysing the signals for all other fabrics, a distinct difference is noticeable between the signals from a woven material compared to the signals from a knitted fabric. Knitted fabrics are, in general, less stiff structures (larger extensions see 3.10.5 below) and therefore will extend or shear more easily when dragged across a surface which is clearly visible in the signal of sensor 1 in Figure 3.34. The voltage level of sensor 1 starts to drop already before the actual true slip-phase (i.e., voltage transition) signifying that the material is either shearing in the direction of pulling or exhibiting a micro-slip movement before the actual sliding. Sensor 2 also is registering some extension though starts later in time whereas sensor 3, located at the end of the fabric, only measures the actual slip. In comparison with the knitted materials, woven materials have a much smaller extensibility and therefore do not show much stretching or shearing during the 'stick-phase' (see Figure 3.35). Hence, the voltage of the sensors does not change a lot until the actual slip-phase, and the signal resembles more the signal for the rigid Perspex sled. With regard to the actual time for slipping, the knitted materials take on average 26 ms whereas the woven materials slip slightly faster in about 20 ms time. Of course, one has to take into account that these figures are only a rough indication considering the manual operation of pulling the fabrics. Unfortunately, a delay between the individual slip-phases proved rather hard to quantify, mainly because the starting of each slip-phase was difficult to pinpoint exactly. In addition, the filtering which was required to remove the noise from the signal reduced the sharpness of the transitions even further.

The above experiment, however, reveals that some fabrics do not move as a rigid body but extended or sheared first when dragged along a surface. Dependent on the material stiffness, tension is built up internally from the pulling side onwards where minute fluctuation is registered. Next, when the tension at some part in the fabric strip is equal to the static friction of the remaining stationary part (viz., end of the strip), the fabric breaks away from the table surface and suddenly slips forward. Consequently, the tension in the fabric is reduced and a new sticking phase is initialised again. Hence, one can say that fabrics are moving in a kind of 'caterpillar' way where a continuous stretch-release cycle moves the fabric forwards when slid along a surface. Therefore, this phenomenon can be modelled appropriately as masses with spring-damper elements in between as will be discussed in section 3.10.4 and 3.10.6 below.

3.10.3 Stick-Slip Traces

Previous tests with the 'diode-bench' could not quantify the frictional force in the stick-slip traces hence some friction tests need to be performed on the set 3 fabrics at very low sliding speeds (i.e., 0.12-0.2-0.24 mm/s). As on the 'diode bench' (3.10.1), the table surface of the friction tester is covered with an identical acetate sheet. A different fabric sample (60 x 300-mm) is used for each

velocity test comprising six tests in total per fabric, one test per day. All fabrics have been tested in the same direction as previously in the 'diode bench' tests.

From the results in Table 3-8, it can be seen that for most of the fabrics the friction goes up with an increasing velocity, only KA1 shows a downward trend. Two categories of stick-slip, different to the above woven/knit classification, can be distinguished. Fabrics KA3, Ac1 and Pa1 display an irregular (aperiodic) stick-slip trace as in Figure 3.36, all other fabrics give a more regular (periodic) trace as seen in Figure 3.37. The difference in traces is also noticeable from the friction coefficients in Table 3-8. The irregular traces give a smaller dynamic ripple, σ_{rip} , except Pa1, which gives overall a large value possibly because of its non-woven structure.

Furthermore, when testing larger samples the friction does not only increase as expected (see section 3.7 above), but the stick-slip for fabric KA3 and Ac1 also now becomes regular. This is intuitively understandable because a larger piece of fabric has a greater mass to move and will therefore have more drag when sliding over a surface. Further, when the area is kept constant and the normal load is increased, Hosseini Ravandi *et al.* [Hosseini Ravandi 94] reported an increase in stick-slip amplitude. Yet, the friction coefficient in itself declines with an increased pressure complying with the normal pressure-friction law. On the other hand, when the velocity is increased eventually the stick-slip should disappear. However, this must be happening at a speed higher than the maximum speed (0.24 mm/s) used in these tests. At this sliding speed, only the friction trace of fabric L2 becomes irregular.

Another interesting fact in a stick-slip trace of a fabric is the periodicity of the signal and its relation to the geometrical structure of the fabric. Few studies on fabric-fabric [Ajayi 92b, 95] and on fabric-Perspex [Hosseini Ravandi 94] have reported a distinct relation between the number of peaks in a stick-slip trace and the yarn spacing. A similar approach to Hosseini Ravandi's [Hosseini Ravandi 94] spectral density analysis will be applied to the stick-slip traces here.

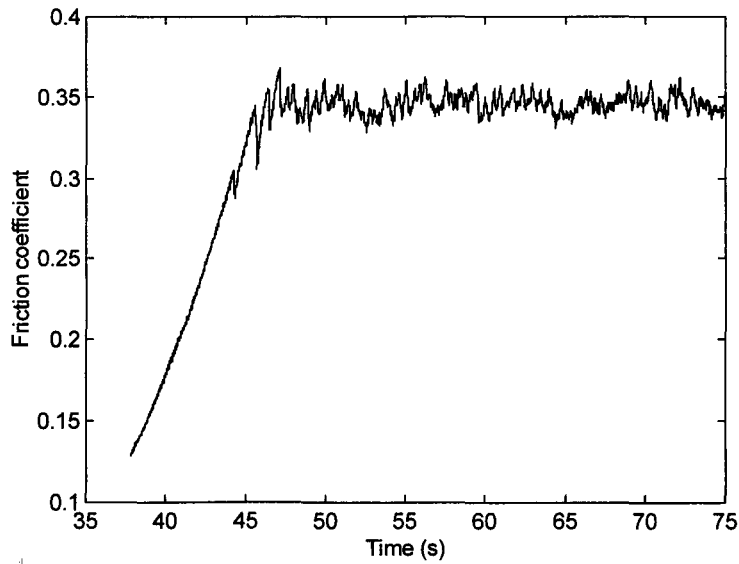


Figure 3.36. Irregular stick-slip trace of KA3 on acetate

Standard conditions, velocity: 0.12 mm/s, acetate surface, mass sample: 3.64 g, area of the sample: 60 x 300 mm, static friction coefficient: 0.370, dynamic friction coefficient: 0.368, dynamic ripple: 0.007

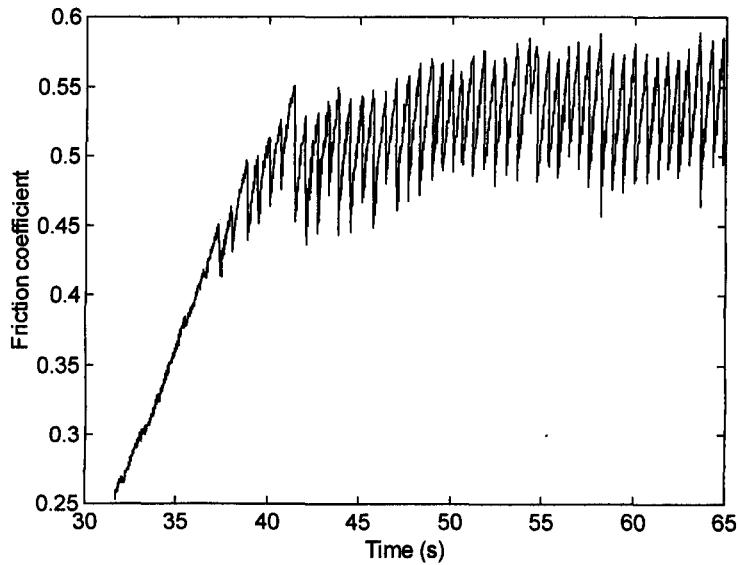


Figure 3.37. Regular stick-slip trace of C3 on acetate

Standard conditions, velocity: 0.12 mm/s, acetate surface, mass sample: 1.87 g, area of the sample: 60 x 300 mm, static friction coefficient: 0.573, dynamic friction coefficient: 0.556, dynamic ripple: 0.027

Table 3-8. Friction coefficients for set 3 fabrics at stick-slip conditions

Fabric code		0.12 mm/s			0.20 mm/s			0.24 mm/s		
		μ_s	μ_d	σ_{rip}	μ_s	μ_d	σ_{rip}	μ_s	μ_d	σ_{rip}
C3	Warp	0.544	0.537	0.029	0.566	0.536	0.028	0.587	0.580	0.031
KC3	Wale	0.639	0.628	0.033	0.706	0.685	0.039	0.728	0.696	0.034
KA1	Wale	0.584	0.541	0.036	0.600	0.557	0.032	0.560	0.521	0.030
KA3	Course	0.361	0.349	0.010	0.346	0.335	0.010	0.353	0.346	0.017
Ac1	Warp	0.513	0.509	0.012	0.529	0.524	0.009	0.553	0.540	0.017
L2	Weft	0.679	0.653	0.029	0.704	0.704	0.019	0.767	0.762	0.027
Pa1	-	0.938	0.923	0.024	0.950	0.922	0.022	0.961	0.941	0.029

Standard conditions, acetate surface, sample area: 60 x 300 mm

Sampling frequency: 60 Hz for 0.12 mm/s and 0.20 mm/s, 75 Hz for 0.24 mm/s

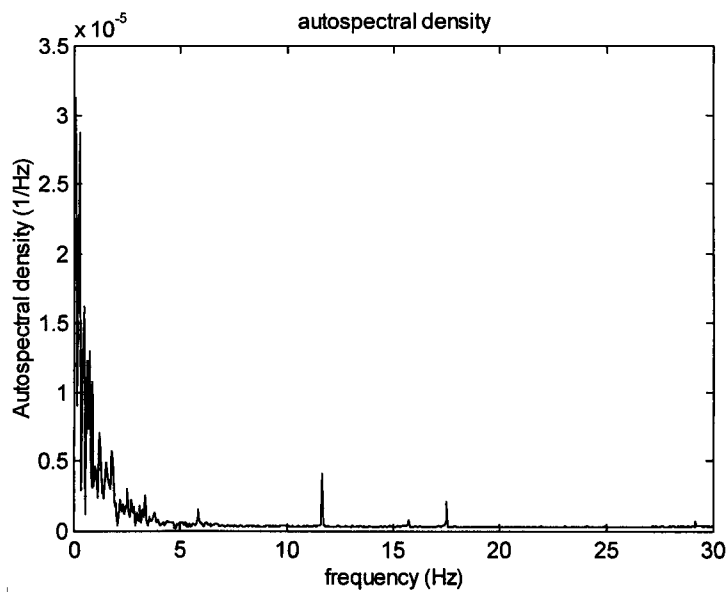


Figure 3.38. Autospectral density of stick-slip trace of KA3

Notice that the units of the spectral density function are in 1/Hz since friction is dimensionless

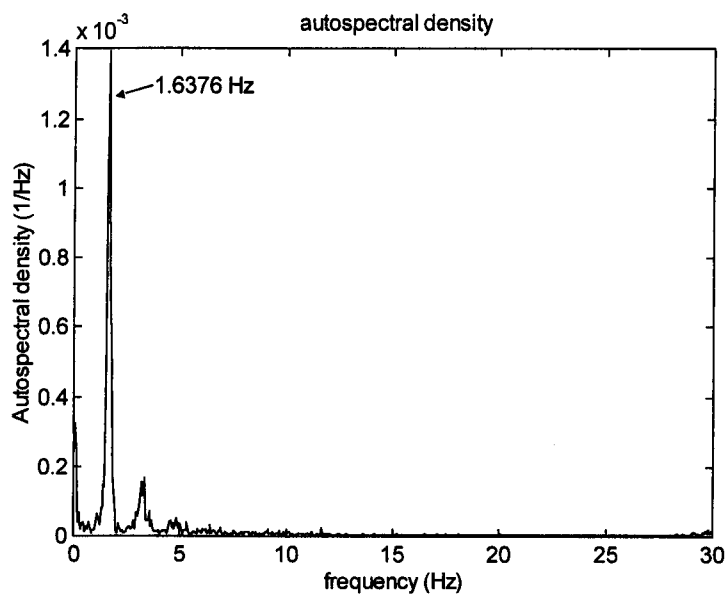


Figure 3.39. Autospectral density of stick-slip trace of C3

The autospectral density function of a time signal will simply detect the periodicity of the signal by calculating the FFT (fast Fourier transform) over several windows of the data. The calculations were performed in MATLAB™ [MATLAB 88] and used a Chebyshev window of 1024 data points shifting over the total data array. A typical autospectral density plot is given in Figure 3.38 and Figure 3.39 for an irregular and regular stick-slip trace respectively. A sharp frequency peak is visible for all fabrics with regular stick-slip whereas the irregular traces display a band of frequencies close to DC showing no periodicity at all hence the name irregular. The frequency value, f_s , of the peak

in the regular traces is converted to wavelength, λ , when a fabric is sliding over a surface with a velocity, v , as follows:

$$\lambda = \frac{v}{f} \quad (3.9)$$

However, the wavelength of the first peak in all fabrics with regular stick-slip does not correspond to the yarn space in the direction of sliding as was found by Hosseini Ravandi *et al.* [Hosseini Ravandi 94]. Referring to Table 3-9, the values for the wavelengths, λ , are on average 5 to 7 times smaller than the yarn space in the travelling direction. Consequently, the peaks must be caused by a combined effect of stretching and releasing of the protruding yarn in both directions of the fabric (i.e., sliding direction and the direction perpendicular to it). Compared with Hosseini Ravandi *et al.* results, the peaks found here are in accordance with their 'second and third' broad peaks of the spectral analysis. Hosseini Ravandi *et al.* reported that for an increased normal load, the stick-slip amplitude increases, and their 'second and third' peak shifts to a higher frequency in the spectral analysis. Thus in analogy, for a lower normal force (e.g., only the weight of the fabric), the first peak corresponding to the yarn spacing might well disappear and the broader second and third peak(s) will shift towards a lower frequency.

Table 3-9. Results from autospectral density analysis for regular stick-slip traces

Fabric code		Wavelength, λ , of first peak (μm)			
		Yarn space (μm)	at 0.12 mm/s	at 0.20 mm/s	at 0.24 mm/s
C3	Warp	333.3	61	67	50
KC3	Wale	555.5	72	97	63
KA1	Wale	1000.0	139	130	84
L2	Weft	416.6	69	60	-

When plotting the wavelength of the first peak as a function of the yarn spacing a linear correlation is found as shown in Figure 3.40. This is in agreement with [Ajayi 92b] and [Hosseini Ravandi 94], and indicates that with an increasing yarn density, the surface structure of the fabric becomes more regular. The next part in this section studies the classical friction model, which will be used to simulate the stick-slip behaviour in fabrics.

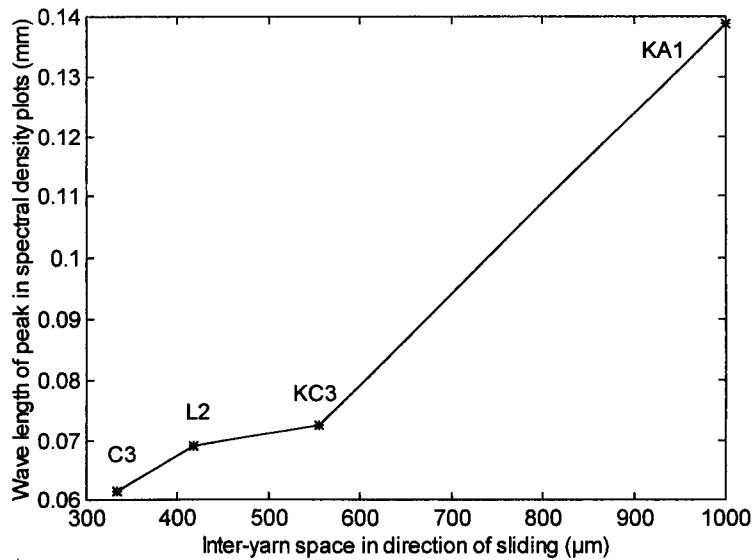


Figure 3.40. Variation of the wavelength peaks for different yarn spacing (0.12 mm/s)

3.10.4 Theoretical Stick-Slip Model

Since friction at microscopic level is caused by surface irregularities obstructing each other during sliding, an accurate representation would entail the theory of random processes. Haessig and Friedland [Haessig 90] proposed a position dependent model that faithfully described the physical mechanism of stick-slip with bristles representing for example the molecular bonds. The bristles are connected to the top surface and assumed to snap when the strain in the bristle exceeds a certain level and form another new bond with a smaller strain. The model is claimed to be very accurate though is computationally complicated and does not allow damping. However, the frictional force is usually represented as a function of velocity rather than position.

From Figure 3.41, it can be seen that at zero velocity the function can have multiple values between positive and negative static friction representing the sticking phase. Only when the magnitude of the external force exceeds the static friction will the body begin to slide or slip. This discontinuity at the origin is not only physically unrealistic but also unacceptable in simulations. One approach to overcoming this discontinuity has been to linearize this region as seen in Figure 3.41. This approximation, commonly known as the 'classical friction model', suffers from the problem that acceleration of the body is possible during the stick-phase where the external forces are lower than the maximum frictional force. The friction in Figure 3.41 is pictured as velocity independent though a velocity dependency can be programmed. Furthermore, the very steep slope around zero velocity can cause numerical difficulties due to very short integration times. Karnopp [Karnopp 85] has developed an alternative approach to overcome the discontinuity in the classical model by reducing the order of the system at every instant that the relative velocity becomes zero. Yet, the Karnopp model is difficult to incorporate in a simulation model because it requires the derivation of separate sets of equations for each possible sticking and slipping condition but only one equation is valid at a time. For a single mass system, there are two sets of equations but a three mass system will need already eight sets of

equations. In addition, Karnopp still supposes a finite region surrounding the zero velocity since an exact value of zero is never possible in digital computation. Nevertheless, the author opted for the simpler classical model approximated with a very steep rise near zero velocity.

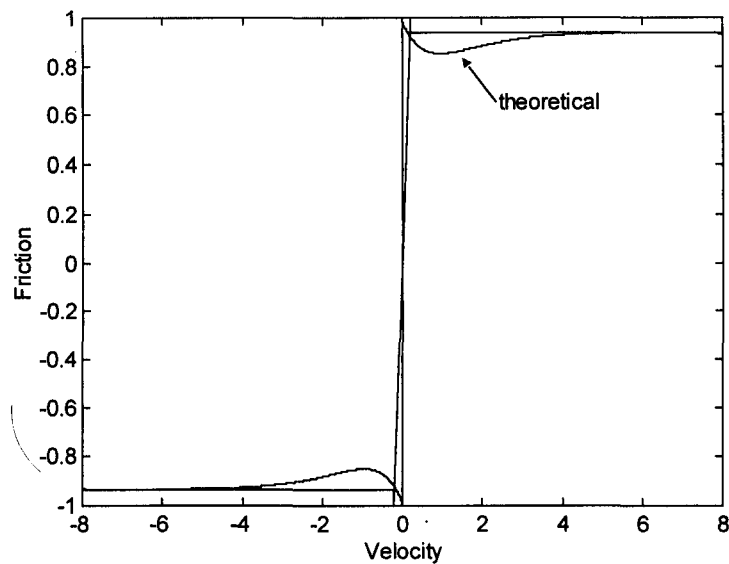


Figure 3.41. Classical and approximated friction model

To gain a basic understanding of stick-slip, assume a single spring-mass model with viscous damping [Derjaguin 57] as pictured in Figure 3.42. Suppose that the supporting table is driven at a constant speed, v , and that initially the spring, k , is not extended. When the surface now moves, the mass sticks to the table and the spring and damper extend until the spring and damper force reaches a value equal to the static frictional force, F_s . As soon as the mass starts to slip, the frictional force falls rapidly to the dynamical force, F_d , and the unbalance between static and dynamic frictional force causes a sudden acceleration of the mass. Consequently, the velocity of the mass also increases until the spring-damper force has fallen to the dynamical friction force. At this moment, there are two possibilities during the deceleration, either the mass velocity becomes zero or tends to the table velocity, v , and stick-slip vanishes. If the mass velocity falls to zero then again theoretically there are two possibilities, either a new stick phase starts or the mass jumps back to its original position. However, the latter is excluded from this analysis since it does not occur for a static friction smaller than three times the dynamic friction, which is normally the case [Derjaguin 57]. Furthermore, the time dependence of friction during the stationary contact is also omitted. Tests on two solid surfaces have shown that the static friction gradually increases (i.e., exponential) as the stick time increases [Kato 72].

Let X denote the movement of the mass then the spring extension, x , (positive in the direction of the table movement) can be written as follows:

$$\begin{aligned} x &= X - vt \\ \frac{dx}{dt} &= \frac{dX}{dt} - v \end{aligned} \quad (3.10)$$

Considering that the table velocity, v , is constant, the acceleration of both mass and spring will be identical and the equation of motion of the mass will be:

$$\begin{aligned} m\ddot{X} &= -c\dot{x} - kx - F_d(v) \\ \text{or } m\ddot{x} + c\dot{x} + kx &= -F_d(v) \end{aligned} \quad (3.11)$$

The dynamic frictional force expressed by, $F_d(v)$, is velocity dependent and works opposite to the direction of motion. Adapting the notation in terms of the damping ratio, ζ , (i.e., ratio of actual damping coefficient, c , over critical damping, c_c) and the undamped natural frequency, ω_n , given respectively by:

$$\zeta = \frac{c}{2\sqrt{mk}} \quad \text{and} \quad \omega_n = \sqrt{k/m} \quad (3.12)$$

Equation (3.11) becomes:

$$\ddot{x} + 2\zeta\omega_n\dot{x} + \omega_n^2x = \frac{-F_d(v)}{m} \quad (3.13)$$

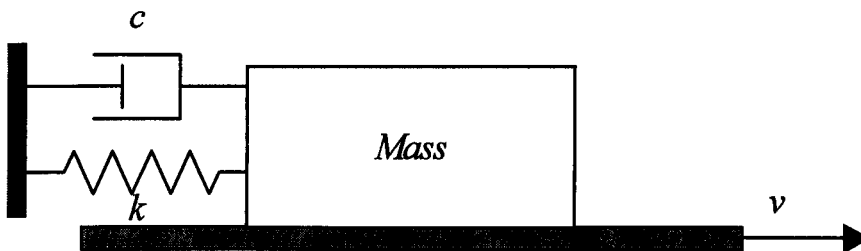


Figure 3.42. Theoretical spring damper model

The solution of the 2nd order differential Equation (3.13) comprises a homogeneous and a particular term of the following kind, with A and B integration constants:

$$\begin{aligned} x_{\text{hom}} &= \frac{-F_d(v)}{m\omega_n^2} \\ x_{\text{part}} &= e^{-\zeta\omega_n t} (A \cos \omega' t + B \sin \omega' t) \quad \text{with} \quad \omega' = \omega_n \sqrt{1 - \zeta^2} \end{aligned} \quad (3.14)$$

Differentiating the particular solution of Equation (3.14) gives the velocity as follows:

$$\dot{x} = e^{-\zeta\omega_n t} [(-\omega_n \zeta A + \omega' B) \cos \omega' t - (\omega_n \zeta B + \omega' A) \sin \omega' t] \quad (3.15)$$

Assuming now, that ($t=0$) at the moment of transition from sticking to slipping, the following conditions apply:

$$c\dot{x} + kx = -F_s \quad \text{and} \quad \frac{dx}{dt} = -v \quad \text{and} \quad \frac{d^2 X}{dt^2} = -\frac{F_s - F_d}{m} \quad (3.16)$$

Using these initial conditions, the integration constants A and B can be determined and so the final solution of Equation (3.13) is obtained as follows:

$$x = x_{\text{hom}} + e^{-\zeta\omega_n t} \left[(2\zeta v_1 - \Phi) \cos \omega' t + \frac{1}{\sqrt{1-\zeta^2}} (2\zeta^2 v_1 - \zeta\Phi - v_1) \sin \omega' t \right] \quad (3.17)$$

with $\Phi = \frac{F_s - F_d}{k}$ and $v_1 = \frac{v}{\omega_n}$

Differentiating the particular solution will give the velocity and acceleration respectively as:

$$\dot{x} = \omega_n e^{-\zeta\omega_n t} \left[-v_1 \cos \omega' t - \frac{(\zeta v_1 - \Phi)}{\sqrt{1-\zeta^2}} \sin \omega' t \right] \quad (3.18)$$

$$\ddot{x} = \omega_n^2 e^{-\zeta\omega_n t} \left[\Phi \cos \omega' t + \frac{(v_1 - \zeta\Phi)}{\sqrt{1-\zeta^2}} \sin \omega' t \right] \quad (3.19)$$

The mass will only stick to the table surface when its relative velocity is zero or in other words when $\dot{x} = -v$ (Equation (3.18) at $t=0$). The severity of the sticking phase will also be dependent on the initial acceleration given to the mass. From Equation (3.19), it can be seen that the acceleration at ($t=0$) is dependent on Φ , or on the difference between the static and dynamic frictional force. Hence, a larger discrepancy between the static and the dynamical force will result in a longer stick-phase or on the other hand, no difference would make stick-slip theoretically infeasible. In addition, stick-slip will end when the damping of the system, ζ , is large enough. Furthermore, Derjaguin *et al.* [Derjaguin 57] determined the critical velocity where stick-slip friction stops. When the mass is in the sticking phase, its velocity is equal to the table velocity and consequently the acceleration will be zero. Thus, Equation (3.19) becomes zero for:

$$\tan \omega' t = \frac{\sqrt{1-\zeta^2} \Phi}{\zeta\Phi - v_1} \quad (3.20)$$

Obviously, the first sticking phase ($t=0$) will fulfil Equation (3.20). However, a second relation can be found by substituting Equation (3.20) in Equation (3.18) where during the stick-phase the velocity is

equal to the table velocity. This results in a critical velocity, v_c , constituting the boundary between the region of stick-slip and normal sliding. Unfortunately, the relation needs to be solved numerically.

The above theory can be extended for a multiple-mass system though the analytical solution is cumbersome and therefore excluded from this section. However, a multiple-mass system will be used in simulations in section 3.10.6. Further, note that this approach only simulates the gradual extension of fabric and does not account for any shear. In order to simulate the stick-slip behaviour in fabrics, the elasticity and internal damping of the material need to be known, hence, some measurement of these parameters are conducted in the following section.

3.10.5 Defining Parameters for Spring-Damper Model

Considering that the stick-slip is a dynamical phenomenon, the parameters (i.e., the spring and the viscous damper) necessary to describe this behaviour might be too. Besides, the damping of a material cannot be measured statically, so a dynamic measuring technique needs to be applied. A method similar to Alptekin's procedure for measuring the longitudinal vibration in yarns, summarised in the literature review (chapter 2), would be appropriate. However, the fabric would need to be tested hanging under its own weight to prevent it from sagging. Thus, simply hanging a fabric strip with a weight on a vibrating exciter, pictured in Figure 3.43, will reveal the same results.

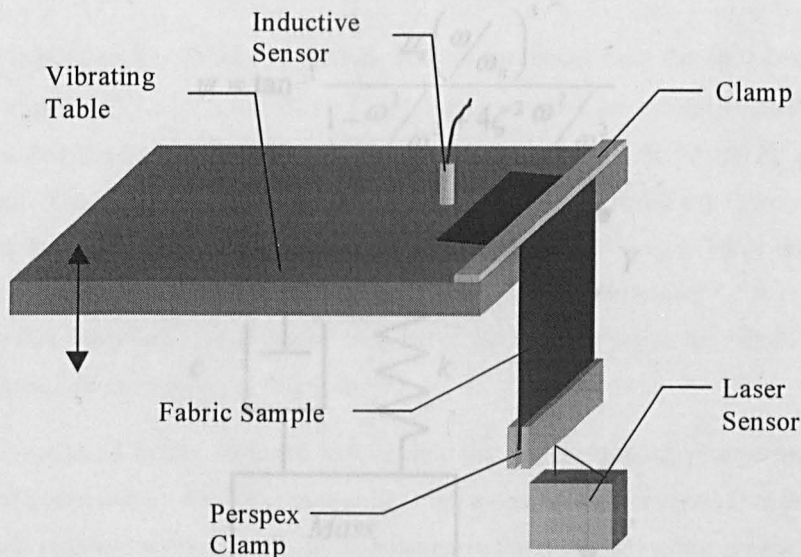


Figure 3.43. A sketch of the longitudinal vibration measurement of fabric

The experiment consists in measuring the displacement and phase difference of the fabric-mass combination relative to the vibrational motion of the table. A 6-cm wide fabric strip is clamped at one end to the table edge and hangs down with a lightweight Perspex clamp (15.87 g) connected at the other fabric end (total fabric length is 14-cm). The Perspex clasp has a dual purpose, serving as a weight to straighten the fabric vertically and acting as a target for the laser sensor (LD1605-4 by $\mu\epsilon$ ®). Further, the table motion is measured with a non-contacting inductive sensor (Gapteck 2004 see

Appendix B), and both sensor signals are logged and analysed by the computer. The test set-up is similar to the experiments in chapter 5 where to reader is referred to for further details.

Theoretically, the experiment can be approached as a single degree-of-freedom (SDOF) spring-damper (viscous) model [Harris 95], which is excited at the base (see Figure 3.44). Consider the motion of the foundation has a sinusoidally varying displacement, Y , with time given as follows:

$$Y = u_0 \sin(\omega t) \quad (3.21)$$

In the steady-state, the displacement of the mass, y , is defined as:

$$y = T_r u_0 \sin(\omega t - \psi) \quad (3.22)$$

with T_r and ψ the transmissibility and phase-shift (see Figure 3.45) respectively expressed in function of the frequency ratio (ω/ω_n) as follows:

$$T_r = \frac{\sqrt{1 + \left(2\zeta \frac{\omega}{\omega_n}\right)^2}}{\sqrt{\left(1 - \frac{\omega^2}{\omega_n^2}\right)^2 + \left(2\zeta \frac{\omega}{\omega_n}\right)^2}} \quad (3.23)$$

$$\psi = \tan^{-1} \frac{2\zeta \left(\frac{\omega}{\omega_n}\right)^3}{1 - \frac{\omega^2}{\omega_n^2} + 4\zeta^2 \frac{\omega^2}{\omega_n^2}}$$

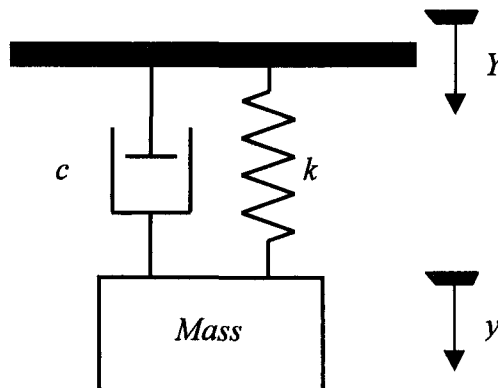


Figure 3.44. SDOF Spring-damper model force-vibrated at the base

The transmissibility, T_r , is a non-dimensional ratio of the response amplitude of the mass to the excitation amplitude or in other words, it represents the magnitude of the transfer function of the system. In particular for this system, the motion transmissibility is numerically identical to the force transmissibility [Harris 95]. Note that the phase picture in Figure 3.45 differs from a classical damped harmonic oscillator in which the mass is excited. The phase angle, ψ , for a damped base excited

system does not tend to -180° but goes to -90° at infinite frequency. Only an undamped system ($\zeta = 0$) gives a $0-180^\circ$ phase-shift, a damping coefficient of 0.5, for instance, will give immediately a 90° shift.

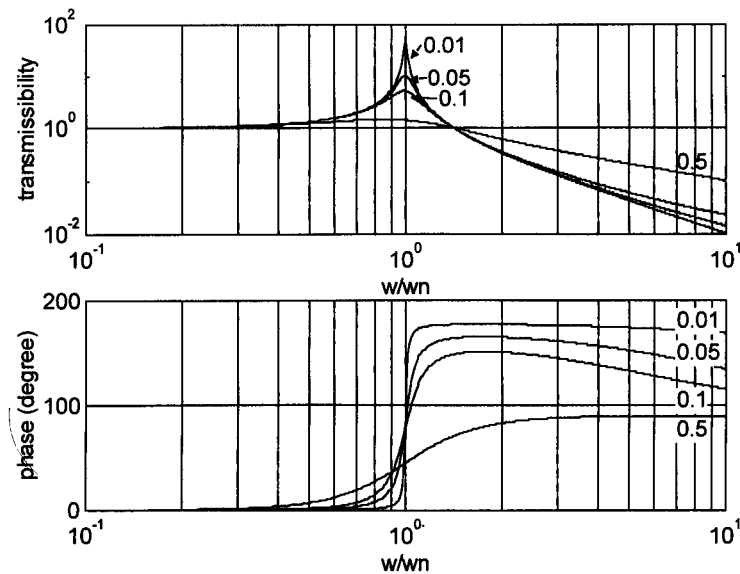


Figure 3.45. Frequency response for different damping ratios of a base excited viscous-damped system

The experiments have been performed on fresh specimens from the set 3 fabrics in a standard testing atmosphere ($20^\circ\pm 1^\circ\text{C}$, $65\pm 4\%$ r.h.). All fabric samples have been vibrated at $50\text{-}\mu\text{m}$ (u_0) amplitude and scanned at different frequencies, starting from 7 Hz up to 60-100 Hz depending on the type of fabric. The amplitude was chosen small enough in order to avoid any flexural waves or ripple in the fabric though remained sufficiently measurable for the laser sensor. Three tests are performed consecutively for each fabric type. The tests showed a good repeatability (r^2 0.97) and have been averaged before analysing. The averaged frequency responses for the seven fabrics (C3 to Pa1) are given in Figure 3.46 to Figure 3.52 respectively.

A glance at all figures indicates immediately that we are dealing with second order systems, which are characterised by the -90° phase-shift at resonance. A further increase in frequency reduces the amplitude response or transmissibility and increases the phase difference gradually to -180° . Yet, three fabric samples form an exception to this. C3 and L2, and to a lesser extent Ac1, do not give a 180° phase-shift (the ripple in the amplitude plot of Ac1 is caused by sideways flapping of the fabric). Remarkably, these three fabrics are all woven materials.

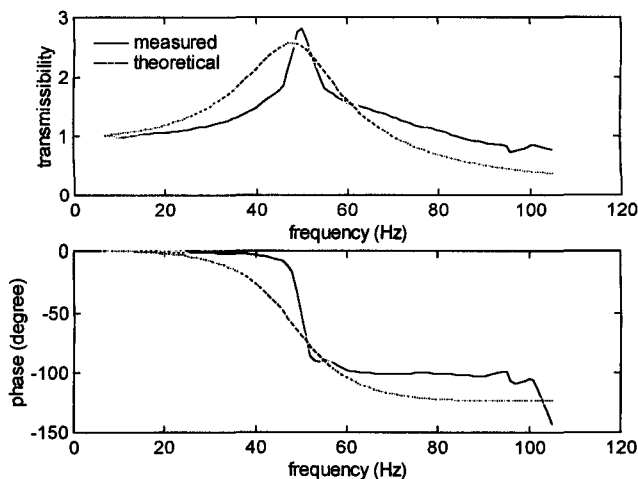


Figure 3.46. Transmissibility of C3 at 50 μm excitation

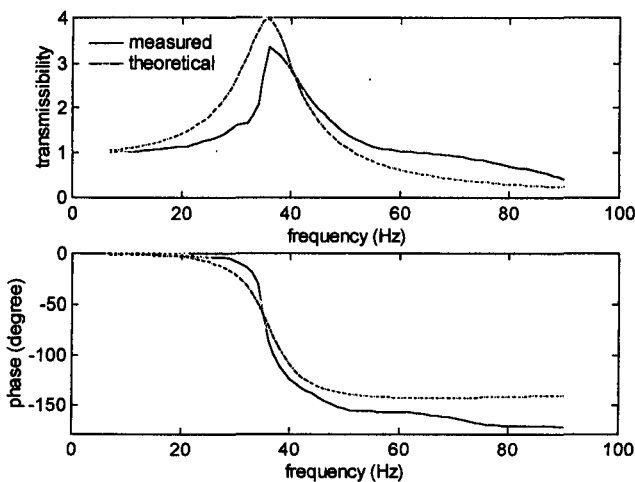


Figure 3.47. Transmissibility of KC3 at 50 μm excitation

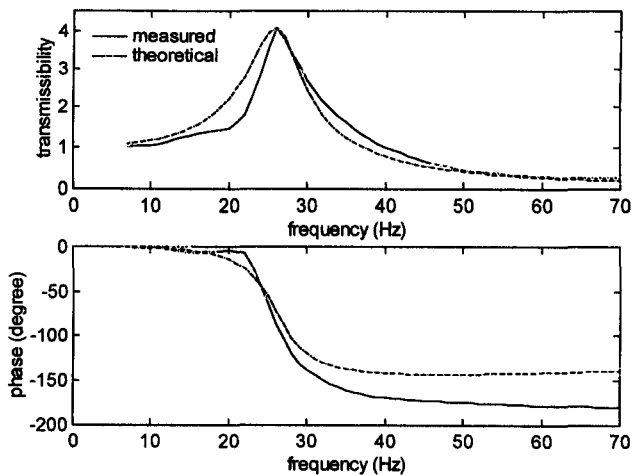


Figure 3.48. Transmissibility of KA1 at 50 μm excitation

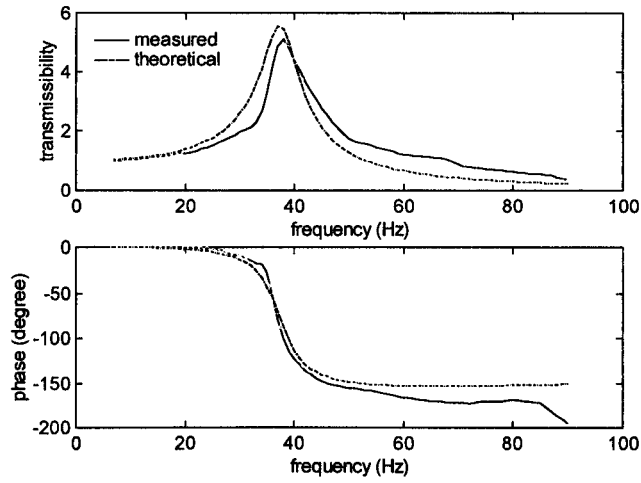


Figure 3.49. Transmissibility of KA3 at 50 μm excitation

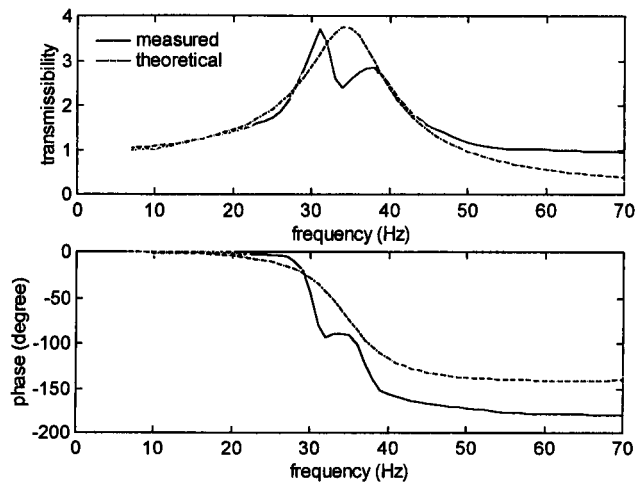


Figure 3.50. Transmissibility of Ac1 at 50 μm excitation

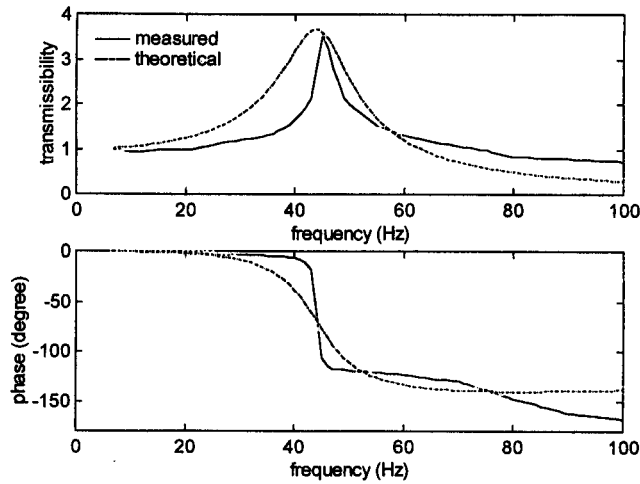


Figure 3.51. Transmissibility of L2 at 50 μm excitation

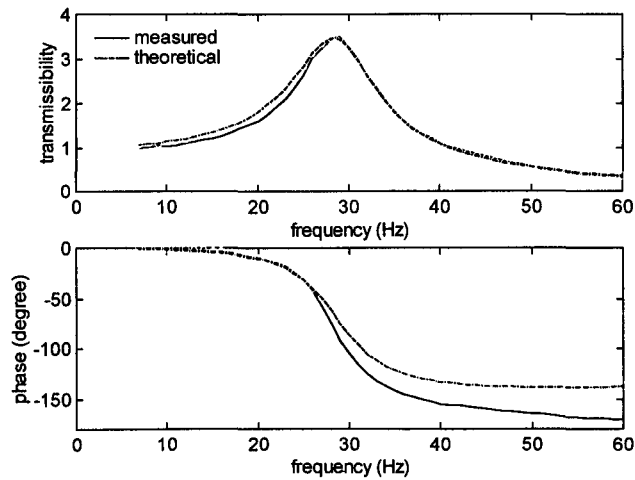


Figure 3.52. Transmissibility of Pa1 at 50 μm excitation

Nevertheless, a spring-damper model is successfully proposed to all fabric types (see theoretical graphs in Figure 3.46 to Figure 3.52), especially the non-woven material Pa1 matches perfectly the theoretical curve. The resonance frequency, f_{res} , spring constant, k , and damping coefficient, c , are summarised in Table 3-10 for all seven fabric samples respectively together with the cross-correlation, r^2 , validating the theoretical model. The two parameters, k and c , for the model have been calculated as follows. The resonance frequency has been estimated from the phase plot because of the smoother transition (viz., smaller errors) and used to calculate the spring constant according to Equation (3.12). The damping coefficient has been deduced from a MATLAB™ [MATLAB 88] simulation (i.e., function 'invfreqs') that uses an equation error method to identify the best model from the magnitude and phase data. Unfortunately, the function gives different coefficients for the numerator (1st order polynomial) and denominator (2nd order polynomial), which is possibly the best fit but has no physical significance. Yet, the denominator coefficients are approximating the measured data coefficients, in particular, the resonance frequency. Hence, the damping ratio, ζ , from the simulation is used to calculate (Equation (3.12)) the damping coefficient of the fabric.

Table 3-10. Estimated spring-damper coefficients from longitudinal vibration measurements for set 3 fabrics

Fabric code		f_{res} (Hz)	k (N/m)	ζ	c (N s/m)	r^2 for T_r	r^2 for ψ
C3	Warp	49.6	1628	0.215	2.246	0.864	0.974
KC3	Wale	36.4	883	0.131	1.012	0.888	0.994
KA1	Wale	26.2	473	0.127	0.730	0.957	0.996
KA3	Course	37.6	982	0.091	0.758	0.937	0.996
Ac1	Warp	35.0	808	0.138	1.014	0.933	0.994
L2	Weft	44.6	1347	0.142	1.364	0.869	0.997
Pa1	-	28.9	538	0.151	0.893	0.996	0.999

Standard conditions, excitation amplitude: 50 μm , r^2 : correlation coefficient between theoretical and measured data

From Table 3-10, it can be seen that the woven materials (C3, Ac1 and L2) are generally identified as stiffer materials considering their higher resonance frequency and resulting spring constant. Furthermore, a higher damping is also found for these materials. On the other hand, the knitted materials on average are more extendable and therefore give a lower resonance frequency, especially KA1, which has a very open structure. These results tie in very well with previous findings from the diode bench measurements in 3.10.2 above.

Comparing now the resonance frequency from Table 3-10 with the stick-slip frequencies (wavelengths) from the autospectral density function in Table 3-9, no direct numerical relation can be established apart from the samples having the same ranking. For example, fabric C3 has the highest resonance frequency and gives also the highest stick-slip frequency. The fact that there is no obvious relationship is somehow expected regarding that friction, which brings in another stiffness effect (i.e., material surface relation, referred as the Dahl effect), is excluded in the longitudinal vibration.

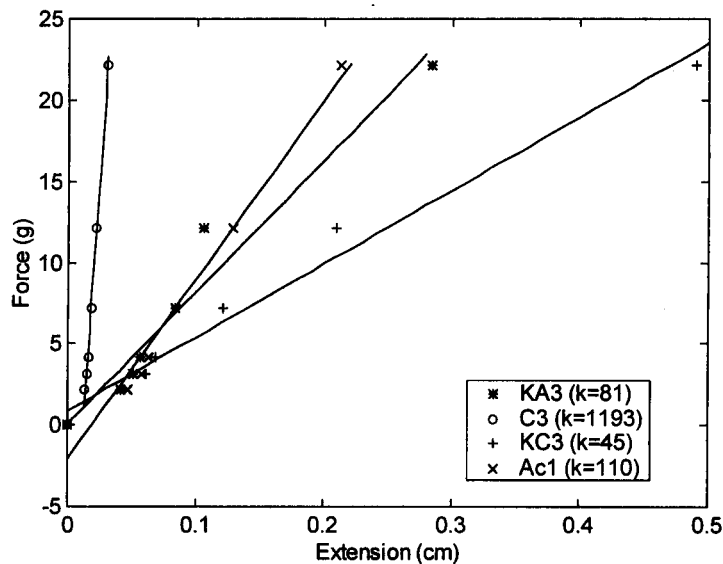


Figure 3.53. Static extension measurements for some set 3 fabrics

Standard conditions, averaged data of six measurements per fabric (one measurement per day) fit to a first order polynomial (least square method)

Furthermore, when measuring the extension statically, much smaller values are found (see Figure 3.53) compared to the dynamic equivalent deduced from the resonance frequency. In particular, the static extension of the knitted sample, KC3 and KA3, differs a factor 12 to 20 respectively (viz., larger extension). Yet, knitted and woven materials are likely to have a different extension process. For knitted materials, the structure will be stretched first followed by the fibres whereas for woven materials, the trellis like structure is extending a lot less so that the extension mainly comes from the fibres. The static fabric stiffness has simply been measured by hanging small weights at the bottom edge of the fabric strip and reading its corresponding extension with a travelling microscope. However, this method is rather crude considering that the fabrics are not exposed to a gradually increasing force and that the extensions are very small, which makes them susceptible to

errors. Yet, it has to be said also that the dynamical force at the resonance frequency is 3-5 times larger (i.e., peak transmissibility 3-5) than the maximum static force used in the stiffness tests. This would thus imply that either the static force-extension curves from Figure 3.53 change their gradient severely at larger forces or that the static and dynamic stiffness (longitudinal) are totally different parameters. The latter is more acceptable since similar conclusions were made for 3D fabrics (TABI) by Clayton *et al.* [Clayton 92].

In the next and final section, the theoretical model from section 3.10.4 will be implemented in a SIMULINK™ environment using the experimentally determined parameters k and c together with the friction coefficients. The simulated results will be tested and verified against the measured stick-slip traces from section 3.10.3.

3.10.6 Stick-Slip Simulation

The differential equation for the classical stick-slip model, defined in Equation (3.11), is translated into a block diagram in SIMULINK™ and verified with the data of the seven set 3 fabrics (see Appendix E). Note, however, that the fabric stick-slip is not modelled as a stationary body on a moving surface but as a body, which is dragged over a stationary surface. Both cases are mathematically identical anyway. Further, the model has been extended to a two-mass and four-mass system and validated with a stiff and extendable fabric respectively C3 and KC3. The SIMULINK™ software package [SIMULINK 93] is an extension to MATLAB™ and used for simulating dynamic systems. Regarding the non-linearity of stick-slip, the Gear algorithm [Kahaner 89] was found to be the most suitable numerical integration method. Gear is a predictor-corrector method that works well on systems, which have a mixture of fast and slow dynamics (i.e., stiff systems) as in this case here. The actual step size during integration is variable and only determined by the pre-set tolerance (10e-08).

When measuring the individual model parameters in 3.10.5, a large discrepancy was found between the static and dynamic stiffness. Despite the fact that the stick-phase, which is a static mechanism, is dominating the total stick-slip process at low speeds, both the static stiffness and dynamic stiffness have been included individually in a single-mass model. The damping coefficients, c , are calculated with the appropriate fabric mass and spring constant from the damping ratios, ζ , which were measured from the longitudinal vibration tests in 3.10.5. Finally, the frictional force, which is simulated as velocity independent, is defined by two points in both the positive and negative velocity direction: (F_s, v_1) represents the static friction and (F_d, v_2) the dynamic friction. Note that F_d is not the minimum frictional force reached at the slip-phase but the dynamic frictional force, which is the average of several stick-slip cycles (Table 3-8). The slope determined by (F_s, v_1) is made as small as possible ($v_1 = 1e-10$ m/s) to minimise the associated numerical stiffness and is well away from the sliding speed v_0 (0.12 mm/s) used in the simulations. The friction model parameters for all set 3 fabrics are listed in Table E-5 (Appendix E) for a single-mass model.

Table 3-11. Simulated stick-slip times for a single-mass model

Fabric code		Experimental	Simulated	Simulated	Simulated critical
		t_{sls} (s) ⁺	(dynamic) t_{sls} (s) [*]	(static) t_{sls} (s) [*]	velocity, v_c (m/s) [*]
C3	<i>Warp</i>	0.65	0.01	0.01	2e-04
KC3	<i>Wale</i>	0.53	0.02	0.3	2e-03
KA1	<i>Wale</i>	1.21	0.07	0.7	4e-03
KA3	<i>Course</i>	Irregular	Irregular	Irregular	6e-04
Ac1	<i>Warp</i>	Irregular	Irregular	0.07	4e-04
L2	<i>Weft</i>	0.53	0.01	0.01	3e-04
Pa1	-	Irregular	Slip	Slip	-

(+) Values measured from the first tests at 0.12 mm/s, (*) at a sliding speed of 0.12 mm/s

Generally, the simulated stick-slip traces (with dynamic and static stiffness) resemble the experimental results numerically though the frequency of the simulated traces is far too small. From Table 3-11, it can be seen that the simulated stick-slip time, t_{sls} , when using the dynamic stiffness deviates enormously in all fabrics from the experimental stick-slip time. This is somewhat expected because the dominating stick-phase is after all a static mechanism and the forces involved during stick-slip are minute (viz., much lower than the testing conditions in 3.10.5). So, in other words, the dynamic stiffness, which is much larger than the static stiffness, cannot be used to simulate stick-slip. When simulating the model with the static stiffness only the knitted materials, which in general have a lower stiffness compared to woven fabrics, return a stick-slip time in the order of the measured values (0.5-1.21 s). The remaining divergences must be ascribed to errors in the experimental parameters (e.g., the damping might be slightly non-linear) but mainly to the simplification of simulating the friction as velocity independent. As seen in 3.9 the sliding velocity can have a significant effect on the friction especially at low velocity. Furthermore, Table 3-11 shows also the simulated critical velocity, v_c , at which stick-slip ceases to exist. This critical velocity is closely connected to the damping coefficient hence the larger values for the knitted materials.

Figure 3.54 to Figure 3.56 represents the simulated time history of a single mass model, the displacement of the mass and spring, and the velocity of the spring respectively for KC3. The jagged staircase type of curve, typical for stick-slip, is clearly exhibited in Figure 3.54. The stick-phase is linearly increasing until the static friction is reached where slip is suddenly initiated. Note the chopped part during the slip-phase, which is not a simulation deficiency but partly caused by the sudden fall in friction from the static to the dynamic value. The second half of the jump is due to the spring kicking the mass forward, and thereby reducing the friction further. A similar looking graph is found by Haessig and Friedland [Haessig 90] when applying the classical model to simulate a solid body. Obviously, the spring extension in Figure 3.55 has an identical looking shape to the frictional force

since the spring is the only physically extendable link in the model (viz., damping unit is only active at the slip). Finally, each slip coincides with a huge increase in velocity of the spring and the mass ($v_{max} = \mu_s g \sqrt{m/k}$), pictured in Figure 3.56. A regular (periodic) stick-slip differentiates here from an irregular stick-slip in that for a regular trace each slip reaches the same maximum velocity. The model is now further extended into a two-mass system and verified again for C3 and for KC3.

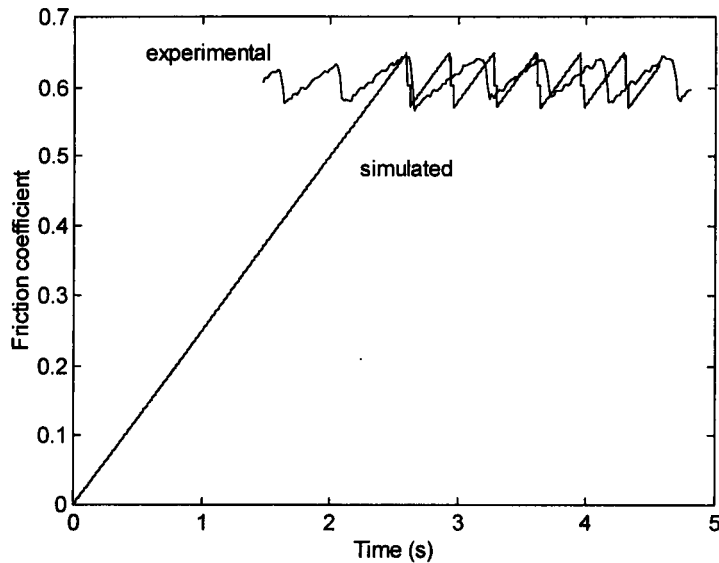


Figure 3.54. Comparison between the simulated and experimental stick-slip for KC3

Simulation parameters; m : 2.2 g, k : 45 N/m, c : 0.08244 N s/m, μ_s : 0.64, μ_d : 0.61

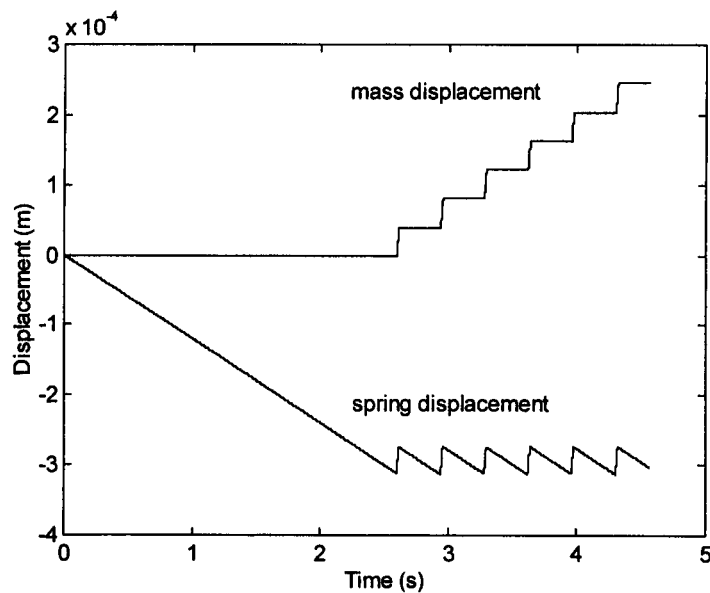


Figure 3.55. Displacement of spring and mass in a single-mass model (KC3)

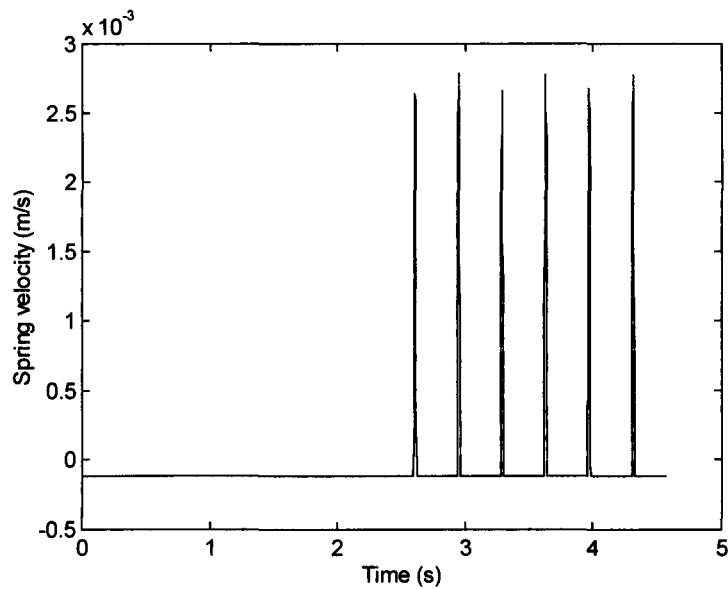


Figure 3.56. Spring velocity in a single-mass model (KC3)

When modelling a fabric strip as a two-mass system (Appendix E), obviously the mass is equally split in two but the spring constant and damping ratio, ζ , between each mass should remain the same as for a one mass model. It would be expected that the fabric stiffness of a 2-cm fabric strip is the same as for a 200-cm long strip. Hence, when using these parameters in the simulation, the stick-slip time reduces even further compared to the single mass model and the minimum friction for slip slightly increases. Furthermore, in the case of fabric C3, the stick-slip of the first mass disappears completely. Only when the total stiffness is split in two, a similar stick-slip time is obtained as for a single-mass model (see Figure 3.57).

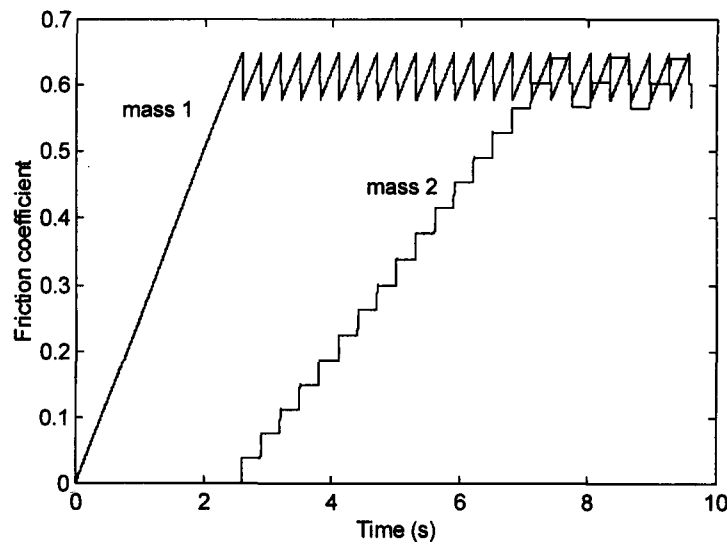


Figure 3.57. Simulated stick-slip for a two-mass model (KC3)

Simulation parameters; $m_1 = m_2$: 1.1 g, k : 22.5 N/m, $c_1 = c_2$: 0.04122 N s/m, μ_s : 0.64, μ_d : 0.61

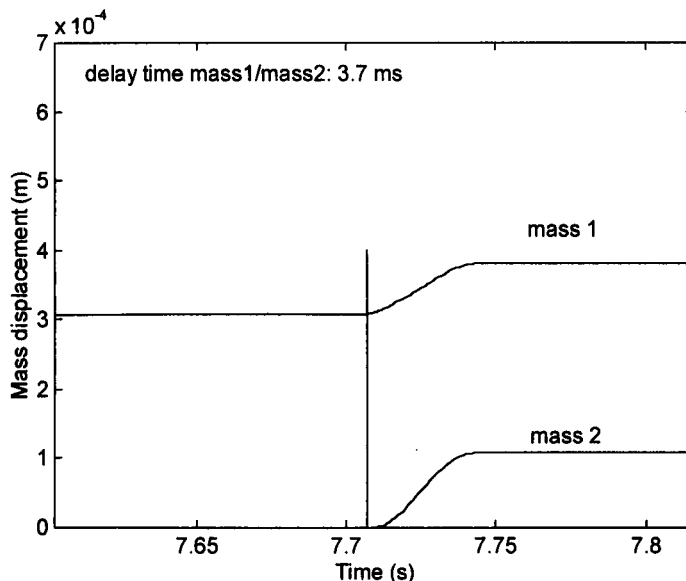


Figure 3.58. Simulated mass displacement (enlargement) of KC3 with a two-mass model

Simulation parameters; $m_1 = m_2$: 1.1 g, k : 22.5 N/m, $c_1 = c_2$: 0.04122 N s/m, μ_s : 0.64, μ_d : 0.61

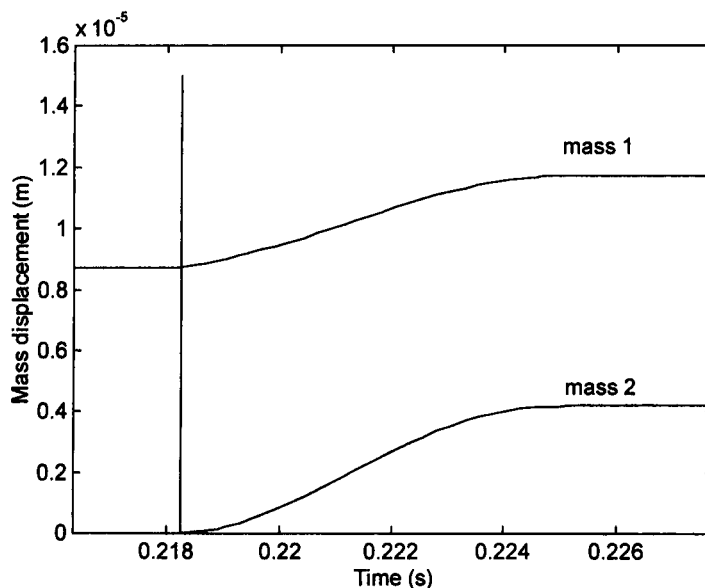


Figure 3.59. Simulated mass displacement (enlargement) of C3 with a two-mass model

Simulation parameters; $m_1 = m_2$: 0.935 g, k : 596 N/m, $c_1 = c_2$: 0.32112 N s/m, μ_s : 0.57, μ_d : 0.52

Figure 3.57 shows the simulated time history of KC3 for both masses. Note the difference in trace for the two masses. The first mass (mass 1, pulling mass) displays a typical stick-slip trace with a 0.3 s step, but the second mass (mass 2) is following a square wave. Thus, if for example stick-slip is measured on a regular friction apparatus where the fabric strip is connected to a force sensor, only the first signal of mass 1 will be registered. Figure 3.58 and Figure 3.59 picture the mass

displacements of KC3 and C3 respectively. A larger time delay has been found for KC3 between the two masses compared to C3. This agrees with the results from the diode bench in 3.10.2 although no concrete numbers can be given.

The model is now easily extendable to an n-dimensional mass model. For example, a four-mass model (Appendix E) has been developed and tested again with the experimental parameters of KC3 and C3. Unfortunately, the simulation for C3 becomes unstable but results for KC3 resemble very much the traces captured on the diode bench. However, a comparison of both simulated and experimental stick-slip traces, given in Appendix E, indicates that the simulated stick-slip time is now larger than the experimental.

To conclude, the above simulations have shown that a fabric strip sliding over a surface can be modelled as a 'lumped' system of masses and springs though the correct stick-slip time is hard to achieve. For low order models, the stick-slip time is too small whereas for a four-mass model for example, the simulated time is too large. In addition, this section showed that stick-slip needs to be simulated with the static fabric stiffness, which for an n-dimensional mass model is split equally in between the masses.

3.11 Summary

The extensiveness of this chapter indicates clearly the numerous factors to which friction is susceptible. The various experiments have been concentrated on friction between fabrics and non-fibrous materials, more specifically aluminium, Formica and rubber. Yet, the study differs from others in that all the tests were performed under zero or very small loaded conditions. This revealed effects such as the static charging, which are usually lost under normal force tests.

The literature in the previous chapter pointed out the importance of the contact area in friction hence the surface roughness of both the sliding surfaces and the fabrics needed to be quantified. Laser scanning of the fabrics found a rougher surface in the warp direction than in the weft direction. Similar conclusions have been reported by Ramgulam *et al.* [Ramgulam 93] and are generally attributed to a larger yarn sett in the warp direction. The majority of friction experiments has been conducted on a fixed set of fabric specimens. Using new samples for each test would have apart from requiring a huge amount of fabric also introduced another source of variation as friction differs slightly from one place in a roll to another. On the other hand, using the same samples in different tests carried the risk of 'wearing' the surface. Successive friction tests have shown a 3-15% increase in friction, which is totally opposite to fabric-fabric friction where a decrease has been found [Carr 88], [Ajayi 92a]. However, including a relaxation period of 24 hours between the individual tests brings the surface back to its original state. Relating the fabric roughness to the friction coefficient revealed an inverse linear relationship for both knitted and woven fabrics where the 'smoothest' fabrics give the highest friction.

Considering the absorbency of many fibres (e.g., wool, cotton or flax), the environmental conditions for testing regarding temperature and humidity had a significant effect on frictional

properties of fabric. All tested fabrics acclimatised exponentially in about 3-10 min. when the relative humidity was suddenly increased from 0% r.h. to 65% r.h. However, the friction coefficients increased percentage wise more than the regain indicating that additional factors such as the fabric geometry have been changing. The absorption of water does increase not only the specific mass of the fabric but also causes the hydrophilic fibres to swell which, when woven or knitted into a structure, results in a smoother surface and consequently increased friction. The friction coefficient of all fabrics, even man-made as for example nylon, increases substantially from a relative humidity of 60% r.h. onwards. When drying the samples, however, higher values of friction have been measured except for cotton indicating a hysteresis similar to the changes in the mass (regain). An advantage of testing at higher humidity (> 40% r.h.) is that electrostatic charge cannot develop. Experiments at low humidity showed the importance of ionising the surrounding air when carrying out friction tests in these conditions. The tests indicated a relationship between the frictional responsiveness to humidity and the sensitivity to charging. Fabrics such as polyester and wool, who do not change a lot in friction coefficient with increasing humidity, were found very susceptible to static charge at low humidities.

The experiments in this chapter did not allow any classification according to the content of the fibre material considering the diversity in construction of the samples. However, sliding the various samples over different surfaces namely aluminium, Formica and rubber provided a respective rise in friction. All fabrics produced the highest friction when tested on rubber and the lowest when slid over the aluminium surface, nevertheless the surface roughness of rubber and aluminium is nearly identical. Hence, one might postulate that the shear strength for fabric-rubber is larger than for fabric-aluminium.

Considering the above effects on friction properties, it should be no surprise that fabrics do not obey the classical linear friction-laws (Amontons' Laws). Firstly, the friction coefficient decreases relatively quick when a normal pressure is initially applied and gradually aims towards a constant value. Secondly, doubling (2-dm^2) or quadrupling (4-dm^2) the sample area gives a 2-15% higher friction coefficient. The knitted fabrics, who on average measured a higher friction against all three sliding surfaces, have been more responsive to pressure changes than the woven samples. This is likely due to their structure, which is more compressible. Wilson's equation, already well established for describing the pressure relation in fabric-fabric friction, has been successfully applied here to fabric-non-fabric friction. A similar though weak inverse linear relation has been found between the frictional index, n , and the coefficient C . Yet, the yarn type of the fabrics, which was found to affect the relationship for fabric-fabric friction, has not been verified as a major influence here. Instead, a distinct grouping of the model parameters according to the sliding surface has been exposed.

Furthermore, the sliding velocity was also found to modify fabric friction. A notable drop in friction was detected at initially low sliding speed (0.5-2.0 mm/s) followed by a slow rise in friction for a further increasing speed. The effect, however, was more pronounced against a rubber surface than against aluminium. The striking similarity with the hydrodynamic lubrication of journal bearings introduced an empirical law, which has been applied effectively in fabrics to describe the friction-velocity relation.

Finally, great attention has been given to what happens when fabrics slide at very low speeds. The friction does not only increase in number but also the movement of the fabric becomes discontinuous at these conditions. This behaviour, generally known as stick-slip, has been measured, modelled and simulated. Considering that fabrics are extendable, the fabric strip does not move as one entity when sliding over a surface but in what has been referred to as a caterpillar movement. Depending on the material extension or shear, the fabric strip extends or shears first in the direction of pulling and suddenly breaks away from the sliding surface when the internal tension equals the static friction. A novel measuring technique has been introduced to visualise this movement in a fabric strip. In addition, stick-slip has been measured in the traditional way by attaching a fabric strip to a purpose built load cell. Two kinds of stick-slip emerged in the tests; some fabrics slipped periodically displaying the typical sawtooth trace whereas others slipped aperiodically. An autospectral density analysis of the time histories revealed an indirect dependency in some fabrics with the yarn density in the direction of sliding. However, a direct linear relation between the stick-slip frequency, the sliding velocity and the yarn spacing as reported by Hosseini Ravandi *et al.* [Hosseini Ravandi 94] has not been demonstrated in this study because of the absence of normal force. Further, a classical friction model has been proposed in which a fabric strip, presented as a lumped mass with springs and dampers, simulates stick-slip. Some crucial model parameters have been measured in order to make the simulation more realistic. The fabric damping, only dynamically measurable, has been obtained through a longitudinal vibration test. The experimental results revealed that fabric behaved as a typical second order system with a 90° degrees phase shift at resonance between one end of the fabric and the other. At the same time, the dynamic stiffness of the fabrics was deduced from the experimental resonance frequency though was found much larger than the static fabric extension in particular for the knitted fabrics. Consequently, when simulating stick-slip with the dynamic extensibility, the stick-slip frequency was far away from the experimental values. This was somewhat expected considering that the stick-phase responsible for the largest part of the cycle is a static process. Overall, the simulations agreed numerically though the timing remained a problem even when using the static extension. This mainly needs to be attributed to the fact that the friction has been modelled as velocity independent and to the crude measurement of the fabric extension. On the other hand, when increasing the order of the model, the stick-slip time was overestimated.

So, fabric friction can vary for a number of reasons and care is necessary when measuring friction and comparing results. In the following chapter the static and impact compressibility of set 1 fabrics will be measured and analysed. Again, the tests will not be performed at the standard pressure interval but at lower pressures, which determines the more characterising part of fabric compression.

4 Low Force Compression Characteristics

The measurement of fabric compression does not only form an integral part of objective fabric characterisation in terms of handle and comfort but it is also one of the important fabric properties for successful garment automation. A better understanding of the fabric structure with its different layers may be useful for automatic fabric inspection and image analysis. Further, the analysis of impact compressibility might help us understand the action of certain gripping mechanisms and elucidate the problems sometimes encountered in sewing dynamics where the pressure foot is continuously 'bouncing' on the fabric. In the first half of this chapter, the compression is measured statically and the corresponding KES-FB3 parameters are calculated and compared between the individual fabrics. Further, as a way of comparison, the zero pressure thickness is measured with a laser sensor as a non-contacting technique. Next, three different approaches to the well known van Wyk model are applied both to the woven and knitted fabric samples of set 1 and verified against the experimental data. The second half of this chapter investigates the impact compression on fabric in which a new and simple measurement technique, based on a pendulum, is introduced. The results are calculated from the successive losses in potential energy during the impacts and compared with the static compressibility.

4.1 Static Compression

4.1.1 Instrumentation and Method

A compression or thickness test is mostly a dual parameter test in which the force or pressure and the corresponding distance need to be measured simultaneously. A hand operated compression apparatus, sketched in Figure 4.1, has been built in-house. The testing device electronically measures the applied pressure through a miniature 50-cN load-cell (OMEGA® LCF-50, total range 100-cN compression and tension) which is sandwiched between a parallel moveable platform and the pressure foot. The reducing fabric thickness is measured with a 2-mm range inductive displacement sensor (TQ 401/5M) attached to the moveable platform. Both sensors are connected via a PC30AT card (12-bit conversion) to a computer, which logs the data.

The compression tester has been built according to the ASTM D1777 specifications with a \varnothing 50.0-mm anvil and \varnothing 35.7-mm pressure foot. This disk diameter here was chosen deliberately to give an effective area of 10 cm². As a matter of comparison, the KES-FB3 compression tester has only a measuring area of 2-cm², which therefore will give compression results with higher standard deviations [Dupuis 95]. Further, both compressing surfaces were lapped to give a mirror finish and are parallel to within 10 μ m. The parallelism is maintained through a moveable platform, which slides on Teflon® bushes over four precision steel shafts. A photograph of the rig and further details on the sensors can be found in Appendix B.

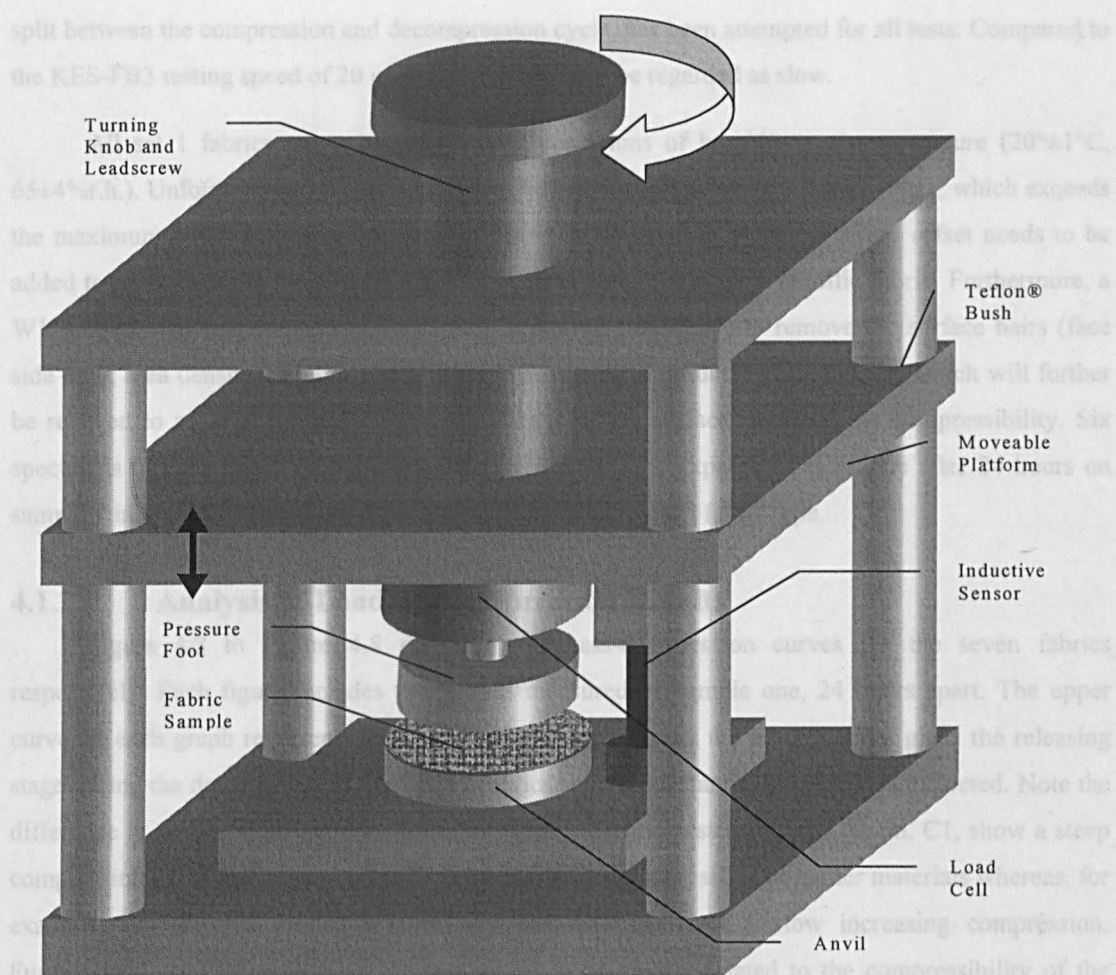


Figure 4.1. A sketch of the experimental compression rig

A typical compression test is performed as follows. A circular fabric sample with a diameter identical to the anvil ($\text{Ø } 50.0\text{-mm}$) is placed on the anvil with the fabric face up. The fabric specimen should be handled with care to avoid any wrinkling or altering of the fabric surface. In order to reduce any irreversible slippage effects common for very low pressure measurements, the fabric specimen is first compressed quickly to maximum pressure (10 cN/cm^2), held for 30-s and released again before the actual test starts. A similar approach was taken by de Jong *et al.* [de Jong 86] with a maximum pressure of 50 gf/cm^2 (maximum pressure used in the KES-FB3). After 'pre-compressing' the fabric, the pressure foot is brought up again by slowly turning the spindle anti clockwise until a minimum force (\approx zero) is reached, which becomes the starting point of the compression test. The pressure is then gradually increased stepwise (3-5 cN), while individual measurements of the force and displacement are taken. A delay of 5 seconds is allowed before each increment is logged by the computer (average of 1000 points sampled at 100 Hz) enabling the pressure changes to stabilise. When the maximum pressure of approximately 10 cN/cm^2 ($\approx 10 \text{ gf/cm}^2$) is achieved, the spindle is turned anti clockwise and the test is reversed in a similar way until the zero pressure point is reached again. Since time is an important factor in compressibility tests, a total test time of 33 min., equally

split between the compression and decompression cycle, has been attempted for all tests. Compared to the KES-FB3 testing speed of 20 $\mu\text{m/s}$ this test here can be regarded as slow.

All set 1 fabrics are tested in standard conditions of humidity and temperature ($20^{\circ}\pm 1^{\circ}\text{C}$, $65\pm 4\%\text{r.h.}$). Unfortunately, W1 has a thickness within the experimental pressure range, which exceeds the maximum 2-mm displacement range of the inductive sensor. Hence, a 2-mm offset needs to be added to the measuring range with a precision shim when testing this specific fabric. Furthermore, a W1 sample, which is considered very hairy, is shaven (manually) to remove the surface hairs (face side only, area density 328 g/m^2) and included in the test. Introducing this sample, which will further be referred to as W1b, should show the influence of the surface fibres on the compressibility. Six specimens of each fabric type are tested consecutively. The experiment is redone after 24 hours on sample 1 in order to find the repeatability and relaxation of each fabric type.

4.1.2 Analysis of Loading-Compression Results

Figure 4.2 to Figure 4.8 give the thickness-compression curves for the seven fabrics respectively. Each figure includes two graphs measured on sample one, 24 hours apart. The upper curve on each graph represents the compression stage whereas the bottom curve gives the releasing stage during the decompression. Hence, all fabrics show a substantial hysteresis as expected. Note the difference in steepness between the different fabrics. The polyester, P1, and denim, C1, show a steep compression curve and can therefore be regarded as less compressible or harder materials whereas, for example, the woollen fabric, W1, is very soft and measures a slow increasing compression. Furthermore, the repeatability of the test seems to be closely related to the compressibility of the sample and hence deviates more for C1 and P1. Dupuis *et al.* [Dupuis 95] report a standard deviation for the KES-FB compression tester ranging from $5\text{e-}03$ to $2\text{e-}02$ mm when testing identical fabrics under the same conditions. Despite the weak pressure used here, the repeatability of the compression is very high: some repeated tests are almost identical to the original test. However, the fabrics for which the repeated curve does not coincide with the original compression curve all seem to be increased in stiffness (shift to the right of the graphs). This increase, which is within the range of the inherent hysteresis of the apparatus (i.e., 10 μm see Appendix B), can indicate either a permanent set of the fabric or the need for a longer relaxation period.

In general, the compression-thickness curves are useful in visualising the compressibility of a material though comparing different materials with each other in this way is rather hard. For that, the KES-FB3 parameters, which allow a much better correlation between the materials have been derived (see 2.2.1) and are given in Table 4-1. The four parameters namely, *WC*, the work; *LC*, the linearity; *RC*, the hysteresis and *EMC*, which is the relative compression, are the average of six fabric specimens.

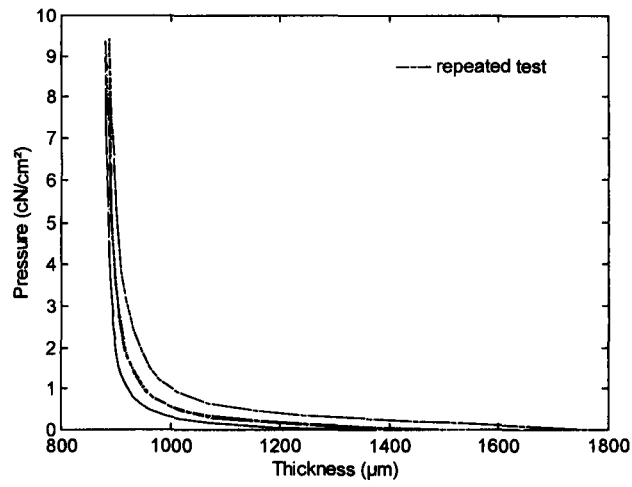


Figure 4.2. Compression hysteresis for C1

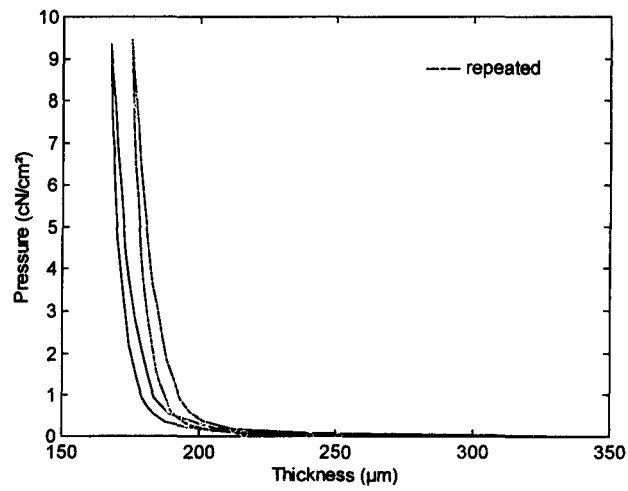


Figure 4.3. Compression hysteresis for P1

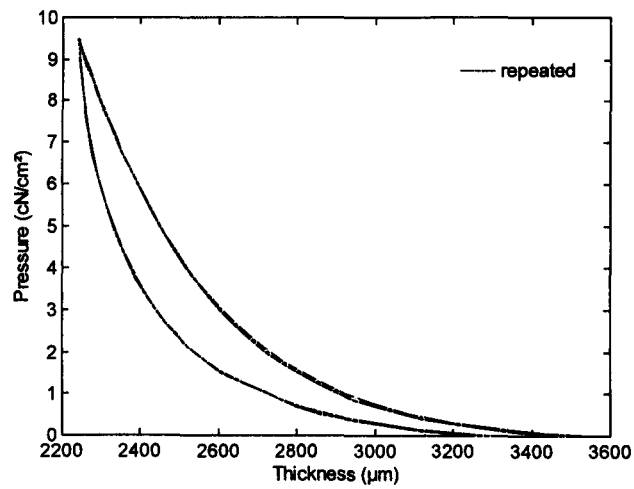


Figure 4.4. Compression hysteresis for W1

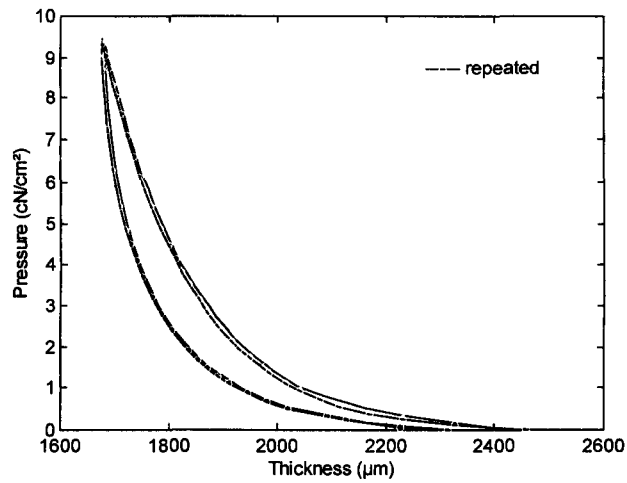


Figure 4.5. Compression hysteresis of W1b (shaven W1)

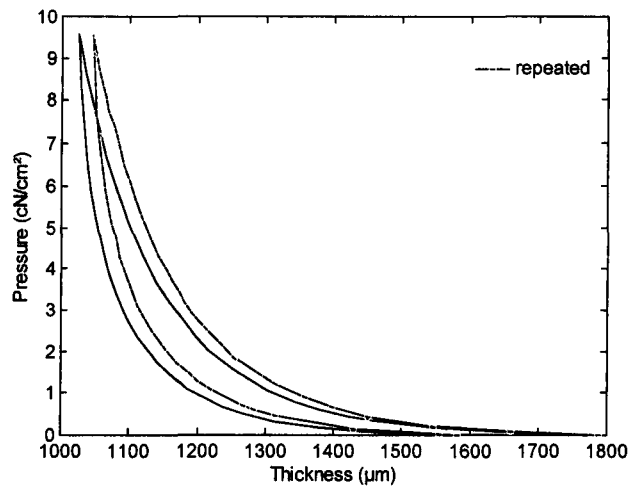


Figure 4.6. Compression hysteresis for KC1

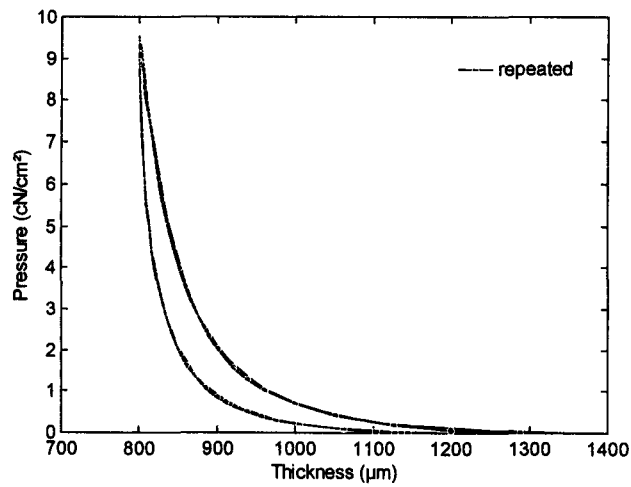


Figure 4.7. Compression hysteresis for KC11

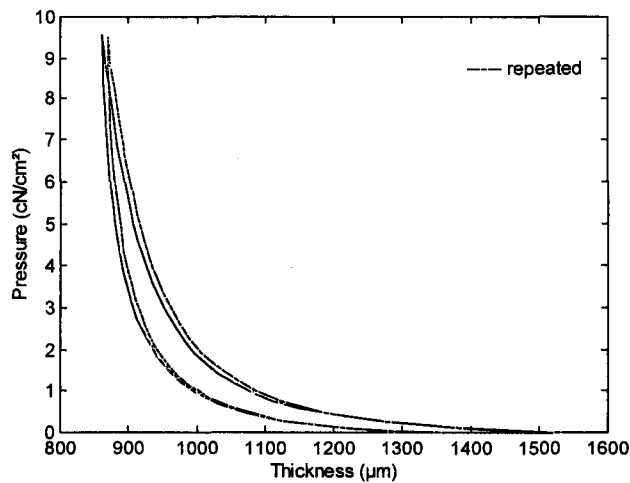


Figure 4.8. Compression hysteresis for KA11

The diversity in material thickness (0.25-3.5 mm) amongst the different fabrics in the test is well reflected in the KES-F parameters. First, the compressional work, WC (cN/cm), which is strictly speaking not an expression of the work but a kind of springiness of the material, varies from 0.008 cN/cm for P1 to 0.294 cN/cm for W1. A more compressible material such as the wool sample W1 gives a larger value of WC , yet this is opposite to mechanical spring constants where a larger value indicates a stiffer spring. Furthermore, W1b, which only differs from W1 in the surface layer, shows a near 50% reduction for WC . This indicates that the surface layer of a fabric has a large contribution to the compressibility (springiness) of the material. However, a direct relation between the surface roughness and WC would not be expected as seen in Figure 4.9. A material such as denim (C1) for example, has been characterised as rough because of its ribbed structure and is a 'hard' fabric whereas at the same time the polyester, P1, is a very smooth fabric but is also very incompressible. A second distinctive parameter for compression is the linearity of the compression, LC . If the thickness of the fabric decreases linearly with increasing pressure, the value of LC would be one. However, all fabrics compress nonlinearly and give a value for LC ranging between 0.14 for C1 to 0.47 for W1. A similar interval for the linearity ($LC = 0.22-0.50$) was found by de Jong *et al.* [de Jong 86] though an explanation for the difference between the various fabrics is not available in the literature. Again, the 'harder' fabrics C1 and P1 have a lower value for LC , which from Figure 4.2 and Figure 4.3 indicates a steeper rising compression. Note the large standard deviation for P1. This is common for 'harder' fabrics because the LC -value is very sensitive to the low-pressure thickness, which is more difficult to measure for these fabrics.

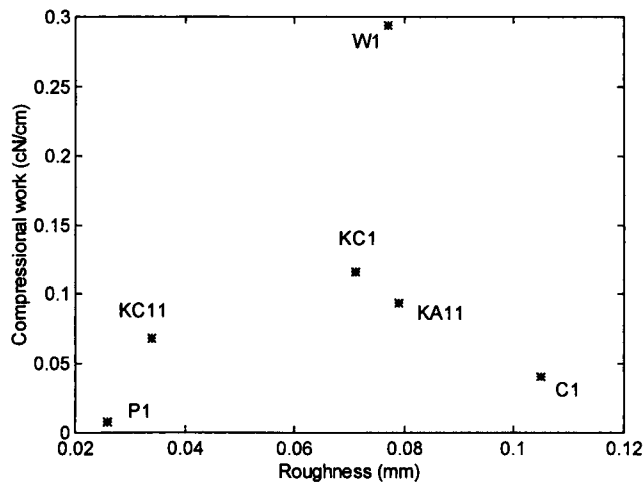


Figure 4.9. Surface roughness of the set 1 fabrics as a function of their 'springiness' (WC)

The third KES-FB3 parameter, RC , represents the hysteresis in the compression graph. In Table 4-1, it can be seen that a more or less similar value (i.e., $\approx 0.55\%$) is calculated for all fabric samples. Yet, from the compression graphs, in particular Figure 4.2 and Figure 4.3, one could wrongly conclude that the hysteresis for fabric C1 and P1 is much smaller compared to the other fabrics because RC is calculated relatively. Finally, the dimensionless EMC parameter expresses the compressibility of a fabric. The smaller the value of EMC the more incompressible the fabric is, as for example seen in case of P1. Further, it should be noted that all knitted fabrics have a very similar value of EMC , which could be due to their structure (equal loop density) whereas the woven materials are more diversified (a high sett for P1 but low sett for C1).

Table 4-1. KES-FB3 compression parameters (see 2.2.1) for set 1 fabrics (+ W1b)

Fabric code	WC (cN/cm)		LC (-)		RC (%)		EMC (-)	
	Mean	Std	Mean	Std	Mean	Std	Mean	Std
C1	0.041	0.006	0.144	0.015	56.63	2.75	0.408	0.033
P1	0.008	0.001	0.245	0.113	63.10	5.16	0.319	0.125
W1	0.294	0.006	0.471	0.006	59.89	0.41	0.372	0.004
W1b	0.150	0.012	0.420	0.015	57.39	2.08	0.322	0.006
KC1	0.116	0.004	0.337	0.013	54.23	1.30	0.408	0.015
KC11	0.068	0.006	0.266	0.010	50.17	0.47	0.406	0.016
KA11	0.093	0.008	0.290	0.015	57.55	0.69	0.431	0.006

Mean: average of six specimens tested under the same conditions, Std: standard deviation

4.1.3 Some Other Thickness Measurement Techniques

As a comparison, the averaged maximum and minimum thickness of the various fabrics has also been measured with the laser sensor and the micrometer respectively. For the measurements with the laser sensor, three points in a circular area (similar to the pressure foot area) have been measured and averaged for each specimen. From Table 4-2, it can be seen that, on average, the laser sensor underestimates the zero pressure thickness by 5-26% compared to thickness measured with the inductive sensor in the compression tester. This discrepancy in thickness measurement could support the findings of Hu and Newton [Hu 97] with regard to the existence of a second fabric layer between the protruding surface hairs and the core of the fabric. The laser does probably not detect the protruding surface hairs on the fabrics, which in the previous compression tests are responsible for very minute forces at the beginning of the compression. On the other hand, the thickness for the polyester P1, which is very susceptible to wrinkles due to its low bending stiffness (note the long low pressure change in Figure 4.3), is hugely overestimated by the laser sensor. Yet, thin fabrics will easily introduce larger errors. Further, the minimum thickness has been measured with a micrometer, which due to the larger pressure involved, measures a smaller minimum thickness than in the previous compression tests for all fabrics but C1. The thickness measured by the micrometer (and T_{\max}^+ when applied larger pressure on the micrometer) can be compared with the 'incompressible volume' from van Wyk's model in the next section.

Table 4-2. Average min-max thicknesses of set 1 fabrics measured with different systems

Fabric code	T_0 (mm) compression	T_0^* (mm) laser sensor	Difference compression /laser (%)	T_m (mm) compression	T^+ (mm) micrometer	T_{\max}^+ (mm) micrometer
C1	1.480	1.404	5.4	0.873	0.947	0.600
P1	0.255	0.379	-48.6	0.168	0.174	0.150
W1	3.541	2.961	19.6	2.223	0.884	0.540
W1b	2.336	1.913	22.1	1.582	0.757	0.585
KC1	1.778	1.404	26.6	1.052	0.612	0.400
KC11	1.334	1.082	23.3	0.792	0.417	0.250
KA11	1.561	1.555	0.4	0.892	0.638	0.470

(*) average value of the six specimens measured at 3 different spots (18 measurements in total), (m) maximum pressure used in static compression experiment, (+) thickness measured with micrometer (Mitutoyo 0-25 mm), ratchet slips between 5-10 N (according to manufacturer though not precisely quantified) with pressure diameter \varnothing 6.1 mm, (max +) thickness measured under higher pressure by tightening the micrometer over the set ratchet slip

4.1.4 Approximation of the Loading-Compression Results

From the literature review in (2.2), it can be concluded that up to now only two modelling approaches for compression in fabrics have been successful. On one hand, there is the van Wyk model, which has been refined over the years especially in replacing the nebulous *K-constant*, which represents the fibre orientation and on the other hand, there is a recent energy approach [Lee 92]. All other models are in fact curve fittings, which lack physical background. Van Wyk's model [van Wyk 46a, b] has been applied here because of its simplicity. The model will be checked for all tested fabrics at very low pressures ($< 10 \text{ cN/cm}^2$), which is the most varying and interesting part of the pressure-thickness curve. Furthermore, van Wyk's equation has to the best of the author's knowledge not been verified for knitted materials.

In the above, compression has been displayed as a function of the thickness variation of the fabric yet in the following discussion the volume per unit area, $V \text{ (mm}^3\text{)}$, will be used which is numerically equal to the thickness. The van Wyk equation can be implemented in three different formats. At first, there is the original Equation (2.25), $P = KE \frac{m^3}{\rho^3} \left(\frac{l}{V^3} - \frac{l}{V_0^3} \right)$ (E : Young's modulus), which is derived directly from the compression of wool wads. Applying now this formula to the experimental data renders compression curves for all seven fabrics, which have a more or less similar shape to the experimental curves though with a severe offset at the asymptote. This divergence is caused by omitting the 'incompressible' volume, V' , which becomes significant when compressing fibre assemblies to a small enough volume ($P > 0.5 \text{ cN/cm}^2$). Van Wyk himself corrected the original equation to the more detailed Equation (2.26), $P = KE \frac{m^3}{\rho^3} \left[\frac{l}{(V - V')^3} - \frac{l}{(V_0 - V')^3} \right]$, which can now further be approached in two ways [de Jong 86], [Dupuis 95]. Either V_0 , which is the volume at zero pressure, is relatively high compared to V and can therefore be ignored or V , V' and V_0 have the same order of magnitude and cannot be neglected. Let us first assume that V_0 is relatively high, then the incompressible volume, V' , and the mechanical parameters, $KE m^3 / \rho^3$, which further will be referred to as a' , can be calculated from the compression energy, W , as follows:

$$\begin{aligned}
 W &= - \int_0^P P dv \\
 &= - \int_{V_0}^V \frac{a'}{(v - V')^3} dv \\
 &= \frac{a'}{2} \frac{1}{(V - V')^2}
 \end{aligned} \tag{4.1}$$

The reader should be reminded that v is representing a volume, which changes with pressure. The above approximation has the enormous advantage that no constant needs to be 'guessed' because there

are two equations and two unknowns. So, V' and a' can be calculated easily from the energy, W , the maximum measured pressure, P_{max} , and the volume, V_{max} , as follows:

$$V' = V_{max} - \frac{2W}{P_{max}} \quad \text{and} \quad a' = \frac{8W^3}{P_{max}^2} \quad (4.2)$$

Both parameters V' and a' for the different fabrics are given in Table 4-3. Comparing now the calculated V' with the measured values from the micrometer then, in general, the calculated value is higher than the measured values except in the case of the more 'incompressible' fabrics P1 and C1. In fact, V' for P1 is exactly the measured value when increasing the force on the micrometer. Looking at the full scale, the calculated compression is close to the experimentally measured values ($r^2 > 0.92$) as can be seen in Figure 4.10 to Figure 4.16, but diverges at very low pressure. This could be somewhat anticipated considering that V_0 has not been included in the calculations. Besides, Equation (2.26) goes to infinity for zero pressure and therefore $P = 0$ cN/cm² needed even to be excluded from the calculated curves.

The final approximation is of course to use the full van Wyk equation (2.26). However, three constants a' , V' and V_0 are unknown but again only two equations are available, hence one constant needs to be estimated. Writing the three parameters as a function of the energy, W , gives the following equation:

$$\begin{aligned} W &= - \int_0^P P dv \\ &= - \int_{V_0}^V a' \left[\frac{1}{(v - V')^3} - \frac{1}{(V_0 - V')^3} \right] dv \\ &= \frac{P}{2} (V - V') + 1.5a' \frac{(V - V_0)}{(V_0 - V')^3} \end{aligned} \quad (4.3)$$

The compression load curves have been calculated by gradually varying the 'incompressible' volume, V' , obtained from the two-parameter model until the best fit ($r^2 > 0.98$). The volume V' is found to be between 0.6 to 0.9 of the volume (or thickness) at maximum test pressure (10 cN/cm²). From Table 4-3, it can be seen that V' does not vary much for both models, only in case of the two wool samples, W1 and W1b, is V' further reduced. De Jong *et al.* [de Jong 86] also reported a similar V' ranging between 0.5 to 0.9 of the maximum volume at 50 gf/cm² when comparing the two approaches. However, it needs to be said that the three parameter model is very sensitive to changes in the substituted value of V' , which results in considerable 'precision' of the estimated values of V' . Compared to the two-parameter model, the three-parameter model gives a compression curve, which is nearly indistinguishable from the experimental curve as seen in Figure 4.10 to Figure 4.16. Yet, both models calculate the load compression characteristics for woven materials as well as knitted materials extremely well. The only weak part in the van Wyk equation is the exact implication of a' and V' , which will be clarified more in section 4.1.5 below.

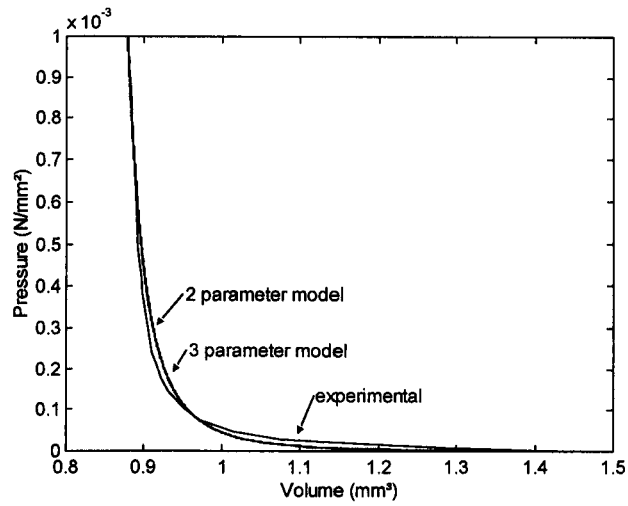


Figure 4.10. Van Wyk approximations to the compression of C1

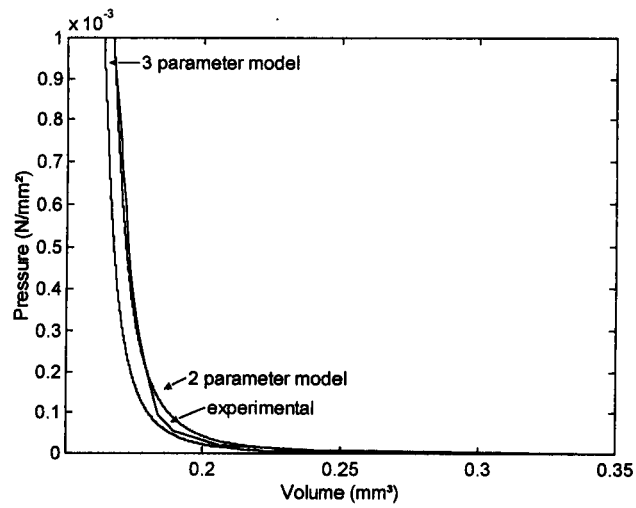


Figure 4.11. Van Wyk approximations to the compression of P1

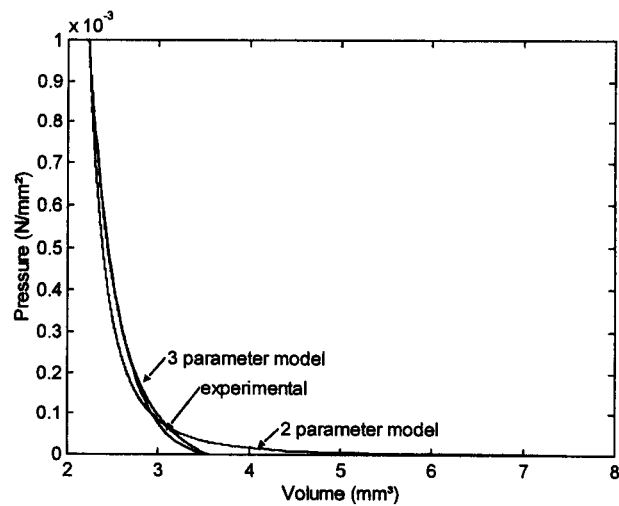


Figure 4.12. Van Wyk approximations to the compression of W1

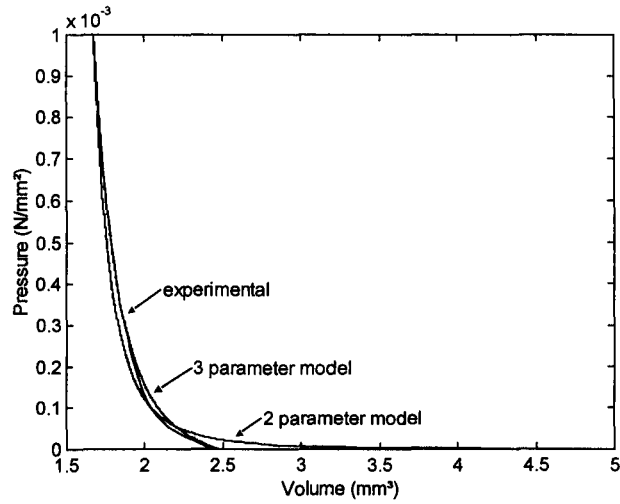


Figure 4.13. Van Wyk approximations to the compression of W1b

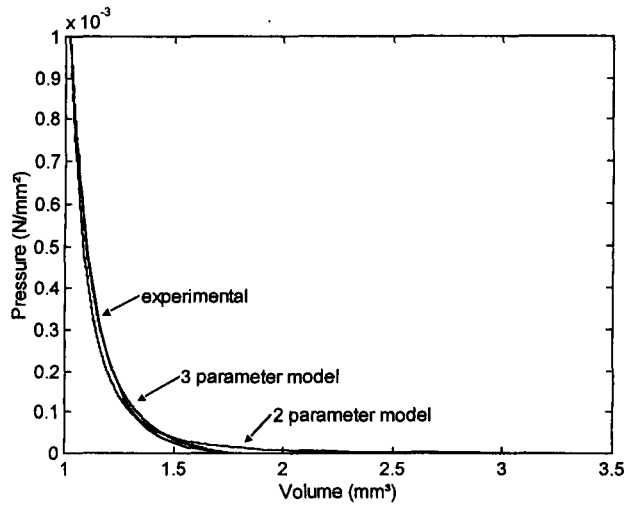


Figure 4.14. Van Wyk approximations to the compression of KCI

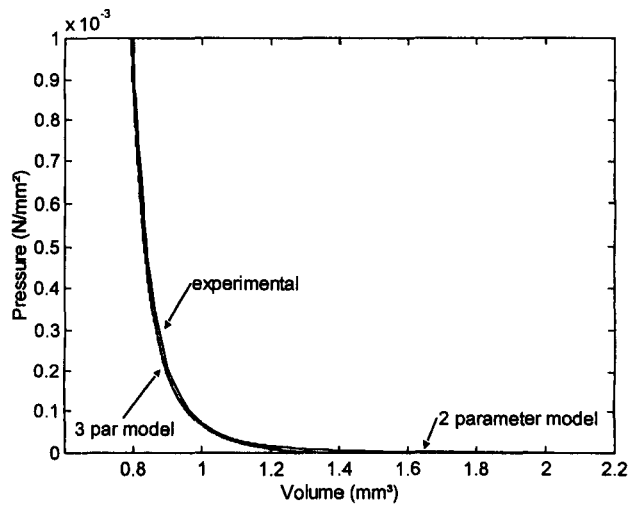


Figure 4.15. Van Wyk approximations to the compression of KC11

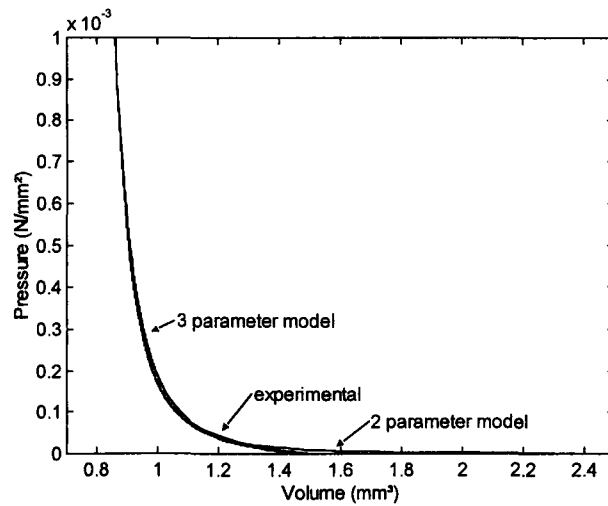


Figure 4.16. Van Wyk approximations to the compression of KA11

Table 4-3. Van Wyk parameters a' and V' for the two and three parameter model

Fabric code	Two Parameter Model			Three Parameter Model			T^+ (mm) micrometer	T_{\max}^+ (mm) micrometer
	a' (Nmm^7)	V' (mm^3)	r^2	a' (Nmm^7)	V' (mm^3)	r^2		
C1	2.9e-07	0.812	0.98	3.1e-07	0.810	0.98	0.947	0.600
P1	5.6e-09	0.149	0.99	3.0e-09	0.149	0.98	0.174	0.150
W1	2.2e-04	1.626	0.92	7.8e-03	1.330	0.99	0.884	0.540
W1b	3.3e-05	1.354	0.94	9.4e-05	1.230	0.99	0.757	0.585
KC1	1.4e-05	0.777	0.97	2.8e-05	0.720	0.99	0.612	0.400
KC11	2.7e-06	0.657	0.98	3.5e-06	0.640	0.99	0.417	0.250
KA11	5.2e-06	0.686	0.98	7.9e-06	0.660	0.99	0.638	0.470

Note that V' for the two-parameter model has been calculated whereas V' for the three-parameter model is an optimised value

4.1.5 Interpretation of the van Wyk Parameters a' and V'

In analogy with de Jong *et al.* [de Jong 86], let us first explain the physical significance of V' , what has up to now been referred to as the 'incompressible' volume. This volume cannot be defined as the volume of the fibres in the fabric excluding the air but has to be interpreted as the volume of the inner fabric core, which is relatively incompressible for pressures lower than 50 cN/cm². Knowing the fibre density, ρ , and the area density, m_a , of the fabric, the packing of the fibres for this volume V' (or core thickness T' per unit area) can be calculated as follows:

$$m_a / \rho T' \quad (4.4)$$

The corresponding packing fractions for the fabrics are given in Table 4-4. Note that a packing fraction of one relates to a solid sheet of material. The results in Table 4-4 are more spread comparing to the interval of 0.35-0.53 found by de Jong *et al.* [de Jong 86] for a group of 40 worsted woven fabrics (i.e., cotton, wool and polyester). As expected, the 'harder' fabrics C1 and P1 give a higher packing fraction whereas the more easily compressed fabrics give a lower packing fraction. Further, we can see that both woollen fabrics W1 and W1b have the same packing, which only confirms that the inner core of the fabrics is identical. Regarding the packing fraction for the knitted materials, these lower values correspond to a loosely packed core that could be due to their structure. A knitted structure is genuinely more '3-dimensional' compared to a woven structure.

Table 4-4. Packing fraction of the 'incompressible' volume, V' , for set 1 fabrics (+ W1b)

Fabric code	Area density, m_a (g/m ²)	Fibre density, ρ (g/cm ³) at 65% r.h. [Morton 97]	'Incompressible' thickness, T' (= V') (m)	Packing fraction
C1	517	1.52	0.810	0.42
P1	105	1.39	0.149	0.51
W1	352	1.31	1.330	0.20
W1b	328	1.31	1.230	0.20
KC1	257	1.52	0.720	0.23
KC11	183	1.52	0.640	0.19
KA11	264	1.19	0.660	0.34

The second constant in van Wyk's equation, which needs some more clarification, is a' grouping together the Young's modulus, E , the density, ρ , and the mass, m . If the core layer of the fabric is not compressed, which is definitely the case for pressures lower than 10 cN/cm², then the

mass must denote the mass of the compressed surface hairs. Thus, knowing the mechanical parameters and assuming the K -constant equal to 0.01 [van Wyk 46b], [de Jong 86], the compressed fibre mass in the surface layers of the fabric can be calculated as follows:

$$m = \sqrt[3]{\frac{\alpha'}{KE}} \rho \quad (4.5)$$

Unfortunately, the Young's modulus, E , for the set 1 fabrics has not been measured in this study. Hence, the compressed fibre mass, given in Table 4-5, has only been calculated for a few fabrics by taking an approximate value for E (i.e., E is dependent on the fibre diameter) from the literature [Dunlop 81]. Obviously, the compressed fibre mass is only a small percentage of the total fabric mass. De Jong *et al.* [de Jong 86] for instance, measured a mass of the surface fibres in the range 3-20 g/m² for a swatch of woven fabrics between 167-323 g/m². Similar values are found here, except in the case of the more hairy wool fabric, W1, where the compressed surface layer represents almost a quarter of the total fabric mass (still in the assumption that $K = 0.01$). Note the huge reduction in compressed fibre mass of W1b, which is expected when removing the surface hairs.

Table 4-5. Estimated compressed fibre mass in the surface layer of some set 1 fabrics

Fabric code	Young's Modulus *, E (N/mm ²)	Compressed fibre mass, m (g/m ²)	Percentage of the total fabric mass (%)
P1	4700	0.55	0.53
W1	3800	77.58	22.04
W1b	3800	17.77	5.42
KA11	3100	7.16	2.71

* [Dunlop 81]

The above analysis indicates clearly that a woven fabric under compression can be modelled as a three-layer structure, as discussed in the literature review (2.2.1). Only the outer layer containing the surface hairs or crowns is compressed and obeys van Wyk's compression law both in case of woven and knitted fabrics and for various textile materials. However, the three-parameter model approximates the experimental compression result better than the two-parameter model, in particular at very low pressure. The above compression results have all been obtained in a static manner. Yet, previous results on fabric extension in section (3.10.5) as well as some papers in the literature [van Wyk 46a], [Dunlop 89, 91] and [Clayton 92] have indicated a difference between static and dynamic parameters. Hence, the second half of this chapter will investigate low frequency compression (i.e., few Hertz) but first a novel measuring technique will be discussed.

4.2 Impact Compression

4.2.1 Instrumentation and Method

A swinging pendulum has been built to dynamically compress a fabric sample under test. The instrument designed is based on a device originating from Henning [Henning 34], known as the 'Pendultex', which has also been used by van Wyk [van Wyk 46a] in his famous study on the compression of wool fibres in bulk. The instrument is based on the principle of measuring the compressional resistance by the consequent damping of the pendulum. The number of swings during which the amplitude decreases is recorded and is inversely proportional to the compressional resistance of the fabric sample.

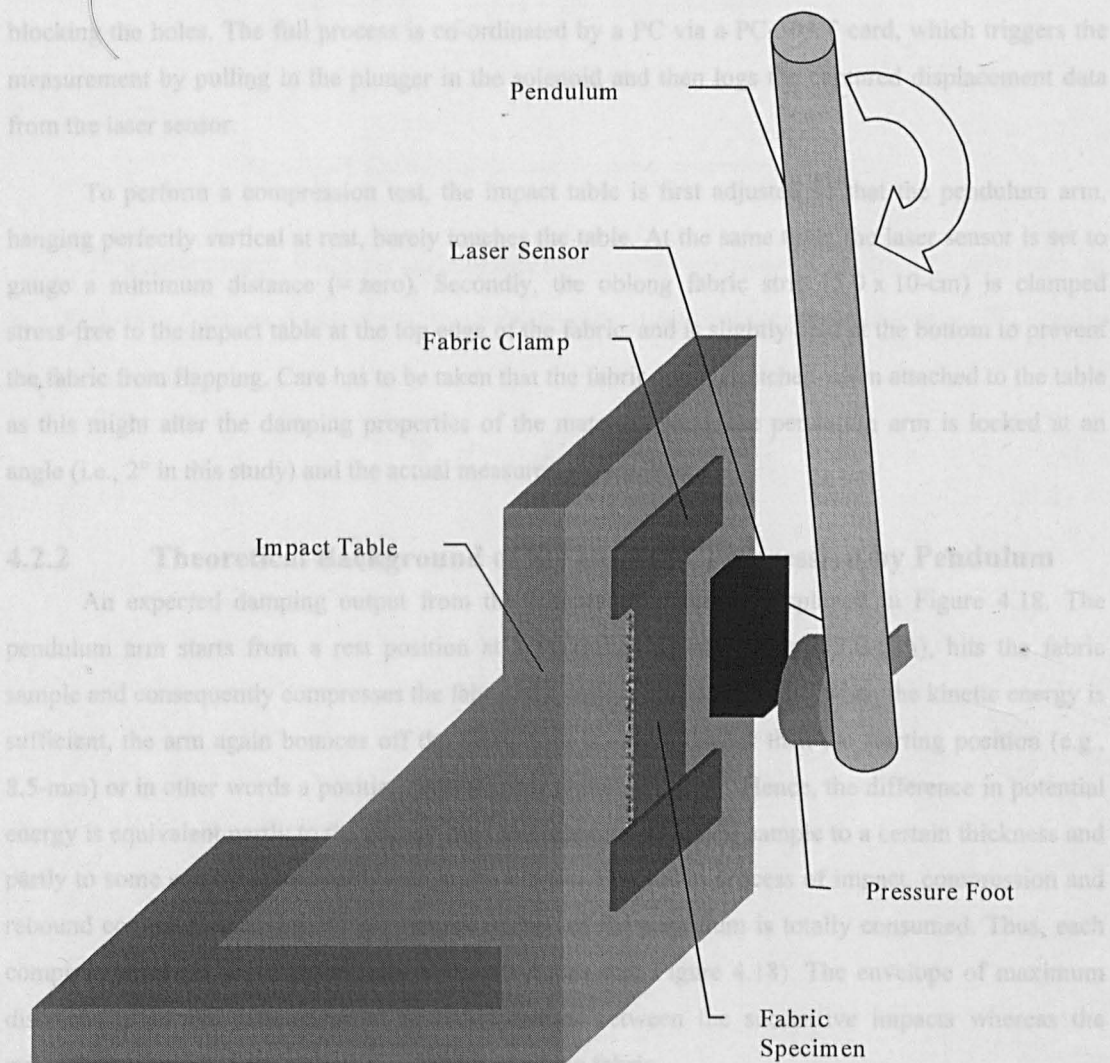


Figure 4.17. Sketch of the impact compression measuring device

Since fabric compression is studied here instead of fibre compression, the pendulum used in this study and sketched in Figure 4.17 (see Appendix B), is less sophisticated in construction than the original 'Pendultex', which comprised of a lever and piston mechanism to compress the enclosed

fibres in a compartment. The instrument here simply consists of a pendulum with mirror finished pressure foot (10 cm^2), which impacts on the fabric sample attached to a 'rigid' vertical plate (i.e., impact table). The pendulum arm is centred in a rod, which is suspended on precision bearings and housed at the top of a large aluminium framework. A solenoid mechanism connected to the suspension rod releases the pendulum arm automatically from a pre-determined variable angle. In addition, a 1550-g mass on the pendulum arm giving an overall weight of 4.5-kg can be balanced to give variable impact forces on the fabric sample. The impact table is adjustable relative to the pressure foot and houses the laser sensor, which measures the varying impact amplitude by pointing the laser beam to a metal indicator at the side of the pressure foot. Furthermore, several small holes were drilled in the impact table at the fabric area to avoid possible air damping. However, results afterwards showed that air damping was negligible even when impacting the table with no fabric sample and blocking the holes. The full process is co-ordinated by a PC via a PC-30AT card, which triggers the measurement by pulling in the plunger in the solenoid and then logs the captured displacement data from the laser sensor.

To perform a compression test, the impact table is first adjusted so that the pendulum arm, hanging perfectly vertical at rest, barely touches the table. At the same time, the laser sensor is set to gauge a minimum distance (\approx zero). Secondly, the oblong fabric strip ($5.0 \times 10\text{-cm}$) is clamped stress-free to the impact table at the top edge of the fabric, and is slightly held at the bottom to prevent the fabric from flapping. Care has to be taken that the fabric is not stretched when attached to the table as this might alter the damping properties of the material. Next, the pendulum arm is locked at an angle (i.e., 2° in this study) and the actual measurement can start.

4.2.2 Theoretical Background of the Impact Compression by Pendulum

An expected damping output from the compression tests is displayed in Figure 4.18. The pendulum arm starts from a rest position at a maximum distance (e.g., 13.0-mm), hits the fabric sample and consequently compresses the fabric to a certain thickness. Next, when the kinetic energy is sufficient, the arm again bounces off the fabric to a distance smaller than the starting position (e.g., 8.5-mm) or in other words a position with a lower potential energy. Hence, the difference in potential energy is equivalent partly to the energy used to compress the fabric sample to a certain thickness and partly to some energy unavoidably lost in the system. The above process of impact, compression and rebound continues until the initial potential energy of the pendulum is totally consumed. Thus, each compression graph is characterised by two envelopes (see Figure 4.18). The envelope of maximum distances gives the differences in potential energy between the successive impacts whereas the minima correspond to the compressed thickness of the fabric.

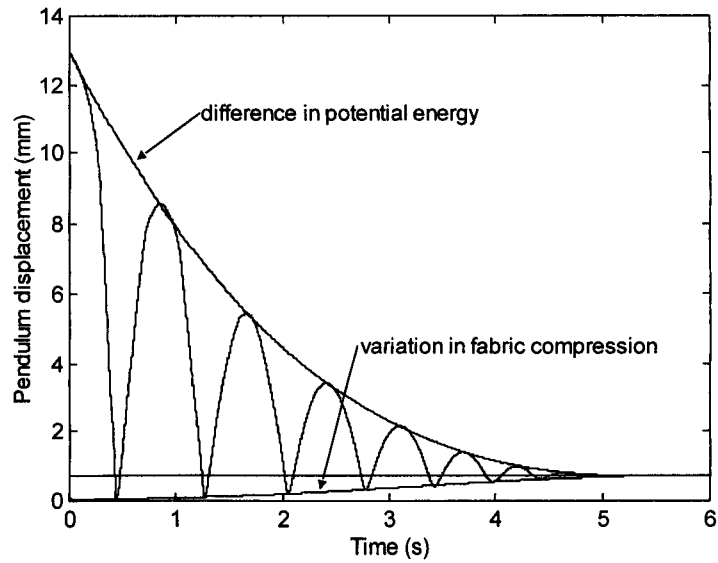


Figure 4.18. Theoretical dynamic pendulum compression of fabric

Thus theoretically, if θ is the angle of inclination of the pendulum in Figure 4.19 with mass, m , at a distance l_m from the centre of gravity to the pivoting point then the potential energy, W_p , can be written as follows:

$$\begin{aligned} W_p &= mgl_m(1 - \cos\theta) \\ &= 2mgl_m \sin^2 \frac{\theta}{2} \end{aligned} \quad (4.6)$$

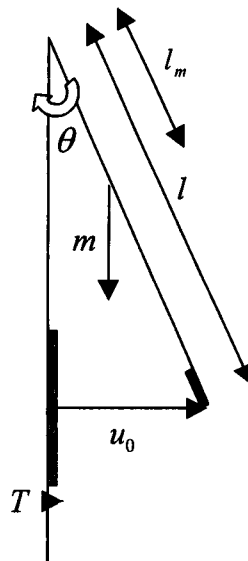


Figure 4.19. Force diagram of a simple pendulum

After impact, the pendulum arm only rebounds to an angle θ_1 since part of the potential energy is converted in work lost during the compressing of the fabric, W , and part is lost in the natural damping of the pendulum, Z . Hence, the difference in potential energy between the first two impacts can be written as:

$$W + Z = 2mgl_m \left(\sin^2 \frac{\theta}{2} - \sin^2 \frac{\theta_1}{2} \right) \quad (4.7)$$

Since θ is not measured directly but the amplitude, u_0 , (viz., distance between the impact table and the pendulum), Equation (4.7) becomes:

$$\begin{aligned} W + Z &= 2mgl_m \left[\left(\frac{u_0}{2l} \right)^2 - \left(\frac{u_1}{2l} \right)^2 \right] \\ &= \frac{mgl_m}{2l^2} (u_0^2 - u_1^2) \end{aligned} \quad (4.8)$$

So, the amplitude of the pendulum arm gradually dies out and the successive energy differences for the corresponding fabric compressions can each be calculated according to Equation (4.8). However, in order to find purely the compression energy of the fabric, W , a correction has to be applied for the natural damping of the pendulum, Z . This will be evaluated first in the next section.

4.2.3 Results

The natural damping of the pendulum is obtained by observing successive amplitudes for the pendulum in free oscillation as seen in Figure 4.20. The impact table is therefore removed and the laser sensor is attached near the top of the rig pointing towards the pendulum arm. The arm is released from an angle of 2° (identical as for the fabric) and purely damped due to bearing friction and air resistance. Applying now Equation (4.7) with W equal to zero, the successive energy loss for each inclination angle, θ , can be calculated. As expected, the pendulum damping in Figure 4.21 is nearly linear, except at extremely small angles. Thus, a pendulum loss, Z , will need to be subtracted from each impact. However, when fabric or any other material is attached to the impact table, an angle of zero degrees can never be obtained since the material thickness offsets the pendulum arm. Hence, the loss of the pendulum has to be calculated according to the travelled distance or more specifically to the angular distance. For example, if the pendulum compresses a material to a thickness of 2.67 mm then the arm is still at an angle of 0.2° . So, if the pendulum starts from an angle, $\theta = 0.3^\circ$, and rebounds to an angle, $\theta_1 = 0.25^\circ$, then a total angle of 0.15° has been covered which corresponds to an energy loss of 4.0×10^{-6} Nm. The reader should be reminded that the energy for a half swing in Figure 4.21 still needs to be divided by two as the pendulum arm moves forwards and backwards during that swing (viz., twice the angle displacement).

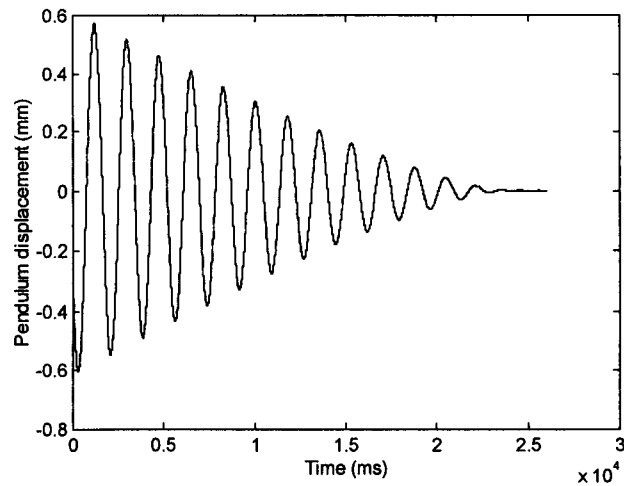


Figure 4.20. Free oscillation of the impact pendulum

Release angle: 2° , sampling frequency: 250 Hz, negative displacement for pendulum coming towards the laser sensor

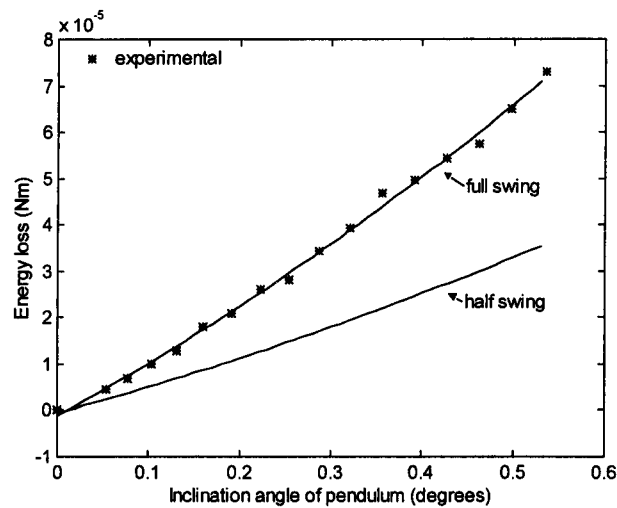


Figure 4.21. Energy loss of the pendulum in free oscillation

Figure 4.22 to Figure 4.24 display the raw impact response (i.e., pendulum loss included) for KC11, C1 and W1 respectively as examples of woven structures with variable compressibility and a knitted structure. Similar looking graphs are found for KC1, KA11 and P1 although the compression of P1 is as tiny as its static compression. A sample of W1b has not been tested. Due to a limited sensing range of 4-mm, the first impacts of each test are clipped and therefore omitted from the figures and calculations. Further, note the thickness offset for the respective fabrics. Yet, this thickness does not correspond to the zero pressure thickness considering that the pressure foot and pendulum arm rest against the fabric surface but conforms to an equivalent thickness for a static compression of $0.2\text{--}0.4\text{ cN/cm}^2$.

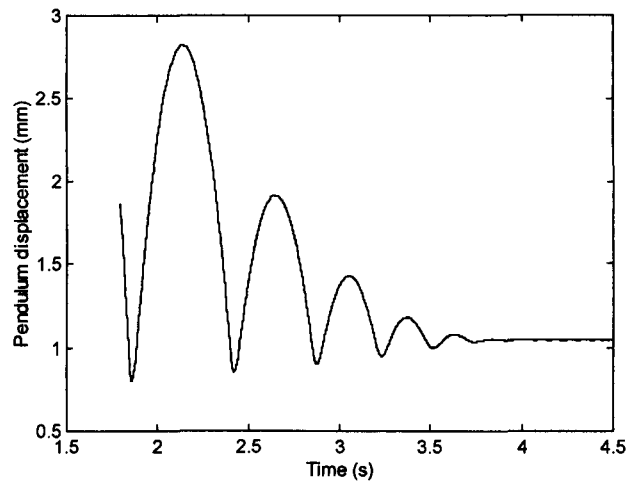


Figure 4.22. Impact response of KC11

Release angle: 2° , sampling frequency: 1000 Hz, 'non-compressed' fabric thickness: 1.044 mm

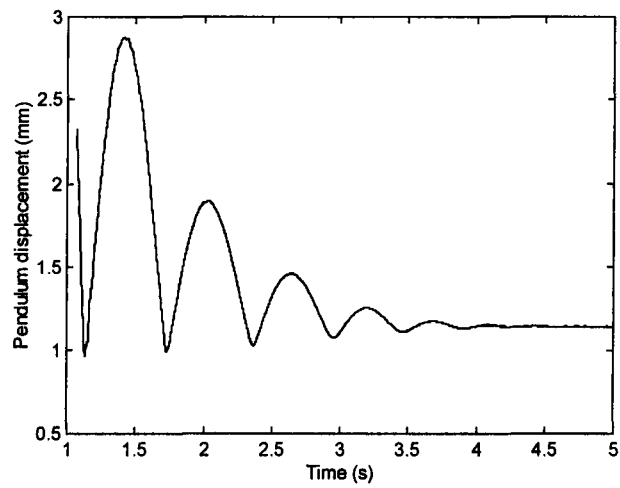


Figure 4.23. Impact response of C1

Release angle: 2° , sampling frequency: 1000 Hz, 'non-compressed' fabric thickness: 1.145 mm

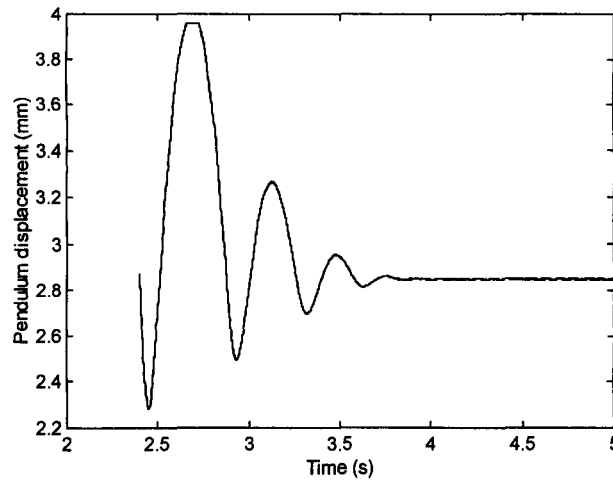


Figure 4.24. Impact response of W1

Release angle: 2°, sampling frequency: 1000 Hz, 'non-compressed' fabric thickness: 2.847 mm

Although, static compression and impact compression are fundamentally different mechanisms (see Appendix F), a comparison is made in the next section between the static and dynamic energy required to compress the fabric to the same thickness.

4.3 Comparison between Static and Impact Compression

From the impact response of each fabric, the dynamic compression energy is first computed for the successive impacts by using Equation (4.7). Secondly, the travelled angular distance is calculated for each impact, converted into energy loss of the pendulum, as described in 4.2.3 above, and deducted from the originally measured potential energies. Compared to the static compression energies, which can be calculated from the respective static deflection characteristics, an overall lower dynamic energy is obtained to compress the fabric to an identical thickness. This is, however, not a compacting phenomenon as it is the case in the dynamic compression of bulk fibres where successive compression cycles gradually reduce the fibre volume [van Wyk 46a], [Dunlop 74]. A repeated test for each fabric sample produced the same outcome. In addition, similar results have been found for the dynamic (impact) compression of solid materials (e.g., a spring) and are commented on in Appendix F. During impact, the stresses in the solid material gradually increase until reaching the level of static load but due to the kinetic energy of the impacting load, the solid material is deflected further than its static limit. Hence, theoretically, a suddenly applied load produces a deflection (i.e., compression or elongation) which is twice as great as when obtained with a similar static load [Timoshenko 73]. This results in a constant energy ratio (i.e., dynamic/static) of 0.5. However, as displayed in Figure 4.25 and summarised in Table 4-6, the ratio between the dynamic and static energy is not constant for most fabric samples. Two different proportions can be distinguished.

Fabric KC1, and to a lesser extent W1, shows a constant ratio smaller than one for all successive impacts whereas the other fabrics, KC11, KA11 and C1 give a variable ratio, which starts

above one and gradually decreases. The fact that KC1 and W1 express a quasi-linear relationship is also visible in Table 4-1 where a larger linearity parameter for the static compressions (i.e., LC) was calculated. Unfortunately, in general, the non-linearity of the deflection makes further conclusions difficult and more research is needed. One could conclude from Table 4-6 for instance, that KC1 gives an impact deflection, which is 30% higher compared to when a similar static load is compressing the fabric. Furthermore, all knitted samples have on average the same ratio, which again highlights their structural similarity.

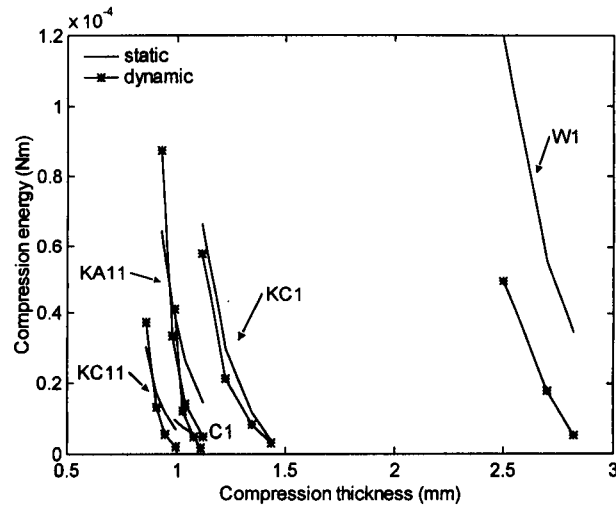


Figure 4.25. Comparison between the static and dynamic energy for similar compression thicknesses

P1 is not displayed in the graph due to the very small values of thickness and energy. The dynamic values are single measurements though the static compression energies are averaged from six samples

Table 4-6. Ratio of the dynamic compression energy to the static compression energy for successive impacts

Fabric code	Dynamic compression energy/static energy					
	C1	P1	W1	KC1	KC11	KA11
	4.188	1.287	0.419	0.871	1.217	1.351
	1.572	0.381	0.324	0.719	0.758	0.798
	0.873		0.153	0.712	0.456	0.532
	0.408			0.812	0.299	0.337
<i>Average</i>	<i>1.760</i>	-	<i>0.299</i>	<i>0.778</i>	<i>0.682</i>	<i>0.754</i>

Impact compression on solid materials (e.g., a spring) gives a ratio of 0.5 (Appendix F)

4.4 Summary

Low force compression measurements on set 1 fabrics, obtained with an in-house built thickness tester, revealed very repeatable results. Only the more incompressible fabrics seem to have a lower repeatability though, despite the fact that all samples have been 'pre-compressed' before testing, this is common to 'harder' fabrics. In order to describe the compression properties of each fabric more precisely, the KES-FB3 compression parameters have been determined for each fabric sample. A good discrimination is found between the different samples characterising the compressional work, linearity and hysteresis, which is common to every sample under compression and release. A wool sample of which the surface hairs have been removed deliberately, showed clearly the variation of the different KES-F parameters when compared to the original. Next, non-contacting thickness measurements with the laser sensor revealed on average a 20% underestimation of the thickness as determined by the previous thickness tester under similar conditions. This discrepancy is likely caused by the laser not detecting the protruding surface hairs, which are responsible for minute forces in the contacting method. Further, the experimental data for both the woven and knitted fabrics has been approximated by van Wyk's model. Although the model was originally developed for wool wads, near indistinguishable fits ($r^2 \approx 0.99$) are obtained for the various woven and knitted fabrics when the full model or three-parameter model is used. However, this model requires a value for the 'incompressible' volume of the fabric, which can be regarded as the relatively incompressible inner core of the fabric counting for 30-60% of the total fabric thickness. Yet, an estimate for this parameter can easily be obtained from the two-parameter approach, which, in essence, diverges at low pressures since the zero pressure volume is excluded from the calculations. Finally, further analysis of the static compression results, showed that at low pressures only the surface hairs of the fabric compress. The difference was particularly clear again between the shaven woollen fabric and its original. This finding, once more, indicates that a woven fabric under compression can be modelled with a three-layer structure as originally proposed by de Jong *et al.* [de Jong 86].

In the second half of this chapter, a novel technique, based on a pendulum, has been introduced to measure the impact compression of fabrics. The number of swings during which the potential energy decreases is inversely proportional to the compressional resistance of the fabric. On average, a smaller compressional energy is required to impact the fabric to the same thickness as when compressed statically. It was found that the fabric can be up to 30% more compressed on impact compared to when the same force is applied statically. It would however be wrong to conclude that the dynamic stiffness of a fabric is therefore lower than its static stiffness since impact compression is a completely different mechanism.

In the next chapter, we will look at another form of dynamically loading fabric, more specifically lateral vibration. Unloaded fabric samples will be subjected to small sinusoidal forces.

5 Vibration Characteristics

The last property investigated in this thesis concerns the out of plane vibration of fabrics. To understand the underlying mechanism first, the fabric's normal displacement is monitored in a 'non conveying' stationary mode by placing the samples on a horizontal vibrating surface. Considering the high probability of a non-linear behaviour, the stationary tests are approached in two different ways. Firstly, the position dependency is studied for an identical excitation at three different positions on the fabric. Secondly, the opposite is done by exploring the amplitude dependency in the centre of the samples at three different excitations. Next, the experimental data from the stationary vibration tests is compared in amplitude and phase with simulated results obtained from a simple Kelvin-Voigt model with hysteresis damping. The second half of this chapter looks into the conveying or transporting of the fabrics and the different influencing factors. Considering the importance of friction in conveying solid material, the friction in fabric conveying is studied first by attaching different surfaces to a vibration unit. Next, the sliding speed of the fabrics at different inclination angles and excitations is measured and compared with theoretical values. Finally, this chapter concludes with some conceptual ideas to position fabric panels on a linear vibratory table. However, first the excitation unit used in the experimental phase is discussed. The rather challenging specifications required the device to be variable in excitation amplitude between 50-200 μm and in a frequency from 10-100 Hz. In addition, different surfaces needed to be attached and the complete rig needed to be able to be inclined at different angles ranging from 0-20°.

5.1 Instrumentation and Method

The vibration unit is built from a 600 W power bass loudspeaker, which is suspended in an aluminium bracket as illustrated in Figure 5.1. The bracket is clamped in a heavy metal framework and can be inclined at different angles. A solid foam structure the exact shape of the loudspeaker cone is glued inside the loudspeaker holding an aluminium honeycomb structure, which serves as table surface. A honeycomb plate (500 x 300 x 12.7-mm) was preferred because of its high mechanical stiffness and relative low weight (583-g). Further, the different test surfaces (i.e., aluminium, Formica and rubber) can be attached to the honeycomb surface in order to vary the friction. The full vibration unit is mounted on rubber bobbins acting as damping units. The instrumentation used in the experiments can be split in two as shown in Figure 5.2: one part takes care of the excitation of the unit another part performs the sensing. The complete experimental set-up is monitored by a computer.

The driving arrangement consists of a function generator and a 550 W MOSFET amplifier. The function generator is set for a sinusoidal wave, which is fed into the power amplifier and eventually fed forward to the loudspeaker. The amplitude of the signal is manually adjusted on the function generator with the frequency controlled from the computer via the VCO facility of the function generator.

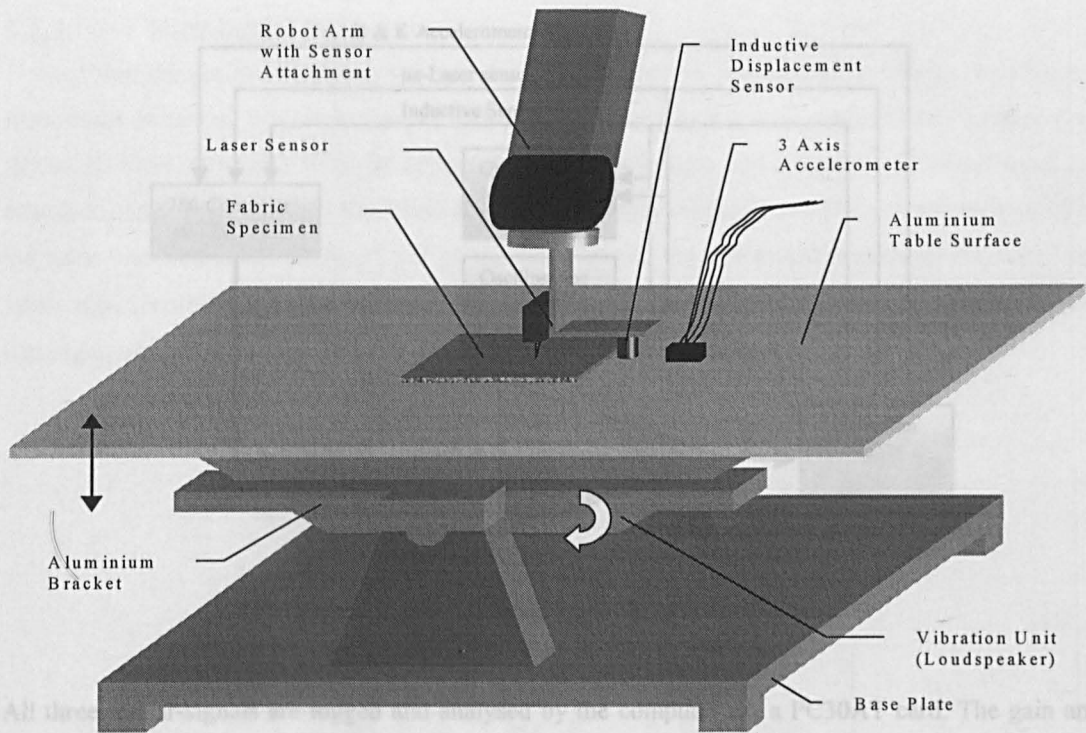


Figure 5.1. Sketch of the out of plane vibration measurements

The vibration is monitored by three individual sensors: two sensors register the table movement while the laser sensor looks at the fabric movement. Both non-contacting sensors (i.e., inductive and laser displacement sensor) are fixed on a bracket at the end-effector of a Unimation PUMA robot arm. On one hand, this allows the sensors to be relocated easily across the table surface and on the other, it secures the sensors well away from any surrounding environmental vibrations. The inductive displacement sensor (Gaptex 2004) is used to measure the table amplitude and frequency (one direction), which further enables us to tune the amplitude on the function generator, bearing in mind that there is no feedback in the measurement system. Hence, the inductive sensor is used as reference during the experiments to adjust the table amplitude. In addition, the triaxial accelerometer (Bruël & Kjør Triaxial Deltatron® 4504) surveys the movement of the table independently in three dimensions. This sensor is particularly useful in determining any phase shift between the three axes considering that the vibration table is not exactly unidirectional over the full frequency range due to a slight eccentricity of the foam cone. The accelerometer is stuck to the table surface with double-sided tape, which allows it to be repositioned. Finally, the fabric movement is gauged with the laser sensor (LD1605-4 by µε®). Although the sensor is not marketed specifically for vibration monitoring as are interferometry sensors, the laser sensor has a bandwidth of 10 kHz and sampling frequency of 40 kHz and will therefore easily measure vibrations of up to 105 Hz. However, one disadvantage of this method of sensing is that the sensor observes only a single point of the fabric sample.

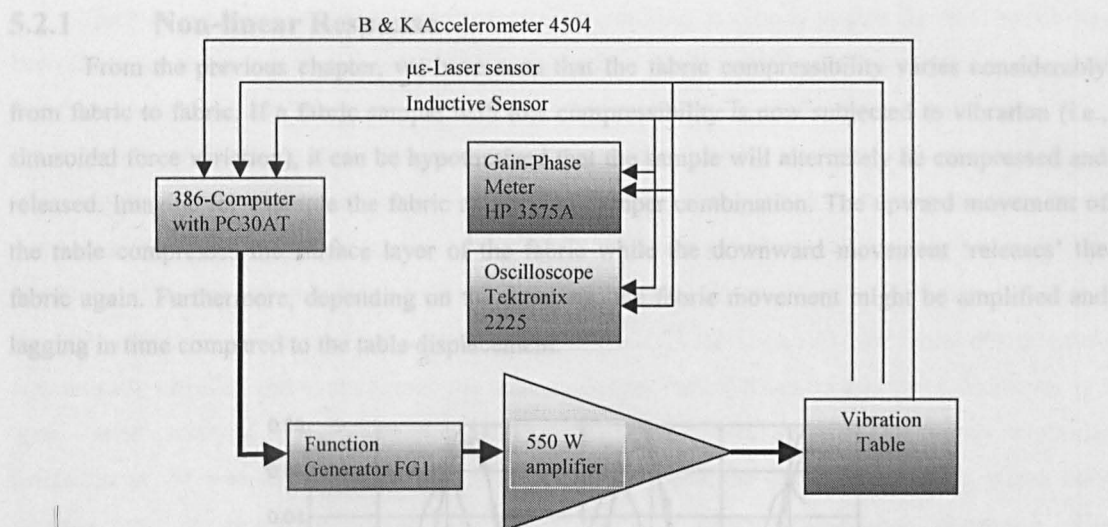


Figure 5.2. Schematic diagram of the equipment set-up

All three sensor-signals are logged and analysed by the computer via a PC30AT card. The gain and phase difference between the table and the fabric are manually checked with a gain phase meter against the computer results, which are calculated from the complex transfer function between the two signals (Spectrum function [MATLAB 88]). An oscilloscope is also included to visualise both the table and the fabric signal. The reader is referred to Appendix B for further details on the measuring equipment.

All vibration tests are performed on only one sample (100 x 100 mm) per fabric type (set 1 plus W1b) as opposed to all previous tests where six samples were always used. However, to increase the repeatability, the vibration tests have been repeated six times successively and averaged. Again, all tests are performed in standard conditions of temperature and humidity. Furthermore, since the table is subject to different modes of vibration, the amplitude of vibration is position dependent. In other words, the excitation of the fabric will differ slightly from the reference amplitude measured by the inductive sensor. Hence, the amplitude of the table at the fabric measuring point is calibrated separately for each experimental condition in order to correct the fabric vibration to the right excitation.

5.2 Stationary Vibration Tests

From the literature review in chapter 2, we know already that carpets and felt pads behave non-linearly when compressed dynamically. Furthermore, as we have just seen in chapter 4, even the static compression of fabric is non-linear. Hence, the stationary vibration tests in this study consist of two experiments. At first, the amplitude of the excitation is kept constant at 100 μm (peak to peak) and the position of measuring is varied along three points at the centre line of the full fabric width. Secondly, the fabric vibration is measured at the centre of the sample but now the amplitude of vibration is changed to three different excitations (i.e., 75 μm , 125 μm and 150 μm). However, we will consider first some raw fabric signals.

5.2.1 Non-linear Response

From the previous chapter, we have seen that the fabric compressibility varies considerably from fabric to fabric. If a fabric sample with low compressibility is now subjected to vibration (i.e., sinusoidal force variation), it can be hypothesized that the sample will alternately be compressed and released. Imagine for example the fabric as a spring-damper combination. The upward movement of the table compresses the surface layer of the fabric while the downward movement 'releases' the fabric again. Furthermore, depending on the damping, the fabric movement might be amplified and lagging in time compared to the table displacement.

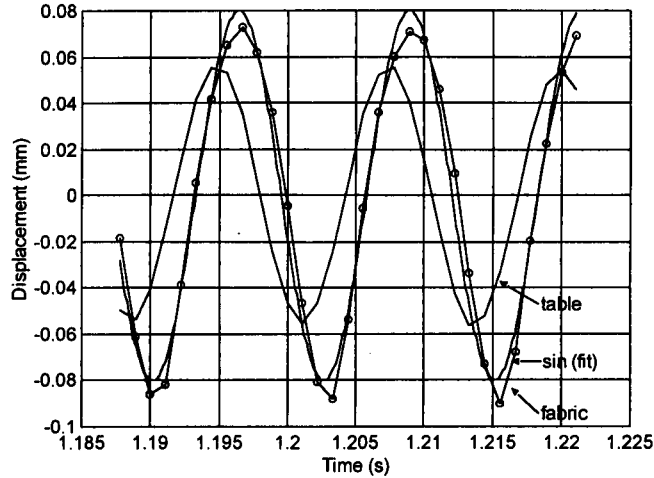


Figure 5.3. Raw data for out of plane vibration of W1

Table excitation (reference): $125\ \mu\text{m}$ (peak to peak), frequency: 79.5 Hz, angle of inclination: 0° , measured at the centre of the fabric in the resonance interval. Note that the table excitation at the point of measurement is slightly less than the reference (inductive sensor)

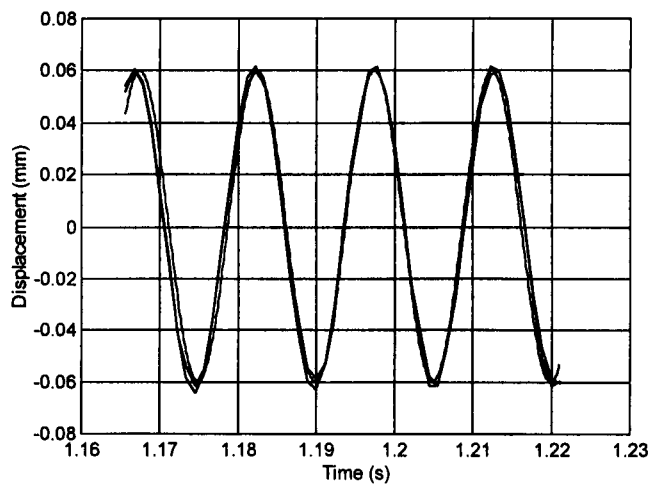


Figure 5.4. Raw data for out of plane vibration of C1

Table excitation (reference): $125\ \mu\text{m}$ (peak to peak), frequency: 65.0 Hz, angle of inclination: 0° , measured at the centre of the fabric in the resonance interval

Such a compression-release phenomenon, for example, is clearly visible for W1, which has been characterised as a relatively easily compressed fabric (see 4.1.2). Figure 5.3, displaying the table and fabric waveform for W1, reveals immediately the enormous lag of the fabric displacement. Yet, the amplitude of the fabric displacement is much larger than the table amplitude and in addition, the fabric displacement is not exactly sinusoidal, as is the driving force, but distorted at both ends. When compared with a perfect sine wave with zero mean, the positive waveform (compression) is smaller in amplitude while the negative wave (release) is slightly larger. On the other hand, Figure 5.4, shows the table and fabric waveform for the rather incompressible C1 fabric (4.1.2). The fabric displacement is practically identical and in phase with the table excitation, hence, it can be said that C1 behaves as a quasi 'solid' material when vibrated. Regarding the other fabric samples: P1 shows a similar behaviour as C1 whereas all other fabrics behave as W1 with the exception of KC1, which only vibrates with an amplified displacement though without compression-release symptoms. The following results in this chapter will be presented as frequency responses in which the magnitude is expressed as the ratio between the fabric displacement and the table excitation. The fabric peak to peak displacement, y_{pp} , for each frequency measurement is calculated from the standard deviation of the displacement, σ , as follows:

$$y_{pp} = 2\sqrt{2}\sigma \quad (5.1)$$

Although, the fabric displacement is not exactly sinusoidal, the positive and negative distortions will compensate each other.

5.2.2 Position Dependency of the Vibrating Fabric

The vibrational behaviour of the fabric is studied in three different places on the fabric, pos1-pos3, as pictured in Figure 5.5. Position one and three (pos1, 3) are symmetrical, 3-cm from the centre line, and therefore still well away from the border of the fabric avoiding possible edge effects. Each sample is placed at the centre of the vibrating table however the principal direction of the fabric (i.e., warp or weft) is indifferent for the stationary tests.

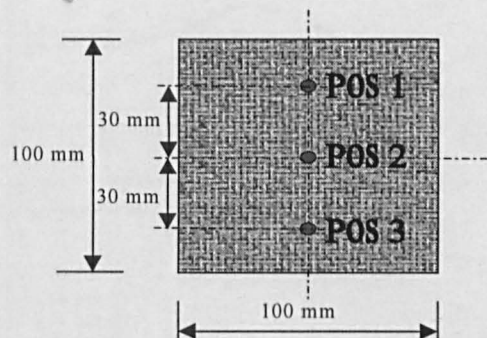


Figure 5.5. Location of the measuring spots on a fabric sample

The frequency responses for the seven fabrics are given in Figure 5.6 to Figure 5.12 respectively. In essence, two types of response can be differentiated. The more incompressible fabrics,

C1 and P1 show a small amplification, which is almost in phase (-6° to -8°) with the table excitation. All other samples exhibit a larger gain with the fabric being between 30° to 110° out of phase with the table. For a few fabrics such as KC1, W1, KA1 and P1, the highest gain is measured at the centre of the fabric (pos2) though there is no further consistency in the results. Some fabrics, as for example W1 and P1, show a similar frequency response for position one and three as if there were some position dependency whereas KC1, for instance, has the same results for the three positions.

Thus, a single point measurement did not reveal any position dependency or evidence of a standing wave (two-dimensional) in the fabric. However, other measuring techniques including three or more sensors capturing the displacement simultaneously or interferometric approaches would be more suitable to investigate the possibility of space distributed waves. This might also clarify the in-plane 'stiffening effect' of vibrating fabrics mentioned in the exploratory study on automated handling by Arthur D. Little Inc. [Saibel 68].

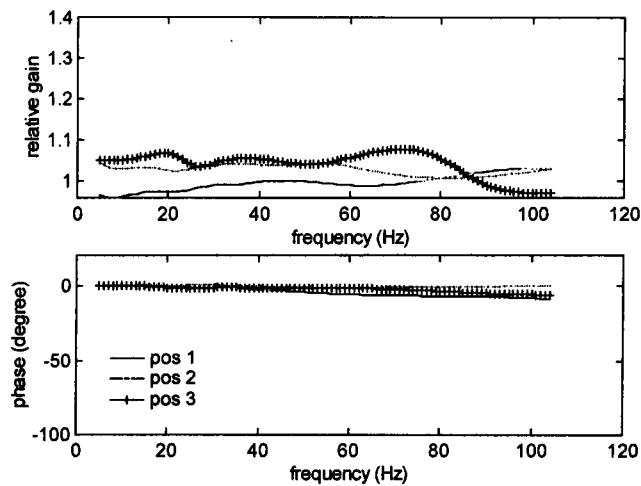


Figure 5.6. Frequency response of C1 measured at three different points

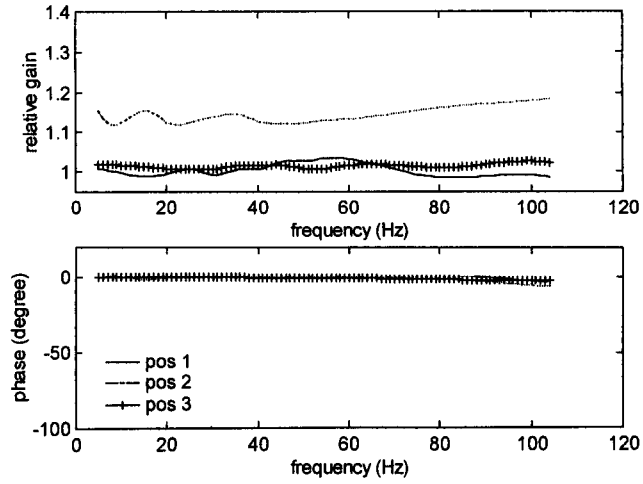


Figure 5.7. Frequency response of $P1$ measured at three different points

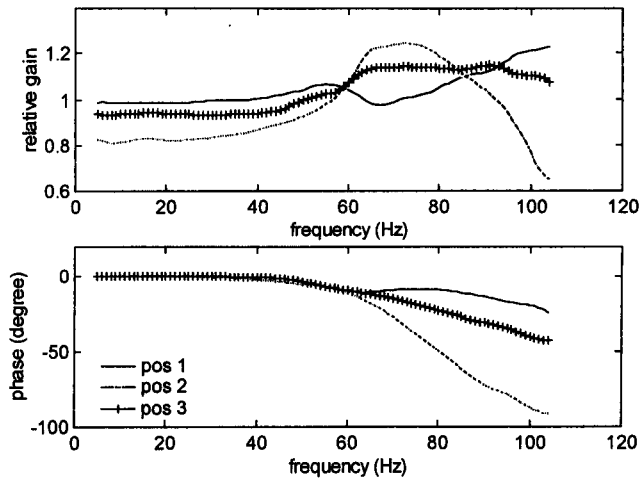


Figure 5.8. Frequency response of $W1$ measured at three different points

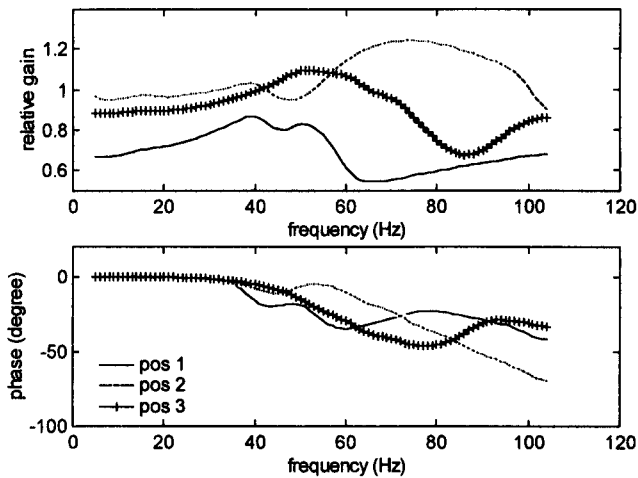


Figure 5.9. Frequency response of $W1b$ measured at three different points

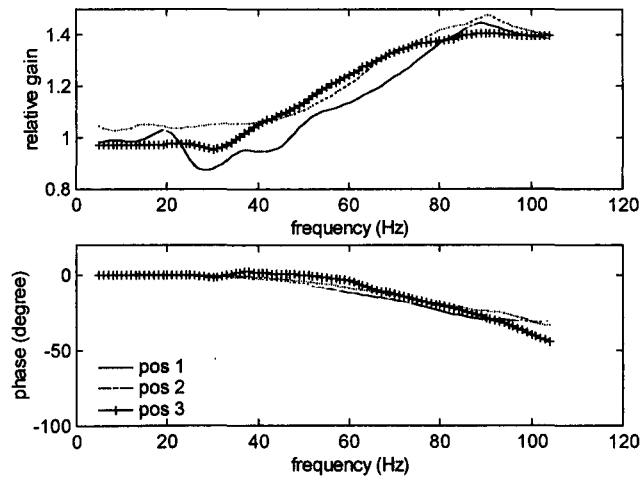


Figure 5.10. Frequency response of KC1 measured at three different points

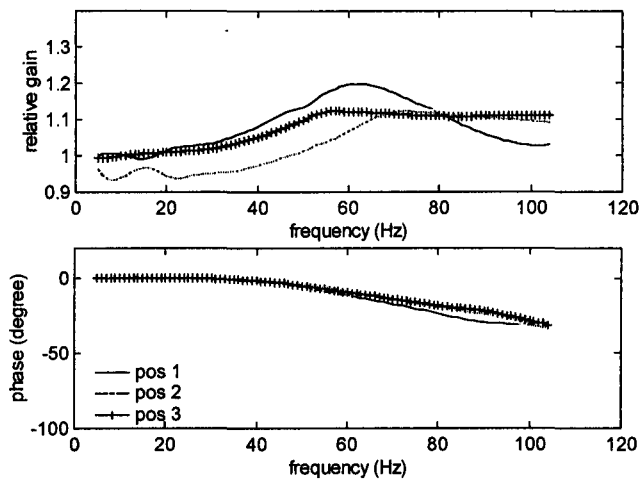


Figure 5.11. Frequency response of KC11 measured at three different points

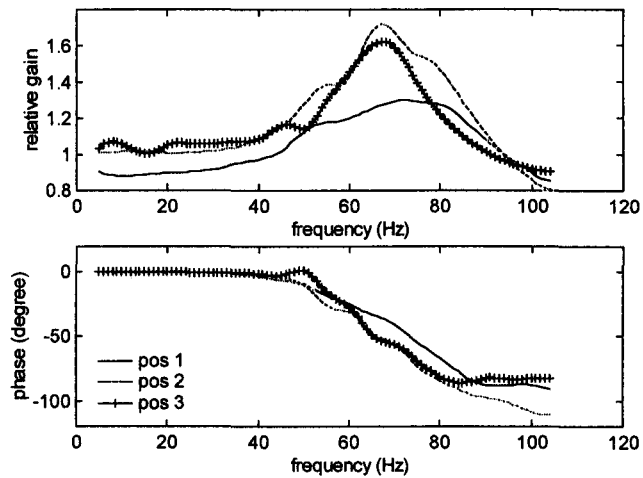


Figure 5.12. Frequency response of KA11 measured at three different points

5.2.3 Amplitude Dependency of the Vibrating Fabric

A second set of stationary vibration tests is performed to check the amplitude dependency of the vibrating fabric. The frequency response at three different excitations (i.e., 75 μm , 125 μm and 150 μm) has been measured at the centre of each fabric sample (pos2). Again, the results, given respectively in Figure 5.13 to Figure 5.19, reveal a contrasting response between C1-P1 and the other fabric samples. Fabric C1 and P1 previously characterised as more incompressible, measure an almost invariable frequency response where both amplitude and phase hardly change in the frequency range 5-105 Hz. On the other hand, all other fabric samples show a typical resonance characteristic with maximum gains in the region of 60-90 Hz and phase shifts ranging from -40° for KC11 to -120° for KA11 at the maximum frequency of 105 Hz. Furthermore, a brief look at all figures indicates an amplitude dependency or non-linearity for all frequency responses. First, an increase in driving amplitude shifts the resonance peak to lower frequencies signifying a decrease in stiffness. Secondly, the damping varies with an increase in amplitude: for some fabrics (i.e., KC11, KC1, and W1) the damping increases, for others it decreases (KA11) or even stays constant (W1b). A similar effect has been reported by Clayton and Tinker [Clayton 92] for the TABI material and by Dunlop and Sun [Dunlop 89] and Dunlop [Dunlop 90] for carpets and felt respectively. However, the experimental conditions for all these materials are quite different from the ones here, in particular the loading. Hence, it is quite possible that the damping mechanism will also be different. For instance, frictional damping encountered in fibre slippage during dynamic carpet compression cannot exist when very low forces are used as in this study here.

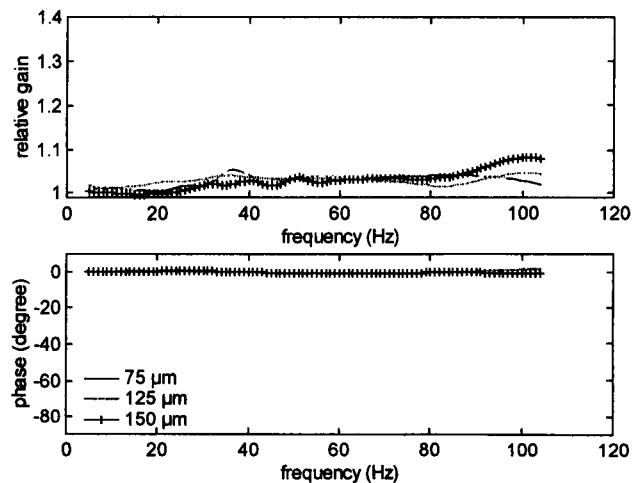


Figure 5.13. Amplitude dependency of C1

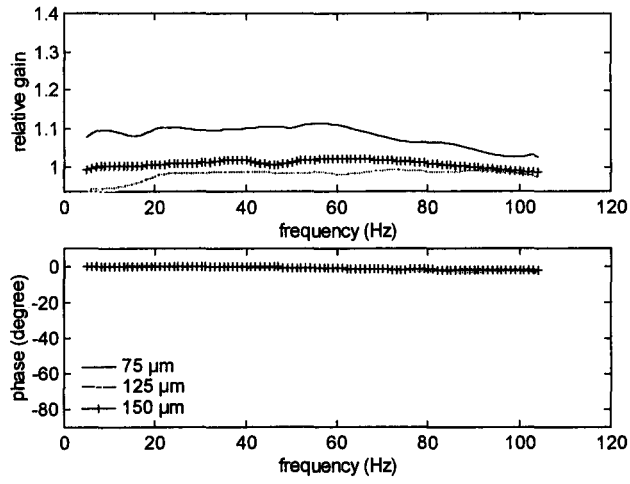


Figure 5.14. Amplitude dependency of P1

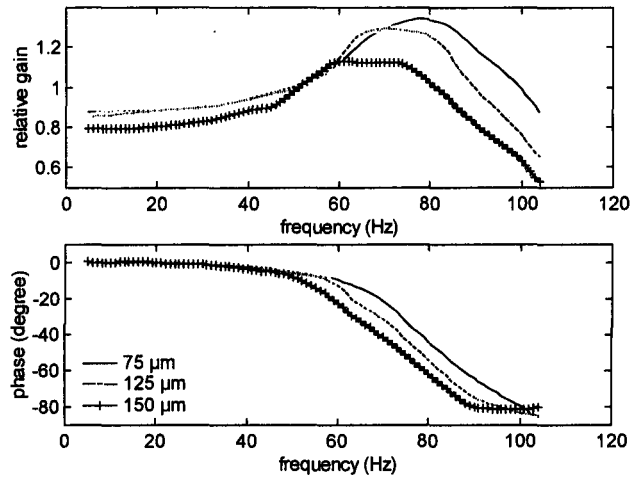


Figure 5.15. Amplitude dependency of W1

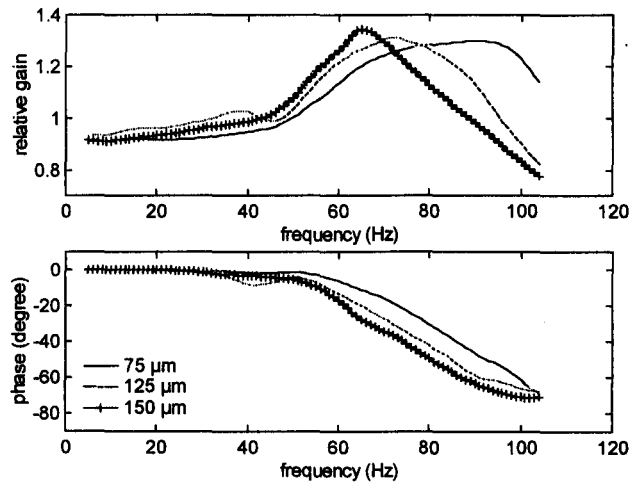


Figure 5.16. Amplitude dependency of W1b

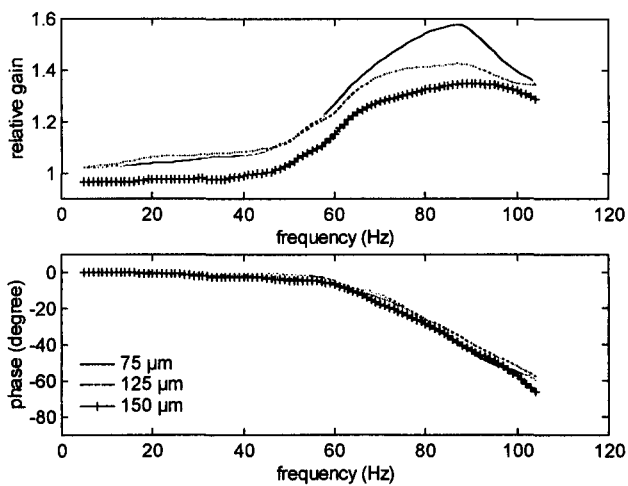


Figure 5.17. Amplitude dependency of $KC1$

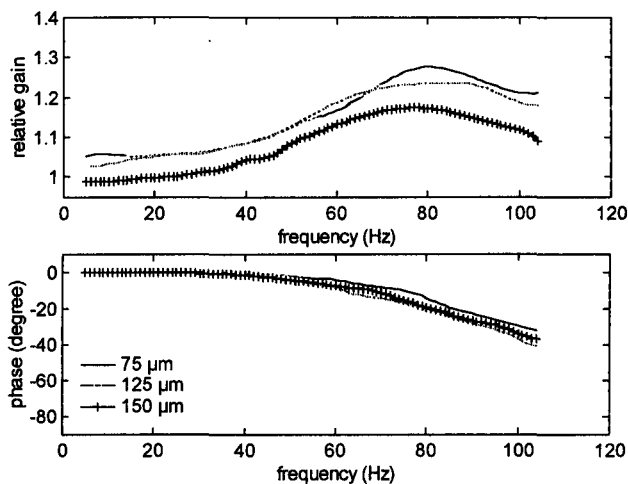


Figure 5.18. Amplitude dependency of $KC11$

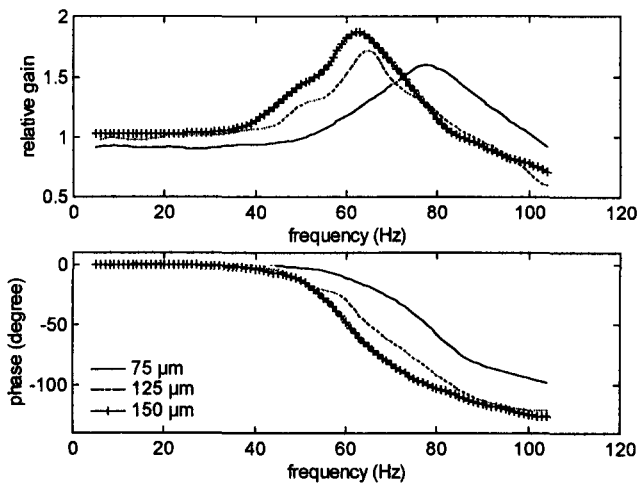


Figure 5.19. Amplitude dependency of $KA11$

Unfortunately, since the fabrics here are unloaded most established techniques for investigating the damping, such as the logarithmic decrement (2.3.1) or the commonly used stress-strain tests, become impracticable. However, a force-displacement relation can be derived here indirectly from the table acceleration. As seen in Figure 5.20, plots of the applied fabric force versus the displacement for W1 and KC11 define a hysteresis loop. The area enclosed by the hysteresis loop is equal to the energy lost per cycle, and the shape of the loop describes to some extent the type of damping [Dahl 84]. An elliptical shape as in Figure 5.20 gives evidence that the damping is mainly viscous (i.e., frequency dependent) or hysteretic (i.e., frequency independent). More pointed ends at the loop of the hysteresis, for example, would indicate that the damping is quadratic whereas a square plot would suggest that the system is frictionally damped.

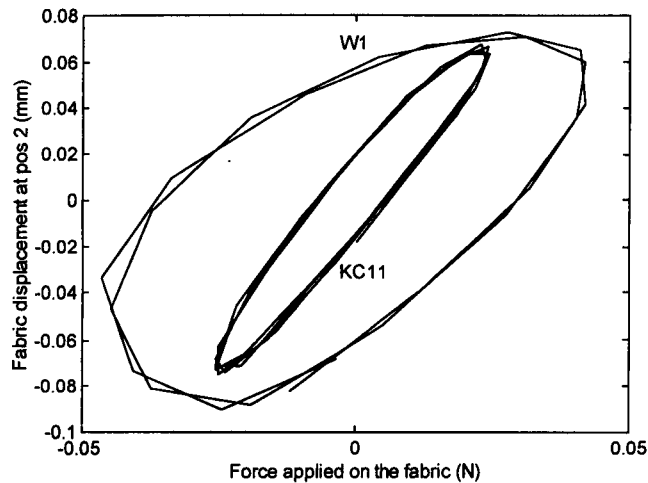


Figure 5.20. Experimental hysteresis for KC11 and W1

Table excitation (reference): 125 μm (peak to peak), frequency: 80 Hz, angle of inclination: 0° , measured at the centre of the fabric (pos2). Force applied on the fabric is not measured directly but derived from the acceleration and the fabric mass

Both viscous and hysteretic damping energy are proportional to the square of the excitation amplitude (see Appendix G), yet hysteresis damping (or structural damping) is also frequency independent. Hysteresis damping is common to materials exhibiting internal friction during low stress cyclic loading (e.g., vibration) [Tongue 96]. Further, the static compression tests in the previous chapter (4.1.2) have already pointed out the existence of a hysteretic damping mechanism in fabric since the compression and release cycle followed a different path on the graph. Although the vibration of fabric is non-linear in stiffness and damping with excitation amplitude, a linear mathematical model will be proposed for each excitation in which the hysteretic damping is approached as an equivalent viscous damping. The method is described in detail in Appendix G, but briefly, the energy dissipated per cycle of a non-linear damping system is equated to the energy dissipated per cycle of an equivalent viscous solution [Bandstra 83]. The equivalent viscous damping coefficient can then be used in a Kelvin–Voigt model as in the next section [Harris 96].

5.2.4 Fabric Vibration Model with Hysteretic Damping

A linear two parameter-model or Kelvin-Voigt model as it is generally referred to in the literature, is proposed to model the lateral vibrational behaviour of fabric for each excitation amplitude. This type of model, shown schematically in Figure 5.21, is the simplest of its kind and consists of a spring in parallel with a dashpot. A series combination of a spring and damper (i.e., Maxwell model) on the other hand, would not provide internal stress and therefore does not approximate viscoelastic solids very well [Bert 73]. Hence, Maxwell models tend to be used more in simulating viscoelastic liquids. Three-parameter models, which include an extra spring or dashpot, are obviously more complex and might give better results but also require an optimisation in order to find the third parameter. However, a parallel configuration of two elements, has some drawbacks. For instance, the creep rate approaches zero for a long duration of loading and a permanent set is impossible irrespective of the loading history [Lazan 68]. Fortunately, these disadvantages only become important when modelling a loaded system and therefore have no influence on the simulation here. The model, proposed in this study (Figure 5.21), differs from most literature models in that it is excited at its base (see also 3.10.5) because the fabric is placed on the vibratory table. Further, the mass in the model is the fabric's mass and not an externally added mass as it is normally the case (viz., spring and damper are only characterising the material).

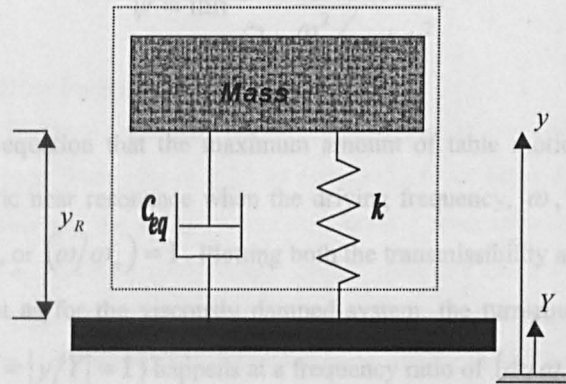


Figure 5.21. Base excited model with hysteretic damping simulating fabric vibration

The steady-state response of a linear Kelvin-Voigt model with hysteretic damping, γ , can be determined by substituting the equivalent viscous damping, c_{eq} , calculated in Appendix G, into the equation of motion to yield:

$$\begin{aligned}
 m\ddot{y} + c_{eq}(\dot{y} - \dot{Y}) + k(y - Y) &= 0 \\
 m\ddot{y} + \frac{\gamma k}{\omega}(\dot{y} - \dot{Y}) + k(y - Y) &= 0
 \end{aligned}
 \tag{5.2}$$

Assuming further that the vibrating table moves sinusoidally in time with the displacement given as $Y(t) = u_0 \sin \omega t$, where u_0 denotes the amplitude of vibration and ω the frequency of oscillation, Equation (5.2) becomes, after some rearrangement:

$$m\ddot{y} + \frac{\gamma k}{\omega} \dot{y} + ky = \gamma k u_0 \cos \omega t + k u_0 \sin \omega t \quad (5.3)$$

The above equation can be thought of as a spring-damper system, which is excited at its mass with two different harmonic inputs. Hence, as mentioned earlier in (3.10.5), the system will again respond differently compared to the classical mass-excited system. In analogy with the viscous model previously introduced in (3.10.5), the transmissibility and phase-shift can be expressed respectively as functions of the frequency ratio (ω/ω_n) , as follows:

$$T_r = \sqrt{\frac{1 + \gamma^2}{\left(1 - \frac{\omega^2}{\omega_n^2}\right)^2 + \gamma^2}} \quad (5.4)$$

$$\psi = \tan^{-1} \frac{\gamma \left(\frac{\omega}{\omega_n}\right)^2}{1 - \frac{\omega^2}{\omega_n^2} + \gamma^2}$$

Note from the above equation that the maximum amount of table motion (i.e., T_r maximum) is transmitted to the fabric near resonance when the driving frequency, ω , is equal to the undamped natural frequency, ω_n , or $(\omega/\omega_n) = 1$. Plotting both the transmissibility and phase relationship as in Figure 5.22 shows that as for the viscously damped system, the turn-round between damping and amplification (viz., $T_r = |y/Y| = 1$) happens at a frequency ratio of $(\omega/\omega_n) = \sqrt{2}$. The differences, however, between the viscous (Figure 3.44) and hysteretic damped system are visible both in the transmissibility and in the phase-shift. For a hysteretic damped system, the transmissibility decays faster after resonance and the phase-shift eventually goes to -180° at infinite frequency whereas for the viscously damped system, the phase tends to -90° at infinity. Further, note that the models have a unity gain at low frequencies. In the next section, we can now compare the measured responses with the theoretical curves and deduce the damping losses and dynamic stiffness.

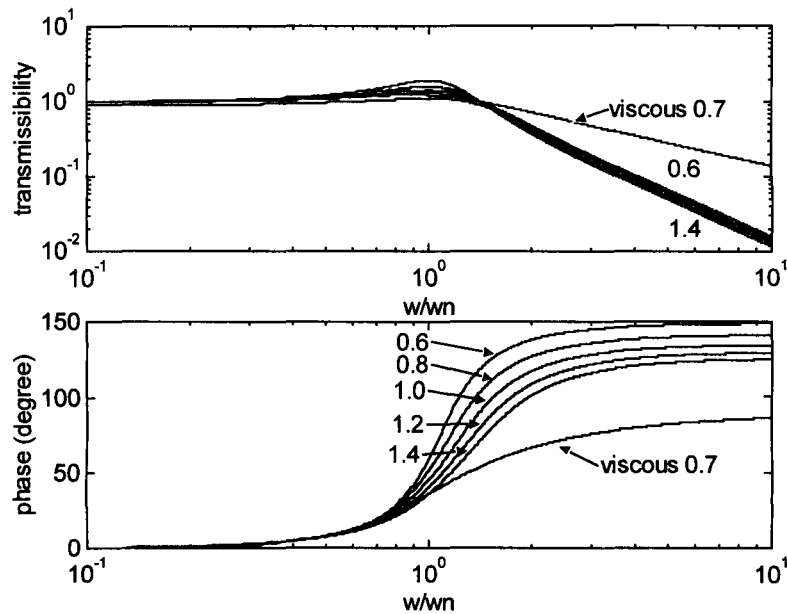


Figure 5.22. Theoretical frequency response of a base excited spring-damper model with hysteretic damping

The curves for hysteretic damping are plotted for different values of γ and as a comparison a viscous damping ($\zeta = 0.7$) is included

5.2.5 Simulation Results

Fabric C1 and P1 have been left out of the simulations because of their invariance (and inconsistency) yet as seen from Figure 5.23 to Figure 5.27, all other fabrics seem to follow the hysteretic model. On average, the phase relationship gives a reasonable fit though the experimental gain is for many tests at low frequency ranges smaller than one and therefore does not match the theoretical unity gain well. However, it should be noted that phase measurements for this type of experiment are probably more accurate than displacement measurements and hence this could well be a measurement error (see 4.1.3). On the other hand, mainly the woollen fabric samples W1 and W1b seem to be susceptible to this low frequency effect which could also be a damping effect caused by the surface hairs in the outer layer creating an extra 'mode' of vibration at low frequency. In addition, this low-frequency damping is reduced for W1b (viz., T_r closer to one) compared to W1.

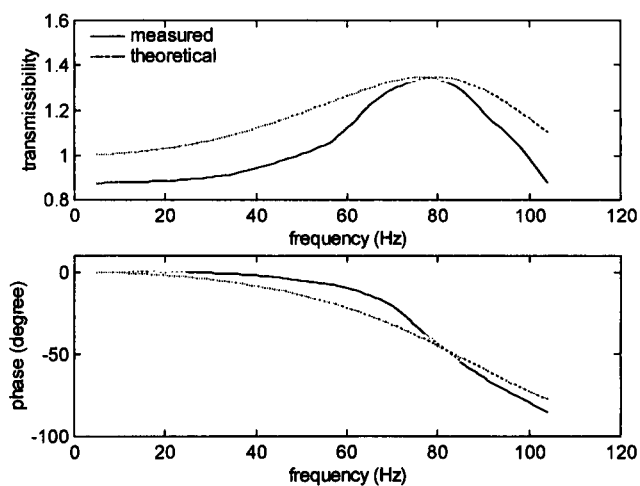


Figure 5.23. Comparison of theoretical and measured frequency response for W1 at 75 μm excitation

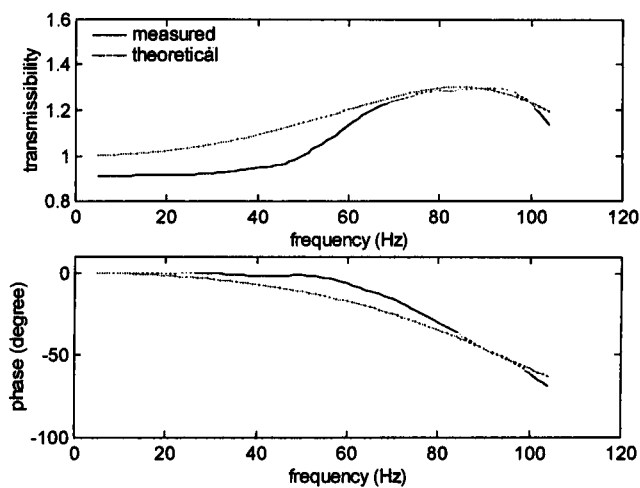


Figure 5.24. Comparison of theoretical and measured frequency response for W1b at 75 μm excitation

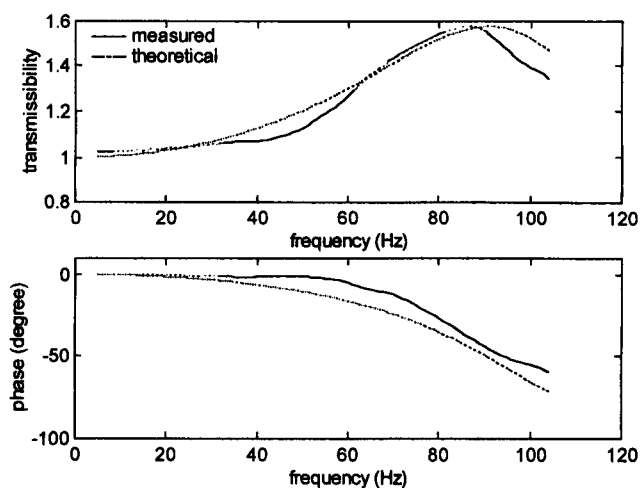


Figure 5.25. Comparison of theoretical and measured frequency response for KC1 at 75 μm excitation

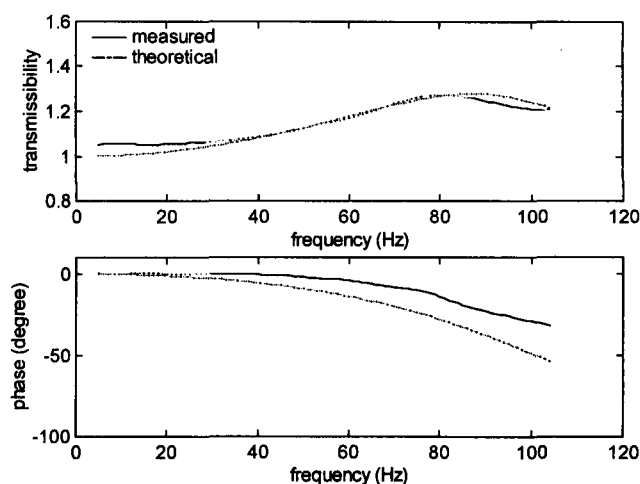


Figure 5.26. Comparison of theoretical and measured frequency response for KC11 at 75 μm excitation

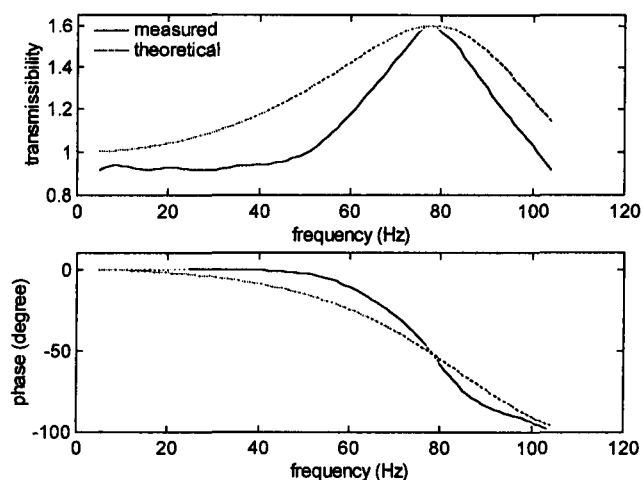


Figure 5.27. Comparison of theoretical and measured frequency response for KA11 at 75 μm excitation

The above figures only display the comparison between the theoretical and the measured data for a 75- μm excitation. All parameters for the other excitation amplitudes (i.e., 125 μm and 150 μm) together with their respective correlation for transmissibility and phase-shift are listed in Table 5-1. All fabrics show a decrease in resonance frequency with an increase in amplitude signifying a 20-40% reduction in stiffness for a near doubling of the excitation. No straightforward relation could be found between the bending stiffness of the fabrics and their corresponding resonance frequency as for flexural vibration [Hearle 61]. As seen from Figure 5.28, a reasonably stiff material such as W1 has the same resonance frequency as KA11, which has a much lower stiffness. Furthermore, C1 and P1, both extremes in bending stiffness, do not even show a resonance peak. Yet, removing the surface hairs such as in W1b seems to increase the resonance frequency when compared with W1. From this finding, it can be postulated that the lateral vibration of fabric is more a dynamic compression than a 'wave' mechanism.

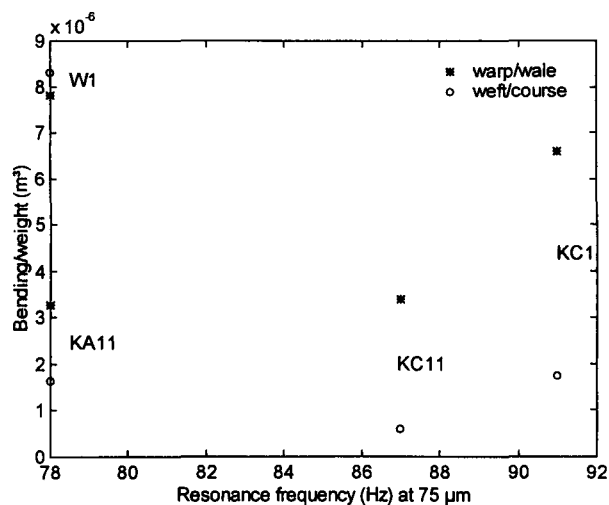


Figure 5.28. Relationship between the bending stiffness and the resonance frequency

Table 5-1. Estimated spring-damper coefficients from vibration measurements of set 1 fabrics

Fabric code	Excitation amplitude (μm)	f_{res} (Hz)	k at ω_n (N/m)	γ	c_{eq} at ω_n (N s/m)	r^2 for T_r	r^2 for ψ
W1	75	78.0	838	1.10	1.881	0.963	0.983
	125	71.6	707	1.20	1.885	0.948	0.986
	150	63.7	558	1.80	2.513	0.937	0.986
W1b	75	84.4	972	1.20	2.200	0.976	0.979
	125	76.4	797	1.20	1.993	0.905	0.990
	150	71.6	701	1.10	1.713	0.918	0.993
KC1	75	90.7	835	0.82	1.201	0.975	0.983
	125	89.1	806	0.98	1.410	0.983	0.989
	150	89.1	806	1.10	1.583	0.980	0.987
KC11	75	87.5	596	1.25	1.354	0.984	0.987
	125	79.6	492	1.35	1.330	0.977	0.995
	150	77.9	473	1.60	1.544	0.978	0.993
KA11	75	77.9	643	0.80	1.051	0.939	0.985
	125	65.3	450	0.70	0.769	0.963	0.995
	150	62.1	408	0.63	0.658	0.968	0.996

Standard testing conditions, r^2 : correlation coefficient between theoretical and measured data

Next, the simulated hysteretic damping, γ , varies on average between 0.6-1.2 for the different fabrics. No uniform trend is evident in the variation of the damping with an amplitude increase: for instance, for KC1, KC11 and W1 the damping increases with increasing excitation whereas for W1b and KA11 the damping reduces. However, when looking at the equivalent damping, on average the

damping for the knitted samples is lower than for the woven samples. Further, the high correlation coefficients ($r^2 > 0.9$) in Table 5-1 reveal that most of the measured data fit the theoretical results despite the offset on the transmissibility of some of the fabrics. Apart from the earlier mentioned low frequency damping this offset is most likely caused by a deficient match of the damping. After all, a pure hysteretic or frequency-independent damping mechanism is very unrealistic since most materials in nature exhibit several contributing damping mechanisms [Crandall 70]. Hence, a more representational damping should also include some viscous and perhaps frictional damping. The latter will become more important should the fabric be preloaded, for instance when vibrating a stack of fabric.

Table 5-2. Comparison between static and dynamic stiffness

Fabric code	Dynamic 'spring' (N/m)	Static 'spring' (N/m)
W1	701	113
W1b	823	147
KC1	816	96
KC11	520	65
KA11	500	66

An average value has been taken for both dynamic and static stiffness considering that the vibration forces (i.e., pressure) for the different amplitudes are very low (0.1-0.2e-04 N/mm²)

Finally, to conclude this section on stationary vibration, the static stiffness measured in the previous chapter is compared with the dynamic stiffness from the vibration tests. The static stiffness has been determined from the slope of the compression characteristics at a compression load equal to that exerted dynamically in the vibration tests at resonance. However, due to the very small variations in resonance and consequently in pressure, an average value of static stiffness (viz., asymptotically near zero static pressure) has been compared with an average dynamic stiffness for the three excitations. From Table 5-2, all static stiffness values are 5-8 times smaller than their corresponding dynamic values. This observation is also made for carpets [Dunlop 89] and felt [Dunlop 90], which has been tested preloaded (i.e., static pressure 4.9 and 7.0 kPa) and for dynamic values calculated from acoustic measurements (i.e., unloaded) [Dunlop 81]. These differences in static and dynamic values can be accounted for in terms of fibre slippage as for carpet and felt. During the static compression much larger displacements are measured (i.e., ≈ 130 -220 μm) than the excitation amplitude for the same pressures thus the fibres in the outer layer are more compacted, hence the reduced static stiffness or spring constant. In addition, the amplitude dependency of the dynamic damping can also be interpreted when looking back at the van Wyk simulations in chapter 4. At very low pressures, the static compression characteristic is already non-linear. Consequently, the area of the hysteresis loop tends to increase disproportionately for larger compressions justifying the increase in damping for larger vibrations. Up to now all vibrational experiments have been stationary, which

means that the fabrics did not move along the table (i.e., horizontal table surface). However, in the next section, the optimal conditions will be investigated which move a fabric panel forward on a vibrating table.

5.3 Vibratory Feeding of Fabric

5.3.1 Experimental Method

From the literature review in section (2.4.2), we have seen that several operating conditions such as the excitation amplitude, u_0 , the frequency, ω , and table inclination (or declination), ϕ , determine the complete movement and motion of an object on a vibrating table. Yet, one of the most important parameters for successful feeding (i.e., efficient speed) is the friction coefficient between the object, in this case fabric, and the table surface (see Appendix H). Hence, the experiments in this section are split into two parts; the first part investigates the influence of friction on vibratory feeding whereas the second part looks at the effect of different table parameters on the velocity. The travelling velocity of each fabric has been obtained by measuring manually with a stopwatch the time it takes a fabric panel to move a certain distance along the table. In order to reduce any timing errors, six measurements are made on the same sample for each test condition and a variable distance is taken according to the velocity (viz., larger speed requires larger distance). Further avoiding any alignment effects of the fabric as discussed in (3.3), only one operating condition, comprised of six tests each, is tested per day.

5.3.2 Friction Dependency

The three engineering surfaces (i.e., aluminium, Formica and rubber) used for friction tests in chapter 4, are now attached individually to the vibratory table surface on which set 1 (including W1b) fabrics (100-mm square) are tested. The table is tilted at an angle of 15 degrees to the horizontal and vibrated at 100- μm peak to peak normal to the surface. The sliding velocities, displayed in Figure 5.31 to Figure 5.37 for each sample, are measured (6 times) at steps of 5-Hz in a range from 10 to 105 Hz. Note however that the scales on the y-axes for the various figures differ from each other. In addition, all fabrics are tested in both principal directions (i.e., warp/wale and weft/course) at 100- μm excitation and a table inclination of 5 degrees. From the figures below, it is striking that the velocity patterns are not monotonically increasing but show peak values at 65 and 95-Hz, in case of aluminium and rubber, and 60 and 95 Hz in case of Formica. Unfortunately, this is caused by an unbalance of the table and has nothing to do with the fabric itself. An analysis of the accelerometer signals at these specific frequencies revealed that a small horizontal displacement of approximately 14- μm is introduced out of phase with the main normal excitation.

As sketched in Figure 5.29, when inclining the table, this combined excitation leads to an elliptical motion of the table, which in fact enhances the conveying [Redford 75], hence the increase in sliding velocity at these particular frequencies. Further note that due to the heavier Formica surface, the first out of phase vibration shifts to a lower frequency (60-Hz) compared to the aluminium and rubber surface.

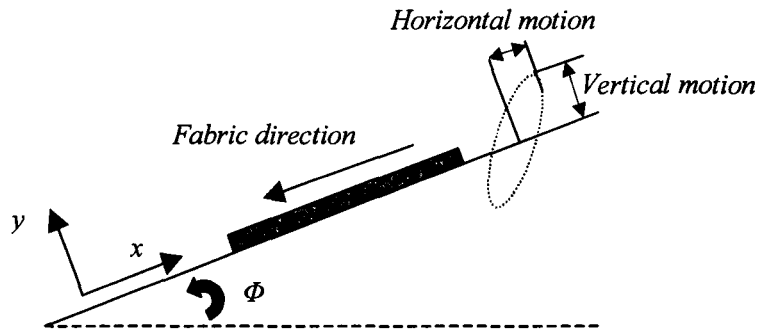


Figure 5.29. Out of phase motion when inclining the table

Consider now first the directionality of the fabric. Due to the low inclination, the fabric samples only start sliding from 60-Hz onwards, which is well over the flight-free excitation limit (i.e., vertical line in Figure 5.31 to Figure 5.37). Only fabric KA11, which has the best performance of all samples, starts sliding at the flight-free limit. A comparison between fabric W1 and W1b reveals that removing the surface hairs improved the conveying velocity, which partly can be attributed to the lower friction coefficient of W1b (μ weft 0.25). In general, the sliding velocity of all fabrics in both principal fabric directions is very much the same. To a certain extent, this is expected since the friction does not vary much in both directions. However, in Figure 5.30 when plotting the sliding speed as a function of the friction for one operating condition, it is clear that the lower friction coefficient of the knitted fabrics in the course direction results in a more rapid conveying. Yet, for the woven samples this is not the case, a lower friction does not convey the samples faster, on the contrary.

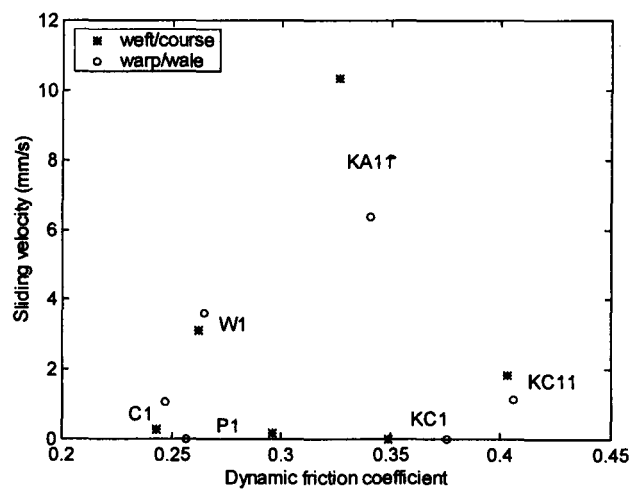


Figure 5.30. Vibratory feeding of fabric samples on an aluminium surface in both principal directions

Table is excited at $100 \mu\text{m} - 100 \text{ Hz}$ and inclined at 5°

However, the directional difference in bending stiffness does not seem to be directly responsible for this since again no obvious relationship has been found. On the other hand, external vibrations can affect the friction between two surfaces (viz., decrease or increase) as in metals for example [Skåre 92], though the exact influence of vibrations here on fabric friction remains unknown. Next, a better discrimination of sliding velocities is obtained when using different surfaces.

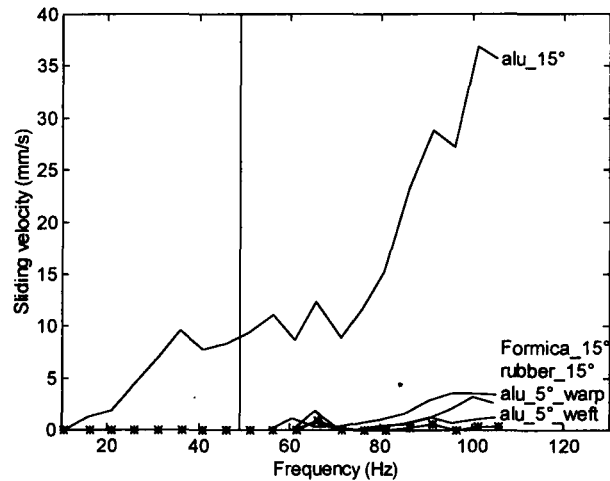


Figure 5.31. Friction dependency for vibratory feeding of C1

Table is excited at $100 \mu\text{m}$, fabric slides in the warp (wale) direction for the 15° experiments, the straight vertical line marks the theoretical end of the flight-free conveying (same remarks apply to Figure 5.32 to Figure 5.37 below)

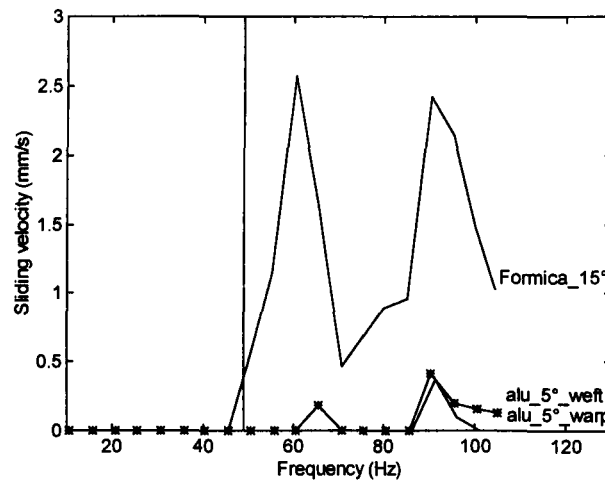


Figure 5.32. Friction dependency for vibratory feeding of P1

Rubber 15° is not included in the graph since fabric P1 does not slide on a rubber surface. Further P1 slips very irregularly on an aluminium surface when inclined at 15° hence, the results are also omitted from the above graph

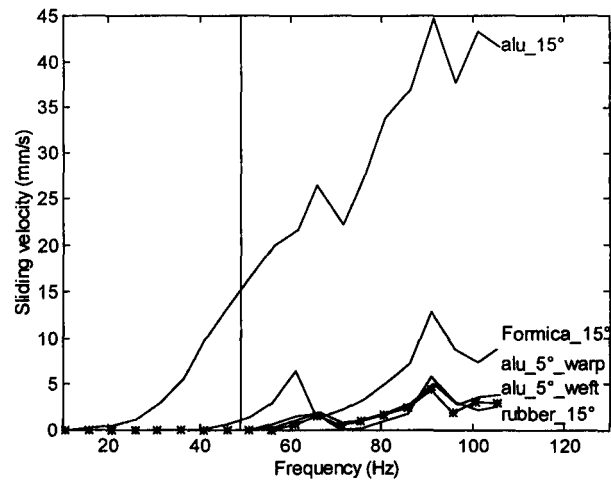


Figure 5.33. Friction dependency for vibratory feeding of W1

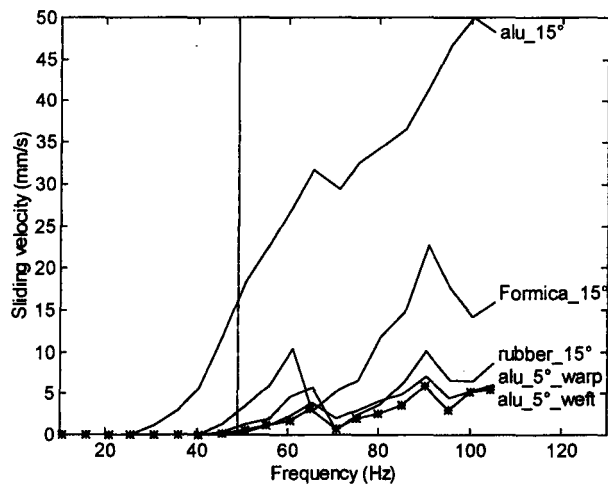


Figure 5.34. Friction dependency for vibratory feeding of W1b

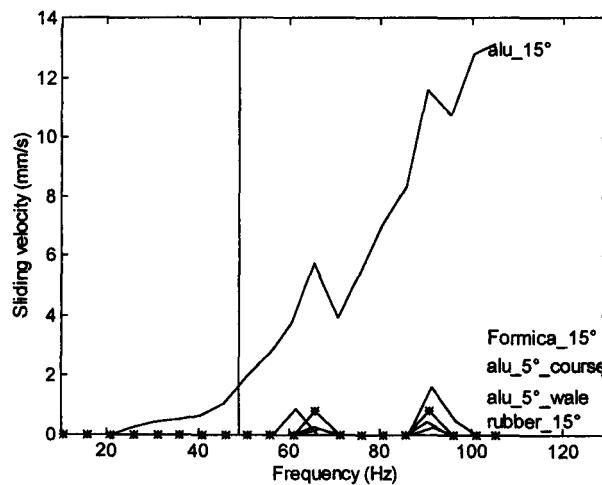


Figure 5.35. Friction dependency for vibratory feeding of KC1

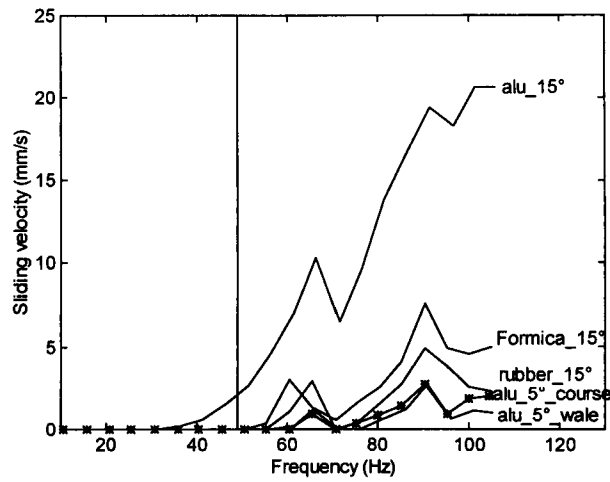


Figure 5.36. Friction dependency for vibratory feeding of KC11

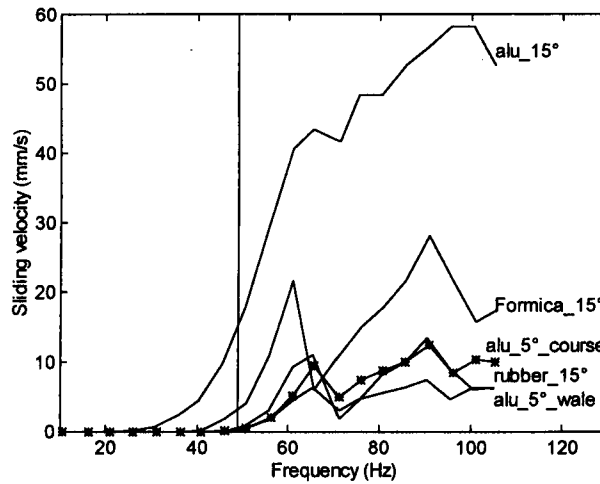


Figure 5.37. Friction dependency for vibratory feeding of KA11

A glimpse at Figure 5.31 to Figure 5.37 shows immediately that the aluminium surface gives by far the highest sliding speed for all fabric samples followed respectively by the Formica and the rubber surface. Note that the table needed an inclination of 15 degrees before the fabrics even started to slide on the rubber surface. Figure 5.38 plots the sliding velocity in relation to the friction for one operating condition and shows that, despite the smaller friction, fabrics on the Formica surface do not convey much faster than the rubber surface. Overall, an aluminium surface is most effective though still large discrepancies in sliding velocities are noted between the different fabrics. For instance, KA11 will be conveyed three times faster than KC11 in identical conditions. These differences in conveying speed between the individual fabric samples might be explained in terms of fabric damping. If a fabric possesses a large damping, then all the vibration energy will be absorbed in the fabric instead of being used for conveying. For instance, as for fabrics C1 and P1, in a stationary position the fabric will follow the table motion exactly (viz., no resonance frequency or phase-shift) and will therefore convey very slowly. On the other hand, KA11 exhibited a large resonance

frequency and phase-shift, and consequently conveys very rapidly. If however the sliding velocity is plot against the equivalent lateral viscous damping as Figure 5.39 no such relationship is directly obvious.

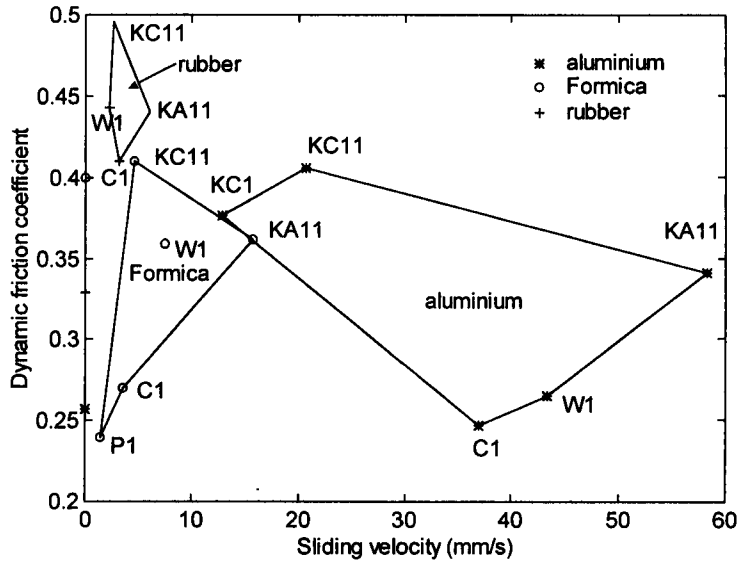


Figure 5.38. Conveying velocity of fabrics on different surfaces

Table is excited at $100 \mu\text{m} - 100 \text{ Hz}$ and inclined at 15° , all fabric samples are sliding in the warp or wale direction

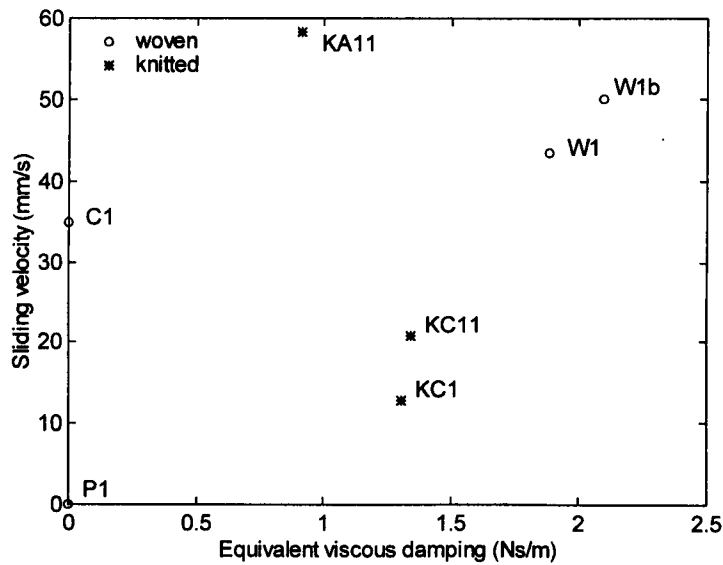


Figure 5.39. Relationship between the fabric damping and the sliding velocity

Table with aluminium surface is excited at $100 \mu\text{m} - 100 \text{ Hz}$ and inclined at 15° , the damping coefficients of fabric P1 and C1 have not been determined

The above results showed that an out of phase vibration is the most optimal condition for conveying fabrics although this was not initially the intention. In the next section, the amplitude and inclination angle is changed to see their effect on fabric conveying.

5.3.3 Table Dependency

As anticipated, Figure 5.40 to Figure 5.46 giving the sliding velocity in relation to table inclination, show an increase in sliding velocity for an increase in table inclination. Note however that the sliding speed does not increase linearly with the table inclination (see Appendix H). In addition, all fabrics start sliding at a lower excitation frequency when the table is tilted more. Compared to a theoretical prediction for a 'solid' (i.e., large damping), most of the fabrics do not differ greatly. Only the samples W1, W1b and KA11, which have a smaller damping, diverge more (different slope) from the calculated velocity. Notice further that the inclination for the calculated velocities of the woven materials is 12.5° instead of 15° as for the knitted materials since theoretically all woven materials would slide down at 15° ($\mu_{\text{woven}} < \tan \phi$). This indicates either that the inclined plate method for the determination of friction is highly inaccurate for unloaded samples, which is very likely or that in fact, external vibrations are increasing the fabric friction.

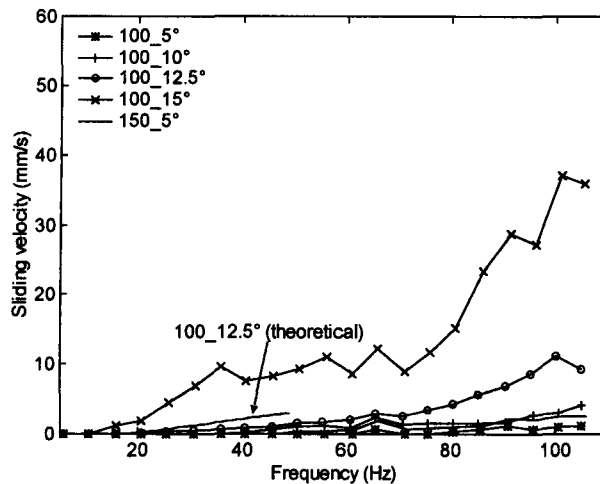


Figure 5.40. Conveying velocity of C1 for an increasing table inclination

The fabric sample is sliding in the warp direction on the aluminium surface, similar for Figure 5.41 to Figure 5.46 with the knitted samples sliding in the wale direction. The theoretical curve is calculated with the previously determined friction coefficient (Table 3-3) on the aluminium surface

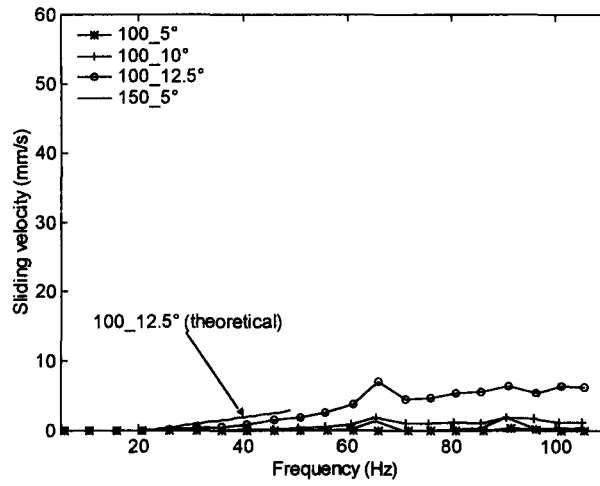


Figure 5.41. Conveying velocity of P1 for an increasing table inclination

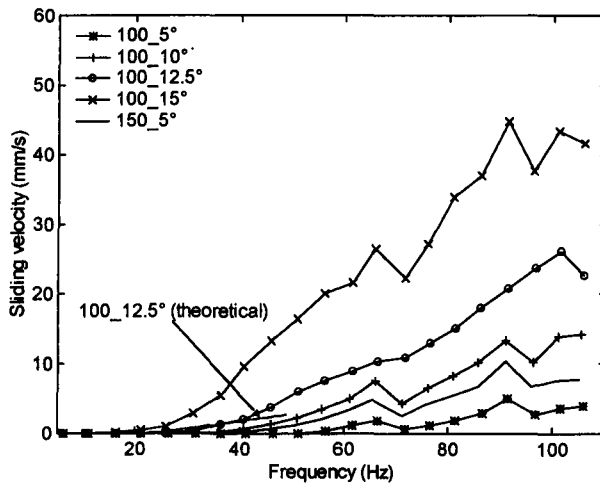


Figure 5.42. Conveying velocity of W1 for an increasing table inclination

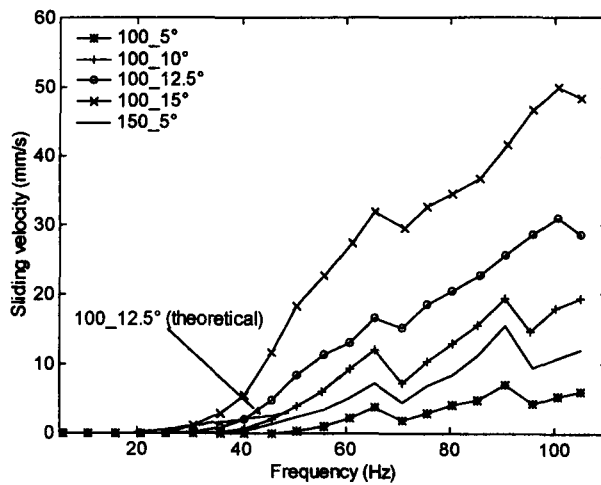


Figure 5.43. Conveying velocity of W1b for an increasing table inclination

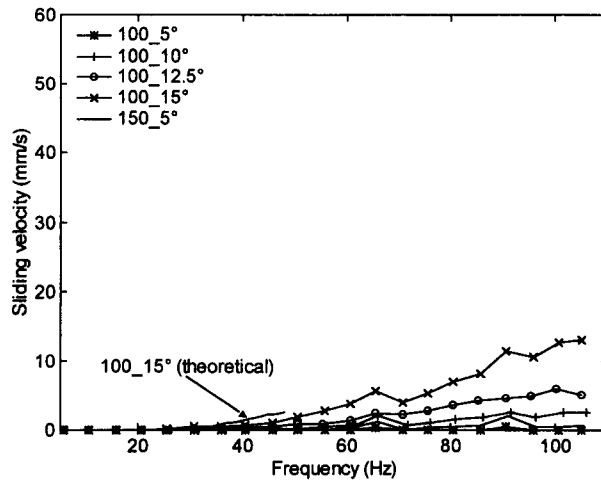


Figure 5.44. Conveying velocity of KCl for an increasing table inclination

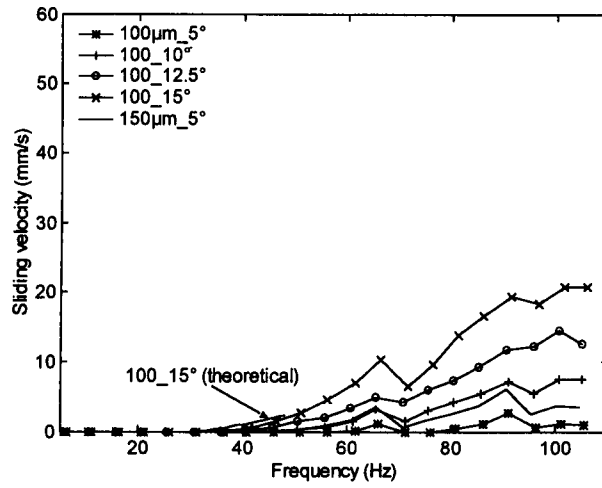


Figure 5.45. Conveying velocity of KCl1 for an increasing table inclination

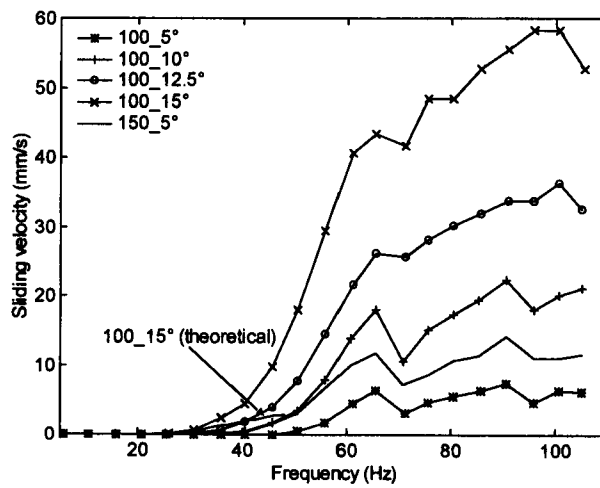


Figure 5.46. Conveying velocity of KA11 for an increasing table inclination

Another obvious way to improve the conveyance of the fabrics is to increase the table excitation though economically this is less preferable since the power consumption will be increased. From Figure 5.40 to Figure 5.46, a 50% increase in amplitude seems nearly to double the feeding although theoretically (i.e., for a solid) such an amplitude increase should convey the materials much faster as can be seen in Figure 5.47. Furthermore, from the predictions (Appendix H), the fabrics should start sliding from 35 Hz onwards whereas experimentally some fabrics only start to convey from an excitation frequency of 45 Hz. This large discrepancy with the theoretical values is likely caused by an increased compression of the material, which consequently results in a reduced sliding of the fabric.

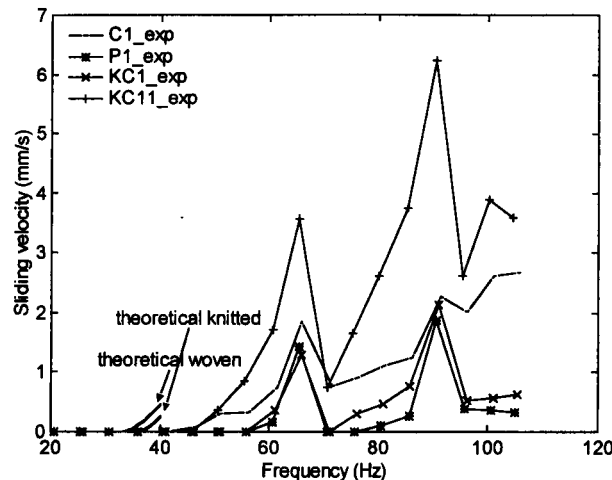


Figure 5.47. Theoretical and experimental sliding velocity of some fabrics for an increased table excitation of $150 \mu\text{m}$

The fabric sample is sliding in the warp (wale) direction on the aluminium surface, with the table inclined at an angle of 5° . The theoretical curve is calculated with the previously determined friction coefficient (Table 3-3) on the aluminium surface

The above analysis has concentrated only on the conveying of fabrics (viz., transporting from one point to another) and the factors that influence this. In general, most fabric types are suitable for vibratory conveying and can be transported efficiently. However, conveyors for solid materials often orientate their objects at the same time as transportation. In the next section, some possible positioning mechanisms will be suggested though the reader should be reminded that none of them have been tested in reality.

5.4 Some Concepts for the Vibratory Orientation of Fabric

In the introduction of this thesis the need and importance of fabric orientation for garment automation has been addressed though the very nature of fabric itself makes this process far more complicated than for solid materials. It was noticed during this research and in the original Apparel Research Foundation study [Saibel 68] that vibrating the fabric stiffens the material to some extent, though the limpness or low in plane stiffness of the fabric remains a problem. For example, when

colliding with guides or fences, which are often used as orientating devices, the panels can easily buckle and crease. Further, the placing of fabric panels on a surface sometimes introduces folds or creases, which can lead to misalignment since only very small creases will be removed during the vibrating process. One advantage however, of the fabric is that its natural resting position is in the fabric plane which reduces the orientation process to two dimensions only. Two main methods shown in Figure 5.50 can be used to orientate materials on a linear vibratory table: one category is based on fences another on variations in the sliding surface. Yet, the huge differences in raw material, panel sizes and shapes will demand an enormous flexibility in the various approaches. Overall, a re-programmable feeding mechanism is preferred to a system, which needs physical modification each time a different panel is introduced. Furthermore, all systems will require limited sensing built into the table to assure that either a fabric panel has arrived at its predetermined position and/or whether the panel is in the correct position or not. In the following two subsections the different implementations presented in Figure 5.50 are elucidated in more detail.

5.4.1 Orientation by Fences

The use of fences to guide and orientate materials is already an established technique in solid parts feeding [Brokowski 93]. The procedure is based on static fences (or rotatable [Mani 85]) rotating the part whenever a corner of the object hits a fence until a flat edge is aligned with that fence. A limitation, however, of this kind of alignment is that contact with the fence should never be broken otherwise the final orientation of the object will no longer be unique [Brokowski 93]. Furthermore, only certain edges of an object are stable as illustrated for example for an arm-shaped panel in Figure 5.48. Panels hitting the fence with an unstable edge will turnaround until a stable edge is reached on which the part can then slide further along that fence.

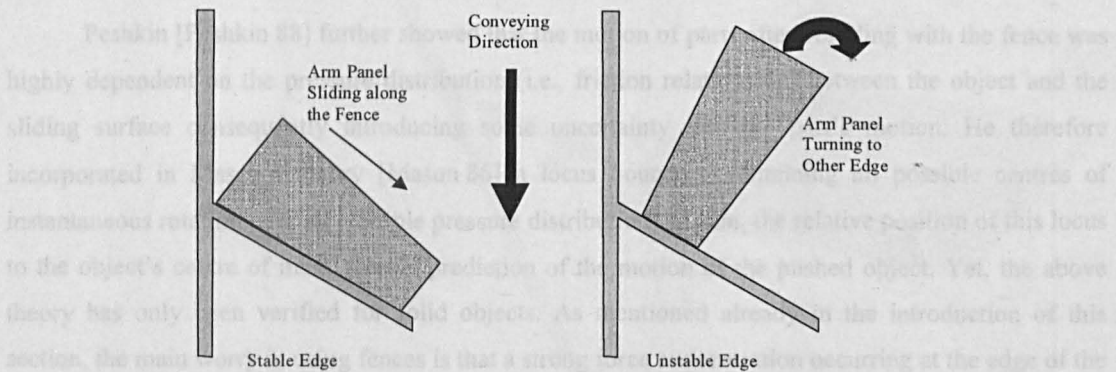


Figure 5.48. Stable and unstable edge alignments of an arm shaped fabric panel

Although several edges of a panel are stable (e.g., both long edges of the arm panel), a sequence of fences at appropriate angles can guarantee that at the end of the cycle the object is aligned along a unique edge. Any planar motion during conveying is either a simple translation or a rotation, however one of the challenging problems in the orientation of objects is to predict which way the object will rotate once it hits a fence. Mason [Mason 84, 86] was one of the first to study this problem.

From a robot manipulation viewpoint, he identified a fundamental rule to tell the direction that a solid part will rotate in when it is pushed by the fingers of a robot hand before grasping. The principle is summarised in Figure 5.49 for a rectangular panel touching a fence at one of its corners. The direction of rotation is determined by three rays starting from the contact point between the object and the fence. Two rays μ_l and μ_r describe the boundaries of a friction cone at an angle, $\alpha = \tan^{-1} \mu$, from the normal while the third ray, v_p , gives the 'velocity' of the fence (push), which is opposite to the sliding direction since the fence is static. These three rays vote, relative to the object's centre of mass, on the direction of rotation. Here, in this case, since two of the three rays are to the left of its centre of mass, the object will turn clockwise.

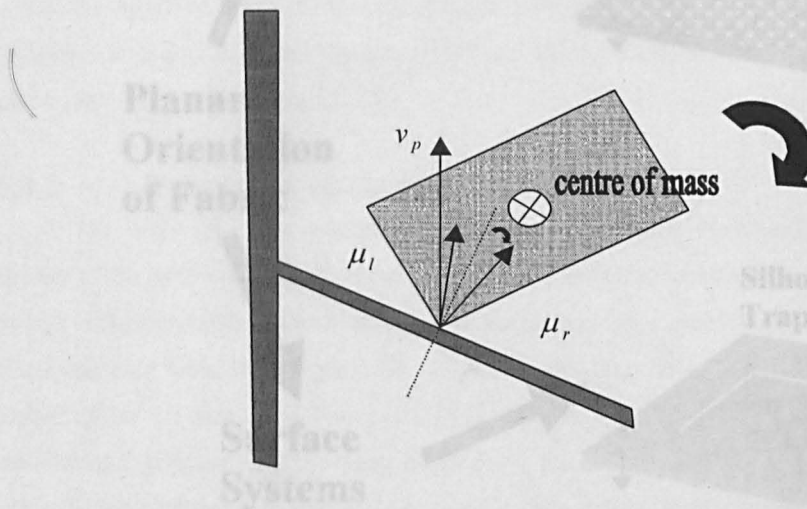


Figure 5.49. Predicting the rotation of a rectangular panel hitting a fence (after [Mason 84])

Peshkin [Peshkin 88] further showed that the motion of parts after colliding with the fence was highly dependent on the pressure distribution (i.e., friction relationship) between the object and the sliding surface consequently introducing some uncertainty into the part's motion. He therefore incorporated in Mason's theory [Mason 86] a locus boundary containing all possible centres of instantaneous rotation over all possible pressure distributions. Again, the relative position of this locus to the object's centre of mass gives a prediction of the motion of the pushed object. Yet, the above theory has only been verified for solid objects. As mentioned already in the introduction of this section, the main worry in using fences is that a strong force concentration occurring at the edge of the fabric can cause buckling. Fabrics are particularly vulnerable to that when the table is inclined at a higher angle, which is sometimes necessary to allow easy sliding as for P1 for example. Unfortunately, many of these fabrics, which convey badly, suffer at the same time from a low bending stiffness, which only worsens the problem.

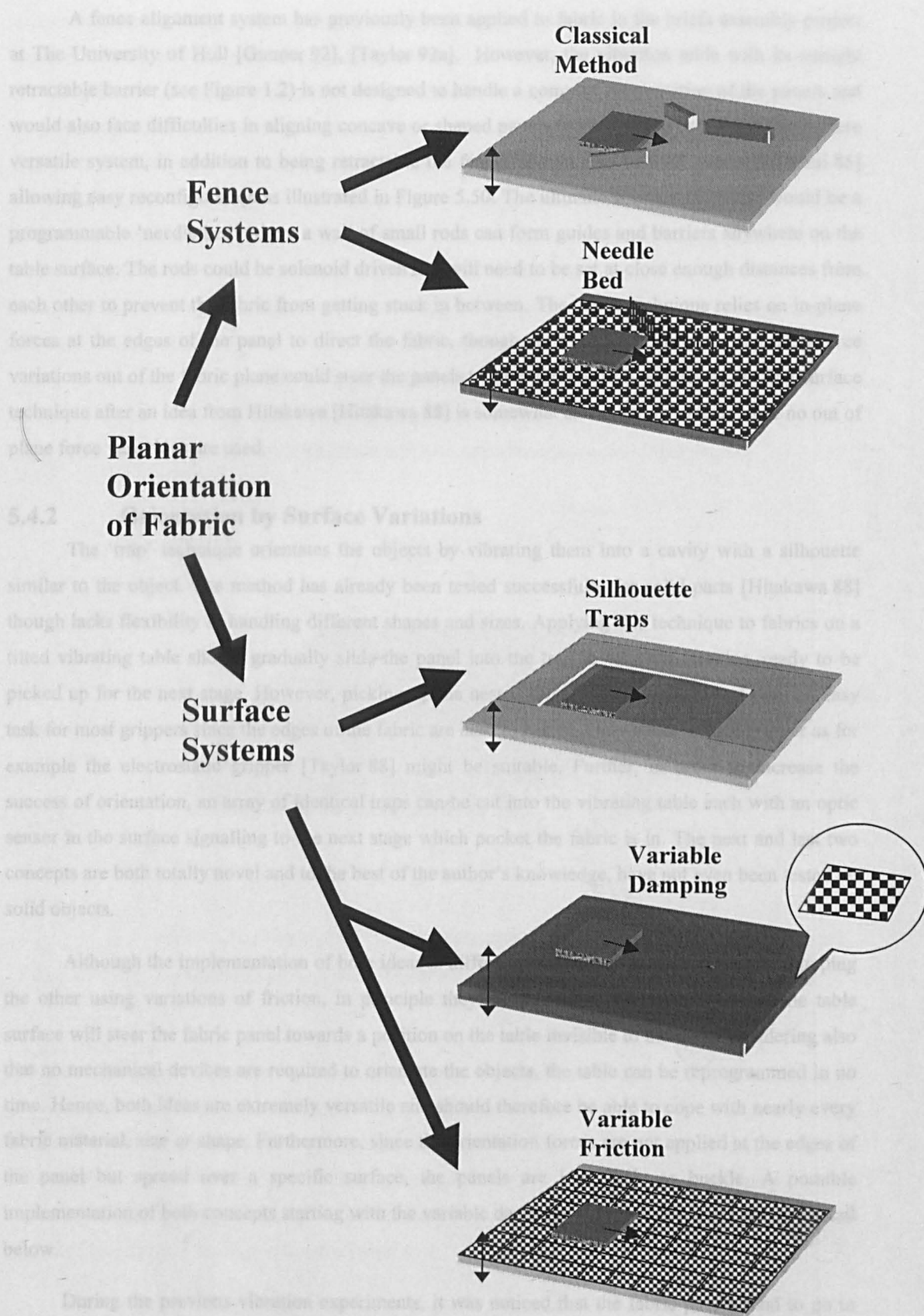


Figure 5.50. Some conceptual ideas of orientating fabric panels on a linear vibratory feeder

A fence alignment system has previously been applied to fabric in the briefs assembly project at The University of Hull [Gunner 92], [Taylor 92a]. However, the vibration table with its straight retractable barrier (see Figure 1.2) is not designed to handle a complex reorientation of the panels and would also face difficulties in aligning concave or shaped panels (e.g., T-shape or I-shape). In a more versatile system, in addition to being retractable the fences should also be 360° rotatable [Mani 85] allowing easy reconfiguration as illustrated in Figure 5.50. The ultimate solution of course would be a programmable 'needle bed' where a wall of small rods can form guides and barriers anywhere on the table surface. The rods could be solenoid driven and will need to be set at close enough distances from each other to prevent the fabric from getting stuck in between. The above technique relies on in-plane forces at the edges of the panel to direct the fabric, though, as in the following section, also force variations out of the fabric plane could steer the panels to a certain position. However, the first surface technique after an idea from Hitakawa [Hitakawa 88] is somewhat an exception to that, since no out of plane force variations are used.

5.4.2 Orientation by Surface Variations

The 'trap' technique orientates the objects by vibrating them into a cavity with a silhouette similar to the object. The method has already been tested successfully for solid parts [Hitakawa 88] though lacks flexibility in handling different shapes and sizes. Applying this technique to fabrics on a tilted vibrating table should gradually slide the panel into the trap in which it remains, ready to be picked up for the next stage. However, picking up the nested fabric panel might be not such an easy task for most grippers since the edges of the fabric are hard to access. Only a flat surface gripper as for example the electrostatic gripper [Taylor 88] might be suitable. Further, in order to increase the success of orientation, an array of identical traps can be cut into the vibrating table each with an optic sensor in the surface signalling to the next stage which pocket the fabric is in. The next and last two concepts are both totally novel and to the best of the author's knowledge, have not even been tested on solid objects.

Although the implementation of both ideas is different, one system using variation of damping the other using variations of friction, in principle they are the same. Field variations in the table surface will steer the fabric panel towards a position on the table invisible to the eye. Considering also that no mechanical devices are required to orientate the objects, the table can be reprogrammed in no time. Hence, both ideas are extremely versatile and should therefore be able to cope with nearly every fabric material, size or shape. Furthermore, since the orientation forces are not applied at the edges of the panel but spread over a specific surface, the panels are less likely to buckle. A possible implementation of both concepts starting with the variable damping system is discussed in more detail below.

During the previous vibration experiments, it was noticed that the fabric panels tend to go to areas with minimum excitation (i.e., minimum energy principle or minimum disturbance). So, if now a path with gradually higher damping (viz., lower excitation) can be programmed on the vibrating table, the fabric will be forced to follow it. One can think about it as a valley with a river flowing through. Eventually, the fabric panel will be directed to a specific place on the table, where it is in an

orientated position ready for the next stage in the automation cycle. This preordained position should represent the highest damping of the whole table and have an exact silhouette as the panel. A device featuring this kind of properties can be constructed by incorporating the programmable compliant surface designed at The University of Hull [Taylor 94c] into an inclined vibrating table as sketched in Figure 5.51. The variable compliance is obtained by electrically changing the viscosity of an electrorheological fluid (ER), which is trapped in between a flexible conductive surface and an array of electrodes embedded into the vibrating table. An ER fluid, which is made from a suspension of dielectric solid or polymeric particles in an insulating base oil, behaves under normal conditions as a Newtonian fluid though transforms to a plastic state on applying an electric field. By then feeding a different voltage of several kV to the various electrodes, the fluid above each electrode surface will change its viscosity proportionally to the field strength and consequently create a different damping at this place on the table. This metamorphosis happens in milliseconds and has lead already to a host of other applications in shock absorption, noise isolation and vibration control [Stanway 96].

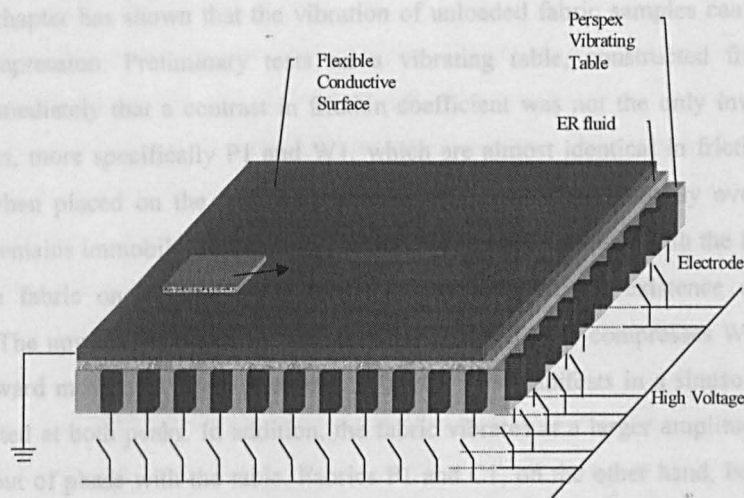


Figure 5.51. Cross sectional view of an electrorheological orienting table

The sketched surface profile is highly out of proportion with the rest of the figure and will only vary 1 to 2 mm at the most in reality

The above description, however, assumes that the path is programmed before the fabric is placed on the table (viz., static approach) though it is also perfectly possible to have a dynamic system with feedback where the surface profile changes continuously. In addition, the ER-effect also works with sinusoidal voltages allowing the surface to be modulated by superimposing different smaller excitations on the already existing table amplitude. The next and last concept uses electrostatic fields to change locally the friction on the table surface.

The analysis on fabric conveying in section (5.3.2) has shown that the friction of the table surface is an important parameter in the process. Increasing the friction by changing the table surface to rubber reduced the sliding velocity of most fabric panels severely even such that some fabrics stopped moving. If now the friction in one particular area of the table is gradually increased then the fabric will stick on that place when passing over it. Furthermore, if that higher friction area has the

exact outline as the fabric panel then the panel should stop sliding and orientate according to the predetermined shape in the table. A different friction coefficient can obviously be obtained by having different sliding surfaces though this is not very flexible. A far more adaptable system could use electrostatics for it has been shown in chapter 3 (section 3.5) that charges on fabric can enormously increase the friction. For example, a mosaic of electroadhesive cells as sketched in Figure 5.50 can easily be built into the surface of a vibrating table. The voltage, which will be much lower for instance than the 2 kV used for the electrostatic gripper [Monkman 89], is supplied individually to each cell and therefore allows the configuration of any friction shape or pattern on the table.

The above described passive orientating methods all have great potential in aligning fabric panels though a full reorientation of a panel as sometimes required in an assembly line with solid objects is believed to be extremely difficult with fabrics.

5.5 Summary

This chapter has shown that the vibration of unloaded fabric samples can be interpreted as a dynamic compression. Preliminary tests on a vibrating table, constructed from a loudspeaker, exhibited immediately that a contrast in friction coefficient was not the only involving factor. Two woven fabrics, more specifically P1 and W1, which are almost identical in friction, behaved totally differently when placed on the inclined vibrating table. W1 slides steadily over the table surface whereas P1 remains immobile. A look at the amplitude signals, captured with the laser when normally vibrating the fabric on a horizontal table, further confirmed the existence of a compressional mechanism. The upward movement of a sinusoidally excited table compresses W1 slightly inasmuch as the downward movement again releases the fabric. This manifests in a sinusoidal response of the fabric, distorted at both peaks. In addition, the fabric vibrates at a larger amplitude than it is excited with and is out of phase with the table. Fabrics P1 and C1, on the other hand, behave exactly as the table excitation, the fabrics vibrating in phase with the table and showing no signs of compression. Further, measuring the fabric's frequency response at three different places in the fabric did not reveal any position dependency or evidence of a standing wave. Yet, it needs saying that a single point measurement is not a very convenient method to investigate position dependency, better measuring techniques should look at the individual positions in the fabric simultaneously.

A second set of stationary vibration tests has investigated the amplitude dependence in the fabric centre. All fabrics, apart from C1 and P1, displayed a resonance characteristic with maximum gains varying from 1.1 to 1.8 in a frequency range from 60-90 Hz, and phase lags between 40-120° at maximum frequency. Comparing the different frequency responses for an increase in amplitude shows a shift of the resonance peak towards lower frequencies, which in terms of fabric stiffness signifies a 20-40% reduction for a near doubling of the excitation. This amplitude dependency of the vibration could be anticipated somewhat since the static compression in chapter 4 already indicated a non-linear behaviour. Although the dynamic compression force is minute even at the highest excitation, the static stiffness is for all fabrics 5 to 8 times smaller than the dynamic stiffness. These differences in stiffness have to be explained in terms of fibre slippage. For a similar force, larger displacements have been

measured for the static compression than for the vibrations, hence the outer fabric layer will be more compacted and consequently the static stiffness is found to be higher. Also previous reports on the dynamic compression of carpet and felt by Dunlop *et al.* [Dunlop 89, 90] showed a similar non-linear effect at the resonance frequency despite the loaded conditions of their experiments. Regarding the fabric damping, a non-uniform variation is found: for some fabrics such as KC11, KC1 and W1 the damping increased with amplitude, for KA11 it decreased whereas for W1b it remained constant. Although the real material damping is probably a combination of several mechanisms, hysteresis damping, which is common to materials subjected to low-stress cycling and present already in the static compression, seemed most appropriate to model the behaviour. Hence, both damping and stiffness have been combined in parallel to model the fabric vibration. The base excited Kelvin-Voigt model, which is in fact a linear approximation despite the non-linearities in stiffness and damping, gives on average a good first approximation to the experimental data. Yet, the phase shift seems overall to match the simulated results much better than the gain. Furthermore, no relationship could be found between the bending stiffness and the resonance frequency of the respective fabrics.

The second half of the chapter has looked into the conveying or transporting of fabric panels on a vibratory table. Obviously, one of the most important parameters is friction since all fabrics are conveyed by sliding over the table surface. Directionally, no great difference in sliding speed has been found; note that the friction does not vary much between the principal fabric directions. However, a much larger variation in sliding speed is noted when changing the surface of the vibratory table, for instance a rubber surface reduced sliding speeds by a factor of 10 compared to the aluminium surface. Despite the small discrepancies in friction for an identical surface, large differences in sliding speed have been measured for the various fabrics. These differences in conveying speed might be attributed to variations in fabric damping where all the vibration energy can be absorbed in highly damped fabric instead of being used for conveying. However, no clear relationship was found between the sliding speed and the equivalent lateral damping or the bending stiffness. Furthermore, unintentionally, it has been shown as for solids that an out of phase vibration is most efficient in conveying fabrics. Peak sliding velocities were noticed throughout all the experiments at frequencies of 60-65 Hz and 90 Hz caused by some imperfections of the table (loudspeaker) in its tilted positions. Other increases in the sliding velocity have been obtained by simply tilting the table at a larger angle or increasing the excitation amplitude. However, when comparing the sliding velocities with some theoretical results, the table inclination seems to be the most effective and economical method. Finally, this chapter has been concluded with some conceptual ideas on orientating and aligning fabric panels. Two main approaches are proposed; one technique is based on fences, a second is based on surface variations. However, apart from a simple alignment device used in a previous project at The University of Hull, none of these ideas have been implemented or tested on fabrics yet and therefore represent part of the future work. The next and last chapter concludes this thesis and summarises the many suggestions for further research.

6 Conclusion and Future Work

This thesis has investigated two of the four essential fabric properties fundamental for the garment automation: friction and compression. Yet, both properties have been approached from a slightly different angle to the literature. The frictional effects have been studied between fabrics and non-fibrous materials and this at minute normal forces whereas the compression characteristics were analysed only up to one fifth of the pressure used in the standard KES-F tests. Furthermore, the out of plane vibration of fabric panels has been examined, again in unloaded conditions. This fabric manipulation offers a whole range of new opportunities to orientate and align fabric panels, vital to textile automation.

6.1 Low Force Friction Characteristics

Previous work on friction has been concentrated on fabric-fabric or fabric-non-fabric friction but at medium to large loads; this thesis has looked into fabric-non-fabric friction at zero or slightly loaded conditions. Considering that friction is a surface property, the condition of each sliding surface has proven to be crucial. In general, the smoother the fabric surface the larger the friction will be or looking at it directionally, most fabrics have a larger friction in the warp direction since the yarn density is normally higher in that direction. If we, on the other hand, compare woven and knitted materials then it is noted that, on average, the knitted structures give higher friction coefficients. Yet, an even greater effect has been found when the type of sliding surface is changed. For all fabrics, the friction coefficients against aluminium are the lowest, against rubber the highest and intermediate for Formica. The reason for this is thought to be a contrast in shear strength between the various sliding materials, although more work is required on the subject. A classification of friction, ranked according to the raw material, has not been given in this thesis since the weave or knit will alter the friction considerably.

More evidence on the importance of the surface conditions is found when sliding the fabric successively over the surface. Tests have shown a 3-15% increase in friction, which is restored back to normality after a relaxation period of 24 hours. These variations in friction do not seem to show any hysteresis though this is definitely not the case when the environmental conditions change. It is a well-known fact that many fabrics are hygroscopic and therefore absorb moisture, which partly enhances the comfort of wearing but also changes the properties of the material. The regain of the fabric increases significantly and at the same time alters the surface and the structure of the fabric. Hence, it is postulated that the smoother surface caused by the swelling of the fibres consequently increase the friction substantially from a relative humidity of 60% onwards. In case of the man-made fabrics, the increase in friction might be explained more in terms of a lubrication effect caused by water clinging to the fibres. Drying the fabrics, however, brings the friction back down but to a higher value than started with originally. The humidity influence on fabrics undoubtedly needs more attention and not only for friction but for all other fabric properties too. A study, which disentangles the humidity influences on the materials as well as on the structures, would benefit both the garment

automation and the textile design world. One of the few advantages of higher humidities is that static charges cannot develop. Although electrostatic forces are small, they can have a significant effect on automated equipment when fabrics are unloaded (i.e., 2-7 times increase in friction coefficient for wool and man-made materials). Evidence collected to date suggests that, as a rule, fabrics, which are less susceptible to humidity changes, are found more sensitive to static charging.

On the other hand, loading fabrics modifies their frictional behaviour; the frictional force is not directly proportional to the normal force but asymptotically aims towards a constant value at higher pressure and is, in addition, dependent on the geometric area. In other words, the classical friction laws or Amontons' Laws as they are sometimes referred to, do not apply to fabric. As an alternative, Wilson's equations, which are already well established for describing the pressure relation in fabric-fabric friction, have been successfully applied for fabric-non-fabric friction. Yet, the model parameters are found here to cluster according to the non-fibrous sliding surface. Although experiments in this thesis did not indicate a direct link between the compressibility and the pressure dependency of friction, more studies should be made. It is speculated by Viallier [Viallier 92] and Ajayi [Ajayi 97b] that easily compressible fabrics will also be more sensitive to friction variations induced by a pressure increase.

Furthermore, great attention has been given to the influence of velocity on friction both at moderate and extremely low speeds. At moderate speeds, the friction-velocity pattern has shown a striking resemblance to that of journal bearings where the friction reaches a minimum value around 0.5-2.0 mm/s then rises slowly to a more steady value at higher velocities. Although the fabrics are not lubricated as such, it is found that an adapted empirical tribology law describes the curves effectively. When sliding the fabric panels at extremely low speed however, the friction not only increases in value but also becomes discontinuous in that an alternating pattern of sticking and slipping is observed. The introduction of a novel measuring technique, in which three IR-beams simultaneously shine through the fabric, further revealed a non-uniform movement in some fabrics. The movement, which has been described as that of a caterpillar, stretches or shears first the fabric until the internal tension reaches the static friction at which point the fabric then suddenly slips forward. For the fabrics, surfaces and velocities used, it is observed that the slip movement emerges in a time span of 18 ms though because of signal noise it was impossible to detect any delay in between the three successive signals. A future development with small angle lasers and a motorised pulling mechanism could definitely improve this experiment. Further, a classic friction model where a fabric strip is presented as a lumped mass connected with springs and dampers has been applied to this problem. Crucial model parameters such as the damping and the spring constant have been measured directly on the fabric through a longitudinal vibration test, though stick-slip simulations showed a better agreement with the experiments when using static stiffness. Obviously, the model simplifies the reality in that the friction has been regarded as velocity independent. A bristle model, in which bonds between the surface and the fabric are continuously formed and broken would introduce some randomness in the process and would probably be a good substitute for further analysis.

6.2 Low Force Compression Characteristics

Low force static compression on woven and knitted materials has been approximated with van Wyk's equations. The experimental results, which have been obtained with an in-house built thickness tester, are very repeatable and virtually indistinguishable from the calculated traces when using the full three-parameter approach. However, this model requires, apart from the nebulous K -constant, also the volume of the incompressible inner core of the fabric, which on average accounts for 30-60% of the total fabric thickness but which cannot be measured directly. Fortunately, an estimate of this volume for each fabric could be extracted from the two-parameter model, which, by definition, cannot model low force compression since it excludes the volume at zero pressures and therefore diverges to infinity. Yet, the simplicity of the van Wyk equation makes it still more successful compared to the complex energy models, despite the vague definition of the K -constant. More research on compression should hopefully give a better understanding of this constant and investigate how it is related to the different fabric structures in particular. Further analysis of the compression results here has proven that for low pressures only the surface hairs of the fabric deform. At the same time, these protruding surface hairs are responsible for underestimating non-contacting thickness measurements with the laser sensor.

In addition to the static compressions, a novel technique has been introduced to measure impact compression. The method is based on a pendulum successively impacting the fabric and thereby gradually reducing the number of swings, which is inversely proportional to the compressional resistance of the fabric. On average, a smaller compressional energy is required to impact the fabrics to the same thickness as in the static compression. Although the fundamental mechanisms of static and impact compression are different, the fabrics could be 30% more compressed on impact with the same force as for a static compression. This is however not purely a fabric property since a suddenly applied load on a spring produces a deflection twice as great as when obtained with a similar static load. Further work on impact compression should include a force sensor in the rig, which would allow modelling of the fabric impact in analogy with work that has been carried out on a surrogate human pelvis [Robinovitch 97].

6.3 Vibration Characteristics

A further investigation of the dynamic compression characteristics has been obtained by vibrating unloaded fabrics out of plane. Previous work on carpet and felt compression has been carried out by Dunlop *et al.* [Dunlop 89, 90] but again under loaded conditions. A sinusoidal excitation normal to the fabric was shown to compress and decompress some fabrics respectively during the upward and downward movement of the table. This has manifested in sinusoidal fabric responses, which apart from being distorted at both peaks, are amplified and out of phase with the table excitation. On the other hand, fabrics, which had already proved statically hard to compress, vibrate in a similar way to the table and are difficult to convey.

A non-linear characteristic, common to most fabric properties, also appears in fabric vibrations. Two types of non-linearity have been studied, position dependency and amplitude dependency.

However, position dependency of the vibration could not be indicated in the fabric panels since only a single point measurement-technique is used. Future work should investigate fabric vibrations with a multi-point measuring technique or interferometry, which will capture the full fabric dynamics at once. This could reveal a possible existence of a 2D standing wave, which would then clarify the in-plane 'stiffening effect' of vibrating fabric. On the other hand, a doubling in excitation amplitude reduces the out of plane stiffness locally by 20 to 40%, thereby shifting all resonant peaks, situated between 60-90 Hz, to a lower frequency. Despite, the minute dynamic compression on the unloaded samples, the static stiffness is for all fabrics 5 to 8 times smaller than the dynamic stiffness. This discrepancy has been explained in terms of fibre slippage where for a static compression the outer surface layer can be more compacted. With regard to the damping, however, a non-uniform variation is found between the different fabrics. Although the exact damping mechanism in fabrics is likely to be a combination of several mechanisms, a hysteretic damping has been proposed by the author as part of a base excited linear Kelvin-Voigt model. A good first approximation with the experimental results is obtained although, the phase shifts, which experimentally vary between -40 to -120° at maximum frequency, seem to agree better than the gains. A further improvement on the modelling will have to concentrate on either implementing extra parameters or switching to Finite Element Methods, as classical mechanics become too complex when looking at 2D vibration.

Finally, as an application for garment automation, vibratory conveying of fabric panels has been investigated. By tilting a linear table perpendicular to the direction of vibration, a panel placed at the top of the table will steadily slide down the table. However, as for solid object conveying, the friction between the fabric and the table has proven to be a fundamental factor in improving the sliding velocity, the smaller the friction the faster the conveying. Tests with a rubber coated surface, for instance, slow-down the feeding rate by a factor of ten, which is far more than the individual friction difference. Yet, despite the small diversifications in friction between the different fabrics against the same surface, large variations in sliding speed have been registered. These differences might be ascribed to the damping of the fabric though no such a relationship could be indicated. Two obvious ways to increase the sliding are to increase the excitation amplitude of the table or to tilt the table at a larger angle. The latter has proven to be more effective and energy efficient. Furthermore, it has been shown as for solids that out of phase vibration is probably the most efficient way of all to convey fabrics. A small horizontal vibration added to the main vertical movement gives the table an elliptical motion, which provides the fabric with a little forward throw, and so enormously enhances the sliding speed. This thesis investigated only the transporting mechanism and the factors directly influencing this. It should be noted that while the fabrics are sliding down the table, the panels could be orientated or aligned. Two main approaches for planar orientation have been proposed. One technique following that of Little [Little 65] and Taylor [Taylor 92] is based on solid fences or barriers, which guide the fabrics towards the right position. Another set of solutions is proposed on variations in the sliding surface, which create a path for the fabric to follow. However, the main challenge in fabric orientation is due to low in-plane stiffness, preventing the fabric from buckling and folding when contacting the aligning tools. Several conceptual ideas have been presented in the previous chapter to overcome this problem though all need further development and research.

References

- [Abernathy 86] Abernathy, F. H., and Pippins, D., "(TC)²: Apparel, Textile and Education at its Best", *Bobbin Magazine*, Vol. 27, pp. 162-168, September 1986.
- [Ahrens 83] Ahrens, H., "Grundlagenuntersuchungen zur Werkstückzuführung mit Vibrationswendelförderern und Kriterien zur Geräteauslegung, (Fundamental Investigation into Parts Feeding with Bowl Feeders and Criteria for Equipment Design)", Düsseldorf Fortschr.-Ber., VDI-Z, Series 13, No. 23, VDI-Verlag, 1983 (in German).
- [Aisaka 87] Aisaka, N., "Technical Development in Apparel Industry", *JTN*, pp. 47-51, May 1987.
- [Ajayi 88] Ajayi, J. O., "Some Studies of Frictional Properties of Fabrics", Doctoral thesis, University of Strathclyde, Glasgow, 1988.
- [Ajayi 92a] Ajayi, J. O., "Fabric Smoothness, Friction, and Handle", *Textile Research Journal*, Vol. 62, No. 1, pp. 52-59, 1992.
- [Ajayi 92b] Ajayi, J. O., "Effects of Fabric Structure on Frictional Properties", *Textile Research Journal*, Vol. 62, No. 2, pp. 87-93, 1992.
- [Ajayi 94] Ajayi, J. O., and Elder, H. M., "Comparative Studies of Yarn and Fabric Friction", *Journal of Testing and Evaluation*, Vol. 22, No. 5, pp. 463-467, 1994.
- [Ajayi 95a] Ajayi, J. O., Elder, H. M., Kolawole, E. G., Bello, K. A., and Darma, M. U., "Resolution of the Stick-slip Friction Traces of Fabrics", *Journal of the Textile Institute*, Vol. 86, No. 4, pp. 600-609, 1995.
- [Ajayi 95b] Ajayi, J. O., and Elder, H. M., "Effects of Finishing Treatments on Fabric Friction", *Journal of Testing and Evaluation*, Vol. 23, No. 1, pp. 55-58, 1995.
- [Ajayi 97a] Ajayi, J. O., and Elder, H. M., "Effects of Surface Geometry on Fabric Friction", *Journal of Testing and Evaluation*, Vol. 25, No. 2, pp. 182-188, 1997.
- [Ajayi 97b] Ajayi, J. O., and Elder, H. M., "Fabric Friction, Handle, and Compression", *Journal of the Textile Institute*, Vol. 88, Part 1, No. 3, pp. 232-241, 1997.
- [Alptekin 68] Alptekin, A. T., "On Dynamic Mechanical Properties of Fiber Assemblies", Doctoral thesis, North Carolina State University, Raleigh NC, USA, 1968.

- [Amirbayat 92] Amirbayat, J., "Seams of Different Ply Properties: 1 Seam Appearance", *Journal of the Textile Institute*, Vol. 83, No. 2, pp. 209-217, 1992.
- [Amirbayat 95] Amirbayat, J., Alagha, M. J., and Porat, I., "Factors Affected by Machine Settings and Fabric Properties in Knitwear Production: 1 Seam Shrinkage and Thread Consumption", *Journal of the Textile Institute*, Vol. 86, No. 1, pp. 110-118, 1995.
- [Amontons 1699] Amontons, G., "On the Resistance Originating in Machines," *Proceedings of the French Royal Academy of Sciences*, pp. 206-220, 1699.
- [Aono 90] Aono, M., "A Wrinkle Propagation Model for Cloth", *Proceedings of the International Conference on Computer Graphics*, Tokyo, Japan, Springer Verlag, pp. 95-115, 1990.
- [Ashton 94] Ashton, S., "Knitting in the Third Dimension", *Knitting International*, Vol. 1211, pp. 56-58, December 1994.
- [B & K 96] *Triaxial Deltatron® 4504, Data sheet*, Bruël & Kjær, Nærum, Denmark, 1996.
- [B.K. Electronics 93] *MOSFET Power Amplifier Modules*, B. K. Electronics, Southend-on-Sea, Essex, UK, 1993.
- [Baird 63] Baird, K., "Dimensional Stability of Woven Wool Fabrics: Hygral Expansion", *Textile Research Journal*, Vol. 33, No. 12, pp. 973-984, 1963.
- [Ballou 44] Ballou, J. W., and Silverman, S., "Young's Modulus of Elasticity of Fibers and Films by Sound Velocity Measurements", *Journal of the Acoustical Society of America*, Vol. 16, No. 2, pp. 113-119, 1944.
- [Ballou 49] Ballou, J. W., and Smith, J. C., "Dynamic Measurements of Polymer Physical Properties", *Journal of Applied Physics*, Vol. 20, pp. 493-502, 1949.
- [Bandstra 83] Bandstra, J. P., "Comparison of Equivalent Viscous Damping and Nonlinear Damping in Discrete and Continuous Vibrating Systems", *Transactions of the ASME, Journal of Vibration, Acoustics, Stress, and Reliability in Design*, Vol. 105, No. 3, pp. 382-392, 1983.
- [Bandyopadhyay 51] Bandyopadhyay, S. B., "Frictional Properties of Jute and Some Other Long Vegetable Fibers. Part I: General Study of Characters", *Textile Research Journal*, Vol. 21, No. 9, pp. 659-670, 1951.
- [Barndt 90] Barndt, H., Fortess, F., Wiener, M., and Furniss, J. C., "The use of KES and FAST Instruments in Predicting Processability of Fabrics in Sewing", *Proceedings of the 1st International Clothing Conference "Textile Objective Measurement and Automation in Garment Manufacture"*, Bradford (UK),

- 9-11 July 1990, ed. Stylios, G., Ellis Horwood, Chichester, pp. 107-117, 1991.
- [Barrett 96a] Barrett, G. R., Clapp, T. G., and Titus, K. J., "An On-line Fabric Classification Technique Using a Wavelet-Based Neural Network Approach", *Textile Research Journal*, Vol. 66, No. 8, pp. 521-528, 1996.
- [Barrett 96b] Barrett, G. R., Farrington, C. E., and Clapp, T. G., "An XY-Theta Manipulator for Flexible Fabric Part Positioning", *International Journal of Clothing Science and Technology*, Vol. 8, No. 1/2, pp. 33-43, 1996.
- [Berkstresser III 86] Berkstresser III, G. A., and Buchanan, D. R., *Automation and Robotics in the Textile and Apparel Industries*, Noyes Publications, New Jersey, USA, 1986.
- [Berkstresser III 95] Berkstresser III, G. A., Buchanan, D. R., and Grady, P. L., *Automation in the Textile Industry, From Fibers to Apparel*, The Textile Institute, 1995.
- [Bernardon 85] Bernardon, E., and Kondoleon, T. S., "Real Time Robotic Control for Apparel Manufacturing", *Proceeding of the 9th Robots Conference*, Detroit, MI, USA, Vol. 1, pp. 4-46-4-66, 2-6 January 1985.
- [Bert 73] Bert, C. W., "Material Damping: An Introductory Review of Mathematical Models, Measures and Experimental Techniques", *Journal of Sound and Vibration*, Vol. 29, No. 2, pp. 129-153, 1973.
- [Bishop 96] Bishop, D. P., "Fabrics: Sensory and Mechanical Properties", *Textile Progress*, Vol. 26, No. 3, 1996.
- [Bogaty 53] Bogaty, H., Hollies, N. R. S., Hintermaier, J. C., and Harris, M., "The Nature of a Fabric Surface: Thickness-Pressure Relationships", *Textile Research Journal*, Vol. 23, No. 2, pp. 108-114, 1953.
- [Booth 63] Booth, J. H., and McCallion, H., "On Predicting the Mean Conveying Velocity of a Vibratory Conveyor", *Proceedings of the Institution of Mechanical Engineers*, Vol. 178, Pt. 1, No. 20, pp. 521-538, 1963-64.
- [Böttcher 58] Böttcher, S., "Beitrag zur Klärung der Gutbewegung auf Schwingrinnen Teil II: Mathematische Behandlung der Gutbewegung", *Fördern und Heben*, Vol. 4, pp. 235-240, 1958 (in German).
- [Bowden 39] Bowden, F. P., and Leben, L., "The Nature of Sliding and the Analysis of Friction", *Proceedings of the Royal Society*, Vol. A169, pp. 371-391, 1939.
- [Bowden 50] Bowden, F. P., and Tabor, D., "Mechanisms of Metallic Friction", in *The Friction and Lubrication of Solids*, Oxford Clarendon Press, London, pp. 90-121, 1950.

- [Bowden 64] Bowden, F. P., and Tabor, D., "The Friction and Deformation of Polymeric Materials", in *The friction and Lubrication of Solids Part II*, Oxford Clarendon Press, London, pp. 214-241, 1964.
- [Bray 86] Bray, F., and Vento, V., "(TC)² and Beyond: Chapter Two Begins with Singer", *Bobbin Magazine*, Vol. 27, pp. 170-174, September 1986.
- [Brickman 63] Brickman, A. D., "The Vibratory Transport of Bulk Materials", Doctoral thesis, University of Michigan, Mechanical Engineering Department, Ann Arbor, MI, USA, 1963.
- [Briscoe 79] Briscoe, B. J., and Tabor, D., "Friction and Wear of Polymers", *Polymeric Surfaces*, ed., Clark, D. T. and Feast, W. J., John Wiley & Sons, pp. 1-23, 1979.
- [BRITE-EURAM 91] BRITE-EURAM Programme, Synopsis of Current Projects 1990-91, Commission of the European Communities, 1991.
- [Brokowski 93] Brokowski, M., Peshkin, M., and Goldberg, K., "Curved Fences for Part Alignment", *IEEE International Conference on Robotics and Automation*, Atlanta, GA, pp. 467-473, 2-6 May 1993.
- [Buckle 48] Buckle, H., and Pollitt, J., "An Instrument for Measuring the Coefficient of Friction of Yarns against other Materials," *Journal of the Textile Institute*, Vol. 39, No. 6, pp. T199-T210, 1948.
- [Carignan 92] Carignan, M., Yang, Y., Magnenat-Thalmann, N., and Thalmann, D., "Dressing Animated Synthetic Actors with Complex Deformable Clothes", *Proceeding of SIGGRAPH, Computer Graphics*, Vol. 26, No. 2, pp. 99-104, 1992.
- [Carnaby 89] Carnaby, G. A., and Pan, N., "Theory of the Compression Hysteresis of Fibrous Assemblies", *Journal of the Textile Institute*, Vol. 59, No. 5, pp. 275-284, 1989.
- [Carr 88] Carr, W. W., Posey, J. E., and Tincher, W. C., "Frictional Characteristics of Apparel Fabrics", *Textile Research Journal*, Vol. 58, No. 3, pp. 129-136, 1988.
- [Catling 60] Catling, H., "Stick-Slip Friction as a Cause of Torsional Vibration in Textile Drafting Rollers", *Proceedings of the Institution of Mechanical Engineers*, Vol. 174, No. 17, pp. 575-586, 1960.
- [Centronic 95] *High Performance Silicon Photo Detectors, European Edition 2*, Centronic, Inc., Newbury Park, CA, USA, 1995.

- [Chaikin 55] Chaikin, M., and Chamberlain, N. H., "The Propagation of Longitudinal Stress Pulses in Textile Fibers", *Journal of the Textile Institute*, Vol. 46, No. 1, pp. T25-T62, 1955.
- [Chapman 55] Chapman, J. A., Pascoe, M. W., and Tabor, D., "The Friction and Wear of Fibres", *Journal of the Textile Institute*, Vol. 46, No. 1, pp. P3-P22, 1955.
- [Chatfield 70] Chatfield, C., *Statistics for Technology*, Penguin Education, Studies in Applied Statistics, 1970.
- [Chuter 88] Chuter, A. J., "Introduction to Clothing Production Management", BPS Professional Books, Oxford, 1988.
- [Clapp 89] Clapp, T. G., Timble, N., and Gupta, B. S., "Factors Affecting Interfacial Forces between Fabric Plies – A Survey", *Proceeding of the AAMA, 1989 Research Conference*, Atlanta, GA, October 31-November 1, Published by American Apparel Manufacturers Association, Washington DC, 1989.
- [Clapp 91] Clapp, T. G., Timble, N. B., and Gupta, B. S. "The Frictional Behavior of Textile Fabrics", *Journal of Applied Polymer Science: Applied Polymer Symposium 47*, pp. 373-382, 1991.
- [Clapp 92] Clapp, T. G., Little, T. J., Thiel, T. M., and Vass, D. J. "Sewing Dynamics: Objective Measurement of Fabric/Machine Interaction", *International Journal of Clothing Science and Technology*, Vol. 4, No. 2/3, pp. 45-53, 1992.
- [Clayton 29] Clayton, F. H., and Peirce, F. T., "The Influence of Humidity on the Elastic Properties of Cotton, IV The Rigidity of Soda-boiled Cotton, and Effects thereon of History and Temperature", *Journal of the Textile Institute*, Vol. 20, pp. T315-T332, 1929.
- [Clayton 92] Clayton, J. P., and Tinker, M. L., "Characterization of Advanced Flexible Thermal Protection Material for Space Applications", *Journal of Spacecraft and Rockets*, Vol. 29, No. 5, pp. 718-726, 1992.
- [Colgate 89] Colgate, A. I., "Sewing Production Strategies – Short & Quick: The Trick", *Bobbin*, Vol. 30, pp. 64-70, April 1989.
- [Cookson 91] Cookson, P. G., De Boos, A.G., Rocznik, A. F., and Ly, N. G., "Measuring Hygral Expansion in Woven Wool Fabrics", *Textile Research Journal*, Vol. 61, No. 6, pp. 319-327, 1991.
- [Cookson 93] Cookson, P. G., and Slota, I. J., "Hysteresis Effects Associated with the Adsorption and Desorption of Water by Woven Wool Fabrics", *Textile Research Journal*, Vol. 63, No. 9, pp. 495-503, 1993.

- [Coulomb 1785] Coulomb, C. A., "Théorie de machines simples, en ayant égard au frottement de leurs parties, et a la roideur des cordages", *Mémoires Mathématique Physique*, Paris, Vol. X, pp. 161-342, 1785.
- [Crandall 70] Crandall, S. H., "The Role of Damping in Vibration Theory", *Journal of Sound and Vibration*, Vol. 11, No. 1, pp. 3-18, 1970.
- [Crank 49] Crank, J., and Henry, M. E., "A Comparison of the Rates of Conditioning by Different Methods", *The Proceedings of the Physical Society of London*, Vol. B62, pp. 257-269, 1949.
- [Czarnecki 95] Czarnecki, C. A., "Integrating the Cutting and Sewing Room of Garment Manufacture Using Mechatronic Techniques", *Mechatronics*, Vol. 5, No. 2/3, pp. 295-308, 1995.
- [da Vinci 1519] da Vinci, L., *The Notebooks*, translated into English by Edward MacCurdy, Jonathan Cape, London, 1938.
- [Dahl 84] Dahl, S. R., and Rice, R. B., "A Derivation of Equivalent Linear Viscous and Elastic Constants for Viscoelastic Materials", Air Force Wright Aeronautical Labs., AFWAL-TR-84-3064, *Proceedings of the Vibration Damping Workshop*, Long Beach, CA, pp. O-1-O-9, 1984.
- [De Boos 90] De Boos, A. G., and Tester, D. H., "The FAST Approach to Improved Fabric Performance", *Proceedings of the 1st International Clothing Conference "Textile Objective Measurement and Automation in Garment Manufacture"*, Bradford (UK), 9-11 July 1990, ed. Stylios, G., Ellis Horwood, Chichester, pp. 55-66, 1991.
- [de Jong 86] de Jong, S., Snaith, J. W., and Michie, N. A., "A Mechanical Model for the Lateral Compression of Woven Fabrics", *Textile Research Journal*, Vol. 56, No. 12, pp. 759-767, 1986.
- [DeLuca 92] DeLuca, L. B., and Thibodeaux, D. P., "The Relative Importance of Fiber Friction and Torsional and Bending Rigidities in Cotton Sliver, Roving, and Yarn", *Textile Research Journal*, Vol. 62, No. 4, pp. 192-196, 1992.
- [Derjaguin 57] Derjaguin, B. V., Push, V. E., and Tolstoi, D. M., "A Theory of Stick-Slip Sliding of Solids", *Proceedings of the Conference on Lubrication and Wear*, London, Institution of Mechanical Engineers, pp. 257-268, 1957.
- [Dreby 43] Dreby, E. C., "A Friction Meter for Determining the Coefficient of Kinetic Friction of Fabrics", *Journal of Research of the National Bureau of Standards*, Vol. 31, pp. 237-246, 1943.

- [Dunell 51] Dunell, B. A., and Dillon, J. H., "The Measurement of Dynamic Modulus and Energy Losses in Single Textile Filaments Subjected to Forced Longitudinal Vibrations", *Textile Research Journal*, Vol. 21, No. 6, pp. 393-403, 1951.
- [Dunlop 74] Dunlop, J. I., "Characterizing the Compression Properties of Fibre Masses", *Journal of the Textile Institute*, Vol. 65, pp. 532-536, 1974.
- [Dunlop 79] Dunlop, J. I., "Acoustic Emission from Wool during Compression", *Journal of the Textile Institute*, Vol. 70, No. 8, pp. 364-366, 1979.
- [Dunlop 81] Dunlop, J. I., "The Dynamic Bulk Modulus of Fibre Masses", *Journal of the Textile Institute*, Vol. 72, No. 4, pp. 154-161, 1981.
- [Dunlop 83] Dunlop, J. I., "On the Compression Characteristics of Fibre Masses", *Journal of the Textile Institute*, Vol. 74, No. 2, pp. 92-97, 1983.
- [Dunlop 89] Dunlop, J. I., and Sun, J., "The Dynamic Mechanical Response of Carpets", *Journal of the Textile Institute*, Vol. 80, No. 4, pp. 569-578, 1989.
- [Dunlop 90] Dunlop, J. I., "Nonlinear Vibration Properties of Felt Pads", *Journal of the Acoustical Society of America*, Vol. 88, No. 2, pp. 911-917, 1990.
- [Dunlop 91] Dunlop, J. I., and Sun, J., "The Dynamic Mechanical Response of Carpets: An Alternative Measurement Technique", *Journal of the Textile Institute*, Vol. 82, No. 3, pp. 353-359, 1991.
- [Dunlop 92] Dunlop, J. I., "Felt Pad Vibration Properties and Design Criteria", *Journal of the Acoustical Society of America*, Vol. 91, No. 5, pp. 2696-2702, 1992.
- [Dupuis 95] Dupuis, D., Popov, G., and Viallier, P., "Compression of Greystate Fabrics as a Function of Yarn Structure", *Textile Research Journal*, Vol. 65, No. 6, pp. 309-316, 1995.
- [El Mogahzy 93a] El Mogahzy, Y. E., and Gupta, B. S., "Friction in Fibrous Materials, Part II: Experimental Study of the Effects of Structural and Morphological Factors", *Textile Research Journal*, Vol. 63, No. 4, pp. 219-230, 1993.
- [El Mogahzy 93b] El Mogahzy, Y. E., and Broughton, R. M., "A New Approach for Evaluating the Frictional Behavior of Cotton Fibers, Part I: Fundamental Aspects and Measuring Techniques", *Textile Research Journal*, Vol. 63, No. 8, pp. 465-475, 1993.
- [Elder 84] Elder, H. M., Fisher, S., Armstrong, K., and Hutchison, G., "Fabric Softness, Handle, and Compression", *Journal of the Textile Institute*, Vol. 75, No. 1, pp. 37-46, 1984.

- [Ernst 40] Ernst, H., and Merchant, M. E., "Conference on Friction and Surface Finish", *MIT 76*, 1940.
- [Forza 97] Forza, C., and Vinelli, A., "Quick Response in the Textile-Apparel Industry and the Support of Information Technologies", *Integrated Manufacturing Systems*, Vol. 8, No. 3, pp. 125-136, 1997.
- [Gaberson 67] Gaberson, H. A., "Material Transport on Oscillating Conveyors", Doctoral thesis, Massachusetts Institute of Technology, Massachusetts, USA, 1967.
- [Gaberson 72] Gaberson, H. A., "Particle Motion on Oscillating Conveyors. Part 1: The Equations of Motion and the Rules for Predicting Motion Form Transitions", *Transactions of the ASME, Journal of Engineering for Industry*, pp. 50-56, February 1972.
- [Gibson 90] Gibson, I., Taylor, P. M., and Wilkinson, A. J., "Robotics Applied to the Top Taping of Men's Y-front Briefs", *Proceedings of the 1st International Clothing Conference "Textile Objective Measurement and Automation in Garment Manufacture"*, Bradford (UK), 9-11 July 1990, ed. Stylios, G., Ellis Horwood, Chichester, pp. 191-201, 1991.
- [Gonsalves 47] Gonsalves, V. E., "Determination of Denier and Strength of Single Filaments by Vibroscope and Heim Tensile Tester", *Textile Research Journal*, Vol. 17, No. 7, pp. 369-375, 1947.
- [Gonsalves 53] Gonsalves, V. E., "Some Fundamental Questions Concerning the Static Electrification of Textile Yarns: Part I", *Textile Research Journal*, Vol. 23, No. 10, pp. 711-718, 1953.
- [Govindaraj 92] Govindaraj, M., Chen, B., and Koechling, J., "Fabric Properties as Control Factors for Flexible Apparel Production Systems", *International Journal of Clothing Science and Technology*, Vol. 4, No. 2/3, pp. 34-38, 1992.
- [Gunner 92] Gunner, M. B., "Automated 2D Fabric Handling", Doctoral thesis, University of Hull, October 1992.
- [Gupta 91] Gupta, B. S., and El Mogahzy, Y. E., "Friction in Fibrous Materials, Part I: Structural Model", *Textile Research Journal*, Vol. 61, No. 9, pp. 547-555, 1991.
- [Guthrie 65] Guthrie, Jr., J. J., and Morris, J. M., "Electromechanical Feeding and Proportioning of Bulk Solids", *ASME-IEEE Materials Handling Conference*, Pittsburgh, PA, 18-20 October 1965.
- [GWI 85] *Series 2004 Gaptex, General Information*, Graham & White Instruments Ltd., St. Albans, Hertfordshire, UK, 1985.

- [Haessig 90] Haessig, D. A. Jr, and Friedland, B., "On the Modeling and Simulation of Friction", *Proceedings of the 1990 American Control Conference*, San Diego, USA, pp. 1256-1261, 1990.
- [Hall 87] Hall, M. K., Blackwood, B., and Loweth, B., "Methods For Auto-Separation of Fabric Plies from a Cut Stack", *Knitting International*, Vol. 94, No. 1123, pp. 162-166, 1987.
- [Hansen 57] Hansen, W. W., and Tabor, D., "Hydrodynamic Factors in the Friction of Fibers and Yarns", *Textile Research Journal*, Vol. 27, pp. 300-306, 1957.
- [Harris 96] Harris, C. M., *Shock and Vibration Handbook*, 4th edition, McGraw-Hill, 1996.
- [Hearle 61] Hearle, J. W. S., and Turner, D. J., "A Preliminary Study of a Technique for Measuring Flexural Vibrations in Fabrics", *Textile Research Journal*, Vol. 31, pp. 981-986, 1961.
- [Hearle 71] Hearle, J. W. S., and Husain, A. K. M. M., "Studies in Needled Fabrics. Part VIII: The Effect of Friction on the Processing and Properties of Needle-Bonded Fabrics", *Journal of the Textile Institute*, Vol. 62, No. 2, pp. 83-107, 1971.
- [Henning 34] Henning, H. J., "Über die Messung der Bauschelastizität von Textilien", *Melliand Textilber*, Vol. 15, No. 12, pp. 537-540, 1934 (in German).
- [Henry 53a] Henry, P. S. H., "Survey of Generation and Dissipation of Static Electricity", *British Journal of Applied Physics*, Vol. 4, supp. No. 2, pp. S6-S11, 1953.
- [Henry 53b] Henry, P. S. H., "The Role of Asymmetric Rubbing in the Generation of Static Electricity", *British Journal of Applied Physics*, Vol. 4, supp. No. 2, pp. S31-S36, 1953.
- [Henry 53c] Henry, P. S. H., "Electrostatic Eliminators in the Textile Industry", *British Journal of Applied Physics*, Vol. 4, supp. No. 2, pp. S78-S83, 1953.
- [Hersh 55] Hersh, S. P., and Montgomery, D. J., "Static Electrification of Filaments, Experimental Techniques and Results", *Textile Research Journal*, Vol. 25, No. 4, pp. 279-295, 1955.
- [Hertz 1881] Hertz, H., "On the Contact of Elastic Solids", *Journal fur die Reine und Angewandte Mathematik*, Vol. 92, pp. 156-171, 1881.
- [Hillier 49] Hillier, K. W., "A Method of Measuring some Dynamic Elastic Constants and its Application to the Study of High Polymers", *Proceedings of the Physical Society of London*, Vol. B62, pp. 701-713, 1949.

- [Hitakawa 88] Hitakawa, H., "Advanced Parts Orientation System has wide Application", *Assembly Automation*, Vol. 8, No. 3, pp. 147-150, 1988.
- [Hoffman 51] Hoffman, R. M., and Beste, L. F., "Some Relations of Fiber Properties to Fabric Hand", *Textile Research Journal*, Vol. 21, pp. 66-77, 1951.
- [Horino 71] Horino, T., Yabunaka, T., and Morikawa, M., "Study on Viscoelastic Behavior of Carpet. Part 1: Apparatus for Dynamic Measurement in Simple Compression and Complex Dynamic Modulus of Commercial Carpets", *Journal of the Textile Machinery Society of Japan*, Vol. 17, No. 1, pp. 26-32, 1971.
- [Hosseini Ravandi 94] Hosseini Ravandi, S. A., Toriumi, K., and Matsumoto, Y., "Spectral Analysis of the Stick-Slip Motion of Dynamic Friction in the Fabric Surface", *Textile Research Journal*, Vol. 64, No. 4, pp. 224-229, 1994.
- [Hosseini Ravandi 96] Hosseini Ravandi, S. A., and Toriumi, K., "Spectral Analysis of the Yarn-pullout Force from Plain-weave Fabric", *Journal of the Textile Institute*, Vol. 87, Part 1, No. 3, pp. 522-531, 1996.
- [Howell 53] Howell, H. G., and Mazur, J., "Amontons' Law and Fibre Friction", *Journal of the Textile Institute*, Vol. 44, pp. T59-T69, 1953.
- [Howell 59] Howell, H. G., Mieszkis, K. W., and Tabor, D., *Friction in Textiles*, Butterworths Scientific Publications, London, 1959.
- [Hu 97] Hu, J., and Newton, A., "Low-load Lateral-compression Behaviour of Woven Fabrics", *Journal of the Textile Institute*, Vol. 88, Part 1, No. 3, pp. 242-254, 1997.
- [Huffington 60] Huffington, J. D., and Stout, H. P., "The Friction of Fibre Assemblies", *Wear*, Vol. 3, No. 1, pp. 26-42, 1960.
- [Inoue 97] Inoue, M., and Masako, N., "Tensile and Tensile Stress Relaxation Properties of Wool/Cotton Plied Yarns", *Textile Research Journal*, Vol. 67, No. 5, pp. 378-385, 1997.
- [Iype 89] Iype, C., and Porat, I., "Fabric Alignment Using a Robotic Vision System", *International Journal of Clothing Science and Technology*, Vol. 1, No. 1, pp. 39-43, 1989.
- [Jeffries 89] Jeffries, R., "Functional Aspects of High Performance Clothing", *Textile Institute Annual World Conference, "Textile Fashioning the Future Materials, Methods and Markets"*, Nottingham, UK, pp. 119-133, 16-20 October 1989.

- [Jeng 96] Jeng, S. T., and Mo, J. J., "Ballistic Impact Response for Two-Step Braided Three-Dimensional Textile Composites", *AIAA Journal*, Vol. 34, No. 2, pp. 375-384, 1996.
- [Johnson 85] Johnson, R. H., "Stretch and Recovery Performance of Textured Polyester Woven Fabrics", Doctoral thesis, North Carolina State University, Raleigh NC, USA, 1985.
- [Kahaner 89] Kahaner, D., Moler, C. B., and Nash, S., *Numerical Methods and Software*, Prentice Hall, 1989.
- [Kalyanaraman 88a] Kalyanaraman, A. R., "Coefficient of Friction between Yarns and Contact Surfaces", *Indian Journal of Textile Research*, Vol. 13, pp. 1-6, March 1988.
- [Kalyanaraman 88b] Kalyanaraman, A. R., "Yarn-friction Studies with the SITRA Friction-measuring Device", *Journal of the Textile Institute*, Vol. 58, No. 1, pp. 147-151, 1988.
- [Karakerezis 94] Karakerezis, A., Rizzi, M., Ippolito, M., Doulgeri, Z., and Petridis, V., "Handling of Flat Non Rigid Materials with Consideration of Robotic Gripping Systems", *Proceedings of the 5th World Conference on Robotics Research*, Cambridge, MA, USA, 27-29 September 1994.
- [Karnopp 85] Karnopp, D., "Computer Simulation of Stick-Slip Friction in Mechanical Dynamic Systems", *Journal of Dynamic Systems, Measurement and Control*, Vol. 107, No. 1, pp. 100-103, 1985.
- [Kato 72] Kato, S., Sato, N., and Matsubayashi, T., "Some Considerations on Characteristics of Static Friction of Machine Tool Slideway", *Journal of Lubrication Technology*, Vol. 94, No. 3, pp. 234-247, 1972.
- [Kawabata 79] Kawabata, S., and Morooka, H., "Analysis of Frictional Properties of Fabrics", *Journal of Textile Machinery Society Japan*, Vol. 32, No. 5, pp. 57-63, 1979 (in Japanese).
- [Kawabata 80] Kawabata, S., *The Standardization and Analysis of Hand Evaluation*, 2nd ed., Textile Machinery Society of Japan, Osaka, 1980.
- [Kawabata 90] Kawabata, S., Niwa, M., Ito, K., and Nitta, M., "Recent Progress in the Application of Objective Measurement to Clothing Manufacture", *Proceedings of the 1st International Clothing Conference "Textile Objective Measurement and Automation in Garment Manufacture"*, Bradford (UK), 9-11 July 1990, ed. Stylios, G., Ellis Horwood, Chichester, pp. 81-104, 1991.
- [Kawabata 91] Kawabata, S., and Niwa, M., "Objective Measurement of Fabric Mechanical Property and Quality: its Application to Textile and Clothing

- Manufacturing”, *International Journal of Clothing Science and Technology*, Vol. 3, No. 1, pp. 7-18, 1991.
- [Kenins 94] Kenins, P., “Influence of Fiber Type and Moisture on Measured Fabric-to-Skin Friction”, *Textile Research Journal*, Vol. 64, No. 12, pp. 722-728, 1994.
- [Kimball 27] Kimball, A. L., and Lovell, D. E., “Internal Friction in Solids”, *Physical Review Series 2*, Vol. 30, pp. 948-959, 1927.
- [King 70] King, N. E., and Kruger, P. J., “Preliminary Results on the Elastic Moduli of Wool, Mohair, and Kemp Fibers by Ultrasonic Pulse Techniques”, *Textile Research Journal*, Vol. 40, No. 10, pp. 865-871, 1970.
- [King 95] King, J. M., Farrington, C. E., Clapp, T. G., and Barrett, G. R., “Auto-Hand Conveyance System for Apparel Assembly”, *Proceedings of the International Conference on Recent Advances in Mechatronics, ICRAM'95*, Istanbul, Turkey, pp. 476-480, 14-16 August 1995.
- [Komori 77] Komori, T., and Makishima, K., “Numbers of Fiber-to-Fiber Contacts in General Fiber Assemblies”, *Textile Research Journal*, Vol. 47, No. 1, pp. 13-17, 1977.
- [Komori 91] Komori, T., and Itoh, M., “A New Approach to the Theory of the Compression of Fiber Assemblies”, *Textile Research Journal*, Vol. 61, No. 7, pp. 420-428, 1991.
- [Kurt Salomon 88] Kurt Salmon Associates, “Quick Response Implementation”, Kurt Salomon Associates, NY, USA, 1988.
- [Larose 53] Larose, P., “Observations on the Compressibility of Pile Fabrics”, *Textile Research Journal*, Vol. 23, No. 10, pp. 730-735, 1953.
- [Lazan 68] Lazan, B. J., *Damping of Materials and Members in Structural Mechanics*, Oxford Pergamon Press, 1968.
- [Leaf 84] Leaf, G. A. V., *Practical Statistics for the Textile Industry: Part 1, Manual of the Textile Technology*, Textile Institute, Zellweger Uster Ltd., Switzerland, 1984.
- [Lee 85] Lee, D. H., and Lee, J. K., “Initial Compressional Behaviour of Fibre Assembly”, in *Objective Measurement: Applications to Product Design and Process Control*, ed., S. Kawabata, R. Postle, and M. Niwa, The Textile Machinery Society of Japan, Osaka, pp. 613-622, 1985.

- [Lee 92] Lee, D. H., and Carnaby, G. A., "Compressional Energy of the Random Fiber Assembly, Part I: Theory", *Textile Research Journal*, Vol. 62, No. 4, pp. 185-191, 1992.
- [Leech 77] Leech, C., and Mansell, J., "Some Aspects of Wave Propagation in Orthogonal Nets", *International Journal of Mechanical Science*, Vol. 19, pp. 93-102, 1977.
- [Leech 79] Leech, C. M., "The Modelling of Net and Cloth Dynamics", *Journal of the Franklin Institute*, Vol. 307, No. 6, pp. 361-378, 1979.
- [Lincoln 52] Lincoln, B., "Frictional and Elastic Properties of High Polymeric Materials", *British Journal of Applied Physics*, Vol. 3, pp. 260-263, 1952.
- [Lindberg 60] Lindberg, J., Waesterberg, L., and Svenson, R., "Wool Fabrics as Garment Construction Materials", *Journal of the Textile Institute*, Vol. 51, pp. T1475-T1493, 1960.
- [Lipson 72] Lipson, H., *Optical Transform*, Academic Press, New York, 1972.
- [Little 65] Arthur D. Little, "A Study of Automated Handling of Limp Fabrics", *The Apparel Research Foundation, Inc.*, 1965.
- [Lodge 54] Lodge, A. S., and Howell, H. G., "Friction of an Elastic Solid", *The Proceedings of the Physical Society of London*, Vol. B67, pp. 89-97, 1954.
- [Lowder 91] Lowder, R., "Balance: a Delicate Word in Modular Manufacturing", *Bobbin*, Vol. 33, pp. 132-138, November 1991.
- [Lowell 86a] Lowell, J., and Truscott, W. S., "Triboelectrification of Identical Insulators: I. An Experimental Investigation", *Journal of Physics D: Applied Physics*, Vol. 19, No. 7, pp. 1273-1280, 1986.
- [Lowell 86b] Lowell, J., and Truscott, W. S., "Triboelectrification of Identical Insulators: II. Theory and Further Experiments", *Journal of Physics D: Applied Physics*, Vol. 19, No. 7, pp. 1281-1298, 1986.
- [Ly 88] Ly, N. G., and Denby, E. F., "A CSIRO Inter-laboratory Trial of the KES-F for Measuring Fabric Properties", *Journal of the Textile Institute*, Vol. 79, No. 2, pp. 198-219, 1988.
- [Ly 89] Ly, N. G., "Error Analysis of Measurements Made with the KES-F System", *Textile Research Journal*, Vol. 59, No. 1, pp. 17-25, 1989.
- [Lyne 55] Lyne, D. G., "The Dynamic Friction between Cellulose Acetate Yarn and a Cylindrical Metal Surface", *Journal of the Textile Institute*, Vol. 46, pp. P112-P122, 1955.

- [Mahar 87] Mahar, T. J., Dhingra, R. C., and Postle, R., "Measuring and Interpreting Low-Stress Fabric Mechanical and Surface Properties. Part I: Precision of Measurement", *Textile Research Journal*, Vol. 57, No. 6, pp. 357-369, 1987.
- [Mani 85] Mani, M., and Wilson, W. R. D., "A Programmable Orienting System for Flat Parts", *Proceeding of the 13th North American Manufacturing Research Institute Conference*, Berkeley, CA, pp. 427-432, May 1985.
- [Mansell 78] Mansell, J., and Leech, C., "Propagation Fronts Arising from the Impulsive Excitation of Orthogonally Woven Cloth and Nets", *Journal of Applied Mechanics*, Vol. 45, pp. 957-959, 1978.
- [Mansour 75] Mansour, W., Massoud, M., Morcos, W., and Lauzier, C., "The Mechanism of Conveyance with Bristled Tracks", *Transactions of the ASME, Journal of Engineering for Industry*, pp. 167-174, February 1975.
- [Martin 41] Martin, A. J. P., "Tribo-Electricity in Wool and Hair", *Proceedings of the Physical Society of London*, Vol. B53, pp. 186-189, 1941.
- [Mason 84] Mason, T. M., "Mechanics of Pushing", *Proceedings of the Second International Symposium of Robotics Research*, Kyoto, Japan, pp. 421-428, August 1984.
- [Mason 86] Mason, T. M., "Mechanics and Planning of Manipulator Pushing Operations", *The International Journal of Robotics Research*, Vol. 5, No. 3, pp. 53-71, 1986.
- [MATLAB 88] Little, J. N., and Shure, L., *Signal Processing Toolbox for Use with MATLAB™ User's Guide*, The Mathworks, Inc., August 29, 1988.
- [Matsudaira 95] Matsudaira, M., and Qin, H., "Features and Mechanical Parameters of a Fabric's Compressional Property", *Journal of the Textile Institute*, Vol. 86, No. 3, pp. 476-486, 1995.
- [Mercer 47] Mercer, E. H., and Makinson, K. R., "The Frictional Properties of Wool and Other Textile Fibres", *Journal of the Textile Institute*, Vol. 38, No. 5, pp. T227-T240, 1947.
- [Mercier 30] Mercier, A. A. "Coefficient of Friction of Fabrics", *Bureau of Standards Journal of Research*, Vol. 5, No. 1, pp. 243-246, 1930.
- [Meredith 56] Meredith, R., *The Mechanical Properties of Textile Fibres*, North-Holland Publishing Company, Amsterdam, Chapter 6, 1956.
- [Micro-Epsilon 94] *optoNCDT 1605 Non-contact Optical Displacement Measuring System, Instruction Manual*, Micro-Epsilon Messtechnik GmbH, Ortenburg, Germany, 1994.

- [Miura 54] Miura, Y., "The Surface Friction of Fabrics", *Journal of the Society of Textile and Cellulose Industry*, Vol. 10, pp. 21, 1954 (in Japanese).
- [Monkman 89] Monkman, G. J., Taylor, P. M., and Farnworth, G. J., "Principles of Electroadhesion in Clothing Technology", *International Journal of Clothing Science and Technology*, Vol. 1, No. 3, pp. 14-20, 1989.
- [Monkman 96] Monkman, G. J., "A Simple Time Domain Web Measurement and Inspection System", *Measurement Science and Technology*, Vol. 7, No. 4, pp. 661-665, 1996.
- [Montgomery 59] Montgomery, D. J., "Static Electrification of Solids", *Solid State Physics*, Vol. 9, pp. 139-197, 1959.
- [Moore 72] Moore, D. F., and Geyer, W., "A Review of Adhesion Theories for Elastomers", *Wear*, Vol. 22, pp. 113-141, 1972.
- [Morrow 31] Morrow, J. A., "The Frictional Properties of Cotton Materials", *Journal of the Textile Institute*, Vol. 22, pp. T425-T440, 1931.
- [Morton 97] Morton, W. E., and Hearle, J. W. S., *Physical Properties of Textile Fibres*, The Textile Institute, 1997.
- [Myagkov 67] Myagkov, A. T., and Makarov, N. I., "Advantages of a Vibratory Conveyor with an Elliptical Vibratory Motion", *Russian Engineering Journal*, Vol. XLVII, No. 1, pp. 40-42, 1967.
- [Nedderman 90] Nedderman, R. M., and Harding, G. H. L., "The Flight-Free Vibrating Conveyor: Part 1. Basic Theory and Performance Analysis", *Transactions of the International Chemical Engineering*, Vol. 68, Part A, pp. 123-130, 1990.
- [Neubert 75] Neubert, H. K. P., *Instrument Transducers: An Introduction to their Performance and Design*, 2nd edition, Clarendon Press, Oxford, pp. 141-142, 1975.
- [Newport 95] *Infinity™ C Strain Gage Meter, Operator's Manual*, Newport Electronics, Inc., USA, 1995.
- [Nishimatsu 84a] Nishimatsu, T., and Sawaki, T., "Study on Pile Fabrics, Part III: Frictional Properties of Pile Fabrics", *Journal of the Textile Machinery Society of Japan*, Vol. 30, No. 3, pp. 67-71, 1984.
- [Nishimatsu 84b] Nishimatsu, T., and Sawaki, T., "Study on Pile Fabrics, Part IV: Investigation of Factors Affecting Frictional Properties of Pile Fabrics", *Journal of the Textile Machinery Society of Japan*, Vol. 30, No. 4, pp. 100-106, 1984.

- [Off 91] Off, J. W. A., "MITI's New Sewing Concepts", *Apparel Industry Magazine*, pp. 26-31, May 1991.
- [Ohsawa 66] Ohsawa, M., and Namiki, S., "Anisotropy of the Static Friction of Plain-woven Filament Fabrics", *Journal of The Textile Machinery Society of Japan*, Vol. 12, No. 5, pp. 197-203, 1966
- [Okabe 80] Okabe, S., and Yokoyama, Y., "Study of a Vibratory Feeder with Repulsive Surface which has Directional Characteristics", *Transactions of the ASME, Journal of Mechanical Design*, Vol. 102, pp. 94-101, 1980.
- [Okabe 85] Okabe, S., Kamiya, Y., Tsujikado, K., and Yokoyama, Y., "Vibratory Feeding by Nonsinusoidal Vibration-Optimum Wave Form", *Transactions of the ASME, Journal of Vibration, Acoustics, Stress, and Reliability in Design*, Vol. 107, No. 2, pp. 188-195, 1985.
- [Omega 95] *LCF Series Compression Load Cells, Operator's Manual (MO442/0993)*, Omega Technologies Ltd., Broughton Astley, Leicestershire, UK, 1995.
- [Onogi 96] Onogi, Y., Sugiura, N., and Nakaoka, Y., "Dissipation of Triboelectric Charge into Air from Textile Surfaces", *Textile Research Journal*, Vol. 66, No. 5, pp. 337-342, 1996.
- [Onogi 97] Onogi, Y., Sugiura, N., and Matsuda, C., "Temperature Effect on Dissipation of Triboelectric Charge into Air from Textile Surfaces", *Textile Research Journal*, Vol. 67, No. 1, pp. 45-49, 1997.
- [Opto Diode Corp 92] *Opto-electronics Data Book*, Opto Diode Corp., Newbury Park, CA, USA, 1992.
- [Parameswaran 79] Parameswaran, M. A., and Ganapathy, S., "Vibratory Conveying-Analysis and Design: A Review", *Mechanism and Machine Theory*, Vol. 14, pp. 89-97, 1979.
- [Paraschidis 95] Paraschidis, K., Fahantidis, N., Petridis, V., Doulgeri, Z., Petrou, L., and Hasapis, G., "A Robotic System for Handling Textile and Non Rigid Flat Materials", *Computers in Industry*, Vol. 26, No. 3, pp. 303-313, 1995.
- [Park 97] Park, C. K., and Kang, T. J., "Objective Rating of Seam Pucker Using Neural Networks", *Textile Research Journal*, Vol. 67, No. 7, pp. 494-502, 1997.
- [Parker 94] *PDX Series Drive, User Guide*, Unimatic Engineers Ltd., London, UK, 1994.
- [Pascoe 56] Pascoe, M. W., and Tabor, D., "The Friction and Deformation of Polymers", *Proceedings of the Royal Society*, Vol. A235, pp 210-224, 1956.

- [Peirce 30] Peirce, F. T., "The 'handle' of Cloth as a Measurable Quantity", *Journal of the Textile Institute*, Vol. 21, pp. T377-T416, 1930.
- [Peirce 37] Peirce, F. T., "The Geometry of Cloth Structure", *Journal of the Textile Institute*, Vol. 28, pp. T45-T96, 1937.
- [Peshkin 88] Peshkin, M. A., and Sanderson, A. C., "The Motion of a Pushed, Sliding Workpiece", *IEEE Journal of Robotics and Automation*, Vol. 4, No. 6, pp. 569-598, 1988.
- [Postle 71] Postle, R., "The Thickness and Bulk Density of Plain-Knitted Fabrics", *Journal of the Textile Institute*, Vol. 62, No. 4, pp. 219-231, 1971.
- [Rabinowicz 58] Rabinowicz, E., "The Intrinsic Variables affecting the Stick-Slip Process", *The Proceedings of the Physical Society of London*, Vol. B71, pp. 668-675, 1958.
- [Ramer 68] Ramer, E. M., and Richards, H. R., "Correlation of the Electrical Resistivities of Fabrics with their Ability to Develop and to Hold Electrostatic Charges", *Textile Research Journal*, Vol. 38, pp. 28-35, 1968.
- [Ramgulam 93] Ramgulam, R. B., Amirbayat, J., and Porat, I., "Measurement of Fabric Roughness by a Non-contact Method", *Journal of the Textile Institute*, Vol. 84, No. 1, pp. 99-106, 1993.
- [Redford 66] Redford, A. H., "Vibratory Conveyors", Doctoral thesis, Royal College of Advanced Technology, Salford, England, 1966.
- [Redford 67] Redford, A. H., and Boothroyd, G., "Vibratory Feeding", *Proceedings of the Institution of Mechanical Engineers*, Vol. 182, Pt. 1, No. 6, pp. 135-152, 1967-68.
- [Redford 75] Redford, A. H., "A Review of Developments in Out-of-Phase (Elliptical-Throw) Vibratory Conveying", *Annals of the CIRP*, Vol. 24, No. 1, pp. 399-404, 1975.
- [Redman 94] Redman, J. M., Chiappina, P., and Clausen, F., "A Strategy for Modernizing the Apparel Industry", *Issues in Science and Technology*, Vol. 11, No. 1, pp. 61-67, 1994.
- [Robinovitch 97] Robinovitch, S. N., Hayes, W. C., and McMahon, T. A., "Predicting the Impact Response of a Nonlinear Single-Degree-of-Freedom Shock-Absorbing System From the Measured Step Response", *Journal of Biomechanical Engineering*, Vol. 119, No. 3, pp. 221-227, 1997.

- [Röder 53] Röder, H. L., "Measurements of the Influence of Finishing Agents on the Friction of Fibres", *Journal of the Textile Institute*, Vol. 44, No. 6, pp. T247-T265, 1953.
- [Rubenstein 58] Rubenstein, C., "Review on the Factors Influencing the Friction of Fibres, Yarns and Fabrics", *Wear*, Vol. 2, No. 4, pp. 296-310, 1958.
- [Ryan 81] Ryan, A., and Postle, R., "Application of Sonic Wave Theory to the Measurement of the Dynamic Elastic Moduli of Woven and Knitted Fabrics", *Textile Research Journal*, Vol. 51, No. 11, pp. 732-740, 1981.
- [Saibel 68] Saibel, M. R., "ARF Rink Demonstration of Automated Handling Devices", *The Journal of the Apparel Research Foundation, Inc.*, Vol. 2, No. 4, pp. 1-13, 1968.
- [Schallamach 52] Schallamach, A., "The Load Dependence of Rubber Friction", *Proceedings of the Physical Society of London*, Vol. B65, Part 9, pp. 657-661, 1952.
- [Schick 75] Schick, M. J., *Surface Characteristics of Fibers and Textiles*, Fiber Science Series V7, Marcel Dekker, Inc., New York, 1975.
- [Schneider 91] Schneider, A. M., and Holcombe, B. V., "Properties Influencing Coolness to the Touch of Fabrics", *Textile Research Journal*, Vol. 61, No. 8, pp. 488-494, 1991.
- [Schofield 38] Schofield, J., "Researches on Wool Felting", *Journal of the Textile Institute*, Vol. 29, No. 10, pp. T239-T252, 1938.
- [Shishoo 90] Shishoo, R. L., and Choroszy, M., "Analysis of Mechanical and Dimensional Properties of Wool Fabrics Relevant to Garment Making", *Proceedings of the 8th International Wool Textile Research Conference*, Christchurch, New Zealand, Vol. V, pp. V316-V338, 7-14 February 1990.
- [Shishoo 91] Shishoo, R. L., "Relation between Fabric Mechanical Properties and Garment Design and Tailorability", (response to a question), *Proceedings of the 1st International Clothing Conference "Textile Objective Measurement and Automation in Garment Manufacture"*, Bradford (UK), 9-11 July 1990, ed. Stylios, G., Ellis Horwood, Chichester, pp. 135, 1991.
- [Shuck 70] Shuck, R. O., and Loeb, L., "Technique for Comparative Frictional Measurements on Wet Fabrics", *Textile Research Journal*, Vol. 40, pp. 957-958, 1970.
- [Sigma 90] *Stepping Motors, Sigma Motion Control*, Unimatic Engineers Ltd., London, UK, 1990.
- [SIMULINK 93] *SIMULINK User's Guide*, The Mathworks, Inc., 1993.

- [Skåre 92] Skåre, T., and Ståhl, J., "Static and Dynamic Friction Processes under the Influence of External Vibrations", *Wear*, Vol. 154, No. 1, pp. 177-192, 1992.
- [SPRINT 83] SPRINT project RA115, European Commission (DG XIII), 1983.
- [Srinath 88] Srinath, K., and Karmakar, R., "Vibratory Conveying by Non-Sinusoidal Excitation", *Proceedings of the Institution of Mechanical Engineers*, Vol. 202, No. C6, pp. 405-408, 1988.
- [Stanway 96] Stanway, R., Sproston, J. L., and El-Wahed, A. K., "Applications of Electro-Rheological Fluids in Vibration Control: A Survey", *Smart Materials and Structures*, Vol. 5, No. 4, pp. 464-482, 1996.
- [Stearn 71] Stearn, A. E., "The Effect of Anisotropy in the Randomness of Fibre Orientation on Fibre-to-Fibre Contacts", *Journal of the Textile Institute*, Vol. 62, No. 7, pp. 353-360, 1971.
- [Steidel 89] Steidel, R. F., Jr., *An Introduction to Mechanical Vibrations*, 3rd edition, John Wiley & Sons, New York, pp. 189-191, 1989.
- [Stylios 96a] Stylios, G., "Intelligent Textile and Garment Manufacture", *Assembly Automation*, Vol. 16, No. 3, pp. 5-6, 1996.
- [Stylios 96b] Stylios, G., and Sotomi, J. O., "Thinking Sewing Machines for Intelligent Garment Manufacture", *International Journal of Clothing Science and Technology*, Vol. 8, No. 1/2, pp. 44-55, 1996.
- [Sukigara 96] Sukigara, S., Yokura, H., and Niwa, M., "The Effect of Moisture Transfer on the Compression Properties of Wool Futon Padding", *International Journal of Clothing Science and Technology*, Vol. 8, No. 5, pp. 29-41, 1996.
- [Sukigara 97] Sukigara, S., and Niwa, M., "Analysis of 'Wet' Sensation for Lingerie Fabrics", *International Journal of Clothing Science and Technology*, Vol. 9, No. 3, pp. 214-219, 1997.
- [Sun 73] Sun, C. T., Yang, T. Y., "A Continuum Approach Toward Dynamics of Gridworks", *Journal of Applied Mechanics*, Vol. 40, Series E, No. 1, pp. 186-192, 1973.
- [Tabata 88] Tabata, Y., "Electrostatic Properties of Antistatic Cloth Woven Partly with Electrically Conductive Fibers", *IEEE Transactions on Industry Applications*, Vol. 24, No. 2, pp. 245-249, 1988.
- [Takayanagi 63] Takayanagi, M., "Viscoelastic Properties of Crystalline Polymers", *Memoirs of the Faculty of Engineering Kyushu University*, Vol. 23, No. 1, 1963.

- [Taylor 82] Taylor, G. E., Kemp, D. R., Taylor, P. M., and Pugh, A., "Vision Applied to the Orientation of Embroidered Motifs in the Textile Industry", *Proceedings of the 2nd International Conference on Robot Vision and Sensory Control*, Stuttgart, West Germany, pp. 39-46, 2-4 November 1982.
- [Taylor 86] Taylor, P. M., and Bowden, P., "The Use of Multiple Low Cost Vision Sensors in Fabric Pick and Place Tasks", *Proceedings of the IFAC Symposium on Low Cost Automation*, Valencia, Spain, pp. 89-95, 1986.
- [Taylor 88] Taylor, P. M., Monkman, G. J., and Taylor, G. E., "Electrostatic Grippers for Fabric Handling", *Proceeding of the IEEE Conference on Robotics and Automation*, Philadelphia, PA, pp. 431-433, 24-29 April 1988.
- [Taylor 90] Taylor, G., "Apparel Machinery of the 21st Century", *Textile Asia*, pp. 97-103, August 1990.
- [Taylor 91] Taylor, P. M., Wilkinson, A. J., Gibson, I., Palmer, G. S., and Gunner, M. B., "The Robotic Assembly of Underwear", *Proceeding of the IEE Control Conference*, Edinburgh, pp. 1153-1158, 25-28 March 1991.
- [Taylor 92a] Taylor, P. M., and Gunner, M. B., "Mechatronics in Automated Garment Manufacture", *NATO ASI, Advancements and Applications of Mechatronics Design in Textile Engineering*, Side, Turkey, April 5-16th 1992.
- [Taylor 92b] Taylor, P. M., Adams, E. J. A., Gunner, M. B., and Taylor, G. E., "Automated Folding and Sensory Alignment of a Leisure Top", *International Conference on Research in Textiles and Clothing*, July 1992.
- [Taylor 94a] Taylor, P. M., "Handling Flexible Materials in Automation", *Advanced Robotics and Intelligent Machines*, Salford UK, 28-29 March 1994, ed. Gray, J.O. and Caldwell, D. G., IEE Control Engineering Series 51, Bookcraft, Bath, pp. 191-213, 1996.
- [Taylor 94b] Taylor, P. M., Griesser, M. T., Gunner, M. B., Smith, D. R., Song, X. K., Adams, E., "Gripper Design in an Automated System for the Assembly of a Leisurewear Top", *Euricon '94*, Malaga, Spain, Vol. 1, pp. 534-543, 22-26 August 1994.
- [Taylor 94c] Taylor, P. M., Hosseini-Sianaki, A., and Varley, C. J., "An Experimental Investigation into the Application of Electrorheological Fluids in Tactile Display Systems", *Proceeding of the 5th International Conference on Adaptive Surfaces*, Sendai, Japan, pp 407-419, 5-7 December 1994.
- [Terzopoulos 87] Terzopoulos, D., "Elastically Deformable Models", *Computer Graphics*, Vol. 21, No. 4, pp. 205-214, 1987.

- [Tester 90] Tester, D., Michie, N., and de Jong, S., "The Effect of Regain on Fabric Finishing and Fabric Mechanical Properties", *Proceedings of the 8th International Wool Textile Research Conference*, Christchurch, New Zealand, Vol. V, pp. V139-V148, 7-14 February 1990.
- [Thorndike 61] Thorndike, G. H., and Varley, L., "Measurement of the Coefficient of Friction between Samples of the Same Cloth", *Journal of the Textile Institute*, Vol. 52, pp. P255-P271, 1961.
- [Timoshenko 73] Timoshenko, S. P., and Gere, J. M., *Mechanics of Materials*, Van Nostrand Reinhold Company, New York, pp. 34-37, 1973.
- [Tongue 96] Tongue, B. H., *Principles of Vibration*, Oxford University Press, 1996.
- [Tortora 87] Tortora, P. G., *Understanding Textiles*, Macmillan Publishing Company, New York, 1987.
- [Tyler 89] Tyler, D. J., "The Development Phase of the Textile/Clothing Technology Corporation Apparel Automation Project", *International Journal of Clothing Science and Technology*, Vol. 1, No. 2, pp. 11-16, 1989.
- [Tyzzler 47] Tyzzler, F. G., and Hardy, H. C., "The Properties of Felt in the Reduction of Noise and Vibration", *Journal of the Acoustical Society of America*, Vol. 19, No. 5, pp. 872-878, 1947.
- [Uchida 91] Uchida, E., Uyama, Y., Ikada, Y., "Antistatic Properties of Surface-Modified Polyester Fabrics", *Textile Research Journal*, Vol. 61, No. 8, pp. 483-488, 1991.
- [Ukponmwan 94] Ukponmwan, J. O., "Compressibility Analysis of Dry Abraded Woven Fabrics", *Textile Research Journal*, Vol. 64, No. 12, pp. 756-760, 1994.
- [van Wyk 46a] van Wyk, C. M., "A Study of the Compressibility of Wool, with Special Reference to South African Merino Wool", *Onderstepoort Journal of Veterinary Science and Animal Industry*, Vol. 21, No. 1, pp. 99-226, 1946.
- [van Wyk 46b] van Wyk, C. M., "Note on the Compressibility of Wool", *Journal of the Textile Institute*, Vol. 37, pp. T285-T292, 1946.
- [Vangheluwe 96] Vangheluwe, L., and Kiekens, P., "Modeling Mechanical Behavior of Fabric and Warp Yarn During Loom Stops", *Textile Research Journal*, Vol. 66, No. 10, pp. 722-726, 1996.
- [Verret 91] Verret, R., "Technological Developments in the Textile Industry", *Journal of the Textile Institute*, Vol. 82, No. 2, pp. 129-136, 1991.

- [Viallier 92] Viallier, P., and Alliouche, D., "Mechanical and Tactile Compression of Fabrics: Origin of the Unpleasant Tactile Feeling of Fabrics Dried in a Drum", Internal Report, Laboratoire de Physique et Mécanique Textiles, Mulhouse, April 1992.
- [Vibro-meter 95] *Proximity Transducer Type TQ-401, Data sheet 265-041*, Vibro-meter Ltd., Hazel Grove, Cheshire, UK, 1995.
- [Virto 97] Virto, L., and Naik, A., "Frictional Behavior of Textile Fabrics. Part I: Sliding Phenomena of Fabrics on Metallic and Polymeric Solid Surfaces", *Textile Research Journal*, Vol. 67, No. 11, pp. 793-802, 1997.
- [Viswanathan 66] Viswanathan, A., "Friction of Cotton Fibres", *Journal of the Textile Institute*, Vol. 57, No. 6, pp. T263-T264, 1966.
- [Wehner 87] Wehner, J. A., Miller, B., and Rebenfeld, L., "Moisture Induced Changes in Fabric Structure as Evidenced by Air Permeability Measurements", *Textile Research Journal*, Vol. 57, No. 5, pp. 247-256, 1987.
- [Weil 86] Weil, J., "The Synthesis of Cloth Objects", *Proceeding of SIGGRAPH, Computer Graphics*, Vol. 20, No. 4, pp. 49-54, 1986.
- [Wharfedale 93] *Fane Professional Audio Components*, Wharfedale Loudspeakers Ltd., Crossgates, Leeds, UK, 1993.
- [Wilson 63] Wilson, D., "A Study of Fabric-on-Fabric Dynamic Friction", *Journal of the Textile Institute*, Vol. 54, No. 4, pp. T143-T155, 1963.
- [Wilson 66] Wilson, D., and Hammersley, M. J., "Some Aspects of the Frictional Properties of Waxed and Unwaxed Worsted Hosiery Yarns", *Journal of the Textile Institute*, Vol. 57, pp. T199-T216, 1966.
- [Yoon 84] Yoon, H. N., Sawyer, L. C., and Buckley, A., "Improved Comfort Polyester, Part II: Mechanical and Surface Properties", *Textile Research Journal*, Vol. 54, No. 6, pp. 357-365, 1984.
- [Zeto 96] Zeto, W. Y., Dhingra, R. C., Lau, K. P., and Tam, H., "Sewing Performance of Cotton Lycra Knitted Fabrics", *Textile Research Journal*, Vol. 66, No. 4, pp. 282-286, 1996.
- [Zorowski 67] Zorowski, C. F., and Murayama, T., "Wave Propagation and Dynamic Modulus in Continuous-Filament Twisted Yarns", *Textile Research Journal*, Vol. 37, No. 10, pp. 852-860, 1967.
- [Zorowski 70] Zorowski, C. F., Murayama, T., and Alptekin, A. T., "Strain Waves in Twisted Viscoelastic Filament Assemblies", *Proceeding of the 5th*

International Congress on Rheology, Japan, University Park Press, Baltimore, MD, Vol. 3, pp. 295-310, 1970.

- [Żurek 85] Żurek, W., Jankowiak, D., and Frydrych, I., "Surface Frictional Resistance of Fabrics Woven from Filament Yarns", *Textile Research Journal*, Vol. 55, No. 2, pp. 113-121, 1985.

Appendix A Fabric Details

Set One Fabrics

Fabric Code: C1

Material: 100% Cotton

Structure: Left hand three up one down twill

Area Density (g/m^2): 517

Thickness at 0.5 cN/cm^2 (μm): 1034

Fabric Count Warp/Weft (Thread/cm): 19/17

Bending Length Warp/Weft (mm): 60.85/43.60



Fabric Code: P1

Material: 100% Polyester

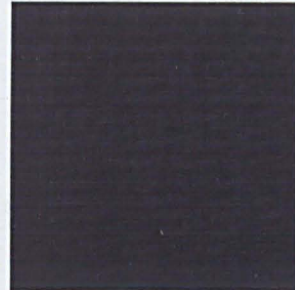
Structure: Plain weave

Area Density (g/m^2): 105

Thickness at 0.5 cN/cm^2 (μm): 190

Fabric Count Warp/Weft(Thread/cm): 46/39

Bending Length Warp/Weft (mm): 13.35/7.8



Fabric Code: W1

Material: 100% Wool

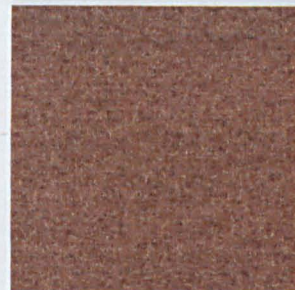
Structure: Broken twill

Area Density (g/m^2): 352

Thickness at 0.5 cN/cm^2 (μm): 3095

Fabric Count Warp/Weft (Thread/cm): 12/13

Bending Length Warp/Weft (mm): 19.85/20.25



Fabric Code: **KC1**

Material: 100% Cotton

structure: Fleece knit

Area Density (g/m²): 257

Thickness at 0.5 cN/cm² (μm): 1428

Fabric Count Wale/Course(Loops/cm): 16/11

Bending Length Wale/Course (mm): 18.75/12.0



Fabric Code: **KC11**

Material: 100% Cotton

Structure: Double-knit stitch

Area Density (g/m²): 183

Thickness at 0.5 cN/cm² (μm): 1030

Fabric Count Wale/Course (Loops/cm): 14/15

Bending Length Wale/Course (mm): 30.1/16.8

Fabric Count Wale/Course(Loops/cm): 16/20



Fabric Code: **KA11**

Material: 100% Acrylic

Structure: Double-knit stitch

Area Density (g/m²): 264

Thickness at 0.5 cN/cm² (μm): 1230

Fabric Count Wale/Course (Loops/cm): 15/10

Bending Length Wale/Course (mm): 14.85/11.75



Set Two Fabrics

Fabric Code: **C2**

Material: 100% Cotton

Structure: Plain weave

Area Density (g/m²): 220

Fabric Count Warp/West (Thread/cm): 24/21



Fabric Code: **KC5**

Material: 100% Cotton

Structure: Plain-knit stitch

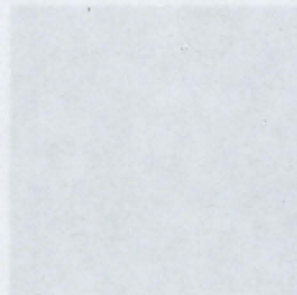
Area Density (g/m²): 118

Fabric Count Wale/Course(Loops/cm): 16/20



Fabric Code: **KC11**

See set 1 fabrics



Fabric Code: **V1**

Material: 100% Viscose Rayon

Structure: Plain weave

Area Density (g/m²): 127

Fabric Count Warp/Weft (Thread/cm): 44/29



Fabric Code: **W2**

Material: 100% Wool (plus backing)

Structure: Even two/two twill

Area Density (g/m²): 215

Fabric Count Warp/Weft (Thread/cm): 23/23



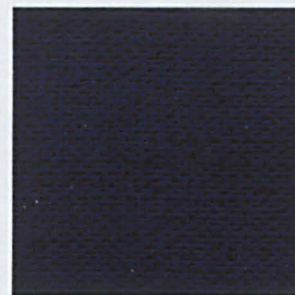
Fabric Code: **L1**

Material: 100% Linen

Structure: Plain weave

Area Density (g/m²): 226

Fabric Count Warp/Weft (Thread/cm): 16/12



Fabric Code: **P2**

Material: 100% Polyester

Structure: Plain weave

Area Density (g/m²): 147

Fabric Count Warp/Weft (Thread/cm): 44/40

Area Density (g/m²): 102

Fabric Count Warp/Weft (Thread/cm): 44/30



Fabric Code: **KN11**

Material: 100% Nylon (plus backing)

Structure: Tricot knit

Area Density (g/m²): 197

Fabric Count Wale/Course (Loops/cm): 19/15

Area Density (g/m²): 128

Fabric Count Wale/Course (Loops/cm): 28/18



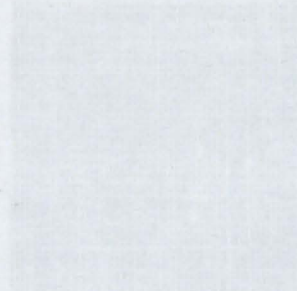
Fabric Code: **L2**

Material: 100% Linen

Structure: Plain weave

Area Density (g/m²): 153

Fabric Count Warp/Weft (Thread/cm): 24/19



Set Three Fabrics

Fabric Code: **C3**

Material: 100% Cotton

Structure: Plain weave

Area Density (g/m²): 102

Fabric Count Warp/Weft (Thread/cm): 44/30



Fabric Code: **KC3**

Material: 100% Cotton

Structure: Plain-knit stitch

Area Density (g/m²): 128

Fabric Count Wale/Course (Loops/cm): 28/18



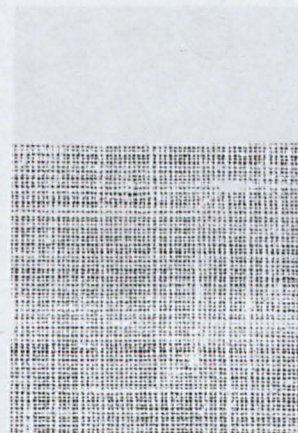
Fabric Code: **L2**

Material: 100% Linen

Structure: Plain weave

Area Density (g/m²): 153

Fabric Count Warp/Weft (Thread/cm): 24/19



Fabric Code: **Ac1**

Material: 100% Acetate

Structure: Plain weave

Area Density (g/m²): 97

Fabric Count Warp/Weft (Thread/cm): 27/26



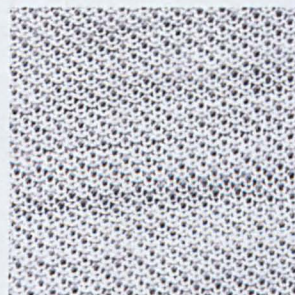
Fabric Code: **KA1**

Material: 100% Acrylic

Structure: Rib-stitch

Area Density (g/m²): 176

Fabric Count Wale/Course (Loops/cm): 9/10



Fabric Code: **KA3**

Material: 100% Acrylic

Structure: Rib-stitch

Area Density (g/m²): 197

Fabric Count Wale/Course (Loops/cm): 12/8

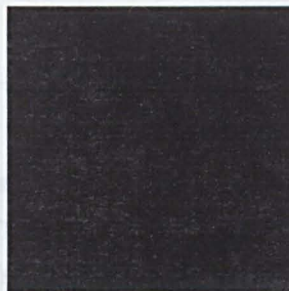


Fabric Code: Pa1

Material: 100% Acrylic

Structure: Non-woven

Area Density (g/m²): 48.3



... in Figure B.1; compr... ar surface
 (250 x 350-mm) to which different surfaces can be attached. T... guides and
 is directly connected to a permanent magnet stepper motor... a 4-mm
 pitch leadscrew. To reduce potential vibrations, generated by the steppers and mechanical
 misalignments, a bi-directional shaft coupling isolates the steppers from the leadscrews. Furthermore,
 a rubber pad physically decouples the motor from the X-Y table and a damping mass in the form of a
 12.6-kg brass plate has been added to the surface. The control of the steppers is provided by a
 MOSFET chopper regulated drive (PDX15-D) with micro stepping options, which gives even at very
 low velocities a smooth motion as seen in Figure B.2.

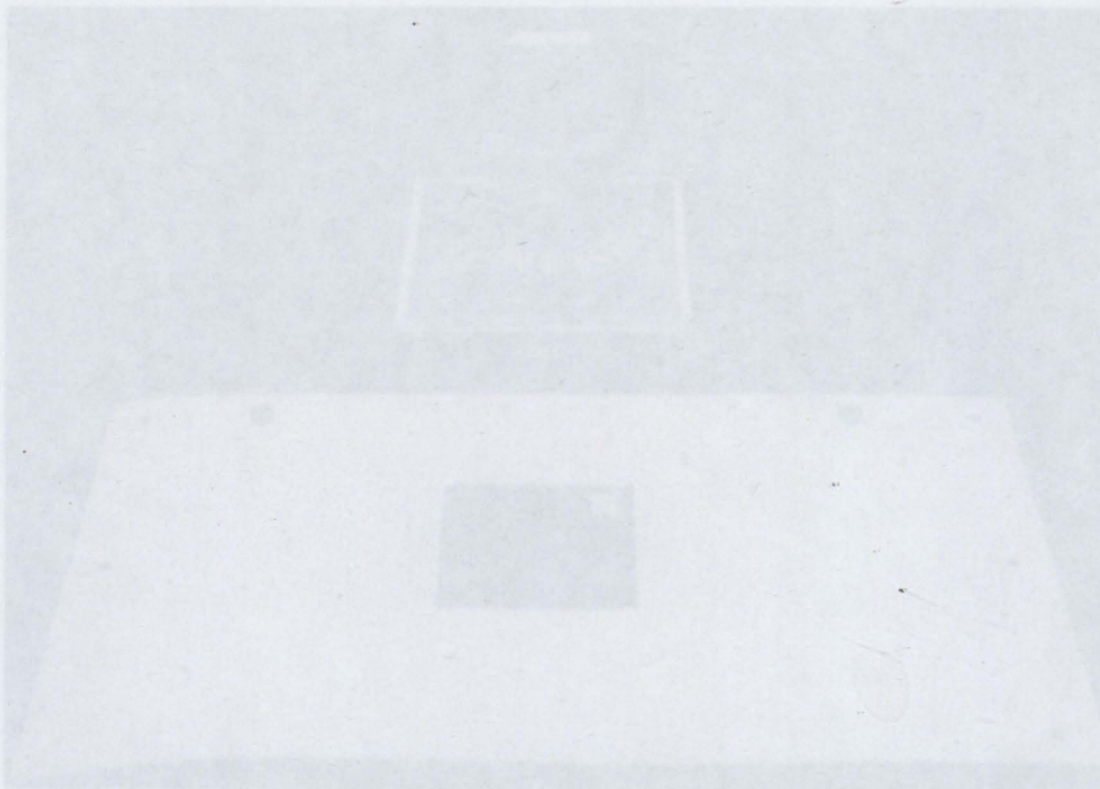


Figure B.1. Picture of the friction table

Table B-1. Specifications of the stepper motor (20-347D100-F015) (Sigma 90)

Parameter	Range
Phases	2
Step angle	1.8°
Windings	4 independent
2 such rotor	

Appendix B Test Equipment

B.1 Friction Measuring Table

The X-Y table, pictured in Figure B.1, comprises a movable rectangular surface (250 x 350-mm) to which different surfaces can be attached. The table slides on camroller guides and is directly connected to a permanent magnet stepper motor (see Table B-1 for details) via a 4-mm pitch leadscrew. To reduce potential vibrations, generated by the steppers and mechanical misalignments, a bi-directional shaft coupling isolates the steppers from the leadscrews. Furthermore, a rubber pad physically decouples the motor from the X-Y table and a damping mass in the form of a 12.6-kg brass plate has been added to the surface. The control of the steppers is provided by a MOSFET chopper regulated drive (PDX15-D) with micro stepping options, which gives even at very low velocities a smooth motion as seen in Figure B.2.

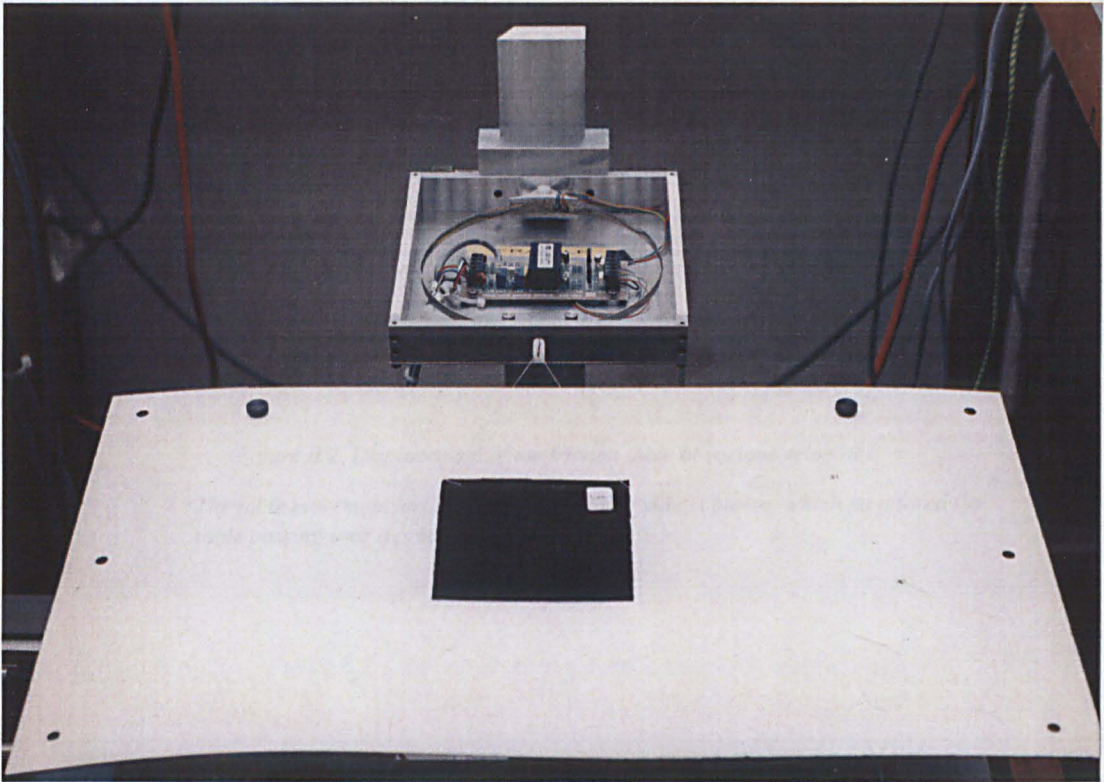


Figure B.1. Picture of the friction table

Table B-1. Specifications of the stepper motor (20-3437D200-F075) [Sigma 90]

Parameter	Range
Phases	2
Step angle	1.8°
Windings	4 independent
2 stack rotor	

Table B-2. Specifications of the PDX15-D series mini-stepping drives [Parker 96]

Parameter	Range
Motor resolution (selectable)	4000 steps/rev
Nominal output current	5 A/phase
Maximum stepping rate	200 kHz at 4000 steps/rev
Nominal chopping frequency	20 kHz
Communication	RS232C

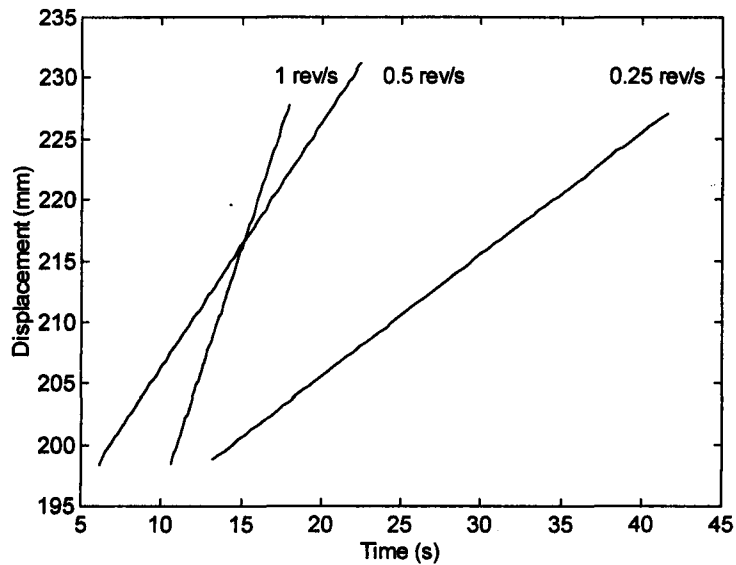


Figure B.2. Displacement of the friction table at various velocities

The table movement has been captured with a video camera, which monitored the table passing over a precision ruler

B.2 The Ring Dynamometer

The dynamometer is constructed from a spring steel ring (\varnothing 150 mm) with four single-axis semiconductor strain gauges (Maywood 919) attached to the mid-length as shown in Figure B.3. The ring is made in-house from a 7-mm wide strip with a thickness of 0.3-mm, which is glued at the boss. The strain gauges are bonded (bonding performed by Maywood Instruments Ltd.) in a full bridge configuration and are temperature compensated minimising thermal elongation. Nevertheless, the ring is still enclosed in an aluminium box together with the amplifier (RS 435-692) to prevent draught from further influencing the sensor.

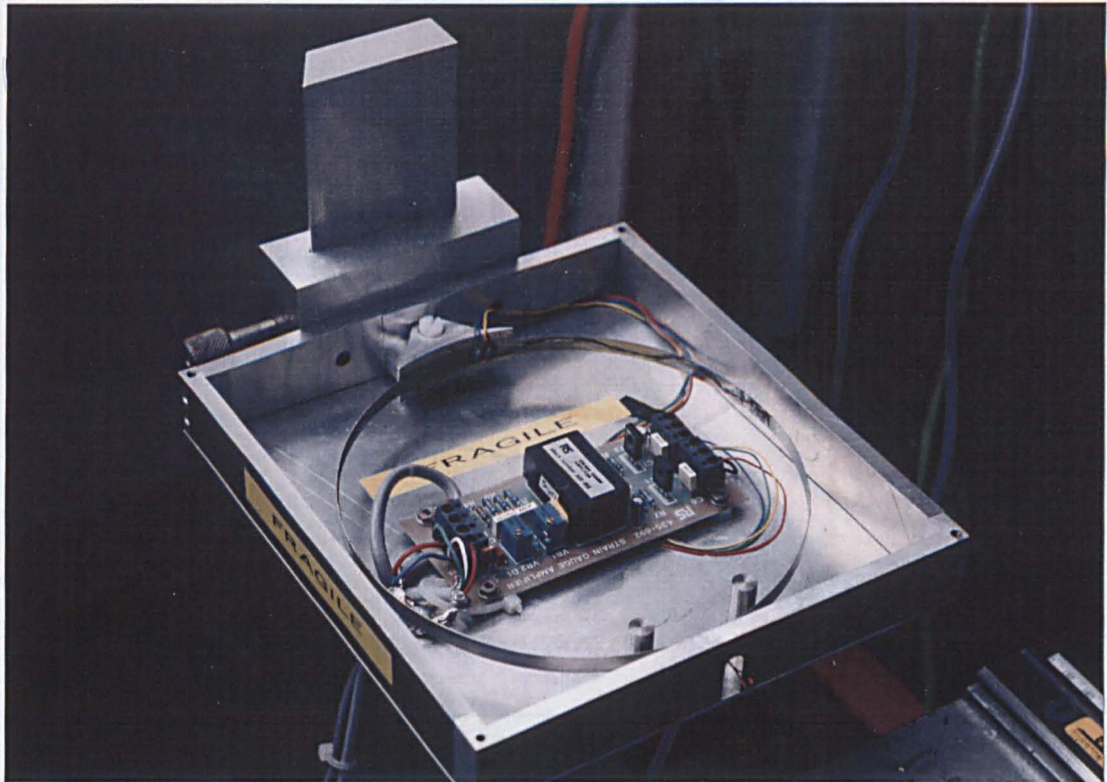


Figure B.3. Close-up of the ring dynamometer and amplifier

The principal advantage of a ring-type tension link as here is its high sensitivity to load without sacrifice in transverse stiffness. The strain distribution in the horizontal diameter of the ring can be regarded as nearly uniform since the bending is minute. As illustrated schematically in Figure B.4 for tension, the outer strain gauges are in compression while the inner gauges are in tension. Considering that the ring thickness, T , is negligible compared to the radius, r , the strain, ε , at the gauge locations for a ring with width, w , can be estimated as follows [Neubert 75]:

$$\varepsilon = \frac{1.08Fr}{EwT^2} \quad T \ll r \quad (\text{B.1})$$

For a spring steel ring, as in this case here, with a Young's modulus, E , of $21 \times 10^{10} \text{ N/m}^2$, subjected to a tension force, F , of 5-g (4.9 cN), Equation (B.1) gives a strain of 3.0×10^{-5} . However, the attachment bracket at the side of the ring might reduce this value appreciably. From Figure B.5, it can be seen that the sensor gives a perfect straight calibration indicating a linear deformation.

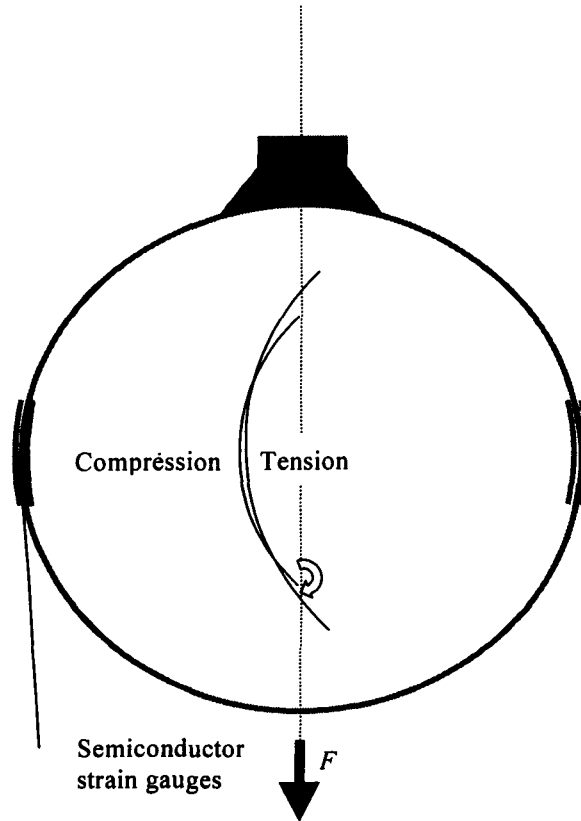


Figure B.4. Ring configuration based on the classical Morehouse proving ring

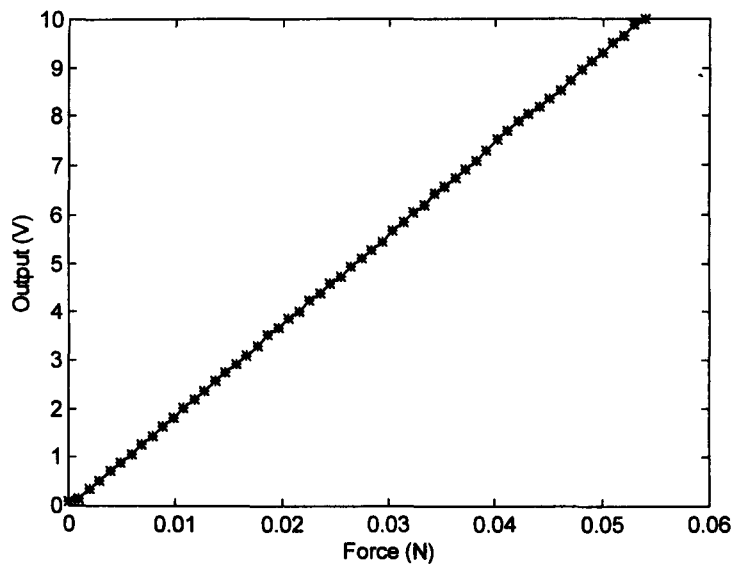


Figure B.5. Calibration graph of the ring dynamometer

B.3 Specifications of the Micro-Epsilon® Laser Sensor (LD1605-4)

The laser sensor uses triangulation as a non-contacting measuring technique and has a measuring range of 4 mm at a 1- μm resolution. As depicted in Figure B.6, a beam of red light projected onto the target, scatters back onto a certain position in the detector and determines so the position of the target. The laser light is pulsed and therefore practically independent of constant ambient light or light fluorescent tubes. Further, the incident light intensity is automatically matched to the reflectivity of the target, which makes that the sensor can easily cope with colour changes or patterns. Error messages displayed by LED-indicators on the signal-conditioning unit indicate whether the target is in range and monitor the light reflection. A summary of the most important technical details is given in Table B-3.

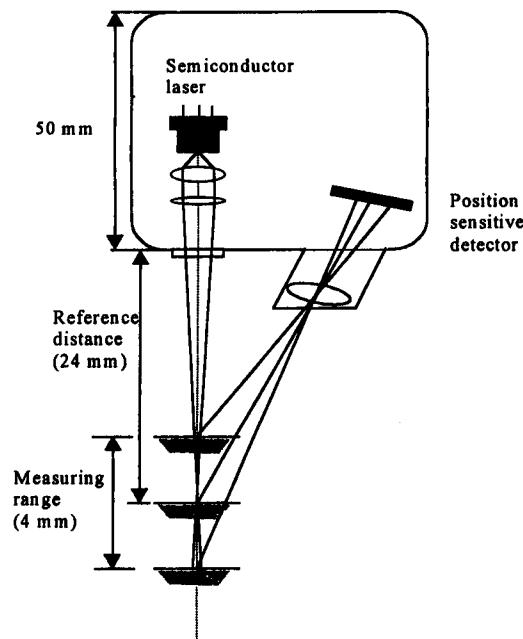


Figure B.6. Triangulation measuring principle [Micro-Epsilon 94]

Table B-3. Technical summary of the LD1605-4 [Micro-Epsilon 94]

Parameter	Range
Measuring range (mm)	± 2
Stand-off midrange (mm)	24
Non-linearity $< \pm 0.3\%$ (μm)	12
Resolution (noise) static (μm)	1
Measuring spot diameter (mm)	0.3
Laser source (class 2)	1 mW, λ 675 nm
Sampling frequency	40 kHz
Analog output	± 10 V
Output impedance	$\approx 0 \Omega$ (10 mA max.)
Rise time (selectable)	0.1/0.2/2 or 20 ms
Temperature stability	0.03%/°K

B.4 Diode Bench

The diode bench, pictured in Figure B.7 and designed to measure stick-slip of fabric panels, comprises three emitter-receiver units embedded in a black Perspex structure, 150-mm apart from each other. The emitters are of the OD-880F series, which use an efficient gallium aluminium arsenide (GaAlAs) infrared emitting diode. The diodes emit 880-nm non-coherent infrared at a half intensity beam angle of 8° when forward biased. Further characteristics are given in Table B-4 and Table B-5. The silicon photodiodes in the bottom plate are an AEPX65. This series offers a very small active area with a good high frequency response even at operating voltages as low as 5-V. More details about the AEPX65 can be found in Table B-6 and Table B-7.

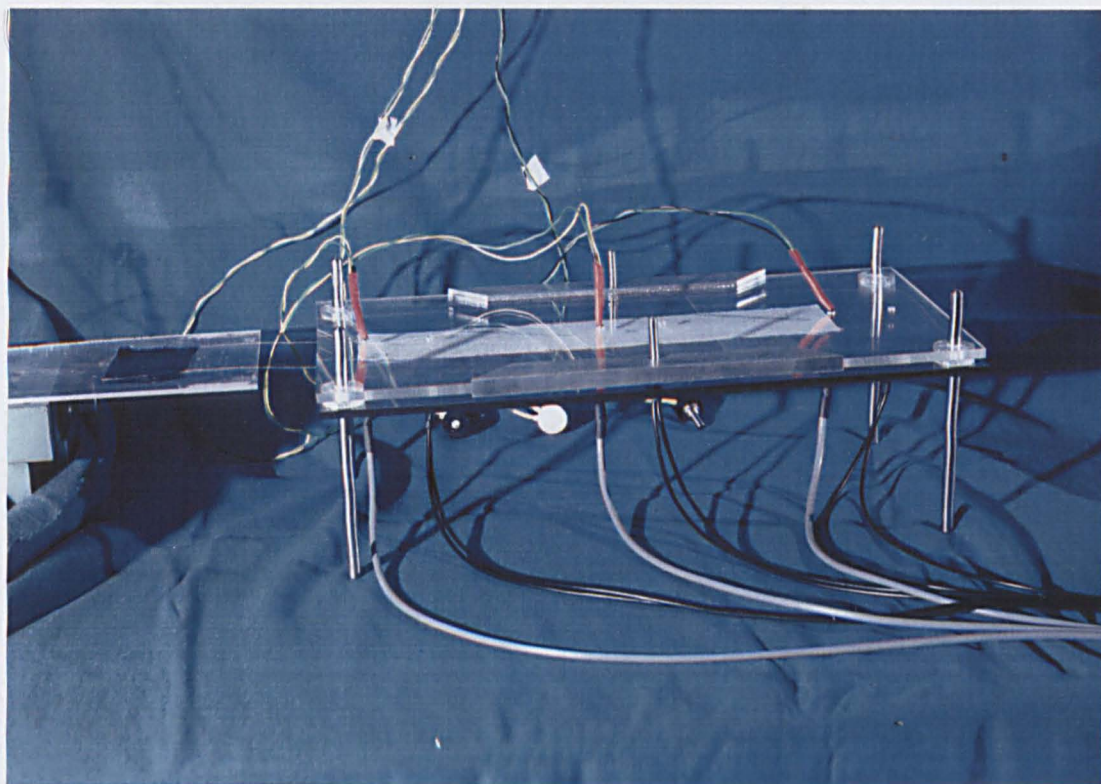


Figure B.7. Diode bench

Table B-4. Electro-optical characteristics of OD-880F at 25°C [Opto Diode Corp. 92]

Parameter	Tests condition	Min.	Typical	Max.	Units
Total power output	Forward current,	15	17		mW
Radiant intensity	$I_f = 100$ mA		135		mW/sr
Peak emission wavelength			880		nm
Spectral bandwidth at 50%	$I_f = 50$ mA		80		nm
Half intensity beam angle			8		degrees
Forward voltage	$I_f = 100$ mA		1.55	1.9	V
Reverse breakdown voltage	$I_r = 10$ μ A	5	30		V
Capacitance	$V_r = 0$ V		17		pF
Rise time			0.5		μ s
Fall time			0.5		μ s

Table B-5. Absolute maximum ratings of OD-880F at 25°C case [Opto Diode Corp. 92]

Power dissipation	190 mW
Continuous forward current	100 mA
Peak forward current (10 μ s, 400 Hz)	3 A
Reverse voltage	5 V

Table B-6. Electro-optical characteristics of AEPX65 at 22°C and 5V reverse [Centronic 95]

Parameter	Tests condition	Min.	Typical	Max.	Units
Active area			0.55		mm ²
Active diameter			0.84		mm
Responsiveness at $\lambda = 820$ nm			0.35		A/W
Dark current			2	10	nA
Noise equivalent power (900 nm)			6.8e-14		WHz ^{-1/2}
Capacitance			6	8	pF
Rise time at $\lambda = 820$ nm	R load 50 Ω			1.0	ns

Table B-7. Absolute maximum ratings of AEPX65 at 22°C [Centronic 95]

DC Reverse voltage	30 V
Peak pulse current (1 μ s, 1% duty cycle)	200 mA
Peak DC current	10 mA

B.5 Static Compression Tester

The static compression tester has been built in-house according to the ASTM D1777 specifications with an anvil of $\text{Ø } 50.0\text{-mm}$ and a pressure foot of $\text{Ø } 35.7\text{-mm}$ giving so an effective compression area of 10 cm^2 . As seen from Figure B.8, the parallelism is maintained through a moveable platform (hand operated), which slides on Teflon® bushes over four precision steel shafts. Both compression surfaces are mirror finished and give an airtight match of less than $10\text{ }\mu\text{m}$ when compressed empty (see Figure B.9).

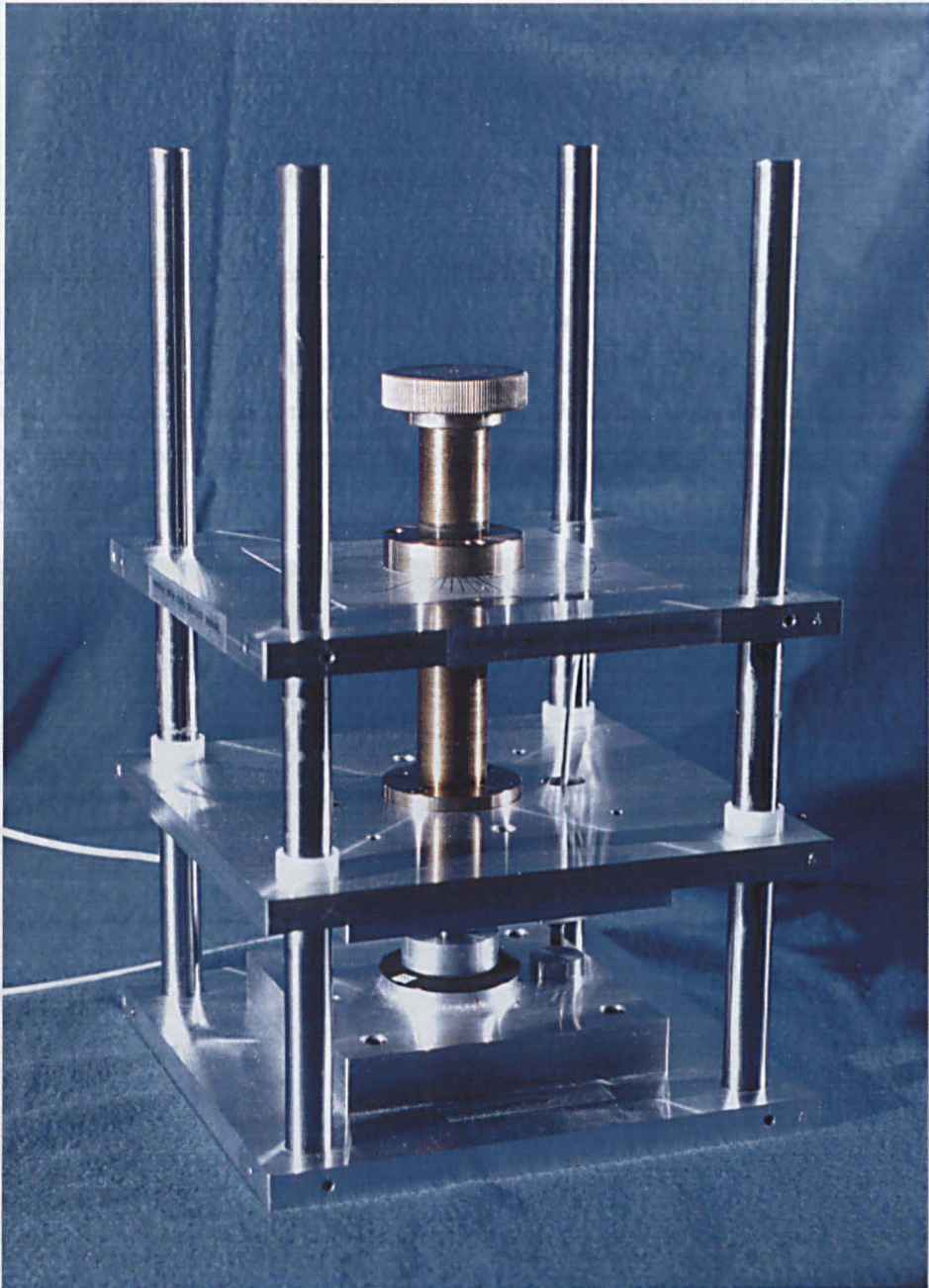


Figure B.8. Static compression tester

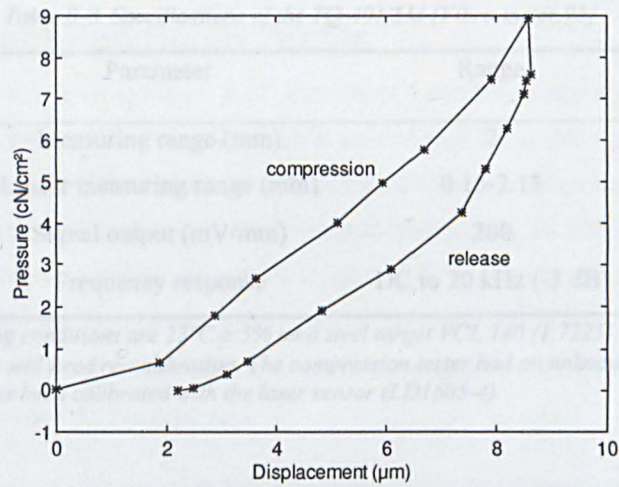


Figure B.9. Inherent hysteresis of the static compression tester

Further, the compression cell comprises a 2-mm range inductive displacement sensor (probe TQ 401/5M and IQS-451 signal conditioner) and a miniature load cell (LCF-50G) of which the specifications are listed in Table B-8 and Table B-9 respectively. A close-up in Figure B.10 shows more detail of the sensors and compression surfaces. The load cell is connected to a DP25-S strain meter [Newport 95], which act as a programmable indicator/controller before feeding the signal into the sampling card (PC30AT).

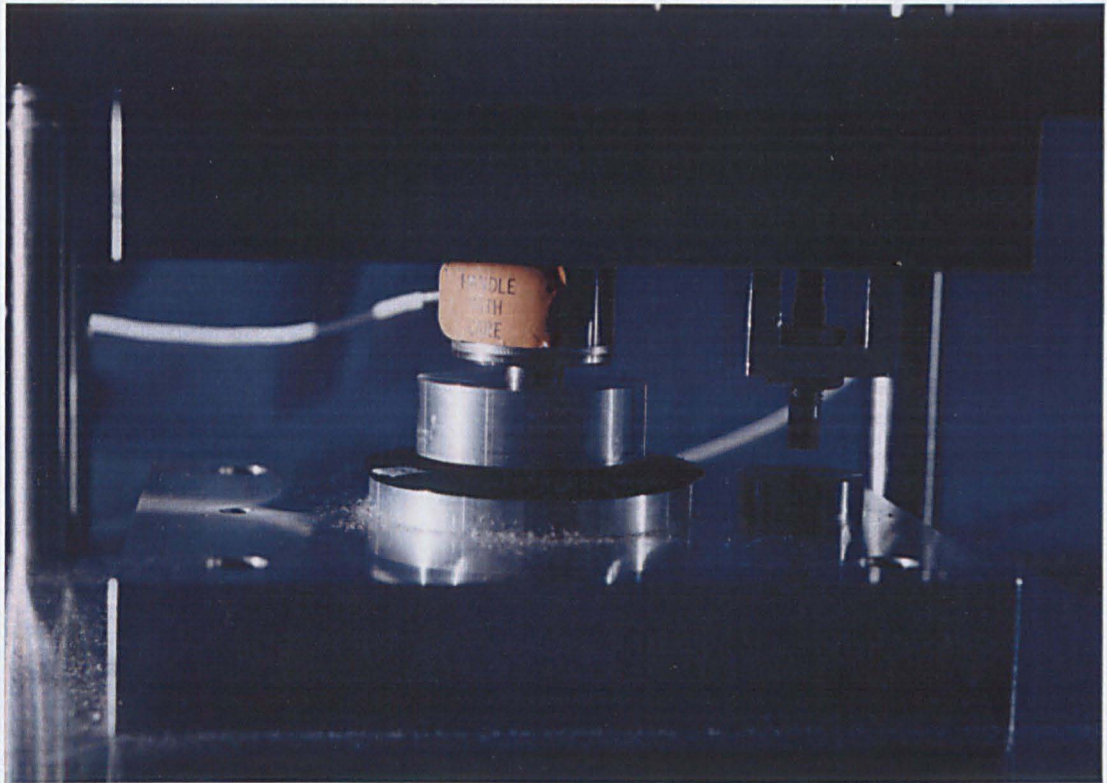


Figure B.10. Close up of the static compression tester

Table B-8. Specifications of the TQ-401/5M [Vibro-meter 95]

Parameter	Range
Measuring range (mm)	2
Linear measuring range (mm)	0.15-2.15
Signal output (mV/mm)	200
Frequency response	DC to 20 kHz (-3 dB)

Testing conditions are 23°C ± 5% on a steel target VCL 140 (1.7225). Different alloys will need re-calibration. The compression tester had an unknown steel target but has been calibrated with the laser sensor (LD1605-4).

Table B-9. Specifications of the LCF-50G [Omega 95]

Parameter	Range
Measuring range (g)	± 50
Signal output (mV/V)	2.63
Linearity and hysteresis	± 0.15% full scale
Zero balance	± 2% max.
Repeatability	± 0.05% full scale
Input resistance (Ω)	608
Output resistance (Ω)	446
Safe overload	150% full scale

B.6 Impact Pendulum Tester

The impact tester, shown in Figure B.11, consists of a pendulum arm (overall length 1315 cm) with mirror finished pressure foot (10 cm^2), which is centred in a rod at the top of a large aluminium framework. The rod is suspended on precision bearings for a smooth rotation and can be released from an adjustable angle with a computer controlled solenoid mechanism. In addition, a dead weight of 1550-g on the pendulum arm giving an overall weight of 4.5-kg can be balanced to give variable impact forces on the fabric sample, which is clamped on the impact table. Further, the impact table is adjustable relative to the pressure foot and houses the laser sensor (LD1605-4), which points to a metal indicator at the side of the pressure foot.

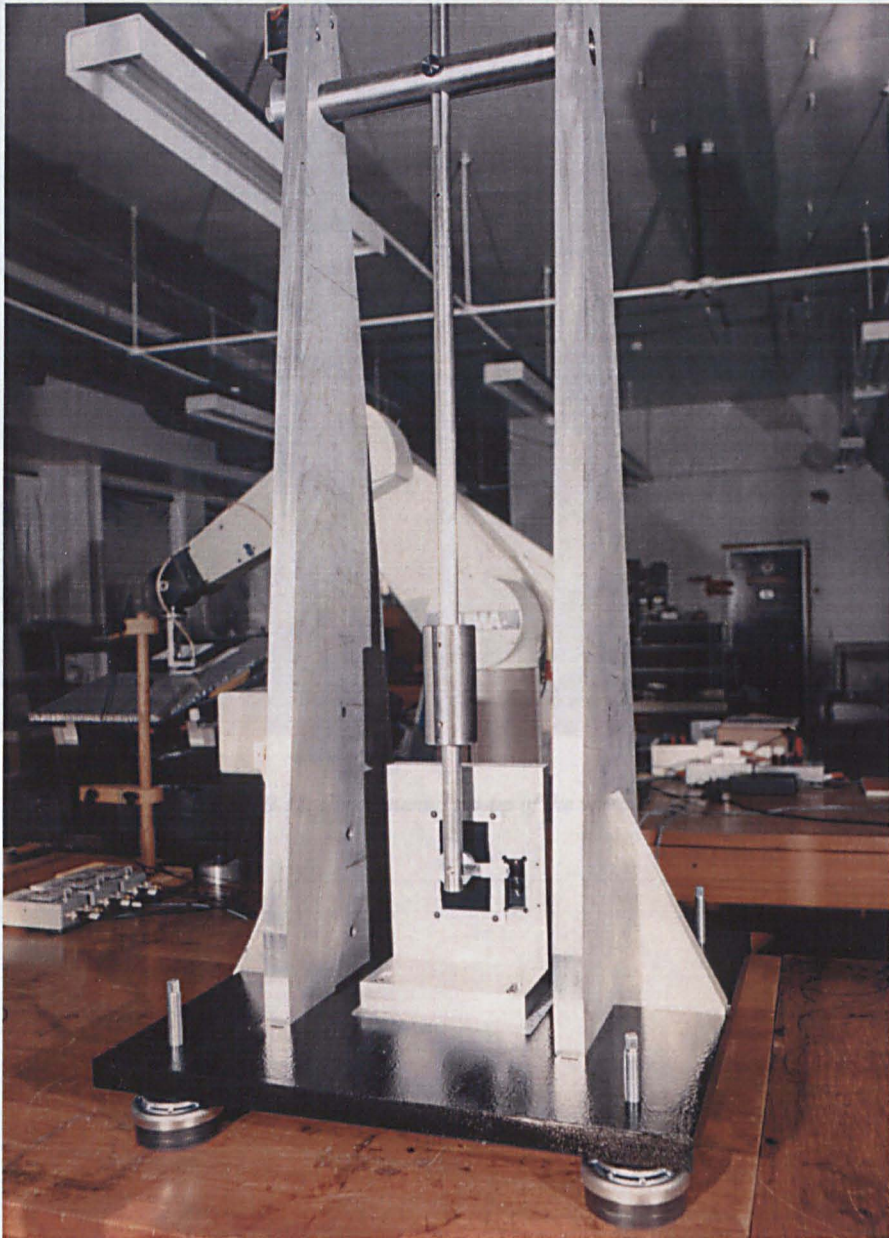


Figure B.11. Total view of the impact tester

B.7 Vibrating Table Unit

Finally, a vibration unit has been built from a 600 W bass loudspeaker (see Table B-10 for details), which is fixed to a rotatable framework that can be clamped at different angles onto a heavy metal base. A solid foam structure made from Tancast™-8 (Trident Foams), not visible in Figure B.12, has been glued inside the speaker cone to provide a flat surface on which the aluminium honeycomb structure (Aim Aviation (HBA) Ltd.) is fixed. The full vibration unit is supported on bobbins (Christie & Grey 60.112) which act as damping units and is powered by a 550 W MOSFET amplifier of which its characteristics are listed in Table B-11.



Figure B.12. Experimental set-up of the vibration unit

B.8 Gaptek 2004 Non-contact Micro Displacement Transducer

The 2004 Gaptek Series is a 'gap-to-voltage' non-contacting transducer (range up to 10.491251 in 0.5 above) which can be used to measure static as well as dynamic distance between the probe and an observed target. The sensor generates a low energy RF-signal at the probe, which induces eddy currents in the metallic target. Changes in the distance between the probe and the target change the sensor's impedance, and a DC output voltage linearly proportional to the gap distance is given. The specifications of the sensor are given below in Table B-12.

Table B-10. Electro-mechanical specifications of the Colossus 15 XB [Wharfedale 93]

Parameter	Range
Nominal chassis diameter (mm)	381
Impedance (Ω)	8
Power rating (W)	600
Resonance (Hz)	35
Usable frequency range (-6 dB)	30 Hz-1 kHz
Average sensitivity (1 W 1 m)	99 dB
Magnetic gap depth (mm)	9.5
Magnet weight (kg)	3.6
Assembly weight (kg)	10.4
Voice coil diameter (mm)	102
Max. usable excursion (mm)	14

Table B-11. Specifications of the OMP/MF1000 [B.K. Electronics 93]

Parameter	Range
Output R.M.S. into 8 Ω (W)	550
3 dB Power bandwidth (STD)	1 Hz-100 kHz
Damping factor	> 300
Slew rate (V/ μ s)	75
Input sensitivity (STD)	500 mV
Input impedance (Ω)	10000
S/N ratio	110 dB
DC loudspeaker protection	± 3 V DC
Forced fan air cooling	-
Anti thump protection	2 s
Weight (kg)	16.3

B.8 Gaptex 2004 Non-contact Micro Displacement Transducer

The 2004 Gaptex Series is a 'gap-to-voltage' non-contacting transducer (similar as the TQ 401/5M in B.5 above) which can be used to measure static as well as dynamic distance between the probe and an observed target. The sensor generates a low energy RF-signal at the probe, which induces eddy currents in the metallic target. Changes in the distance between the probe and the target change the sensor's impedance, and a DC output voltage linearly proportional to the gap distance is given. The specifications of the sensor are given below in Table B-12.

Table B-12. Specifications of the Gaptek 2004 with probe CG8PO1 [GWI 85]

Parameter	Range
Measuring range (mm)	1.4
Linear measuring range (mm)	0.2-1.6
Resolution (μm)	5
Frequency response	DC to 50 kHz
Output impedance (Ω)	1000
Output voltage (V)	-10
Power supply (unregulated)	-18 to -30 V DC.

B.9 Specifications of the Triaxial Accelerometer (4504)

The accelerometer is a piezoelectric type with a built in preamplifier (DeltaTron®) measuring the accelerations simultaneously in three mutually perpendicular directions. The sensor operates with a constant-current power supply (WB 1372) and gives output signals in the form of voltage modulations on the power supply line. Further, the accelerometer has an extreme low mass and small physical dimensions, which make it ideal for use on the vibrating table. Some specifications of the sensor are listed in Table B-13.

Table B-13. Specifications of the Triaxial DeltaTron® accelerometer type 4504 [B & K 96]

Parameter	Range
Typical sensitivity	9.8 mV/g
Frequency range	1 Hz-15 kHz (X) 1 Hz-10 kHz (Y) 1 Hz-23 kHz (Z)
Mounted resonance frequency	40 kHz (X), 30 kHz (Y), 50 kHz (Z)
Weight (g)	14
Overall dimensions (mm)	22.5 x 17.5 x 11

Appendix C Surface Details

C.1 Instrumentation and Method

The surface scans of the engineering materials used for the friction and vibration tests (i.e., aluminium, Formica and rubber) have been performed on a Form Talysurf Series (Rank Taylor Hobson Ltd.). The measuring device consists of a diamond tipped stylus, which is slowly (0.5 mm/s) traversed over a 10 mm distance across the test surface. The diamond has a tip radius of 1.5-2.5 μm and is spring-loaded (70-100 mgf) onto the surface under test. The traverse unit is placed on an optical bench, which is nominally levelled (viz., parallel) to within 6.0- μm .

The measuring device displays an output of the surface profile either in an unfiltered format or in an analysed format by subtracting the inclination. Together with the analysed profile are several parameters calculated (listed below), which characterise the surface.

- R_a : arithmetic mean of the departure of the roughness profile from the mean line
- R_q : the RMS parameter corresponding to R_a
- R_p : the maximum height of the profile above the mean line within the assessment length
- R_v : the maximum depth of the profile below the mean line within the assessment length
- R_t : the maximum peak to valley height of the profile in the assessment length
($R_p + R_v$)
- R_{sk} : the measure of the symmetry of the profile about the mean line (viz., distinguishes between asymmetrical profiles of the same R_a or R_q)
- R_{ku} : the measure of the sharpness of the surface profile

C.2 Surface Scans

All three engineering surfaces are rectangular (300 x 500 mm) and are provided with two screw-holes at the side for attachment to the X-Y table. The aluminium was supplied in a thin sheet format (see Table C-1) and therefore glued to a stiffer Perspex sheet. A similar process was applied to the rubber.

Table C-1. Specifications of the engineering surfaces

	Aluminium	Formica	Rubber
Material	99% pure	-	Natural Grade B
Thickness	0.15 mm	-	0.9 mm ± 10%
Characteristic	Half hard	White	Antistatic
Supplier	Goodfellow Cambridge Ltd. (AI 000600/10)	-	Four D Rubber Co. Ltd.

Three locations, roughly 5-cm apart, in the centre of each surface (i.e., area of friction testing) have been scanned. The result, R_a , for the three scans are given in Table C-2 and averaged for each material. Furthermore, a printout from a surface scan of each material is given in Figure C.1 to Figure C.3 respectively.

Table C-2. Average surface roughness of engineering materials

	R_a (μm) Aluminium	R_a (μm) Formica	R_a (μm) Rubber
Position 1	0.1461	1.6060	0.7296
Position 2	0.3978	0.5794	0.5930
Position 3	0.1864	0.6932	0.4788
<i>Average</i>	<i>0.2434</i>	<i>0.9595</i>	<i>0.6005</i>

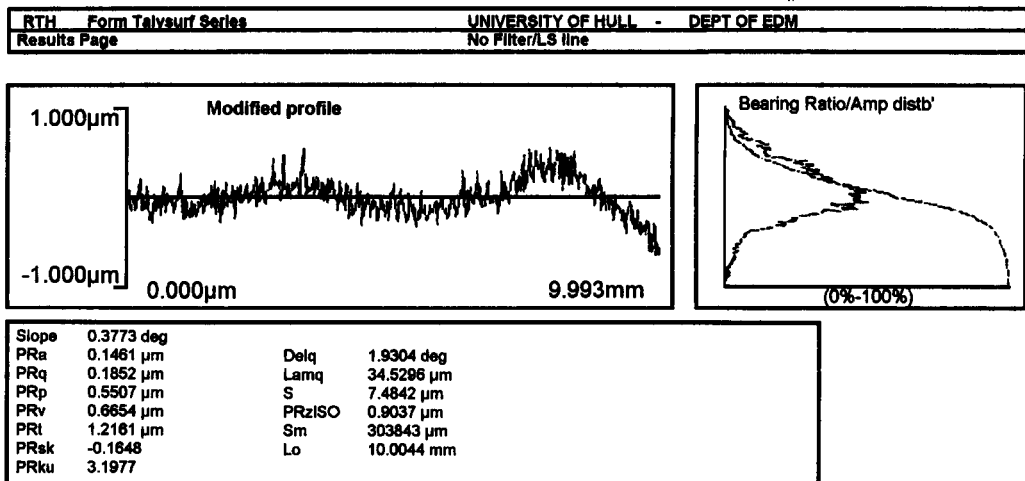


Figure C.1. Roughness profile output of the aluminium surface

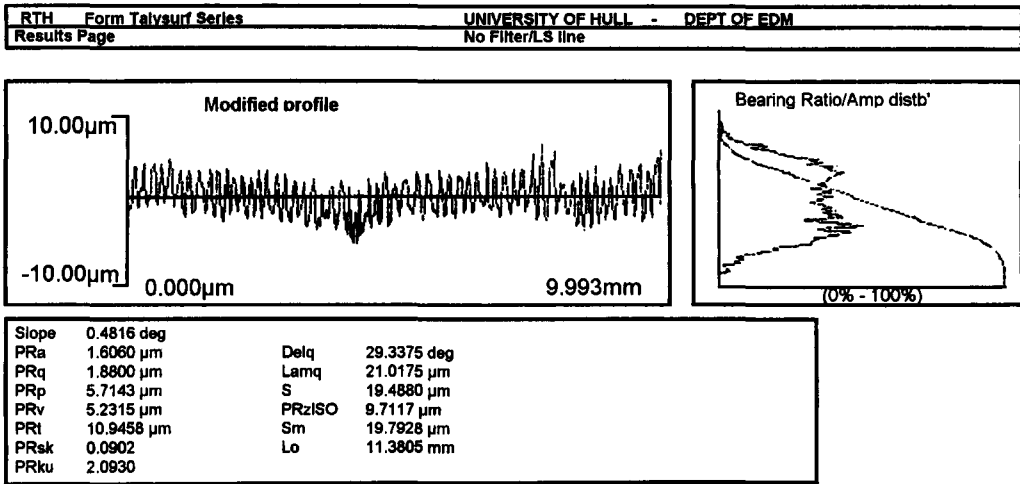


Figure C.2. Roughness profile output of the Formica surface

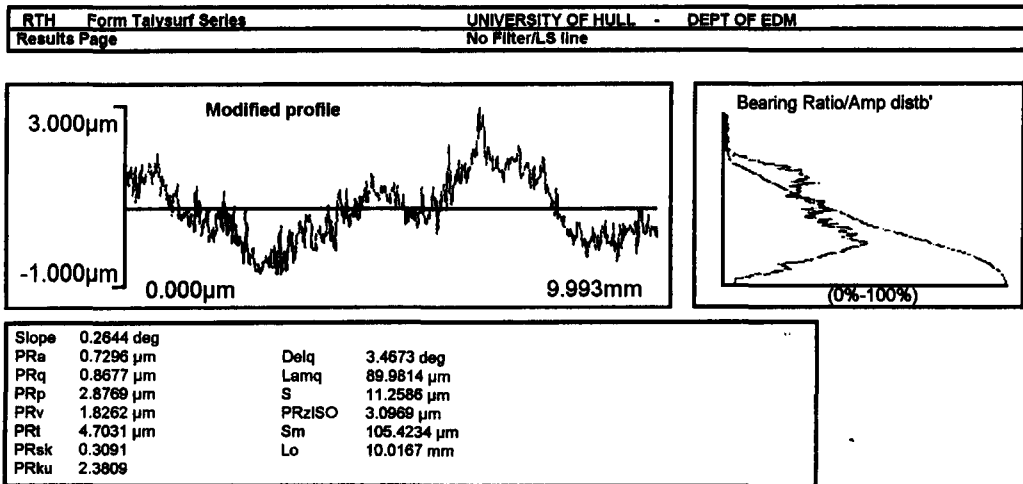


Figure C.3. Roughness profile output of the rubber surface

Appendix D Some Statistical Analysis

When performing experiments there is always that strategic question on how many measurements should be taken for the test to be significant. In particular, tests on low-stress mechanical properties demand a higher level of attention to detail and precision than the traditional high-stress measurements such as breaking extension for example. Furthermore, fabrics are in many ways different from other engineering materials; their mechanical properties can easily vary within a single roll and within a batch. A study by Ly [Ly 89] reported that the variation of measured properties on the KES-F instruments was more pronounced across the width than along the length of the fabric. An insignificant variation of less than 3.8% has been reported along a 1.5-m length of fabric whereas across a similar fabric width, seven KES-F parameters concerning tensile, shear and surface roughness showed a variation greater than 5%. A rough estimate of 10% variation across the breath of the fabric has been quoted by Shishoo [Shishoo 91]. In addition, virtually all mechanical fabric properties are temperature and humidity dependent which brings in another two variables (and source of error).

However on one hand, too many measurements will obviously give accurate results but demands a lot of work while on the other hand a small number of tests might lead to wrong conclusions. The number of required tests and the accuracy obtained from the tests is an important issue, which will be discussed in this appendix, but first it is essential to find out how the measurements are distributed.

D.1 Kind of Distribution

The measurement of mechanical fabric parameters is a discrete process and subject to variations due to a large number of small independent effects in the fabric itself, the apparatus or the method of measurement. Hence, it is reasonable to assume that the mechanical parameters follow a normal (or Gaussian) distribution as many other scientific experiments. One simple test for normality [Leaf 84] is illustrated in Table D-1 on three repeated tests of the frictional data for KC11 (wale direction). The first two columns show the raw data for the respective fabric sample, which is again displayed in ascending order in the third column. The last two columns of Table D-1 give the cumulative normal probability for the 19 samples, s , and their corresponding normal probability (viz., area under the normal distribution curve) respectively. The measurements of the frictional coefficient can be regarded as coming from a normal distribution when the plotted points of μ_d fall close to a straight line as in Figure D.1. Similar results are obtained for the remaining fabrics (set 1) as can be seen from Figure D.2 and for other test conditions (not displayed).

Table D-1. Test for normality on KC11

Sample No.	Dynamic friction coefficient μ_d	μ_d in ascending order (i)	Cumulative normal probability $i/(s+1)$	Standard normal probability [Leaf 84]
1	0.383	0.341	0.05	-1.6449
	0.396	0.358	0.10	-1.2816
	0.385	0.360	0.15	-1.0364
	0.393	0.364	0.20	-0.8416
2	0.409	0.375	0.25	-0.6745
	0.360	0.379	0.30	-0.5244
	0.404	0.383	0.35	-0.3853
3	0.394	0.383	0.40	-0.2533
	0.375	0.385	0.45	-0.1257
	0.390	0.386	0.50	0
4	0.389	0.389	0.55	0.1257
	0.341	0.390	0.60	0.2533
	0.383	0.390	0.65	0.3853
5	0.386	0.391	0.70	0.5244
	0.358	0.393	0.75	0.6745
	0.390	0.394	0.80	0.8416
6	0.391	0.396	0.85	1.0364
	0.364	0.404	0.90	1.2816
	0.379	0.409	0.95	1.6449

Standard conditions, velocity: 1 mm/s, aluminium surface, wale direction, sample area: 1 dm²

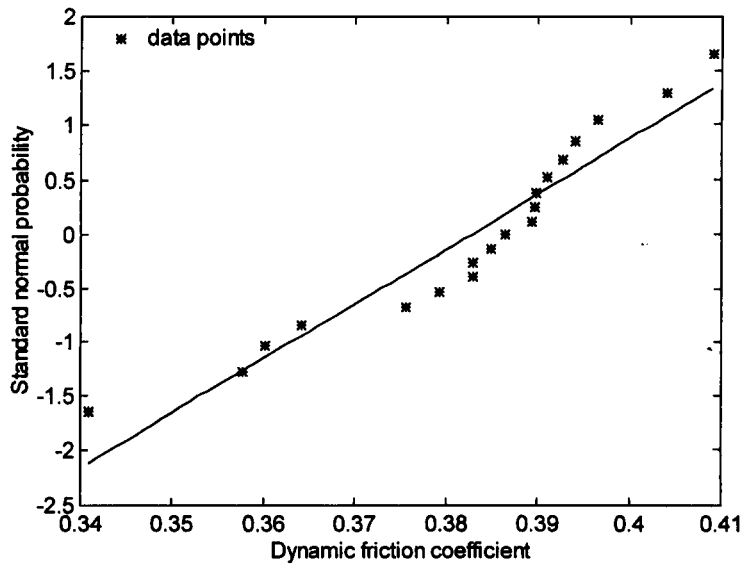


Figure D.1. Graphical representation of the normality test for KC11

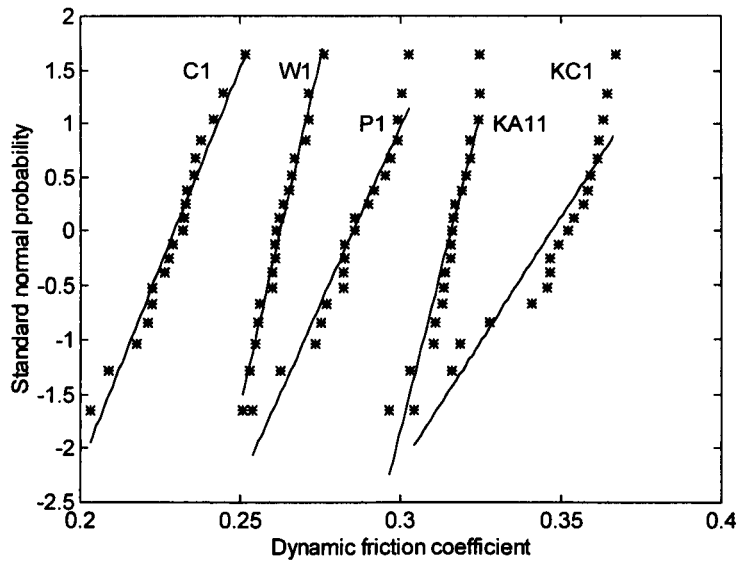


Figure D.2. Normality tests for other set 1 fabrics

Standard conditions, velocity: 1 mm/s, aluminium surface, wale direction, sample area: 1 dm²

Once the distribution of the samples is known, various statistical calculations can be applied on the results. The next question is now how many measurements need to be made so that the mean value of the parameter is a significant representative.

D.2 Number of Samples Required

As more and more measurements of a certain parameter, x , are taken then the average, \bar{x} , is expected to approach the 'true' value. Yet, this is physically impossible regarding the enormous amount of work so a limited number of measurements are taken with the spread of the measurements given as the standard deviation, σ_x . If the measurements are normally distributed then: approximately 68% of the measurements will lie between $\bar{x} \pm \sigma_x$ and 95% between $\bar{x} \pm 2\sigma_x$. In other words, there is 68% (or 95%) probability ('confidence') that any new measurement will lie between the interval $\bar{x} \pm \sigma_x$ (or $\bar{x} \pm 2\sigma_x$). A similar confidence interval can also be defined for the variation of the average value of s measurements though the standard deviation, σ_x , is now substituted by the standard error, $\sigma_{\bar{x}}$, defined as follows [Chatfield 70]:

$$\sigma_{\bar{x}} = \frac{1}{\sqrt{s}} \sigma_x = \sqrt{\frac{\sum_{i=1}^s (x_i - \bar{x})^2}{s(s-1)}} \quad (\text{D.1})$$

The variation of the average, $\sigma_{\bar{x}}$, is very sensitive to the number of measurements because of the use of the 'unknown' σ_x . Therefore, strictly speaking, the distribution of the mean is not normal (or Gaussian) for samples sizes smaller than 30 but follows a Student t-distribution, t_c (viz., kind of Gaussian distribution for small sample size). Regarding that the number of tests on fabric parameters is mostly below 30, a minimum amount of tests is required to give a reasonable standard error. If an error at the 68% confidence limit is required which is in many cases sufficient then the standard error of the measurements is within 11% as can be seen from Table D-2. Increasing the number of tests further than six, increases the work drastically but only gives a minor improvement in the standard error.

Table D-2. Values for the Student t-distribution [Chatfield 70]

Number of samples	t_c for a 68%	t_c for a 95%
	confidence interval	confidence interval
2	1.81	
3	1.31	
4	1.21	3.18
5	1.14	
6	1.11	
7	1.09	
8	1.08	2.36
9	1.06	
10	1.06	
>10	$1+1/2(s-1)$	

So, six samples of each fabric (set 1) have been used throughout most of the tests. This was more preferable than repeating the tests 6 times bearing in mind that successive friction tests for example, increase the coefficient of friction (3.3). Furthermore, this approach also included the variance of the fabric itself.

In the literature, however, the error on measurements is not so much expressed in terms of the standard deviation, σ_x , but rather as the ratio of the standard deviation to the mean otherwise defined as the coefficient of variation, CV (%). With regard to friction measurements for example, Ajayi [Ajayi 92a] mentioned a value for CV less than 10% for five measurements, results in this study give a value between 5% for the lightweight P1 to 2% for KA11. Some levels of precision for the KES-F test resulting of an extensive study by Mahar *et al.* [Mahar 87] will be discussed in the next section.

D.3 Precision of KES-FB Tests of Friction and Compression

Two major inter-laboratory trials [Mahar 87] and [Ly 88] on pure wool and wool blend fabrics have investigated the variations when measuring the KES-F fabric properties. Mahar *et al.* [Mahar 87] collected KES-F data from seven laboratories around the world for a range of 30 wool and wool blend suiting fabrics. A similar approach was followed by Ly *et al.* [Ly 88] though fabrics with a wider

range in thickness and weight were evaluated in their case. An analysis of variance on the data was used to separate the variance of all observations into four categories: changes within the laboratory, changes between the different laboratories, interaction between laboratory and specimen and finally variation between the different fabrics. Here in particular the laboratory-specimen variance is important because it gives an indication of the expected accuracy of fabric measurements. The KES-F surface and compression test figures are listed in Table D-3.

Table D-3. Coefficient of variance for KES-F friction and compression tests [Mahar 87]

KES-FB [Mahar 87]				KES-FB [Mahar 87]			
<i>Parameter</i>	<i>Grand Mean</i>	<i>CV (%)</i>	<i>CV* (%)</i>	<i>Parameter</i>	<i>Grand Mean</i>	<i>CV (%)</i>	<i>CV* (%)</i>
MIU-1	0.19	2.7	2-5	LC (-)	0.35	3.5	11.7
MIU-2	0.20	2.9	2-5	WC (J/m ²) at 50 cN/cm ²	0.19	4.3	8.3
MMD-1	0.024	22.1	-	RC (%)	50	5.0	3.0
MMD-2	0.031	11.7	-	T (mm) at 0.5 cN/cm ²	0.71	2.6	3.1
SMD-1 (μm)	5.6	9.3	-	T (mm) at 2.0 cN/cm ²	0.62	2.1	-
SMD-2 (μm)	5.8	9.1	-				

The suffixes 1 and 2 refer to the warp and weft directions, respectively, MIU: coefficient of friction, MMD: mean deviation of MIU, and SMD: geometrical roughness. The grand mean is calculated as the average of 390 tests comprising 30 wool (wool/synthetic) fabrics. The surface test comprises of five measurements for each fabric sample and the compression tests of three. () Values from this study*

Note that some of the variance is higher in this study compared to figures from Mahar *et al.*, this is probably due to the larger variety of fabrics tested here (i.e., lightweight polyester P1). Results from both Mahar *et al.* and this study showed that lightweight fabrics generally have a more variable mechanical (i.e., compression) and surface characteristic than medium to heavyweight materials.

Furthermore, Mahar *et al.* [Mahar 87] recommend at least four measurements for compression and five for surface tests in order to predict the parameters to an accuracy of 15% at a 95% confidence interval. However, a general rule of three tests per fabric for all mechanical parameters may be taken as a guide [Mahar 87].

Appendix E Friction

E.1 Detailed Friction Results

Table E-1. Friction coefficients for set 1 fabrics against different sliding surfaces

Fabric code		Aluminium			Formica			Rubber		
		μ_s	μ_d	σ_{rip}	μ_s	μ_d	σ_{rip}	μ_s	μ_d	σ_{rip}
C1	Warp	0.235	0.227	0.010	0.288	0.266	0.017	0.430	0.398	0.012
	Weft	0.228	0.217	0.007	0.296	0.275	0.016	0.435	0.409	0.011
P1	Warp	0.270	0.245	0.010	0.293	0.249	0.015	0.339	0.323	0.010
	Weft	0.306	0.282	0.009	0.305	0.262	0.015	0.355	0.330	0.012
W1	Warp	0.273	0.255	0.010	0.367	0.358	0.007	0.448	0.446	0.007
	Weft	0.275	0.258	0.010	0.365	0.362	0.007	0.452	0.444	0.007
KC1	Wale	0.340	0.326	0.006	0.405	0.392	0.010	0.482	0.466	0.009
	Course	0.327	0.316	0.006	0.399	0.385	0.010	0.480	0.462	0.010
KC11	Wale	0.366	0.364	0.005	0.413	0.401	0.009	0.504	0.498	0.009
	Course	0.369	0.372	0.004	0.413	0.408	0.009	0.492	0.493	0.010
KA11	Wale	0.328	0.313	0.006	0.370	0.361	0.009	0.438	0.439	0.008
	Course	0.332	0.314	0.006	0.381	0.370	0.009	0.466	0.455	0.009

Standard conditions, velocity: 1 mm/s, sampling frequency: 75 Hz, sample area: 1 dm²

Table E-2. The effect of the sample area on fabric friction for set 1 samples

Fabric code		Aluminium				Formica				Rubber			
		μ_s	μ_d	σ_{rip}	$\Delta\mu_d$	μ_s	μ_d	σ_{rip}	$\Delta\mu_d$	μ_s	μ_d	σ_{rip}	$\Delta\mu_d$
C1	R1	0.262	0.248	0.010	14.0	0.355	0.319	0.018	16.0	-	-	-	-
	R2*	0.278	0.265	0.008	7.0	-	-	-	-	-	-	-	-
P1	R1	0.326	0.301	0.013	6.5	0.336	0.296	0.025	13.0	0.408	0.380	0.015	15.0
	R2	0.326	0.307	0.009	2.0	0.322	0.293	0.016	-1.0	0.452	0.436	0.012	14.0
W1	R1	0.317	0.295	0.013	14.4	0.434	0.414	0.012	14.4	0.487	0.471	0.011	6.2
	R2	0.336	0.328	0.005	11.3	-	-	-	-	-	-	-	-
KC1	R1	0.393	0.372	0.013	14.0	0.472	0.434	0.017	10.9	0.536	0.502	0.015	7.8
	R2	0.412	0.396	0.010	6.5	-	-	-	-	-	-	-	-
KC11	R1	0.380	0.359	0.014	-1.3	0.483	0.460	0.012	15.0	0.552	0.537	0.013	7.8
	R2	0.425	0.410	0.010	14.0	0.519	0.491	0.012	6.6	-	-	-	-
KA11	R1	0.338	0.320	0.007	2.2	0.413	0.389	0.012	7.5	0.482	0.471	0.012	7.3
	R2	0.371	0.359	0.006	12.0	0.418	0.399	0.011	2.6	-	-	-	-

Dimensions R1: 100 x 200 mm, R2: 200 x 200 mm, R2*: 165 x 173 mm, $\Delta\mu_d$: % difference μ_d 100 cm² – 200 cm² and 200 cm² – 400 cm²

Standard conditions, velocity: 1 mm/s, sampling frequency: 75 Hz

Table E-3. Experimental values of C and n for set 1 fabrics

Fabric code		Aluminium				Formica				Rubber			
		Static		Dynamic		Static		Dynamic		Static		Dynamic	
		$C(N/m^2)$	n										
C1	Warp	-0.55	0.92	-0.57	0.91	-0.64	1.14	-0.59	1.04	-0.28	0.97	-0.36	1.00
	Weft	-0.59	0.96	-0.64	0.98	-0.42	0.94	-0.49	0.96	-0.37	1.02	-0.40	1.01
P1	Warp	-0.51	0.85	-0.56	0.83	-0.52	0.94	-0.61	0.94	-0.42	0.92	-0.47	0.97
	Weft	-0.48	0.88	-0.52	0.87	-0.48	0.96	-0.58	0.96	-0.43	0.98	-0.48	1.01
W1	Warp	-0.49	0.90	-0.55	0.93	-0.39	0.96	-0.43	0.97	-0.39	1.09	-0.35	1.00
	Weft	-0.43	0.84	-0.48	0.86	-0.44	1.03	-0.45	1.02	-0.37	1.02	-0.35	1.01
KC1	Wale	-0.37	0.87	-0.39	0.87	-0.32	0.94	-0.35	0.93	-0.28	0.91	-0.28	0.88
	Course	-0.41	0.91	-0.44	0.93	-0.39	1.01	-0.42	1.00	-0.26	0.91	-0.28	0.90
KC11	Wale	-0.36	0.86	-0.37	0.86	-0.35	0.97	-0.37	0.97	-0.29	0.97	-0.30	0.96
	Course	-0.35	0.89	-0.37	0.85	-0.35	0.96	-0.37	0.96	-0.28	0.95	-0.30	0.95
KA11	Wale	-0.38	0.84	-0.42	0.84	-0.38	0.94	-0.41	0.95	-0.32	0.97	-0.31	0.93
	Course	-0.40	0.86	-0.44	0.87	-0.39	0.96	-0.41	0.95	-0.26	0.91	-0.32	0.95

Standard conditions, velocity: 1 mm/s, sampling frequency: 75 Hz, sample area: 1 dm²

Table E-4. Coefficients a_3 and b for dynamic friction coefficient with variable speed against aluminium and rubber

Fabric code		Aluminium			Rubber		
		a_3	b	r^2	a_3	b	r^2
C1	<i>Warp</i>	0.246	0.023	0.948	0.452	0.036	0.984
	<i>Weft</i>	0.234	0.018	0.834	0.454	0.033	0.944
P1	<i>Warp</i>	0.266	0.040	0.897	0.370	0.075	0.970
	<i>Weft</i>	0.286	0.017	0.734	0.370	0.058	0.908
W1	<i>Warp</i>	0.280	0.020	0.692	0.457	0.011	0.565
	<i>Weft</i>	0.283	0.019	0.731	0.473	0.021	0.868
KC1	<i>Wale</i>	0.348	0.021	0.872	0.512	0.037	0.923
	<i>Course</i>	0.337	0.022	0.783	0.500	0.033	0.887
KC11	<i>Wale</i>	0.375	0.009	0.498	0.518	0.021	0.844
	<i>Course</i>	0.376	0.013	0.687	0.512	0.024	0.647
KA11	<i>Wale</i>	0.325	0.024	0.776	0.470	0.030	0.916
	<i>Course</i>	0.327	0.012	0.590	0.471	0.018	0.727

Standard conditions, sample area: 1 dm²

r^2 : correlation coefficient between model and experimental data

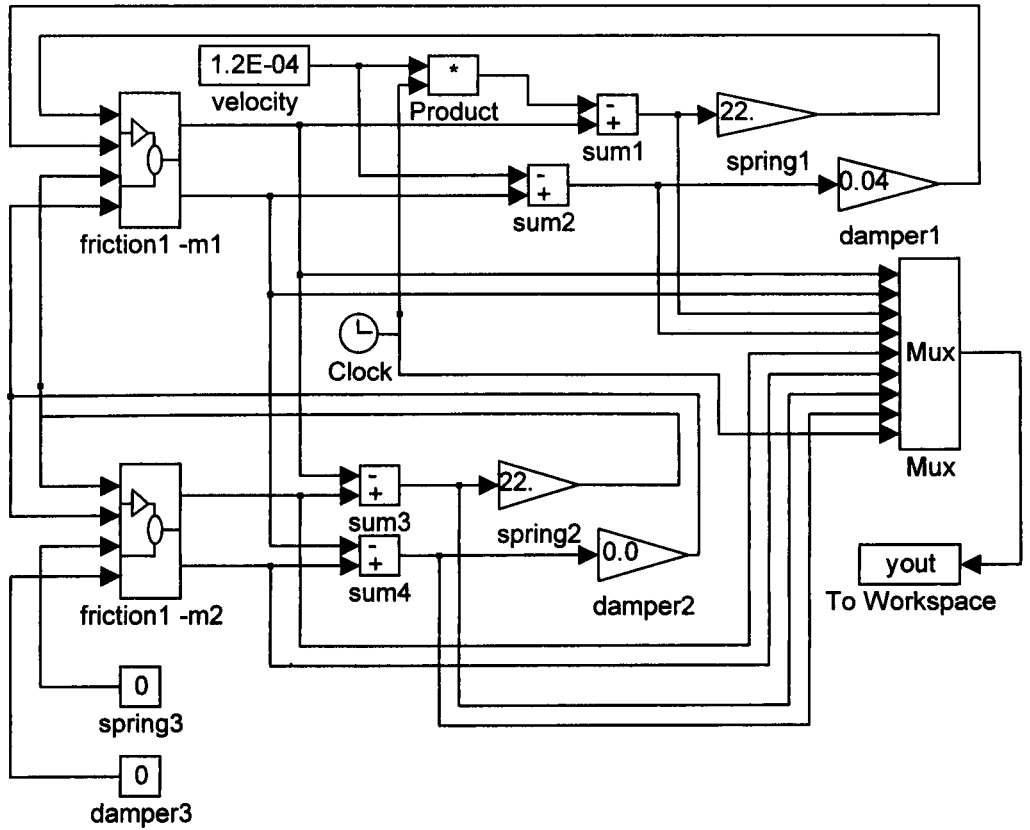


Figure E.2. Two-mass model for simulating stick-slip in fabric

Parameters in the block diagram are set for KC3; $m_1 = m_2$: 1.10 g.
 $k_1 = k_2$: 22.5 N/m, $c_1 = c_2$: 0.0412 N s/m

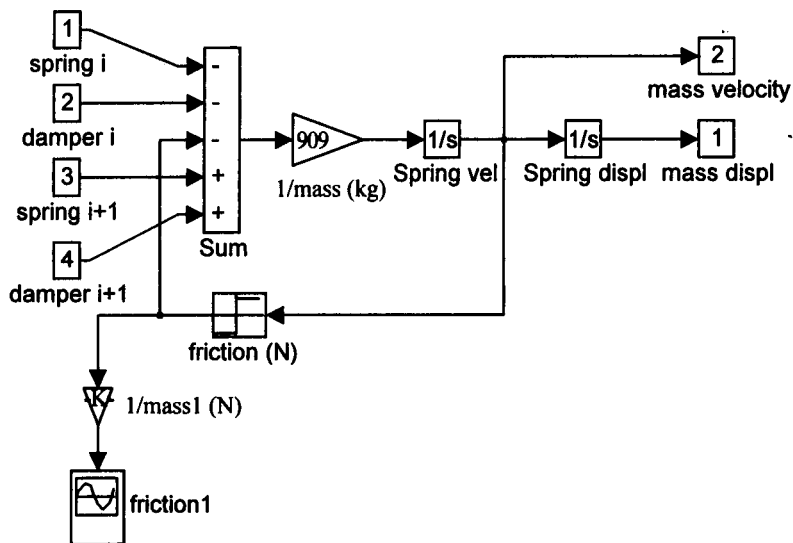


Figure E.3. Representation of a one mass element as a subsystem (friction1_m1) in Figure E.2

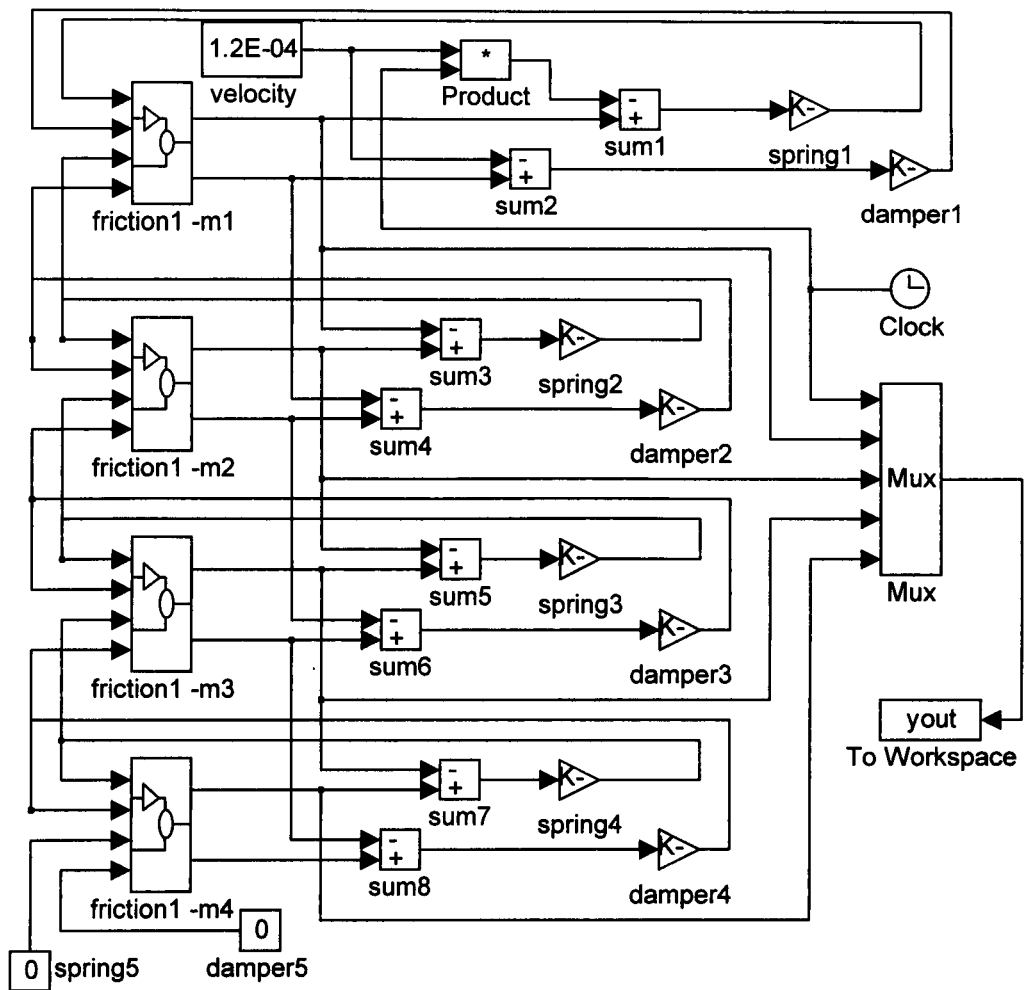


Figure E.4. Four-mass model for simulating stick-slip behaviour in fabrics

Parameters in the block diagram are set for KC3 and are identical for the four masses; m : 0.55 g, k : 11.25 N/m, c : 0.02061 N s/m

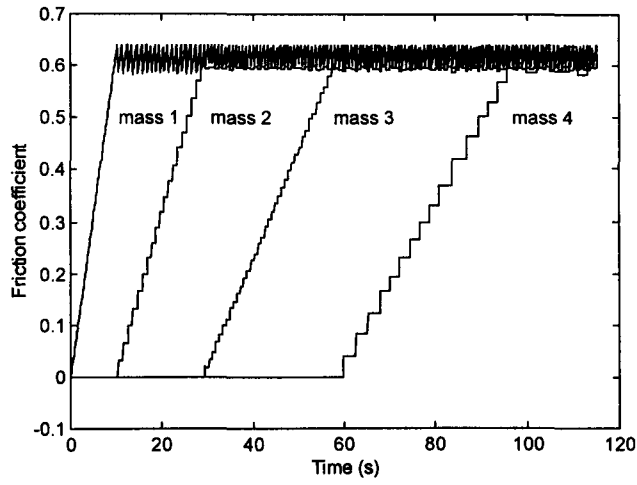


Figure E.5. Simulated friction for KC3 with a four-mass model

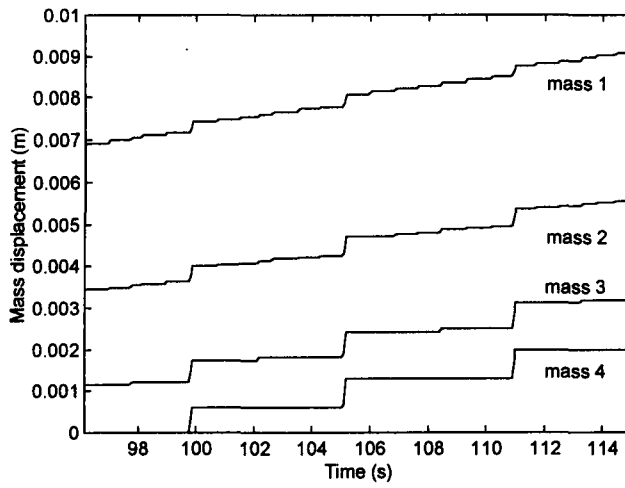


Figure E.6. Simulated mass movement for KC3 with a four-mass model

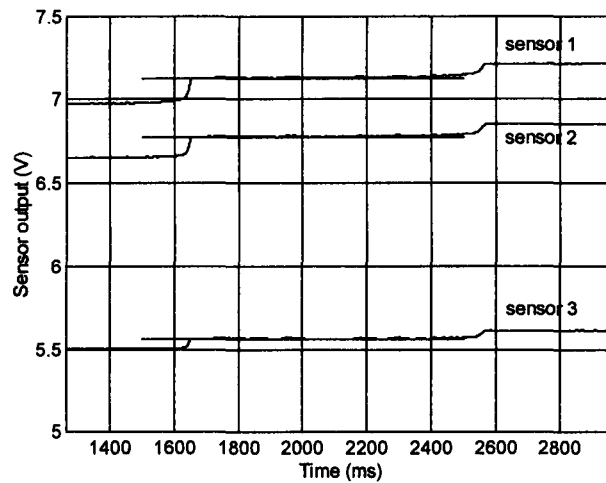


Figure E.7. Experimental movement of fabric parts in KC3 detected on the diode bench
 Straight line is superimposed on the sensor signal during the stick phase

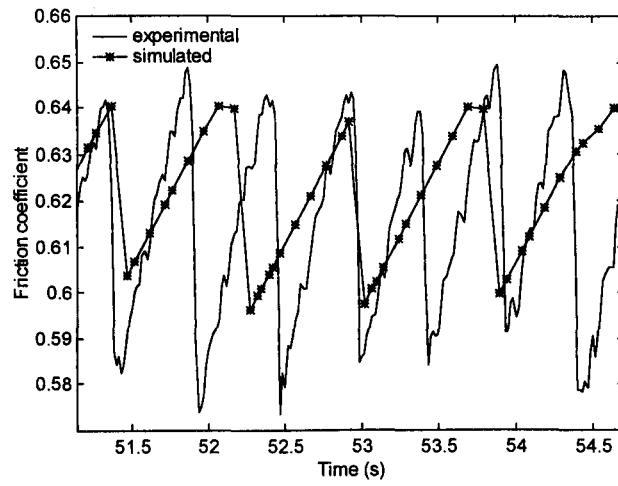


Figure E.8. Comparison between the experimental stick-slip trace from KC3 and the simulated trace with a four-mass model (0.12 mm/s)

Appendix F Spring Impact

A small helical compression spring is compressed statically and impact loaded, as described in chapter 4. The spring with an overall free length of 6.45-mm and $\text{Ø } 4.55\text{-mm}$ is carefully selected to avoid any bottoming during the impact compression. At first, the spring is compressed statically measuring simultaneously force and displacement. A quasi-linear load-deflection characteristic, displayed in Figure F.1, is obtained, giving a spring constant of 5000 N/m. Next, the same spring is impact loaded on the pendulum giving a response as in Figure F.2. The timing in Figure F.2, however, does not correspond to the release time of the pendulum (i.e., 0 seconds is not the start of the test) but has been delayed since the pendulum arm rebounded heavily.

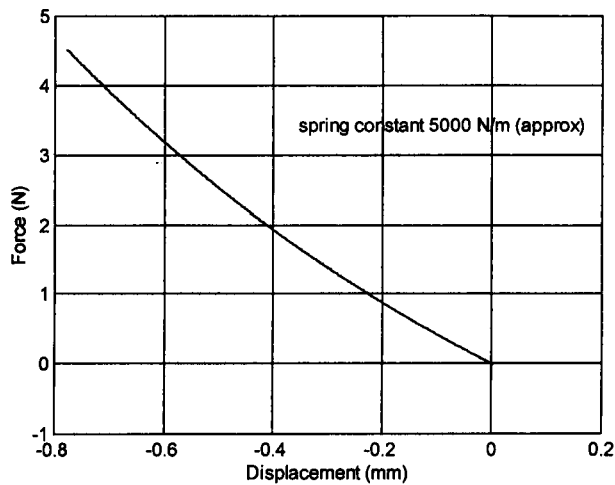


Figure F.1. Load deflection characteristic of test spring

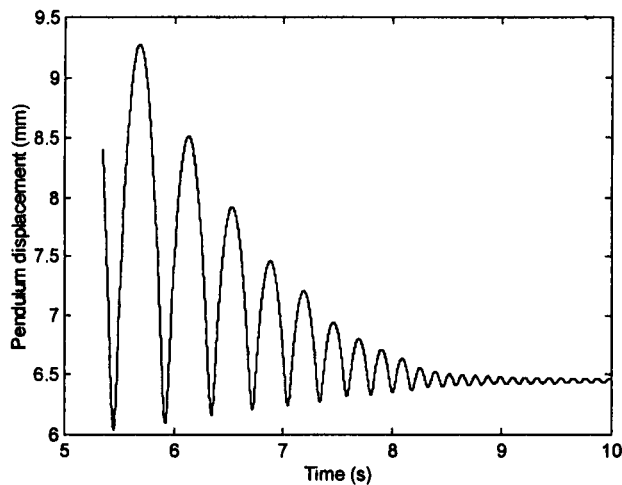


Figure F.2. Pendulum oscillation for test spring

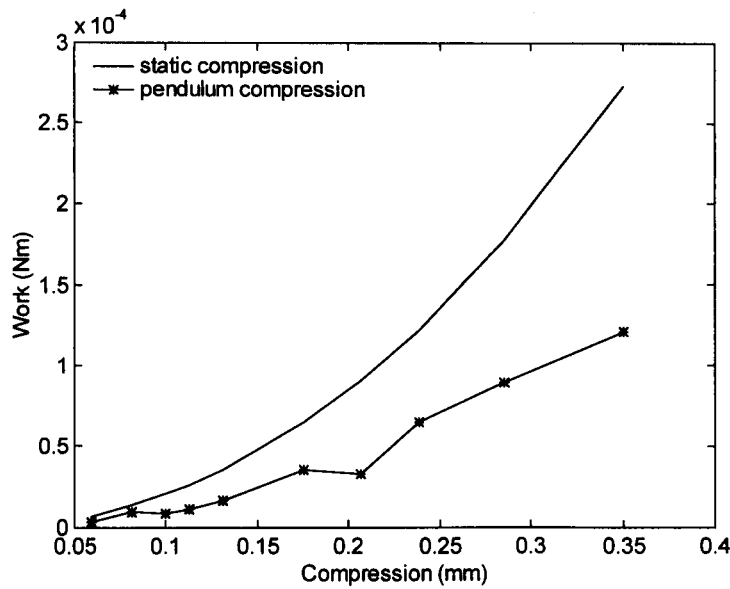


Figure F.3. Comparison between the static and dynamic work for similar compression of the test spring

Table F-1. Static and dynamic compressional work for identical compressions

Spring compression (mm)	Static compression energy (1e-04 Nm)	Dynamic compression energy (1e-04 Nm)	Ratio dynamic/static energy
0.350	1.209	2.733	0.442
0.285	0.896	1.775	0.505
0.239	0.649	1.220	0.532
0.207	0.330	0.905	0.365
0.175	0.351	0.646	0.524
0.131	0.167	0.357	0.467
0.113	0.114	0.259	0.441
0.099	0.087	0.202	0.411
0.081	0.095	0.134	0.711
0.059	0.039	0.068	0.566

Comparing again the static compression energy with the dynamic compression energy, using Equation (4.7), reveals an approximate ratio of 0.50, given in Table F-1 and displayed in Figure F.3. This ratio is however theoretical verifiable as will be explained in this appendix. Consider a mass, m , originally at rest falling from a height, h , onto the spring with free length, l , and spring constant, k , as depicted in Figure F.4. The potential energy of the mass, m , can be written as mgh with g the acceleration of gravity. As the mass falls down, this potential energy is gradually converted into kinetic energy and is eventually totally transformed when the mass strikes the spring. The kinetic energy of the mass is then further transformed into deformation energies, which can be split into two. One part is dissipated into strain compressing the spring with a length, l_d , and another part is converted into heat and localised plastic deformations. A small part of that energy may even remain as

kinetic energy and be used to rebound. Eventually, the rebound will end because of damping effects in the spring and the spring will be at rest supporting the mass. The real mechanical behaviour of such a system is obviously more complex than as described above and requires advanced mechanics, which is beyond the scope of this thesis. However, an approximate analysis can be made by using the concept of strain energy and assuming some simplification [Timoshenko 73].

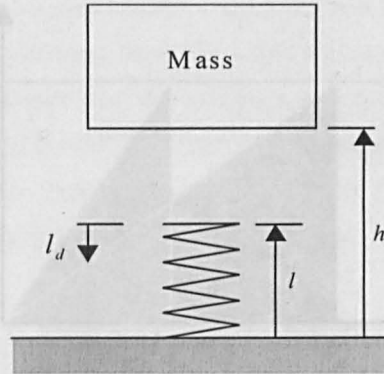


Figure F.4. Impact load on a helical spring

First, we will assume that no rebound takes place (i.e., perfectly plastic impact) and that all the kinetic energy transforms into strain thereby disregarding any energy losses. Further, minute changes in the potential energy of the spring due to the compression are ignored together with any inherent strain already apparent before the impact. Finally, we assume that the stresses in the spring stay within the linearly elastic range and that the distribution is the same as for static loading. The latter is acceptable for low velocities but deviates definitely at high velocity impacts. Based on these assumptions, the maximum dynamic compression, l_d , can be calculated from the principle of energy conservation by equating the potential energy lost by the falling mass to the strain developed in the spring as follows:

$$mg(h + l_d) = \frac{kl_d^2}{2} \quad (\text{F.1})$$

Equation (F.1) is quadratic in l_d and can be solved for its positive root as:

$$l_d = \frac{mg}{k} + \sqrt{\left(\frac{mg}{k}\right)^2 + \frac{2mgh}{k}} \quad (\text{F.2})$$

Introducing now the static compression, $l_s = \frac{mg}{k}$, the preceding equation becomes:

$$l_d = l_s + \sqrt{l_s^2 + 2l_s h} \quad (\text{F.3})$$

In the case of the pendulum, the mass is falling from a very small angle or in other words, h can be considered zero. Hence, the impact load produces a spring deflection twice as large as a deflection

caused by a similar static load (a finding first obtained by J.V. Poncelet (1788-1867)). The ratio between the maximum dynamic deflection and static deflection is sometimes in mechanics referred to as the impact factor. Thus, comparing the static and dynamic compression energy for the same deflection, the dynamic energy will only be half of the required static energy as seen from the shaded area in Figure F.5.

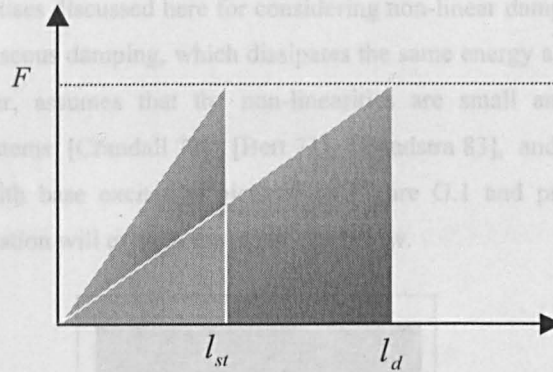


Figure F.5. Theoretical comparison between the static and dynamic compression energy

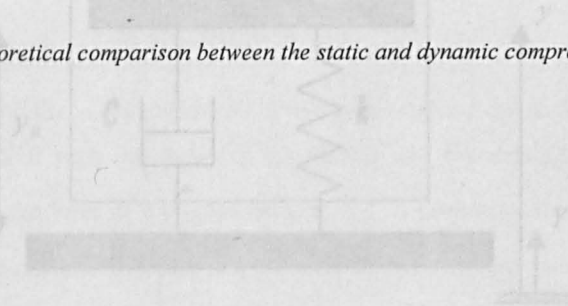


Figure G.1. Base excited spring-damper model

Summing the relevant forces on the mass, m , in Figure G.1, the equation of motion for the base excited system with spring, k , and damper, c , becomes:

$$m\ddot{y} + c(\dot{y} - \dot{Y}) + k(y - Y) = 0 \tag{G.1}$$

Considering that both the mass (x , fabric) and the base are moving harmonically, the relative displacement, y_r , is used throughout the explanation instead of the absolute displacement. Hence, Equation (G.1) can be written as:

$$m\ddot{y}_r + c\dot{y}_r + ky_r = m\omega^2 u_r \sin \omega t \tag{G.2}$$

Appendix G Hysteretic Damping

The normal engineering approach to including damping in vibration models is by using only viscous damping so that the equations of motion are linear and 'economical' to solve. Yet, for many cases, this is an idealised situation where the real damping is often non-linear and more complicated. One of the standard practises discussed here for considering non-linear damping in a dynamic system is to use an equivalent viscous damping, which dissipates the same energy as the non-linear damping. This technique, however, assumes that the non-linearities are small and is only applicable to sinusoidally excited systems [Crandall 70], [Bert 73], [Bandstra 83], and [Tongue 96]. A SDOF spring-damper model with base excitation pictured in Figure G.1 and proposed in chapter 5 for modelling the fabric vibration will explain the technique below.

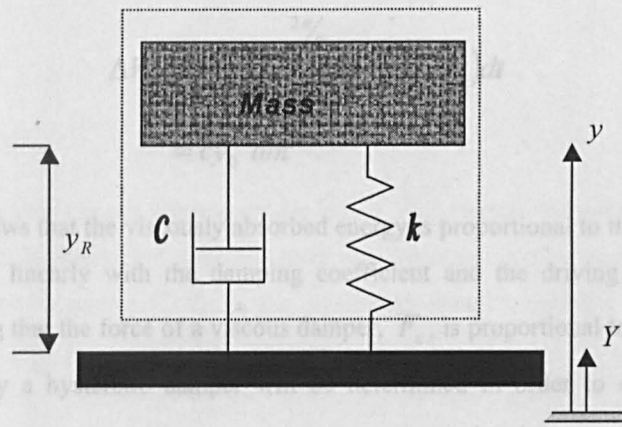


Figure G.1. Base excited spring-damper model

Summing the relevant forces on the mass, m , in Figure G.1, the equation of motion for the base excited system with spring, k , and damper, c , becomes:

$$m\ddot{y} + c(\dot{y} - \dot{Y}) + k(y - Y) = 0 \quad (\text{G.1})$$

Considering that both the mass (i.e., fabric) and the base are moving harmonically, the relative displacement, y_R , is used throughout the explanation instead of the absolute displacement. Hence, Equation (G.1) can be written as:

$$m\ddot{y}_R + c\dot{y}_R + ky_R = m\omega^2 u_0 \sin \omega t, \quad (\text{G.2})$$

with u_0 the amplitude of the absolute displacement. The energy (work), ΔW_v , dissipated per cycle in a viscously damped system with a viscous damping coefficient, c , is then given by:

$$\begin{aligned}\Delta W_v &= \oint F_c dy_R \\ &= \int_0^{2\pi/\omega} \left(c\dot{y}_R \frac{dy_R}{dt} \right) dt \\ &= \int_0^{2\pi/\omega} (c\dot{y}_R^2) dt\end{aligned}\quad (G.3)$$

At steady state $y_R = y_0 \sin(\omega t - \psi)$ and $\dot{y}_R = y_0 \omega \cos(\omega t - \psi)$ hence Equation (G.3) becomes:

$$\begin{aligned}\Delta W_v &= cy_0^2 \omega^2 \int_0^{2\pi/\omega} \cos^2(\omega t - \psi) dt \\ &= cy_0^2 \omega \pi\end{aligned}\quad (G.4)$$

The above result shows that the viscously absorbed energy is proportional to the relative displacement squared, and varies linearly with the damping coefficient and the driving frequency, ω . This is expected considering that the force of a viscous damper, F_c , is proportional to the velocity. Next, the energy dissipated by a hysteretic damper will be determined in order to calculate an equivalent viscous damper.

Viscous damping force is different from hysteretic damping force in that hysteretic damping is frequency independent. However, theoretically, a force that is simply proportional to a displacement (i.e., frequency independent) does not absorb any energy and therefore includes no damping. Yet, being out of phase with the displacement is sufficient for damping to occur. This has been solved mathematically by introducing the concept of complex damping [Kimball 27] where the damping force is represented proportionally as an imaginary term, jy_R (viz., 90° out of phase with the displacement). Applying this concept now to a base excited spring-damper system changes Equation (G.2) into:

$$\begin{aligned}m\ddot{y}_R + jk\gamma y_R + ky_R &= m\omega^2 u_0 \sin \omega t \\ m\ddot{y}_R + (j\gamma + 1)ky_R &= F_m\end{aligned}\quad (G.5)$$

with F_m the total force acting on the mass. The quantity $(j\gamma + 1)k$ is called the complex stiffness with γ the hysteretic (or structural) damping factor. The notion of structural damping, γ , is related to the definition of the damping ratio, ζ , only at resonance (i.e., forcing frequency is equal to the natural frequency) where $\gamma = 2\zeta$. Further, this complex notation is also frequently used in material engineering to describe viscoelastic behaviour, where in analogy the modulus of elasticity or shear is

represented as a complex unit. The structural damping factor is then generally referred to as the loss factor of the material or loss angle (viz., $\tan \delta$).

The energy, ΔW_h , dissipated by a hysteretic damping can now be calculated in a similar way as for the viscous damping in Equation (G.3) yielding:

$$\begin{aligned} \Delta W_h &= \oint F_h dy_R \\ &= \int_0^{2\pi/\omega} \bar{F}_m \cos \omega t (-\omega \bar{F}_m) \frac{(k - \omega^2 m) \sin \omega t - \gamma k \cos \omega t}{(k - \omega^2 m)^2 + (\gamma k)^2} dt \end{aligned} \quad (G.6)$$

Evaluating Equation (G.6) gives:

$$\begin{aligned} \Delta W_h &= \frac{\pi \gamma k \bar{F}_m^2}{(k - \omega^2 m)^2 + (\gamma k)^2} \\ &= \pi \gamma k y_0^2 \end{aligned} \quad (G.7)$$

So, as seen from the above result, the energy dissipated by hysteretic damping is proportional only to the square of the displacement but does not have any frequency dependence. Equating the viscous damping energy from Equation (G.4) to the hysteretic damping energy, an equivalent viscous damping coefficient, c_{eq} , can be derived as follows:

$$\begin{aligned} c y_0^2 \omega \pi &= \pi \gamma k y_0^2 \\ \text{hence} & \\ c_{eq} &= \frac{\gamma k}{\omega} \end{aligned} \quad (G.8)$$

This equivalent damping coefficient can now be implemented in any spring-damper model and act as an 'ordinary' damping coefficient as in (5.2.4). Nevertheless, the equivalent damping is still dependent on the forcing frequency, ω ; a constant value will be assumed in this study for the frequency range 10-100 Hz. Finally, the reader should be reminded that the above analysis strictly applies to harmonically excited systems since other excitations violate the causality requirement (i.e., the response can be dependent on its history but not on its future behaviour [Crandall 70]).

Appendix H Basic Theory of a Single Degree Flight-Free Vibrating Conveyor

In the literature review of section (2.4.1), it has been shown that a vibratory feeder can work in two main modes, namely the contact mode (i.e., flight-free) or the flight mode. The following theoretical analysis explains in detail the operation of flight-free conveying for a normally excited conveyor introduced in chapter 5. The analysis based on the work of Booth and McCallion [Booth 63] and Nedderman and Harding [Nedderman 90] approximates the fabric as a 'solid' point-mass where neither its shape nor the air resistance is assumed to affect the motion. In addition, no differentiation is made between the static and dynamic friction coefficient considering the insignificant variation for unloaded fabrics. Further, it is also presumed that the coefficient of friction remains constant and does not vary with the sliding velocity.

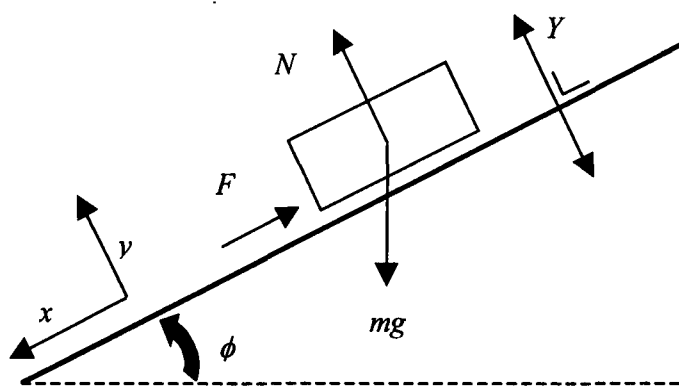


Figure H.1. The co-ordinate system and angles

Figure H.1 shows the co-ordinate system used to describe the motion of the conveying surface and the fabric, the x -axis is directed along the surface and the y -axis is perpendicular to it. The plane track of the conveyor is inclined at an angle, ϕ , to the horizontal and vibrates sinusoidally with an amplitude, u_0 , and angular velocity, ω , normal to the track. The angle of the table inclination, ϕ , must however be less than the angle of static friction (see 2.1.6) to prevent the object from just sliding down. Denoting now by X and Y the co-ordinates of any particular point on the table surface, the displacement, velocity and acceleration of the table may be written respectively as:

$$\begin{aligned} Y &= u_0 \sin \omega t \\ \dot{Y} &= \omega u_0 \cos \omega t \\ \ddot{Y} &= -\omega^2 u_0 \sin \omega t \end{aligned} \quad (\text{H.1})$$

For the fabric to maintain contact with the table, the normal force, N , between the fabric and the table must remain positive or in other words the fabric's velocity, \dot{y} , and acceleration, \ddot{y} , will be equal to

the table's Y-velocity and Y-acceleration. Hence, the dynamic force equilibrium of the fabric with mass, m , and co-ordinates x, y yields in the y -direction:

$$\begin{aligned} m\ddot{y} &= N - mg \cos \phi \\ \text{or} & \\ N &= m(g \cos \phi - \omega^2 u_0 \sin \omega t) \end{aligned} \quad (\text{H.2})$$

Thus, the minimum normal force will arise at the positive half cycle of the displacement sinusoid with $\omega t = 90^\circ$. Further contact between the fabric and the table will be lost if:

$$g \cos \phi < u_0 \omega^2 \quad (\text{H.3})$$

Next, for a situation as illustrated in Figure H.1, only two modes of operation can appear dependent on the frictional force, F , between the fabric and the table; the fabric will either slide down when $F > \mu N$ or remain stationary when $F \leq \mu N$. Upward moving of the fabric panel along the table is excluded. Resolving now the fabric's motion for both modes in the x -direction gives:

- for the stationary phase (R) in a steady state with $|\dot{x}| = 0$ and $F \leq \mu N$:

$$\begin{aligned} mg \sin \phi &= F \\ mg \sin \phi &\leq \mu N \\ g \sin \phi &\leq \mu(g \cos \phi - \omega^2 u_0 \sin \omega t) \\ g \left(\frac{\sin \phi}{\mu} - \cos \phi \right) &\leq \ddot{Y} \end{aligned} \quad (\text{H.4})$$

- for the sliding down phase (B) with $|\dot{x}| > 0$ and $F > \mu N$:

$$\begin{aligned} mg \sin \phi &= F \\ mg \sin \phi &> \mu N \\ g \left(\frac{\sin \phi}{\mu} - \cos \phi \right) &> \ddot{Y} \end{aligned} \quad (\text{H.5})$$

The fabric motion as a function of time is best explained by referring to the acceleration diagram in Figure H.2. Considering that the conveyor operates in flight-free mode both the table and the fabric has an identical Y-acceleration. From Figure H.2, it is seen that the fabric remains stationary during the majority of the cycle, sliding down only appears when the table acceleration fulfils inequality (H.5) between $t1$ and $t2$. The transition times $t1$ and $t2$ between the stationary and sliding phase are

given by $g\left(\frac{\sin \phi}{\mu} - \cos \phi\right) = \ddot{Y}$. Substituting for \ddot{Y} from Equation (H.1) results in:

$$\sin \omega t_{1,2} = \frac{g(\sin \phi - \mu \cos \phi)}{-\mu \omega^2 u_0} \quad (\text{H.6})$$

Applying Equation (H.6) to the parameters of Figure H.2 gives both sliding times $t1 = 0.0041$ ms (i.e., 58.78°) and $t2 = 0.0084$ ms respectively. Note that Equation (H.6) only calculates the starting time $t1$.

Time $t2$ (i.e., stop time) is obtained from the supplementary angle or $(180 - \omega t_1)$.

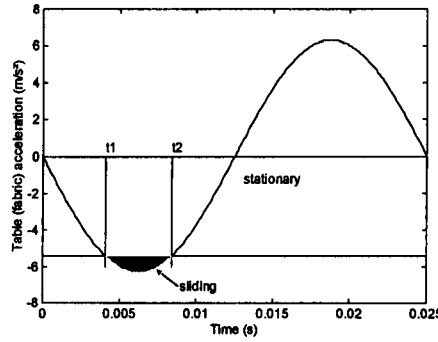


Figure H.2. 'Slip stick' cycle of a vibrating fabric panel

The illustration is calculated for a table inclined at an angle of 10° with an excitation of $100 \mu\text{m}$ and a frequency of 40 Hz, a friction coefficient of 0.4 is assumed between the fabric and the table surface

Thus at time $t1$ the fabric starts to slide down the table. The X-acceleration of the fabric between $t1$ and $t2$ can be calculated by resolving the forces along the X-direction, giving:

$$\begin{aligned} m\ddot{x} &= mg \sin \phi - F \\ \ddot{x} &= g \sin \phi - \mu(g \cos \phi - \omega^2 u_0 \sin \omega t) \\ \ddot{x} &= -\mu \omega^2 u_0 (\sin \omega t_1 - \sin \omega t) \end{aligned} \quad (\text{H.7})$$

Integrating Equation (H.7) from $t1$ gives us the velocity of the fabric as follows:

$$\begin{aligned} \dot{x} &= \int_{t_1}^t -\mu \omega^2 u_0 (\sin \omega t_1 - \sin \omega t) dt \\ &= -\mu \omega u_0 [\omega t \sin \omega t_1 - \cos \omega t]_{t_1}^t \\ &= \mu \omega u_0 [(t_1 - t) \omega \sin \omega t_1 + \cos \omega t_1 - \cos \omega t] \end{aligned} \quad (\text{H.8})$$

Note that both at times t_1 and t_2 the fabric velocity is supposed to be zero or $\dot{x} = 0$. Further, the sliding distance of the fabric per cycle can now be found by integrating the velocity again between t_1 and t_2 giving:

$$\begin{aligned}
 x &= \int_{t_1}^{t_2} \mu \omega u_0 \left[(t_1 - t) \omega \sin \omega t_1 + \cos \omega t_1 - \cos \omega t \right] dt \\
 &= \mu \omega u_0 \left[\left(t_1 t - \frac{t^2}{2} \right) \omega \sin \omega t_1 + t \cos \omega t_1 - \frac{\sin \omega t}{\omega} \right]_{t_1}^{t_2} \quad (\text{H.9}) \\
 &= \mu u_0 \left[\sin \omega t_1 - \sin \omega t_2 + (t_2 - t_1) \omega \cos \omega t_1 - \frac{(\omega t_2 - \omega t_1)^2}{2} \sin \omega t_1 \right]
 \end{aligned}$$

The average conveying velocity for one cycle, v_B , can also be calculated from the sliding distance divided by the cycling period given as follows:

$$v_B = \frac{\omega x}{2\pi} = f x \quad (\text{H.10})$$

To illustrate the above equations, we have used again the same parameters used to generate Figure H.2. A fabric with a friction coefficient of 0.4, on a 10 degrees inclined table, excited with 40 Hz -100 μm peak to peak sinusoid, will slide 2.3 μm per cycle or 91 μm per second.

Finally, Figure H.3 and Figure H.4 display the sliding velocity for flight-free motion under different operating conditions of friction and inclination for a table excitation of respectively 100- μm and 150- μm .

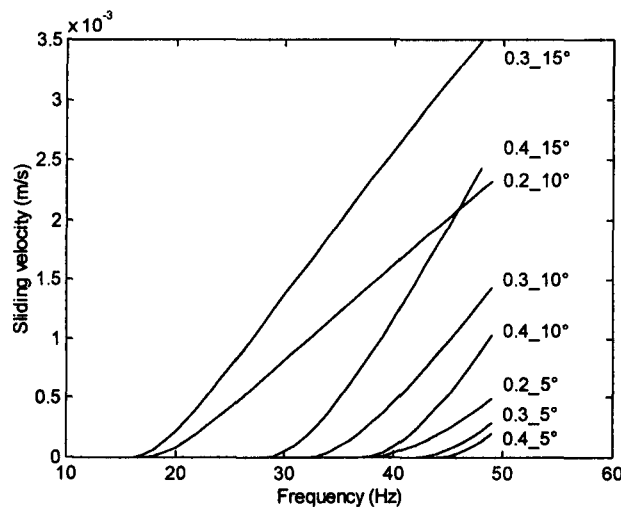


Figure H.3. Theoretical sliding velocity of a solid object in flight-free motion for a table excitation of 100 μm

The first number of the legend gives the friction coefficient, μ ; the second number refers to the inclination angle of the table, ϕ

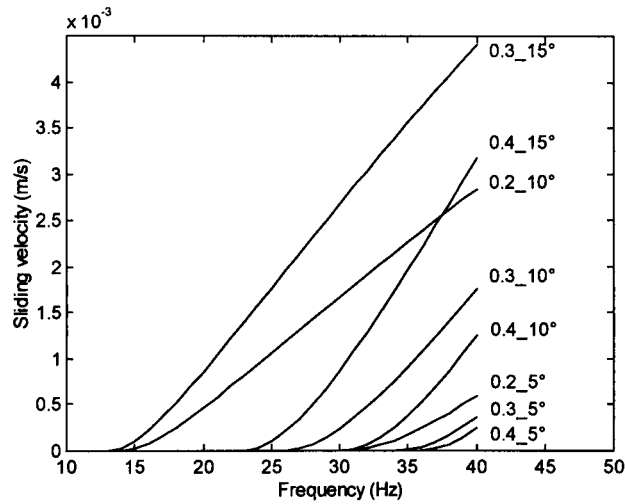


Figure H.4. Theoretical sliding velocity of a solid object in flight-free motion for a table excitation of $150 \mu\text{m}$

The first number of the legend gives the friction coefficient, μ ; the second number refers to the inclination angle of the table, ϕ

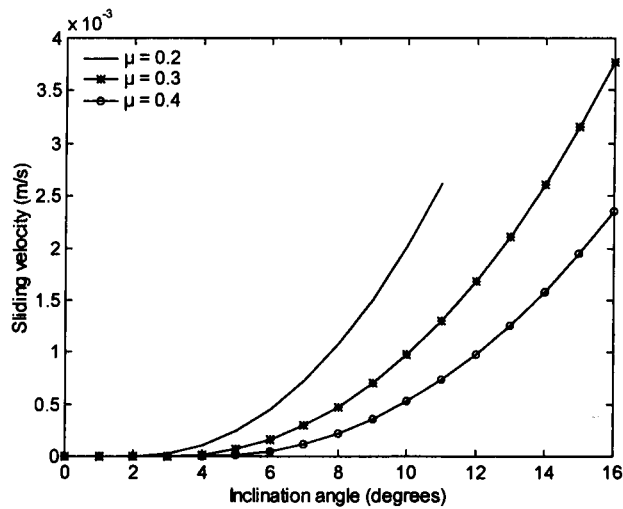


Figure H.5. Theoretical sliding velocity of a solid object in flight-free motion for a variable table inclination

The results are calculated for a table excitation of $100 \mu\text{m}$ at 45 Hz

Both figures clearly indicate that the object obtains a larger sliding velocity for a smaller friction coefficient as can be seen separately for a 45-Hz excitation in Figure H.5. Note also that the velocities are only calculated respectively for frequencies up to 49 Hz and 39 Hz since, theoretically, higher frequencies lift the object off the table (see Equation (H.3)). Comparing both Figure H.3 and Figure H.4, it is also evident that an increase in sliding velocity can be obtained when the excitation amplitude is increased and/or when the table is inclined more as given in Figure H.5.